

DOKUZ EYLÜL UNIVERSITY
GRADUATE SCHOOL OF NATURAL AND APPLIED SCIENCES

**INFLUENCE OF MICA PLATES ON CYCLIC
STRENGTH OF SOILS OF OLD GEDİZ RIVER
DELTA**

by
Ender BAĞARI

July, 2012
ZM R

**INFLUENCE OF MICA PLATES ON CYCLIC
STRENGTH OF SANDY SOILS OF OLD GED Z
RIVER DELTA**

**A Thesis Submitted to the
Graduate School of Natural and Applied Sciences of Dokuz Eylül University
In Partial Fulfillment of the Requirements for the Degree of the Doctor of
Philosophy in Civil Engineering, Geotechnics Program**

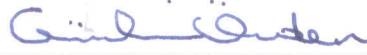
**by
Ender BA ARI**

July, 2012

ZM R

Ph.D. THESIS EXAMINATION RESULT FORM

We have read the thesis entitled “**INFLUENCE OF MICA PLATES ON CYCLIC STRENGTH OF SANDY SOILS OF OLD GEDIZ RIVER DELTA**” completed by **ENDER BAŞARI** under supervision of **ASSOC. PROF. DR. GÜRKAN ÖZDEN** and we certify that in our opinion it is fully adequate, in scope and in quality, as a thesis for the degree of Doctor of Philosophy.



Assoc. Prof. Dr. Gürkan ÖZDEN

Supervisor



Prof. Dr. Arif Şengün KAYALAR

Thesis Committee Member



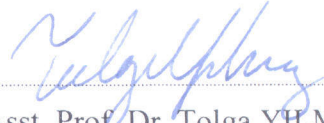
Prof. Dr. Necdet TÜRK

Thesis Committee Member



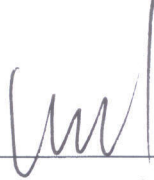
Assoc. Prof. Dr. Selim ALTUN

Examining Committee Member



Asst. Prof. Dr. Tolga YILMAZ

Examining Committee Member



Prof. Dr. Mustafa SABUNCU

Director

Graduate School of Natural and Applied Sciences

ACKNOWLEDGMENTS

Before anything else, I would like to express my sincere thanks to my advisor, Assoc. Prof. Dr. Gürkan Özden, who provided valuable information and guided me during my thesis process. I extend my gratitude to Assoc. Prof. Dr. Gürkan Özden for the technical and mental support he gave me from the very first day of my postgraduate training. I do believe that the guidance and information I received from him will continue to guide my way throughout my life.

I would like to acknowledge the financial support provided by T.R. Prime Ministry State Planning Organization and The Scientific & Technological Research Council of Turkey, TÜB TAK B DEB program.

My special thanks are also for Prof. Dr. Arif engün Kayalar, for valuable comment and contributions in each stage of the my Dissertation.

I would also like to thank Prof. Dr. Necdet Türk for taking time to serve in my thesis committee and valuable contributions.

I would like to thanks for Assoc. Prof. Dr. Selim Altun for his permission for using of Soil Mechanics Laboratory of Ege University and Assist. Prof. Dr. Mustafa Tolga Yılmaz for their valuable comment and helpfull discussions.

Many thanks are due for my friends, colleagues and research assistants of the Soil Mechanics Division of Civil Engineering Department, for their helps, valuable comments and suggestion.

I would like to thanks my family, my mother, father and as well as my brother. They have always supported, helped and encouraged me through all my life. I will always remember their contributions

The last but certainly not the least, I send my special thanks to my wife Aslı and my children. I thank my wife who never left me alone during my studies and always accompanied me. I also thank my children for the irreplaceable love and happiness they brought to my life with their existence.

INFLUENCE OF MICA PLATES CYCLIC STRENGTH OF SANDY SOILS OF OLD GEDIZ RIVER DELTA

ABSTRACT

In this study, the effect of grain shape and fine material content on the cyclic strength properties of sandy soils of Old Gediz River Delta (OGRD) has been experimentally investigated. The test materials were recovered from the sandy soil layers within the liquefaction depth (0^m–20^m) by drilling engineering boreholes in the study area. Sand specimens involving platy mica grains, which were taken from the field, were used in the experimental study. By this way, information on strength and stiffness characteristics of regional sandy soils was acquired with a special emphasis on the influence of mica grains.

Monotonic, cyclic triaxial and bender element tests were carried out on reconstituted prepared test specimens containing varying fractions of sand and mica grains. Size effect of platy grains was also examined using manufactured mica grains in the mixtures. Also, Standard Penetration Test (SPT) was conducted in the field to determine effect of mica on SPT blow counts (N). In the study liquefaction resistance, post liquefaction volume change, shear wave velocity, internal friction angles at different densities and packing density (maximum and minimum void ratios) of the sand mica mixtures were determined.

In conclusion of the study it was determined that mica grains and non-plastic fine materials could significantly reduce to cyclic resistance ratio (CRR) and internal friction angle of OGRD sands. Mica and non-plastic fine materials increase the post liquefaction volumetric strain. It was revealed that mica grains reduce the N values. A relation between N and CRR was proposed for micaceous OGRD sands.

Keywords: Old Gediz River Delta, sand, platy grain, mica, non-plastic fine material, liquefaction resistance, shear wave, post-liquefaction volume change, standard penetration test, cyclic stress ratio, cyclic resistance ratio

YAPRAKSIM KADANELER NESK GED Z NEHR DELTASI KUMLU ZEM NLER N DEV RSEL DAYANIMINA ETK S

ÖZ

Bu doktora çalı masında Eski Gediz Nehri Deltası (EGND) kumlu zeminlerinin dinamik dayanım özelliklerine dane ekleinin ve ince malzeme içeri inin etkisi deneysel olarak ara tırılmı tır. Bu amaç için inceleme sahasında sondajlar yapılarak sıvıla ma derinli i (0^m–20^m) içinde kalan kumlu zemin tabakalarından numuler alınmı tır. Deneysel çalı ma programında araziden elde edilen yapraksı mika daneleri ve kum malzemeler kullanılmı tır. Böylece hem bölgenin kumlu zeminlerinin dinamik davranı ları hakkında, hemde yapraksı danelerin dinamik davranı üzerindeki etkileri hakkında bilgi sahibi olunmu tur.

Farklı mika içeriklerinde hazırlanan numuneler üzerinde monotonik, dinamik ve bender eleman deneyleri yapılmı tır. Yapraksı danelerin boyut etkisi, ticari olarak temin edilen farklı boyuttaki mika danelerinin karı ımlarda kullanılması ile incelenmi tir. Ayrıca, mika danelerinin Standart Penetrasyon Testi (SPT) darbe sayısına (N) etkisini belirlemek amacı ile arazide SPT yapılmı tır. Deneysel çalı mada farklı mika içeriklerindeki numunelerin istiflenme özellikleri (maksimum ve minimum bo luk oranları), farklı sıklıklar için sıvıla ma dirençleri, sıvıla ma sonrası hacim de i imleri, kayma dalgası hızları ve içsel sürtünme açısı de erleri belirlenmi tir.

Çalı ma sonucunda mika danelerinin ve non-plastik ince malzemenin EGND kumlarının devirsel direnç oranlarını (CRR) ve içsel sürtünme açılarını önemli derecede dü ürdü ü görülmü tür. Mika ve non-plastik ince malzeme sıvıla ma sonrası hacim de i imini arttırmı tır. Mika danelerinin N de erlerini dü ürdü ü tespit edilmi tir. Mika içeren EGND kumları için düzeltilmi N ve CRR arasında bir ili ki ortaya konulmu tur.

Anahtar sözcükler: Eski Gediz Nehri Deltası, kum, yapraksı dane, mika, non-plastik ince malzeme, sıvıla ma direnci, kayma dalgası, sıvıla ma sonrası hacim de i imi, standart penetrasyon deneyi, devirsel gerilme oranı, devisel direnç oranı

CONTENTS

	Pages
Ph.D. THESIS EXAMINATION RESULT FORM	ii
ACNOWLEDGMENTS	iii
ABSTRACT	iv
ÖZ	v
CHAPTER ONE – INTRODUCTION	1
1.1 Introduction	1
CHAPTER TWO – LITERATURE REWIEW	4
2.1 Study Area	4
2.2 Liquefaction Phenomenon	5
2.3 Determination of the Liquefaction Potential	8
2.3.1 Evaluation of Cyclic Resistance Ratio (CRR)	10
2.3.2 Evaluation of Cyclic Stress Ratio (CSR)	17
2.3.3 Determination of Safety Factors (FS) Against Liquefaction	21
2.4 Factors Effective on Liquefaction	24
2.4.1 History in Past Earthquakes	24
2.4.2 Geological Structure	25
2.4.3 Grain Size Distribution and Index Properties	25
2.4.4 Relative Density and Stress State	28
2. 4.5 Loading Conditions	30
2.4.6 Vertical Effective Stress and Over Consolidation Ratio	30
2.4.7 Earthquake Background	30
2.4.8. Fine Material Content	32
2.4.9 The Effect of Grain Shape on Behavior	33

CHAPTER THREE – FIELD INVESTIGATIONS AND STUDIES	40
3.1 Geological and Earthquake Characteristics of zmir	40
3.1.1 General Tectonics of the Region	40
3.1.2 Historical Earthquake Affecting the Old Gediz River Delta	43
3.1.3 General Geology of zmir and its Vicinity	44
3.1.4 Aluvial Geomorphology	46
3.2 In Situ Sounding and Laboratory Test Data	48
3.3 Geotechnical Properties of Old Gediz River Delta Soils	50
CHAPTER FOUR – TESTING MATERIALS AND EXPERIMENTAL METHODS	54
4.1 Materials	54
4.2 Experimental Methods	58
4.2.1 Standard Penetration Test (SPT)	58
4.2.2 Index and Physical Properties of Test Materials	61
4.2.3 Determination of Internal Frictional and Repose Angles of Tested Materials	61
4.2.4 Triaxial Tests	62
4.2.4.1 Triaxial Test Apparatus	62
4.2.4.1.1 Tests in DTC-367S Seiken Apparatus	63
4.2.3.1.2 Tests in Controls–Wykeham Farrance Apparatus	63
4.2.4.2 Sample Preparation for Triaxial Tests	64
4.2.4.2.1 Air Pluviation Method	65
4.3.2.2.2 Moist Placement (Tamping) Method	66
4.2.4.3 Monotonic Triaxial Tests	69
4.2.4.4 Load Controlled Cyclic Triaxial Strength Tests	70
4.2.5 Separation Method of Platy and Non-Platy Grains	70
4.2.6 X-Ray Diffraction (XRD) Tests	74
4.2.6 Bender Element Test	76

CHAPTER FIVE – TEST RESULTS	79
5.1 Mica Content of Old Gediz River Delta Sandy Soils	79
5.2 Standard Penetration Test Results	82
5.3 Minimum and Maximum Void Ratios of Sand-Mica Mixtures	87
5.4 Internal Friction Angles of Sand Mica Mixtures	89
5.5 Shear Wave Velocity of Sand Mica Mixtures (Bender Element Tests)	95
5.6 Post-Liquefaction Volumetric Strains	101
5.7 Cyclic Strength (Liquefaction) Test Results	108
 CHAPTER SIX – CONCLUSIONS AND RECOMMENDATIONS	 123
 REFERENCES	 126

APPENDIXES

Appendix – A : Cyclic Strength Tests

Appendix – B : Bender Element Tests

Appendix – C : X-RD Tests

CHAPTER ONE

INTRODUCTION

A significant portion of İzmir, the third largest city and an important industrial center of Turkey, is located on saturated alluvial layers that possess liquefaction potential (Akıncı, et al., 2000; Alper, 2008; Altın, 1993; Başı, 2000; Dadak & Tolay, 2002; Güz, 1970; Kuruoğlu, 2004; Özden, 2000; Utku, et al., 2001). These soil layers are located mostly in the Old Gediz River Delta on the northern part of the city and contain plenty of mica grains due to their geological origins (Candan, 1994; Kayan, 2000; Kuruoğlu, 2004; Özakcan, 2004; Özkan & Çalıkan, 1991; RADIUS, 1999; TGM.RSN.86, 1974). However, liquefaction resistance of these soils was not extensively studied to date.

Research studies made on coarse grain soils with liquefaction potential made great progress in the last three decades. Standard analysis methods for determining liquefaction potential were developed (Youd & Idriss, 2001). As a consequence, in the aftermath of recent earthquakes such as 1995 Great Hanshin Earthquake it was noticed by researchers that fine content might decrease liquefaction resistance, an opinion contrary to the common belief that fines increase liquefaction resistance (Bouckovalas et al., 2003; Ishihara, 1993; Mulilis et al., 1977; Prakash et al., 1998; Seed & Idriss, 1967; Seed & Idriss, 1971; Seed et al., 1985; Thevanayagam & Martin, 2002; Tokimatsu et al., 1990; Vallejo & Mawby, 2000; Walker & Steward, 1989; Xenaki & Athanasopoulos, 2003; Yamamuro et al., 1999; Yoshimi et al., 1984). On the other hand, findings on the liquefaction resistance of sandy and silty soils that contain platy grains (flake or plate shaped such as mica grains) are very limited (Bokhtair et al., 2000; Harris et al., 1984a; Harris et al., 1984b; Lee et al., 2007). It was mentioned that “*finer silts with flaky or platelike particles generally exhibit sufficient cohesion to inhibit liquefaction*” (Kramer, 1996; p.354). As a result of the experimental researches made on saturated sands that contain platy grains, it was determined that platy grains would increase the void ratio of the soil by changing the orientation of the rounded grains (Cho et al., 2006; Georgiannou, 2006; Lee et al., 2007). As a matter of fact, in this study, it was also observed that platy

grains could increase the void ratio of clean sand. Platy grains reduce the stability of the soils by increasing the void ratio of sandy soils and increase compression potential. In other studies, regarding shear strength of both sand and clay size mica grains it was concluded that these grains generally reduced shear strength of soil mixtures (Bokhtair et al., 1999; Bokhtair et al., 2000; Harris et al., 1984a; Harris et al., 1984b; Horn & Dear, 1962; Lee et al., 2007; Santamarina & Cho, 2004; Tiwari & Marui, 2005).

The objective of this thesis study was to investigate influence of flake or plate shaped grains such as mica grains on dynamic behavior of fine sands of OGRD. Although emphasis was given to the experimental research on liquefaction resistance, effect of such grains on SPT-N values was also investigated. The testing program was pursued by means of dynamic triaxial test set-up and bender element test system. The mica mineral present in OGRD soil deposit was separated from natural sand samples so that mica grains would serve as platy grains that were mixed with clean sands in certain proportions. Besides, fabricated crushed mica was also used throughout the testing program.

It is anticipated that the conclusions of the study will allow for more realistic liquefaction analysis about sandy soils of OGRD and will be considered as a contribution to the literature.

During the study, the mineralogical composition of the platy grains obtained from the field within liquefaction depth, was studied. Mineralogical structures of platy grains, was examined by observing thin sections under a microscope and by conducting X-Ray Diffraction (XRD) analyses. Both of these methods have manifested that the platy grains consist of mica minerals. Then, mica grains were separated from the rest of soil grains using some special methods specific to their mineralogy. A method intended for determining the platy grain content of the test soils was developed. With the utilization of the method based on the XRD analyses and the developed correlation were used to determine the mica content of the OGRD soils within the liquefaction depth.

Separated mica and non-platy sand grains were mixed at certain proportions. Tests were carried out at several densities with the purpose of determining the static and dynamic properties of the prepared mixtures. Effect of mica grains on packing density was explored with determining maximum and minimum void ratios of samples in different mica content. Also, SPT was carried out in the investigated fields to determine effects of the mica grains on N values. For this purpose index properties, grain size distribution and mica content of the field samples which is obtained from SPT spoon were determined. In addition, shear wave velocities (V_s) of the sand – mica mixtures were also measured with bender element test to explore mica effects on V_s of the OGRD sand.

In the following chapters of this doctoral thesis, results achieved throughout the experimental program are presented. In this respect, the second chapter is devoted to the literature whereas field studies are presented in the third chapter. The test methods utilized in the testing program and characteristics of the test soils are given in the fourth section. The fifth chapter covers the test results along with their discussions. Finally, conclusions of this study and recommendations for future research are included in the sixth chapter.

CHAPTER TWO

LITERATURE REVIEW

2.1 Study Area

Saturated alluvial layers of the OGRD were the subject material of this research study. Liquefaction analyses in past studies (Dadak & Tolay, 2002; Kuruo lu, 2004; Özden, 2000; Özkan & Çalı an, 1991; RADIUS, 1999) revealed that silty fine sands down to 20 m depth had a high liquefaction potential. These liquefiable soils also contain considerable amount of mica flakes visible as shiny spots in the photograph given in Figure 2.1.



Figure 2.1 Platy mica grains as shiny spots observed in field soils

The experimental research on liquefaction resistance of soils in the region commenced by the help of TUB TAK's financial support to the project “ zmir Metropolü ile Alia a ve Menemen İçelerinde Güvenli Yapı Tasarımı için Zeminin Sismik Davranı larının Modellenmesi – Modelling of Seismic Behavior of Soils for Safe Structural Design in zmir Metropolis with Alia a and Menemen Towns” (Project No:106G159, 2011). The effect of mica grains on liquefaction resistance was particularly touched upon during the study. Additionally, shear wave velocity of micaceous sands was examined via the bender element tests, and monotonic shear

strength tests were performed in the lab in order to investigate basic mechanical characteristics.

2.2 Liquefaction Phenomenon

Liquefaction has been one of the most dramatic causes of damage to the structures and foundations during earthquakes in saturated cohesionless soils (Figure 2.2 through 2.5). Although casualties and damages resulting from liquefaction in earthquakes take part in historical records (Ambraseys & Finkel, 1995), this phenomenon attracted attention of engineers in 20th century in the aftermath of Niigata ($M_s=7.5$) and Great Alaska ($M_w=9.2$) earthquakes occurred in Japan and the USA in 1964. Research programs were launched towards understanding and determination of the liquefaction mechanism in subsequent years (Seed & Idriss, 1967; Seed & Idriss, 1969; Finn et al., 1971; Finn et al., 1977; Seed et al., 1975; Ishihara, et al., 1975). In the wake of these pioneering studies, the research on the subject accelerated. Today, a literature with a quite comprehensive knowledge base was formed.



Figure 2.2 Liquefaction traces and post liquefaction excessive settlement in Adapazarı city center in 1999 Marmara Earthquake (a: <http://sezayozbal.blogspot.com/2011/11/99-depremi-golcuk-adapazar-8.html>, 2011; photo: Özbal S., 1999; b: <http://kisi.deu.edu.tr/huseyin.catal/>, 2011; photo: Çatal H.H., 1999)



Figure 2.3 The loss of bearing capacity of foundation due to liquefaction in 1964 Niigata Earthquake (<http://www.architectureweek.com/2012/0307/>, 2012; Photos by Youd T.L., 1964)

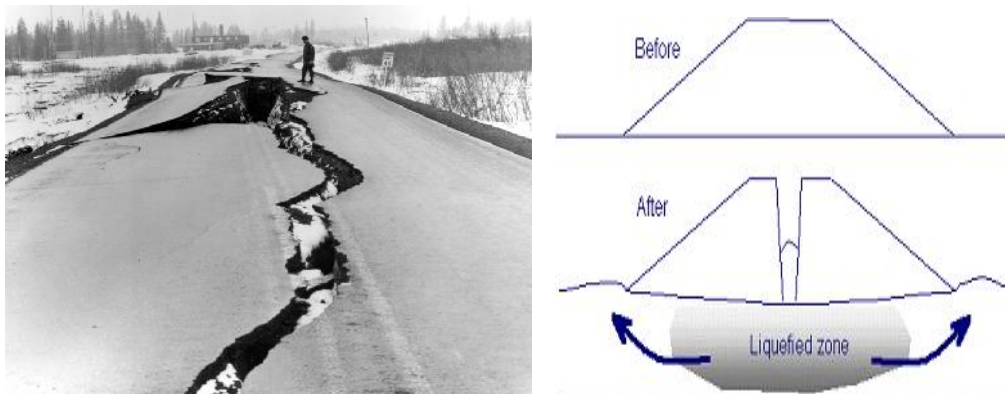


Figure 2.4 The loss of foundation bearing capacity due to liquefaction in 1964 Alaska Earthquake (<http://libraryphoto.cr.usgs.gov/html/lib/batch74/batch74j/batch74z/ake00138.jpg>, 2010, Photo: US army, 1964)

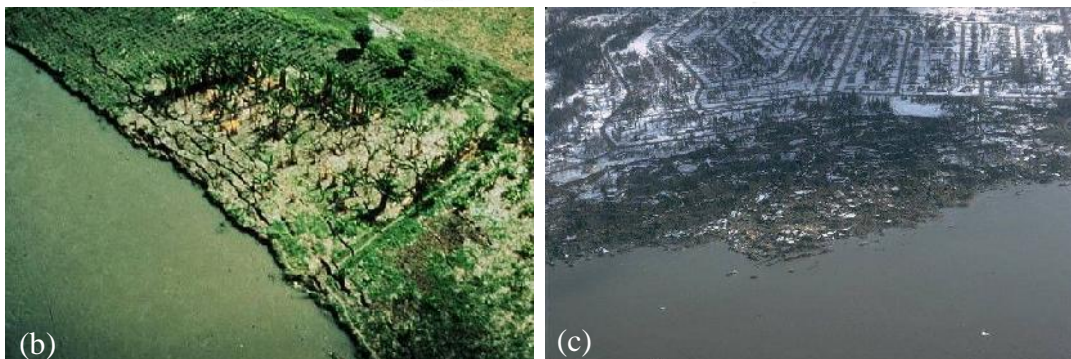
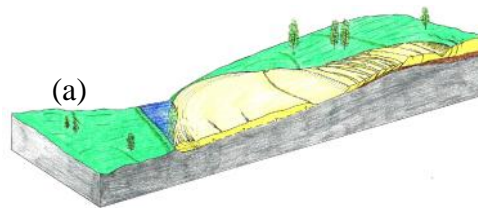


Figure 2.5 Lateral spreading due to liquefaction in (b) Motagua River, Guatemala Earthquake 1976 (c) Alaska, 1964 Alaska Earthquake

a,b: <http://www.ce.washington.edu/~liquefaction/html/what/what2.html>

c: <http://nisee.berkeley.edu/elibrary/Image/S2007>; Photo: Steinbrugge K.V., 1964

Liquefaction in sandy soils and a resultant damage occurred in the city center of Adapazarı and Sapanca during 1999 Marmara earthquake that caused severe damage in the Marmara Region of the country (Figure 2.2). In the aftermath of Sultanda - Çay earthquake in 2002, liquefaction traces in open field were observed (Kuruo lu, 2004). In 1994 Manisa earthquake, it was denoted that liquefaction took place in the district of Saruhanlı in Manisa province (Orhan & Ate , 2010; Orhan & Ate , 2012). Sand volcanoes associated with liquefaction were reported in sandy regions surrounding Demircili village and Yumlu farm in the south of Urla basin in 2005 S1 acık-Seferihisar earthquake (Sözbilir et al., 2009).

The liquefiable fine sand and silt deposits have tendency to densify when they are subjected to dynamic loading. However, the tendency to densify leads to excess pore water pressure generation. This, in turn, causes a decrease in effective stress. As a consequence, the saturated cohesionless soils lose substantial portion of their shear strength once excess pore water pressure gets equal to the initial effective stress and a subsequent reduction in soil volume takes place as the excess pore water pressure dissipates following the ground motion.

If the sand will undergo unlimited deformations without mobilizing significant resistance to deformation, it can be said to be liquefied. If, on the other hand, sand is dense, it may develop a residual pore water pressure, on completion of a full stress cycle, which is equal to the confining pressure (a peak cyclic pore pressure ratio of 100%) but when the cyclic stress is reapplied on the next stress cycle, or if the sand is subjected to monotonic loading, the soil will tend to dilate, the pore pressure will drop if the sand is undrained, and the soil will ultimately develop enough resistance to withstand the applied stress. However, it will have to undergo some degree of deformation to develop the resistance, and as the cyclic loading continues, the amount of deformation required to produce a stable condition may increase. Ultimately, however, for any cyclic loading condition, there appears to be a cyclic strain level at which the soil will be able to withstand any number of cycles of a given stress without further increase in maximum deformation. This is the type of

behavior termed “cyclic mobility” or “development of a peak cyclic pore pressure ratio of 100% with a limited strain potential” (Seed, 1979, p.205-207).

In a typical cyclic triaxial test on sand, “it is observed that the pore pressure builds up steadily as the cyclic axial stress is applied, and eventually approaches a value equal to the initially applied confining pressure, thereby producing an axial strain of about 5% in double amplitude. Such a state has been referred to as initial liquefaction or simply liquefaction” (Ishihara, 2003, p.218). Double amplitude (DA) axial strain is amplitude of axial strains in one cycle, other words it is sum of largest extension and compression axial strains in one cycle. Double amplitude axial or shear strain is illustrated in Figure 2.6. Single amplitude strain can be defined as half of double amplitude strain. Also, 5% double amplitude strain level is used for definition of cyclic strength of reconstituted sand. Cyclic stress ratio required to cause 5%DA axial strain under certain load cycles is often referred to simply as cyclic strength. Required load cycle for cyclic strength of reconstituted sand was defined differently such as 10, 15 and 20 by Mulilis et al. (1975), Seed & Idriss (1971) and Ishihara (2003), respectively.

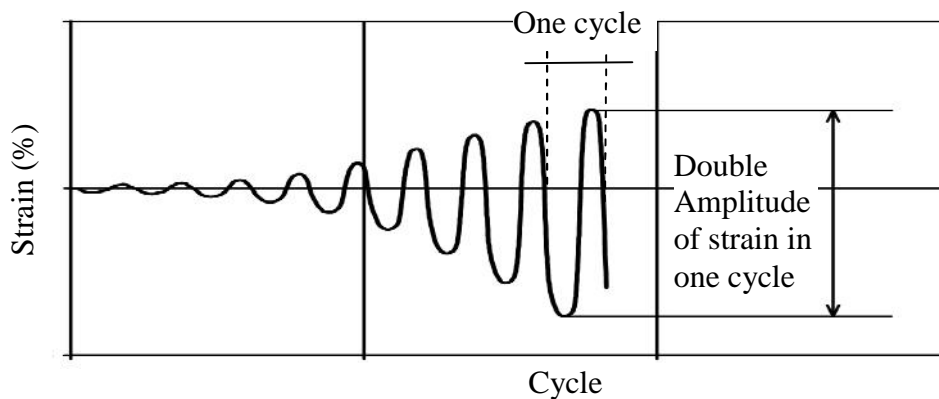


Figure 2.6. Defination of double amplitude strain

2.3 Determination of the Liquefaction Potential

For the selected earthquake and soil conditions, time history of shear stresses induced by the earthquake ground motions at different depths within the soil deposit

are calculated with soil response analyses. Calculated irregular time history of shear stresses is converted to time history of equivalent uniform shear stress. Then converted equivalent uniform shear stress levels are plotted as a function of depth (Figure 2.7). To determine the cyclic shear stresses that cause liquefaction in the same loading cycles of equivalent uniform shear stress (N_{eq}), tests are performed on representative samples for various depths. Shear stress levels obtained by means laboratory tests are plotted as a function of depth as shown in Figure 2.7. After both shear stress levels are plotted as a function of depth, two shear stress levels are compared to determine liquefaction zones.

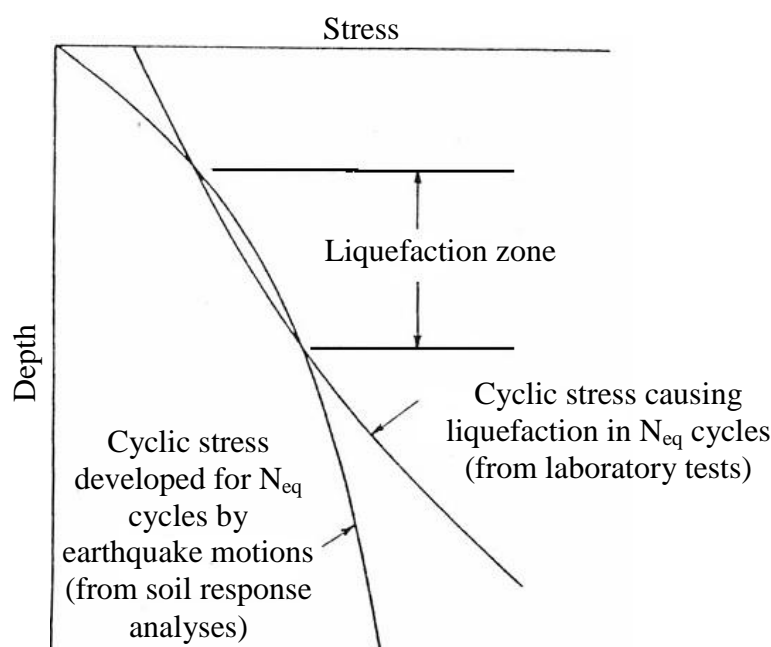


Figure 2.7 Evaluation of liquefaction potential

Investigations and analyses after some major earthquakes (1964 Niigata; 1964 Alaska; 1971 San Fernando) it is recognized that liquefaction cannot be induced at large depths. Although some marginal liquefaction cases at depth of 90 m during 1964 Alaska Earthquake were reported (Seed, 1979), in general, liquefaction can develop within the upper depth of 20 m in saturated sandy soils during earthquakes (Castro, 1975; Castro & Poulos, 1977; Christian & Swiger, 1975; Ishihara & Li, 1972; Peacock & Seed, 1968; Seed, 1979; Seed & Idriss, 1967).

Determination of liquefaction potential has some difficulties and high technical skills with advanced equipments are required. A variety of methods were developed to determine liquefaction potential of saturated layers, such as energy-based criteria, probabilistic analyses and in-situ test – based methods (Arıo lu et al., 2003; Kayen & Mitchell, 1997; Law et al., 1990; Liao et al., 1988; Seed & Idris, 1971; Sönmez & Gökçeo lu, 2005; Youd & Noble, 1997; Youd & Idriss, 1997). Liquefaction resistance criteria based on seismic energy passing through a liquefiable layer and probabilistic analyses of case history data are still under development and not sufficiently formulated for routine engineering practice. They need to be independently tested so that they could be used in general practice (Youd & Idriss, 1997).

For routine liquefaction analysis of sandy soils, the modified Seed-Idriss method, based on in-situ standard penetration tests (SPT) and soil mechanics laboratory test results, is generally preferred because of the presence of extensive database and past experience (Youd & Idriss, 2001). The basis of this method rests on the comparison of the liquefaction resistance ratio of soil (CRR) which is estimated from in-situ SPT test and the cyclic stress ratio (CSR), which is generated by traveling shear waves during an earthquake.

2.3.1 Evaluation of Cyclic Resistance Ratio (CRR)

The cyclic resistance ratio is also known as liquefaction resistance of the soils. The most accurate CRR value of the soils can be determined with tests, which are performed on undisturbed samples. However, it is expensive and very difficult to obtain undisturbed samples from field and to reestablish in situ stress states in the laboratory. In practice, CRR or liquefaction resistance of a soil is not determined with tests on undisturbed samples.

Mainly four field tests have gained common usage for evaluation of CRR or liquefaction resistance, including the cone penetration tests (CPT), the standard penetration test (SPT), the Becker penetration test (BPT) and shear-wave velocity

measurements (V_s). In literature and in practice, SPT and CPT tests are preferred over other methods for the evaluation of the cyclic stress ratio. Although, CPT test provides nearly continuous profile of penetration resistance of the soil layers, on the other hand soil samples cannot be recovered from the soil layers with this in-situ test. SPT provides soil samples and information about penetration resistance of layers.

In the modified Seed-Idriss method which is based on SPT in-situ tests, CRR or liquefaction resistance of soils is estimated using correlations established between SPT blow counts and liquefaction case histories during the past earthquake corresponding to $M=7.5$ earthquake. CRR can be determined through Equation 2.1 or Figure 2.8 as described in the modified Seed-Idriss method (Youd & Idriss, 2001). The term $(N_1)_{60CS}$ corresponds to corrected SPT blow count.

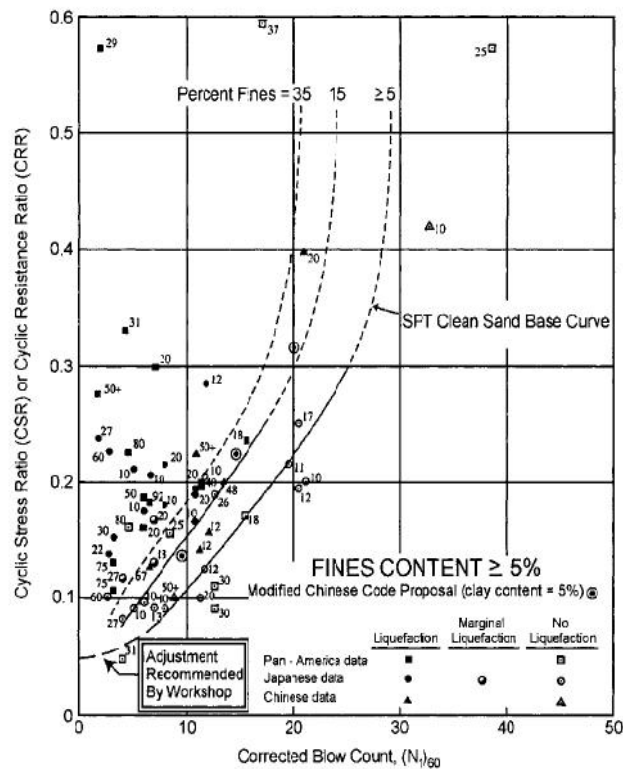


Figure 2.8 CRR- N_{60} curves along with the data from liquefaction case histories (Youd & Idriss; 2001)

$$CRR_{7.5} = \frac{1}{34 - (N_1)_{60CS}} + \frac{(N_1)_{60CS}}{135} + \frac{50}{[10 \cdot (N_1)_{60CS} + 45]^2} - \frac{1}{200} \quad (2.1)$$

Factors such as fine material content, geologic age, static shear stress and overburden effective stress are taken into account along with appropriate correction coefficients in Seed and Idriss method. Such corrections applied in the method are presented below:

Seed et al. (1985), and Youd & Idriss (2001) states that fine material content increases CRR. However, they are not certain whether this augmentation in CRR stems from the increase in CRR along with fine material content or the decrease in SPT value taking place as fine material content increases. The increase in CRR as a function of fine material is accounted for by considering $(N_{60})_{CS}$ in Equation 2.1. $(N_{60})_{CS}$ is calculated through Equation 2.2 to 2.8.

$$(N_1)_{60CS} = r + s(N_1)_{60} \quad (2.2)$$

$$r = 0 \quad \text{for } FC \leq 5\% \quad (2.3)$$

$$r = \exp\left[1.76 - \left(\frac{190}{FC^2}\right)\right] \quad \text{for } 5\% \leq FC \leq 35\% \quad (2.4)$$

$$r = 5.0 \quad \text{for } FC \geq 35\% \quad (2.5)$$

$$s = 1.0 \quad \text{for } FC \leq 5\% \quad (2.6)$$

$$s = \left[0.99 + \left(\frac{FC^{1.5}}{1000}\right)\right] \quad \text{for } 5\% \leq FC \leq 35\% \quad (2.7)$$

$$s = 1.2 \quad \text{for } FC \geq 35\% \quad (2.8)$$

where FC is the fine content in percent and α and β are empirical adjustment factors. Other corrections to SPT blow count are given in Equation 2.9 and 2.10.

$$(N_1)_{60} = N_1 C_E C_B C_R C_S \quad (2.9)$$

$$N_1 = N C_N \quad (2.10)$$

where, N: uncorrected standard penetration resistance in the field; C_N : factor to normalize N to a common reference effective overburden stress; C_E : correction for hammer energy ratio; C_B : correction factor for borehole diameter; C_R : correction

factor for rod length; and C_S : correction for split spoon sampler; σ'_{vo} : effective overburden pressure, and P_a is the atmospheric pressure (Youd & Idriss, 2001). SPT corrected parameters are extensively studied by various researches and SPT corrected coefficients may have some small differences from researcher to researcher (Youd & Idriss, 1997; Liao & Whitman, 1986a; Kayen et al. 1992; Gibbs & Holtz, 1957; Castro, 1995; Skempton, 1986; Robertson & Wride, 1998; Youd & Idriss, 2001).

The correction for overburden stress (C_N) was applied in this study as suggested by Liao & Whitman (1986a). Correction factors for energy ratio, borehole diameter, rod length and sampling method, which were suggested by Skempton (1986) and revised by NCEER-1997 (Youd & Idriss, 1997) were used (Table 2.1).

Table 2.1 Corrections to SPT (Youd & Idriss, 1997)

Factor	Equipment Variable	Term	Correction
Overburden pressure		C_N	$\sqrt{P_a/t'_{vo}} \leq 2.0$
Energy ratio	Donut Hammer	C_E	0.5-1.0
	Safety Hammer		0.7-1.2
	Automatic Hamer		0.8-1.3
Borehole diameter	65-115 mm	C_B	1.00
	150 mm		1.05
	200 mm		1.15
Rod length	< 3.0 m	C_R	0.75
	3-4 m		0.80
	4-6 m		0.85
	6-10 m		0.95
	10-30 m		1.00
	>30 m		<1.00
Sampling method	Standard sampler	C_S	1.0
	Sampler without liner		1.1-1.3

$P_a = 100$ kPa; t'_{vo} : Effective overburden stress

Characterization of in-situ soil properties has been made during in-situ sounding tests or laboratory tests on undisturbed soil samples recovered from in-situ soil deposits. CRR or CSR values of points in Figure 2.8 represent the in-situ conditions derived by means of SPT tests. In routine practice, undisturbed sandy soil samples, which represent the in-situ condition, cannot be recovered from investigated site. In several research programs conducted on sands, soil mechanic tests were performed on both disturbed and reconstituted samples. The test results obtained from disturbed or reconstituted samples must be related to field soil properties, which are derived from SPT in-situ tests.

A widely used parameter related to the classification of reconstituted specimens is the relative density (D_r) (the relative density is also known as density index (I_D)). On the other hand, in-situ test of SPT is characterized by the blow count. Some researchers studied relationships between the SPT blow count and the relative density (Gibbs & Holtz, 1957; Meyerhof, 1957; Skempton, 1986; Ishihara, 1993; Ishihara & Cubrinovski, 1998). Meyerhof, (1957) proposed the relationship in Equation 2.11.

$$D_r = 21 \sqrt{\frac{N}{\sigma'_v + 0.7}} \quad (2.11)$$

Tokimatsu & Seed (1987) used Equation 2.11 proposed by Meyerhof (1957). Relative densities of the laboratory samples were converted to equivalent $(N_1)_{60}$ values by Tokimatsu & Seed (1987) using the relationship given in Figure 2.9. Tokimatsu & Seed (1987) used (N_1) for Japanese data and $(N_1)_{60}$ for US data in Equation 2.11. Curve in Figure 2.9 can be obtained using Equation 2.11. In order to relate the cyclic triaxial test results to $(N_1)_{60}$, which is obtained in the field, the relationship given in the Figure 2.9 was used by Tokimatsu & Seed (1987).

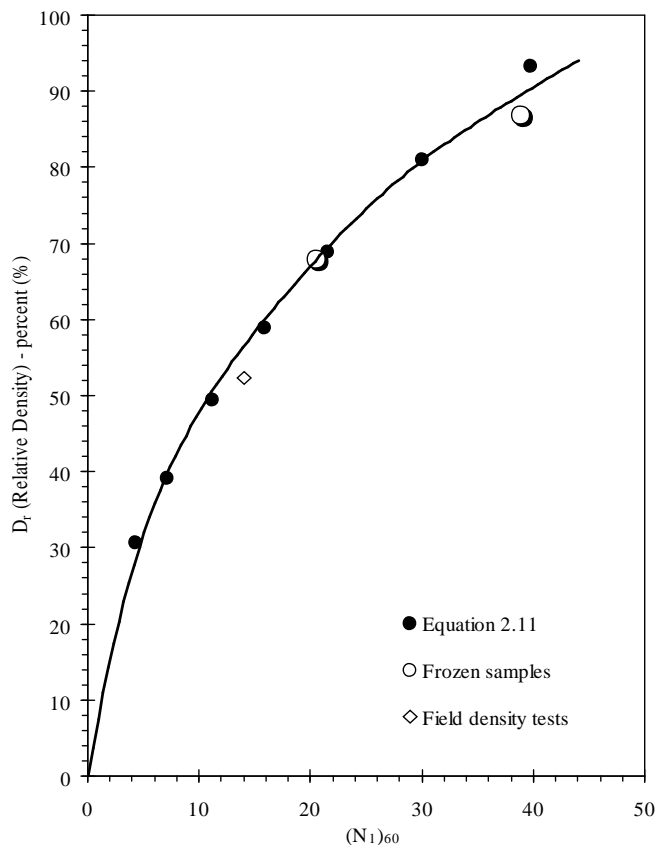


Figure 2.9. Relationship between relative density and $(N_1)_{60}$ (Tokimatsu & Seed, 1987)

When effective overburden pressure (\dagger'_v) is taken into account as 1.0 kg/cm^2 Equation 2.11 can be written as in Equation 2.12 (Meyerhof, 1957).

$$D_r = 16\sqrt{N_1} \quad (2.12)$$

Later from Meyerhof, (1957), as a result of extensive survey over many existing laboratory and in situ test data on the blow count of the SPT, a general form of the correlation was expressed by Skempton (1986) as in Equation 2.13. In the equation a and b are constants which depend mainly on the grain size distributions of soils. The 'a' and 'b' constants which were determined by Skempton (1986) are given in Table 2.2.

$$\frac{N}{D_r^2} = a + b\dagger'_v \quad (2.13)$$

Table 2.2 Skempton's a & b coefficients for various soil properties (Skempton, 1986)

Sand No	Wet or Dry	D ₅₀ (mm)	C _u	Fines (%)	D _r	N ₁	$\frac{N_1}{D_r^2}$	$\frac{N}{D_r^2} = a + b\tau'_v$
(1)	Wet	2.00	5.3	0	0.4 0.6 0.8	7.5 19 37	47 53 58	30 + 22 τ'_v
(2)	Dry and moist	1.50	5.5	0	0.4 0.6 0.8	6.5 14.5 25	40 40 39	18 + 22 τ'_v
(3)	Wet	0.51	2.5	4	0.4 0.6 0.8	7 16 29	44 44 45	21 + 24 τ'_v
(4)	Wet	0.23	1.8	2	0.4 0.6 0.8	5.5 12 21	34 33 33	16 + 17 τ'_v
(5)	Dry	0.30	7	14	0.4 0.6 0.8	4.5 12 23	28 33 36	15 + 18 τ'_v

N₁=NC_N; C_u: Uniformity coefficient; D₅₀: mean grain size of the test samples

Ishihara, (1993) taken into account (τ'_v) as 1.0 kg/cm² and rewritten Equation 2.13 for N₁ instead of N as shown in Equation 2.14. Ishihara (1993) proposed that a+b values must be selected according to mean grain size of the sandy soils.

$$\frac{N_1}{D_r^2} = a + b \quad (2.14)$$

Ishihara & Cubrinovski, (1998) rearranged the relation of Ishihara (1993) which is given in Equation 2.14 using available data in the literature and data that are more recent. Instead of a and b, (e_{max}-e_{min}) was used in the new relation by Ishihara & Cubrinovski, (1998). The proposed relationship between N₁ and D_r is given in Equation 2.15.

$$\frac{N_1}{D_r^2} = \frac{9}{(e_{\max} - e_{\min})^{1.75}} \quad (2.15)$$

2.3.2 Evaluation of Cyclic Stress Ratio (CSR)

During an earthquake, the shear stress was induced at a depth of “z” developed by the upward propagation of horizontal shear waves in the deposits. Assuming the soil column above the depth z behaves as a rigid body, the maximum shear stress for maximum ground surface acceleration (a_{\max}) is simply computed using the Newton’s law of motion ($F=m.a$) at the bottom of a soil element with a thickness of z and unit area of A as illustrated in Figure 2.10. The maximum shear stress ($\tau_{\max-r}$) at the bottom of the rigid soil column due to maximum ground surface acceleration (a_{\max}) can be calculated as Equation 2.16.

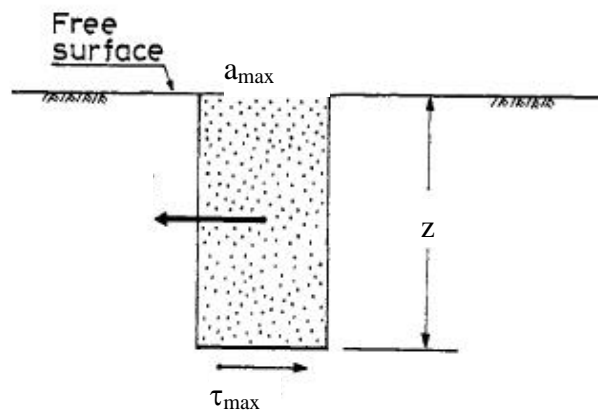


Figure 2.10 Equilibrium of forces near the surface
(Seed & Idriss, 1971; Ishihara, 2003; Das, 1992)

$$\tau_{\max-r} = \frac{\gamma_{vo}}{g} a_{\max} \quad (2.16)$$

where γ is the unit weight of the soil, g is the acceleration of gravity, and σ_{vo} is the vertical overburden stress (Seed & Idriss, 1982).

The Equation 2.16 has been derived for a rigid soil column, the soil column is however not a rigid body and it behaves as a deformable material capable of damping the kinetic energy. So the actual shear stress at depth z which is determined by ground response analysis will be less than the shear stress assuming as the soil as a rigid body. Ratio (r_d) of shear stress calculated for deformable soil body to shear

stress calculated for rigid soil body for different soil profiles at different depth is given Figure 2.11 (Seed & Idriss, 1971; Youd & Idriss, 2001). Derived shear stress for a rigid soil column ($\tau_{\max-r}$) must be corrected with r_d to be able to calculate the shear stress for a deformable soil body ($\tau_{\max-d}$). When the r_d correction is applied, the Equation 2.17 is obtained for the maximum shear stress in a deformable soil column. For routine practice and noncritical projects, using of the average curve of r_d is recommended (Liao & Whitman, 1986b; Seed & Idriss, 1971; Youd & Idriss, 2001). The average value of the r_d can be calculated using Equation 2.18 (Liao & Whitman, 1986b).

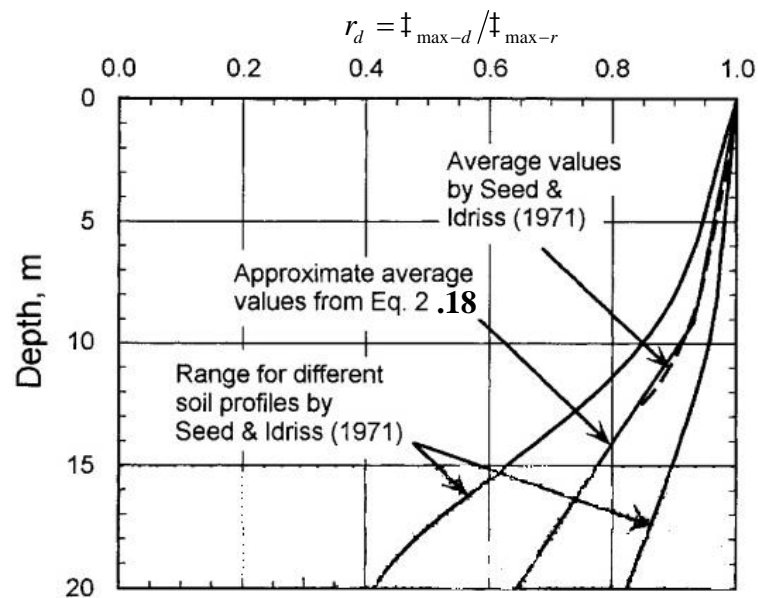


Figure 2.11 Stress reduction coefficient (r_d) versus depth curves developed by Seed & Idriss, 1971 (Seed & Idriss, 1971; Youd & Idriss, 2001).

$$\ddagger_{\max-d} = \left[\frac{\ddagger_{vo}}{g} a_{\max} \right] r_d \quad (2.17)$$

$$\begin{aligned} r_d &= 1.0 - 0.00765z && \text{for } z \leq 9.15\text{m} \\ r_d &= 1.174 - 0.0267z && \text{for } 9.15\text{m} < z \leq 23\text{m} \end{aligned} \quad (2.18)$$

Actual earthquake motions are in irregular characteristics, so time history of the shear stress for a point in the soil will have an irregular form as shown in Figure 2.12. However, the cyclic shear stress amplitudes of laboratory test data, which are

used to estimate liquefaction resistance, are uniform. Therefore, earthquake irregular time history of shear stress must be converted to uniform stress cycles to compare earthquake-induced shear stress with laboratory-determined cyclic resistance. For this purpose, Seed & Idriss (1971) used 65% of the peak cyclic shear stress amplitude ($0.65\tau_{\max}$) induced by the earthquake as average equivalent uniform shear stress ($\tau_{\text{av}}=0.65\tau_{\max}$ where τ_{av} is the average equivalent uniform shear stress). Some researchers such as Halder & Tang, (1981) used different stress level from Seed & Idriss (1971) to develop similar relationships. However, the commonly used level in the literature is 65% (Kramer, 1996). Thus, the average cyclic shear stress induced by an earthquake at any point in a soil deposit can be expressed with Equation 2.19.

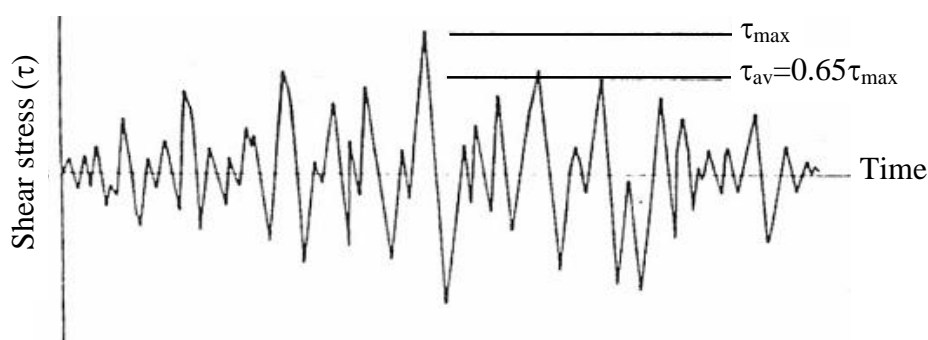


Figure 2.12 Time history of shear stress during an earthquake (Seed & Idriss, 1971)

$$\tau_{\text{av}} = 0.65 \left[\frac{\tau_{\text{vo}}}{g} a_{\text{max}} \right] r_d \quad (2.19)$$

Seed & Idriss (1971) used τ_{av} to determine number of equivalent uniform stress cycles (N_{eq}) for the shear stress time histories recorded during strong ground motions. Equivalent number of uniform stress cycles (N_{eq}) is the number of cycles at certain uniform stress (such as $0.65\tau_{\max}$ according to Seed & Idriss, 1971) that will produce an increase in pore pressure equivalent to the increase in pore pressure due to an irregular time history record. Appropriate number of N_{eq} depends on the duration of ground shaking, and thus on the magnitude of the earthquake. Figure 2.13 shows relation between earthquake magnitude and equivalent number of uniform stress cycles (N_{eq}) for $0.65\tau_{\max}$ according to Seed et al. (1975) and Seed (1979).

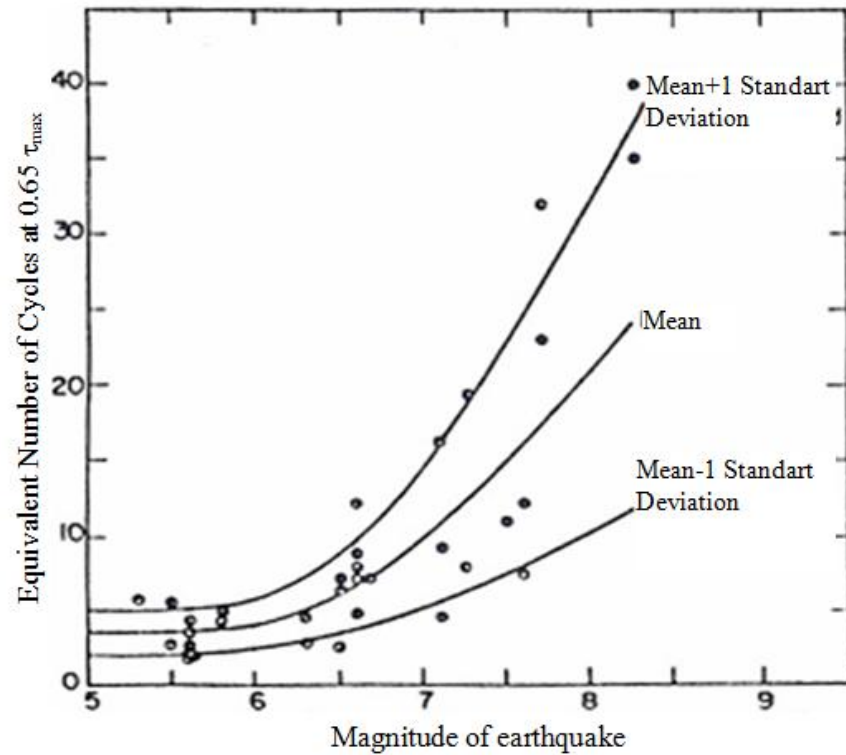


Figure 2.13 Relation between equivalent number of cycles at $0.65 \cdot \tau_{\max}$ and earthquake magnitude (Seed, 1979)

Normalized shear stress due to cyclic loading by the initial effective overburden pressure is called as cyclic stress ratio (CSR). CSR for average equivalent uniform shear stress can be described as in Equation 2.20 (Seed & Idriss, 1971; Youd & Idriss, 2001):

$$\text{CSR} = \frac{\ddagger_{av}}{\ddagger'_{vo}} = \frac{0.65 \ddagger_{\max}}{\ddagger'_{vo}} = 0.65 \frac{a_{\max}}{g} \frac{\ddagger_{vo}}{\ddagger'_{vo}} r_d \quad (2.20)$$

On the other hand, the CSR ($\ddagger_{av}/\ddagger'_{av}$) was calculated differently for different tests. For the cyclic simple shear test, the CSR is taken as the ratio of the cyclic shear stress to the initial vertical effective stress ($\text{CSR} = \tau_{\text{cyc}}/\sigma'_{vo}$) (Kramer, 1996). For the cyclic triaxial test where the samples are isotropically consolidated, CSR is taken as the ratio of the cyclic shear stress (half of the maximum cyclic axial deviator stress) to the initial effective consolidation pressure ($\text{CSR} = \ddagger_{dc}/2\ddagger'_o$) (Ishihara, 2003; Mulilis et al., 1977).

2.3.3 Determination of Safety Factors (F_S) Against Liquefaction

Cyclic stress ratio (CSR) calculated in soil response analyses or estimated with any simplified method for an earthquake and soil condition indicates the cyclic shear stress, which is expected to appear in the soil deposit during an earthquake. Cyclic resistance ratio (CRR) determined by means of laboratory testing program or estimated by means of correlations of in-situ tests indicates the cyclic shear stress level which is the threshold value for the on set of liquefaction of the soil. If the CSR is higher than CRR, it is expected that liquefaction phenomenon will occur for the considered depth, soil conditions and the earthquake magnitude, in the other case it is expected that liquefaction phenomenon will not take place. In the other words, when the ratio of CRR to CSR is equal or lower than 1.0, liquefaction potential exists for the soil deposits at certain depths. The ratio of CRR to CSR (Equation 2.21) is called as the safety factor ($F_S = \text{CRR}/\text{CSR}$) against liquefaction. Curves in Figure 2.8 were drawn for the 7.5 magnitude of earthquake by Seed & et al. (1985). Therefore, determined F_S using Figure 2.8 will represent the safety factor against liquefaction potential for an earthquake of magnitude 7.5.

$$F_s = \frac{\text{CRR}_{7.5}}{\text{CSR}} \quad (2.21)$$

If CRR is estimated with the above mentioned simplified Seed et al. (1985) method (using Equation 2.1 or Figure 2.8), F_S must be corrected for earthquake magnitude. Because of the limited amount of field liquefaction data available during establishment of the Seed et al. (1985) method, data of the earthquakes (Figure 2.13) which have magnitudes other than 7.5 were used by Seed & Idriss (1982). Therefore, Seed & Idriss (1982) developed magnitude-scaling factor (MSF) to be able to use various earthquake magnitudes and laboratory test results. Seed & Idriss (1982) firstly proposed Figure 2.14 as a representative curve, which shows the number of loading cycles required to generate liquefaction for a certain CSR. Representative numbers of stress cycles (equivalent number of uniform stress cycles) for a 7.5 magnitude earthquake was suggested as 15 by Seed & Idriss (1982). Afterwards Seed

& Idriss (1982) along with some investigators studied the equivalent number of uniform stress cycles for soil liquefaction analysis (Arango, 1996; Liu et al., 2001). Liu et al. (2001) recommended that it must be considered together with site conditions, site to earthquake source distance and magnitude of the earthquake while determining the equivalent number of uniform stress cycles for soil liquefaction analysis (Liu et al., 2001). Liu et al. (2001) proposed Figure 2.15 for the equivalent number of uniform stress cycles.

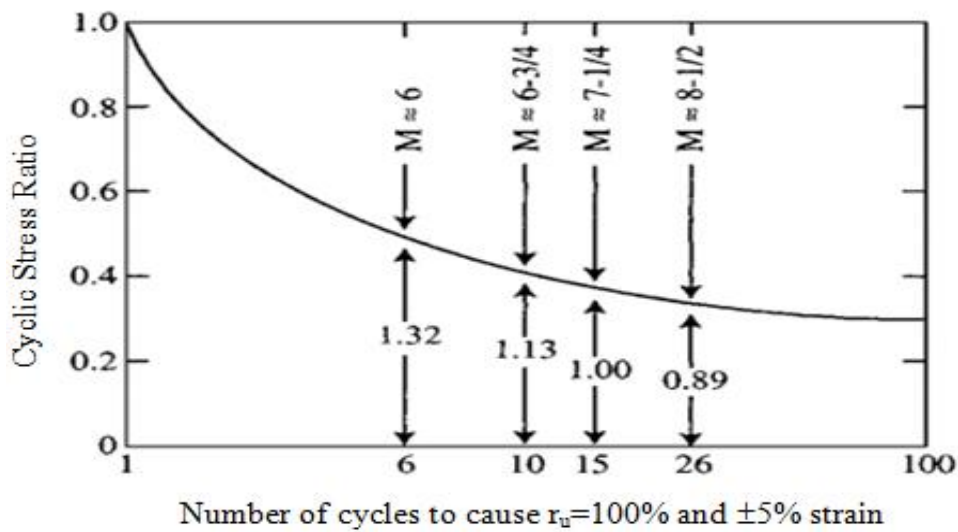


Figure 2.14 Relationship between number of cycles to cause liquefaction and CSR (Reproduced by Youd & Idriss, 2001)

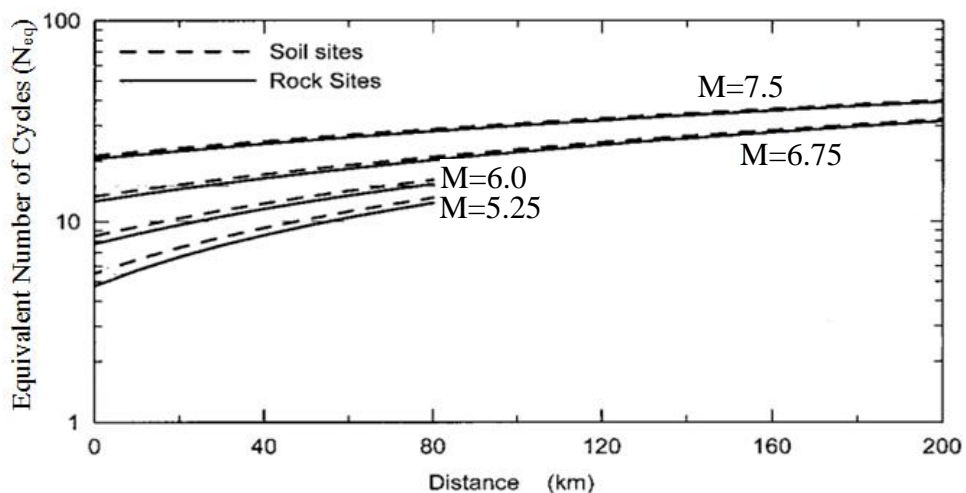


Figure 2.15 Equivalent number of cycles (N_{eq}) with earthquake distance and magnitude for deep soil and shallow stiff soil/rock sites (Liu et al., 2001)

$CRR_{7.5}$ which is expressed with Equation 2.1 indicates boundary of the cyclic stress ratio for the soil can resist without liquefaction for a $M=7.5$ earthquake. In other words, soil would not liquefy until end of the equivalent number of uniform stress cycles (N_{eq}), when it is subjected to uniform cyclic shear stress, which is lower than $CRR_{7.5}$. Cyclic resistance ratio $M=7.5$ can be converted to other magnitudes using magnitude scaling factor (MSF) such as given in Figure 2.14 (Seed & Idriss, 1982). Afterwards, Idriss suggested Equation 2.22 for MSF (Youd & Idriss, 2001). Different magnitude scaling factors given in Figure 2.16 were proposed by some researchers (Ambraseys, 1988; Andrus & Stoke, 1997; Arango, 1996; Idriss, 1999; Seed & Idriss, 1982; Youd & Noble, 1997; Youd & Idriss, 1997).

$$MSF = \frac{10^{2.24}}{M_w^{2.56}} \quad (M_w \text{ is the moment magnitude of earthquake}) \quad (2.22)$$

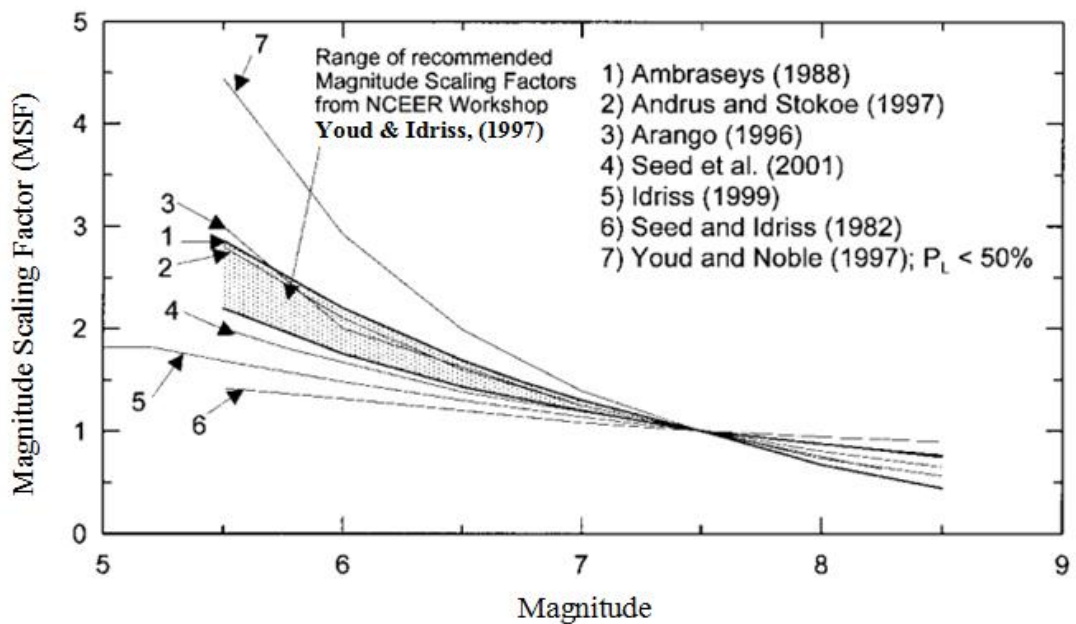


Figure 2.16 Magnitude scaling factors proposed by different researchers

When the magnitude-scaling factor is applied on Equation 2.21, the factor of safety against liquefaction:

$$FS = \frac{CRR_{7.5}}{CSR} MSF \quad (2.23)$$

2.4 Factors Effective on Liquefaction

Certain conditions shall be fulfilled for the liquefaction of a soil layer. The foremost condition among these is the saturation of a cohesionless soil, which is not adequate for occurrence of liquefaction.

2.4.1 History in Past Earthquakes

Unless ground water level and soil conditions alter, it was confirmed by observations in the past earthquakes that previously liquefied soils are re-liquefiable afterwards (Youd, 1984; Youd, 1991). In addition to that, it is known from the past cases that, liquefaction can take place within a certain distance from earthquake epicenter, not only occur on the epicenter of earthquakes. The distances, which may cause liquefaction, changes according to magnitude of the earthquakes are shown in Figure 2.17 (Ambraseys, 1988).

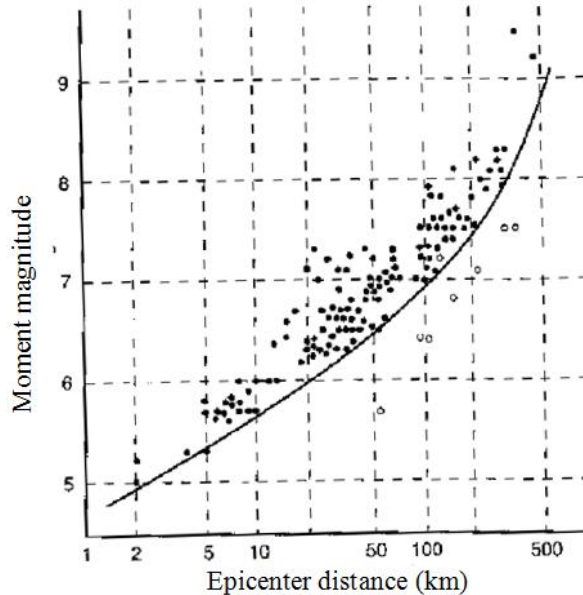


Figure 2.17 Relationship between earthquake magnitude and epicentral distance of earthquake to liquefaction sites for shallow earthquake (Ambraseys 1988)

2.4.2 Geological Structure

Soil layers geologically susceptible to liquefaction generally consist of saturated Holocene alluviums. The liquefaction potential of a loosely deposited uniform granular soil is higher than other soils. The liquefaction resistance of granular soils, where cementation formed among the grains, is also augmented. If saturated man made fills, constitute fine granular materials and they are not compacted properly, they will carry high liquefaction potential as well. Groundwater level is in fact a governing factor on liquefaction. The deeper the water level is, the higher the liquefaction resistance of a site will be. A decrease in the degree of saturation will lead to an increase in the liquefaction resistance (Figure 2.18) (Xia & Hu, 1991).

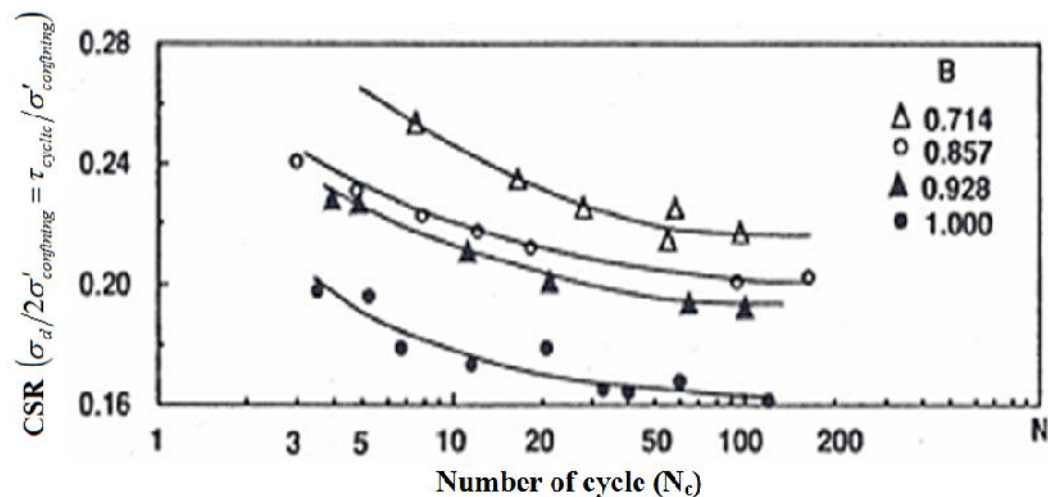


Figure 2.18 Effect of degree of saturation on initial liquefaction (Xia & Hu, 1991)
B: Skempton's pore pressure parameter

2.4.3 Grain Size Distribution and Index Properties

Grain size distribution, grain shape and size of a coarse-grained soil are influential on permeability. The pore water pressure dissipates slower during an earthquake for low permeability soils. Undrained loading conditions relatively come into existence easier in such soils. Besides, soils, which can be densified easily, have higher liquefaction potential.

Rounded sand will be denser than the angular sand grains, when they are compacted under same energy level (Cho et al., 2006). Similarly, it is possible that angular sand grains generate more porous structure in the sedimentation process. High porosity causes loose and high permeable deposition. High porosity could be disadvantageous in liquefaction risk considering in terms of density, otherwise porosity could be advantageous in terms of permeability. Consequently, in the literature it is considered that, rounded soils are usually more susceptible to liquefaction than angular-grained soil (Kramer, 1996). According to observed sand liquefactions in the literature, uniform sands are liquefied easier compared with well-graded sands and fine sands are more easily liquefiable than coarse sands (Tsuchida, 1970).

Grain size affects shear strength as well as permeability. Internal friction angle of fine sands is lower than that of coarse sands. This comparison is also valid for the gravel and coarse sand pair. As internal friction angle reduces, the resistance of soil to cyclic stresses decreases as well. Tsuchida (1970) published grain size distribution ranges of liquefiable soils (Figure 2.19) as a result of a survey conducted on soil profiles, whose liquefaction backgrounds are known. As expected, sands and silty sands form the soil group with the lowest liquefaction resistance. Even though soils in the gravel group are expected to liquefy harder because of high permeability and shear strength and this case was mostly verified via field observations, it is known in rare cases that loose gravels are liquefied during large magnitude earthquakes (Andrus et al., 1991). Although geological age and relative density are dominating factors for liquefaction potential of gravels, fine material content (-No.200%) and boundary conditions that could restrict excess pore water drainage (for instance impervious layers bounding a gravel layer) are also effective. It is known that silts with plasticity (I_p) being less than 10 may liquefy like sands (Ishihara, 1985; Walker & Steward, 1989). As plasticity of fine grains increases, cohesion among grains restricts grain movement and limits the development of excess pore water pressure.

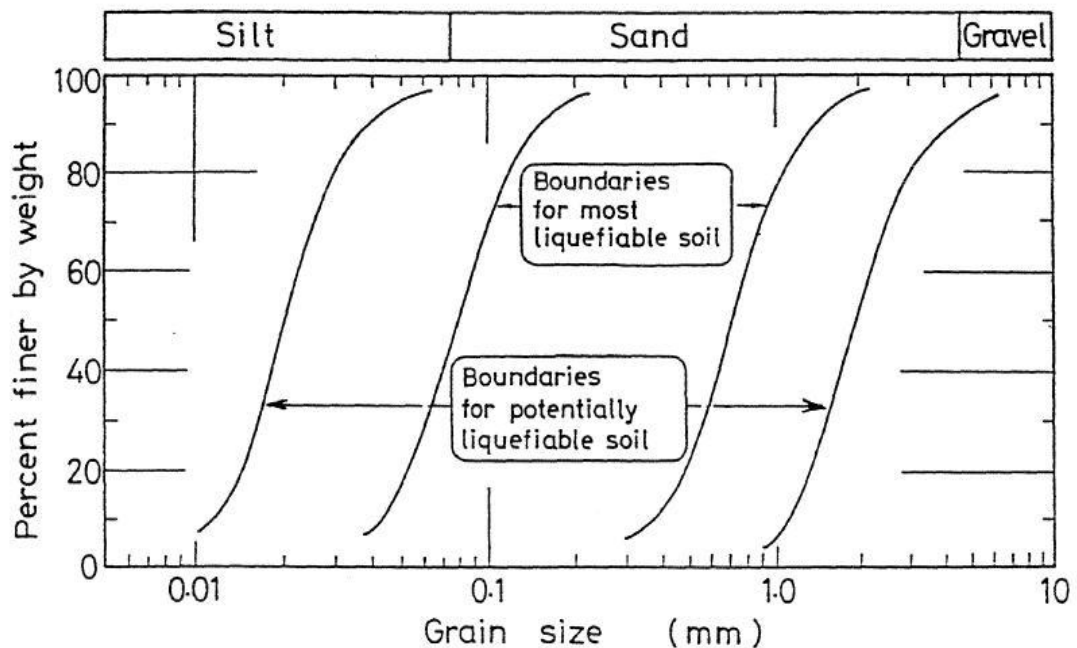


Figure 2.19 Variation grain size distribution of liquefiable soils (Tsuchida, 1970)

The loss of stability and strength experienced in cohesive soils in the early earthquakes is reported by some researchers as liquefaction. A great deal of such soils did not turn into viscous liquid under earthquake loading as sands. But in particular, large deformation of sensitive clays is possible losing majority of their strength and stiffness owing to the development of excess pore water pressure. It should be stated that large-scale failure of slopes consisting of cohesive soils in Alaska might be attributed to the liquefaction of sand and silt pockets present in the slopes. This was formerly defined as liquefaction of sensitive clays. Although clays did experience cyclic softening (also called as cyclic stress failure) during the earthquake, sand and silt pockets liquefied prior to the failure of clays. In order to distinguish cohesive soils that do not undergo liquefaction and those that exhibit stress-strain behavior similar to those of liquefied soils a criterion was proposed by Youd & Gilstrap (1991);

“The ratio of grains smaller than 0.005 mm in soil should be less than 15%.

The liquid limit value pertaining to soil should be $w_{LL} < 35$.

Water content of soil should be higher than 90% of liquid limit ($w_n > 0.9w_{LL}$). In other words, soil has yet to complete its consolidation and is close to the liquid limit state or should be in a liquid consistency. Even such soils have cohesion, it is known that they demonstrate sand behavior in terms of stress-strain”.

2.4.4 Relative Density and Stress State

Even though it is generally said that loose and medium dense sands are susceptible to liquefaction and dense sands the not liquefiable, consolidation pressure and density both play together a determinative role on the liquefaction potential of sandy soil. Regardless the state of density of sand samples subjected to drained triaxial test under a specific confining stress, Casagrande (1940) put forward that they will reach a critical void ratio in large deformations (Figure 2.20). The critical void ratio (CVR) line of a soil sample specified under diverse values of confining stress is representatively shown in Figure 2.21. If soil samples with an initial void ratio-effective confining stress ($e_o-\sigma_o$) point remain above the CVR line, they will tend to get to the critical void ratio by trying to lessen their volume in triaxial compression test. Put it differently, this soil will tend to liquefy in undrained loading conditions. The soil below the CVR line expands under compression loading and acts towards strengthening in the course of undrained loading.

The state in which the soil flows continuously under constant effective confining pressure and constant shear stress at constant volume and constant velocity was defined as steady state of deformation (SSD) (Castro & Poulos 1977). This deformation situation exhibiting a difference under compression and extension loading can be represented by an SSD line in the plane of void ratio-effective confining stress. In general, the SSD line is established slightly below the CVR line. If static shear stresses (τ_s) are higher than shear strength (τ_{ss}) of soils while void ratios and effective confining stress condition above the SSD line, flow liquefaction is expected to occur (Figure 2.22).

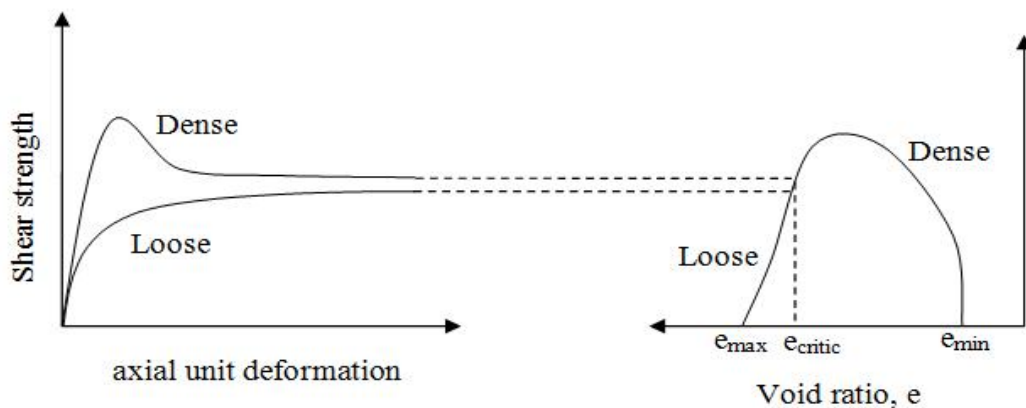


Figure 2.20 The concept of critical void ratio

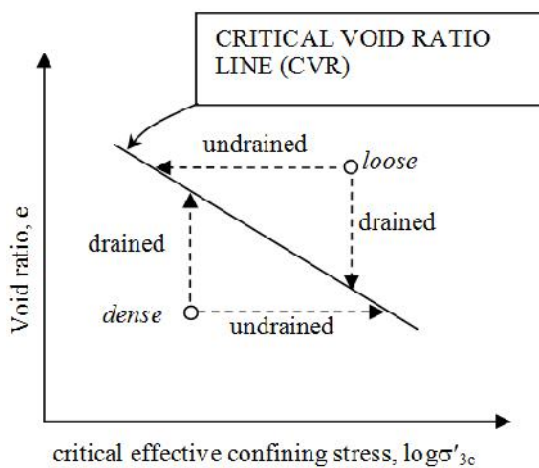


Figure 2.21 Critical void ratio line (CVR)

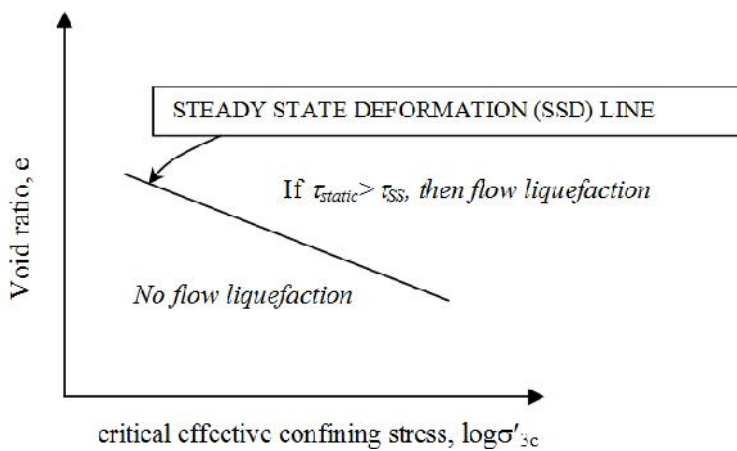


Figure 2.22 Steady State Deformation (SSD) line

2.4.5 Loading Conditions

Liquefaction may take place under conditions of monotonic, immediate loading (shock wave producing burst) and dynamic loading. Liquefaction cases developed as a result of monotonic loading were mostly observed in embankments and natural slopes in the form of flow (Kramer, 1988; Kramer 1996; Ishihara, 2003; Holtz et al., 2011). Dynamic loading can stem from traffic, piling, waves and earthquakes. Earthquake loading stands out among these. Magnitude of an earthquake is characterized by some parameters such as intensity and duration of an earthquake. Magnitude and maximum acceleration of an earthquake are effective on the liquefaction behavior. When liquefaction incidents occurred in the past earthquakes are examined, one can notice that liquefaction was not observed in cases of surface acceleration being $a_{\max} < 0.1g$ and magnitude being $M < 5.0$ (National Research Council of United State, 1985).

2.4.6 Vertical Effective Stress and Over Consolidation Ratio

Due to the fact that shear strength increases with effective stress, the liquefaction potential will reduce accordingly. Cases where liquefaction analyses were made to develop the aforementioned methods are limited to soil layers up to 17 meters from the surface (Youd & Idriss, 2001). In this respect, liquefaction analyses may be performed down to 20 m depth in terms of engineering practice. When curves given in Figure 2.23 examined, even though based on limited number of data, it is seen that as the depth of the liquefiable soil layer from the surface increases, risk of possible deformations it will constitute on the soil surface decreases. Cyclic stress that would generate liquefaction is expected to increase with pre-loading rate and geostatic lateral earth pressure (Ishihara, 1985).

2.4.7 Earthquake Background

If a soil profile is subjected to some earthquakes which cause liquefaction in the past and it is exposed to smaller magnitude earthquakes than past earthquakes, it is

stated that the soil profile does not generate liquefaction due to compacted and hardened by the past earthquakes (Singh, et al. 1980). Although densification and hardening that take place after liquefaction producing earthquakes, loose weak zones are also formed in the soil profiles (National Research Council of United State, 1985). Post earthquake field investigations shown that liquefaction may recur in the same soil profiles when soil and groundwater conditions have remained unchanged (Kramer, 1996; Youd, 1984).

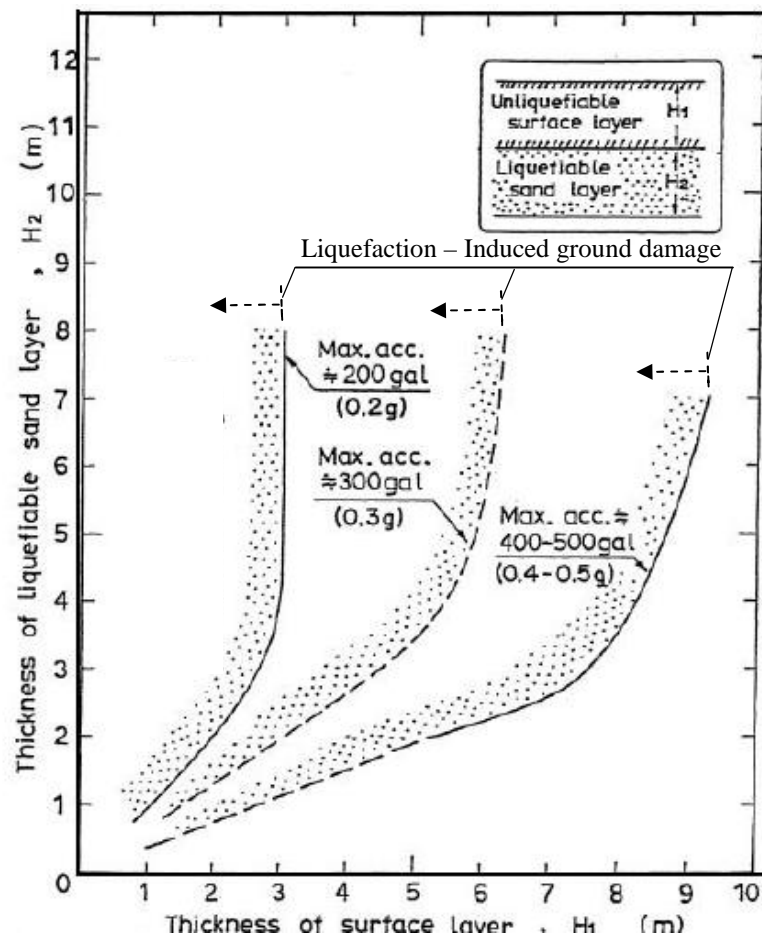


Figure 2.23 Identification of possible deformation on the surface based on H_1 , H_2 and a_{max} parameters (H_1 : liquefiable sand layer thickness, H_2 : non-liquefied soil layer situating above liquefiable sand layer and extending towards the surface, a_{max} : maximum surface acceleration (Ishihara, 1985))

2.4.8 Fine Material Content

In the Seed & Idriss (1982) method, it was stated that liquefaction resistance increases with increasing fine material content and curves demonstrating the correlation between the adjusted SPT resistance (N_{60}) and the liquefaction resistance ratio (CRR) were constructed as a function of fine material content (Figure 2.8). However, whether liquefaction resistance itself increases as a function of fine material content or SPT resistance reduces due to the increase in fine material content has not been clarified, yet. As it is known, SPT is a dynamic field experiment. The increase in fine material content and/or the rise of plasticity of fine materials affect the development of excess pore water pressure and eventually influence SPT resistance. It is known that granular soils containing fine grains (silty sands, clayey sands) were liquefied in previous earthquakes (Seed & Harder, 1990).

Findings compatible with as well as contradictory to curves suggested in Seed et al. (1985) method were obtained in experimental studies. For instance, Troncoso (1990) put forwards that the liquefaction resistance of fine material (<0.075 mm) added sands decreases when tested at the same void ratio. Seed et al. (1985) denoted that fine material increases liquefaction resistance when sands with fines and clean sands at equivalent SPT resistance are compared. In general, it can be said that the liquefaction resistance of sands with low plasticity ($I_p < 10$) fine material at low fines content is lower than clean sand liquefaction resistance. On the other hand, cohesive fine material generally causes considerable increase in liquefaction resistance of sands (Ishihara, 2003; Prakash et al., 1998). Many researchers confirmed that increase of the silt ratio causes a reduction in liquefaction resistance firstly, than beyond a certain value of silt content, the liquefaction resistance increases with silt ratio at the same global void ratio (Zlatovic & Ishihara, 1997; Yamamuro et al., 1999; Thevenayagam, 2007a; Thevenayagam, 2007b). An example to this behavior is presented in Figure 2.24.

As seen in Figure 2.24, after silt ratio (M) exceeds 20%, cyclic stress resistance of the soil increases. The concept of inter-granular void ratio was developed and

proposed to address the effect of silt ratio on sand behavior in a standard framework (Thevanayagam, 2007a; Thevanayagam, 2007b). The recommended equivalent void ratio parameters and the liquefaction resistance of silty sands are attempted to be described with void ratios of fine and coarse materials. In a study performed on silts in different sizes, it is observed that size of the silt grain have significant effects on the liquefaction resistance of the sand (Monkul & Yamamuro, 2011).

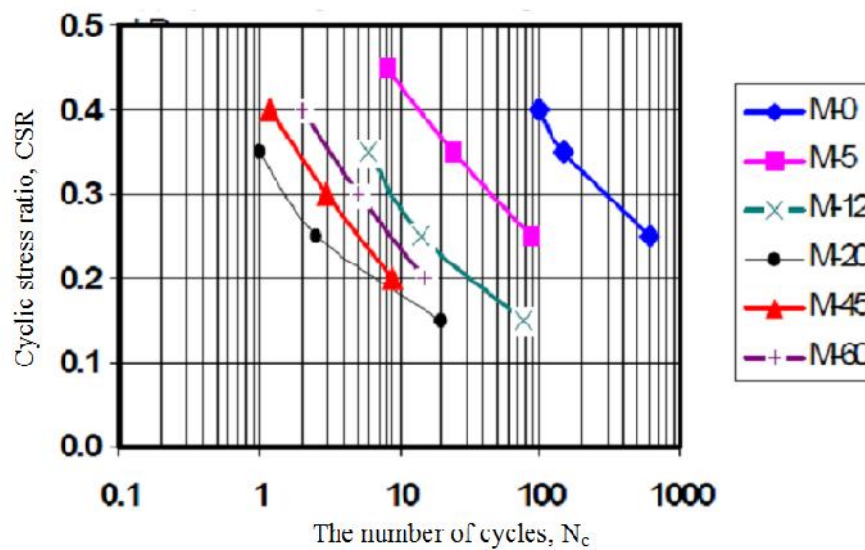


Figure 2.24 Influence of non-plastic fine material content on liquefaction resistance (Thevanayagam, 2007a)

2.4.9 The Effect of Grain Shape

Researches on the effect of grain shape on the liquefaction resistance of sandy soils mostly concentrate on sand grains. As grain shape becomes irregular (angular, sub-angular), voids among grains increase and $e_{\max} - e_{\min}$ values rise. While the stiffness of angular grained sands declines, its compressibility and internal friction increases (Cho et al., 2006).

Harris et al. (1984a), Harris et al. (1984b), Hight et al. (1998), Lee et al. (2007), Georgiannou (2006), Bokhtair et al. (1999) studied behavior of the sand with platy grains. Their study showed that the platy grains cause a decrease in strength parameters and cause an increase in compressibility of sand. Harris et al. (1984a)

studied quartz sand with platy mica grains. In their experimental study, samples were isotropically consolidated followed by drained triaxial compression tests. They also conducted California Bearing Ratio (CBR) and compaction tests on the sand mica mixtures. They proposed new parameters and relations to define behavior of such soils. One of the parameters is defined as F_m : frequency of mica grains (mica amount in every 100 soil grains). The other parameter is MFA: relative mica surface area in unit volume. The variation of w (internal friction angle), c (cohesion), CBR (California bearing ratio), q_{ult} (ultimate bearing capacity) and E_t (tangent deformation modulus) with the mica amount were experimentally explored (Figure 2.25 and Figure 2.26). It was demonstrated that engineering properties are in a nonlinear correlation with mica content (in terms of weight). On the other hand, same parameters exhibit a linear relationship with F_m (Figure 2.27 and Figure 2.28). It was asserted that engineering parameters were associated with the contact of mica-quartz grains and relative mica surface area (MFA) increases linearly with the increase of mica content. Therefore, a linear relationship can be established between engineering properties and the mica content. It was ascertained that a swift and sharp decline arises in strength parameters in values up to 10% by weight while compressibility increases. As a result of experiments, the relative effect of mica content on sand parameters is most pronounced at lower (<10%) weight percentages and tapers off about 10% to 15%. In such cases, it was inferred that platy grains like mica reduce strength parameters of the soil even in small amounts.

Georgiannou (2006) studied the effect of fine materials with distinct shape and sizes within sand on undrained behavior by means of triaxial tests on samples artificially formed and consolidated in non-isotropic conditions. In the test program, two sub-angular quartz sands were used. Maximum and minimum void ratios of the sands were $e_{max}=0.870 - e_{min}=0.526$ and $e_{max}=0.885 - e_{min}=0.537$. Distribution of sand sizes varied medium to fine. One of the additive fine materials used in test program is platy mica grains in silt size. Air pluviation and water sedimentation method was used to obtain homogenous mixtures and provide horizontally orientation of platy grains during preparation of samples. According to study, platy grains reduced stability of the granular structure in both medium and fine sands.

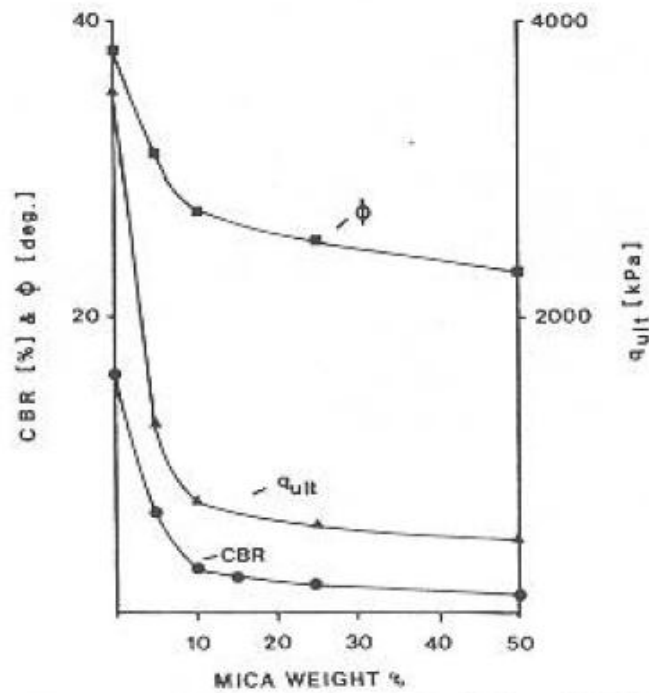


Figure 2.25 Shear strength (ϕ), bearing capacity (q_{ult}), CBR of mica quartz sand mixtures as a function of mica weight percentage (Harris et al., 1984a)

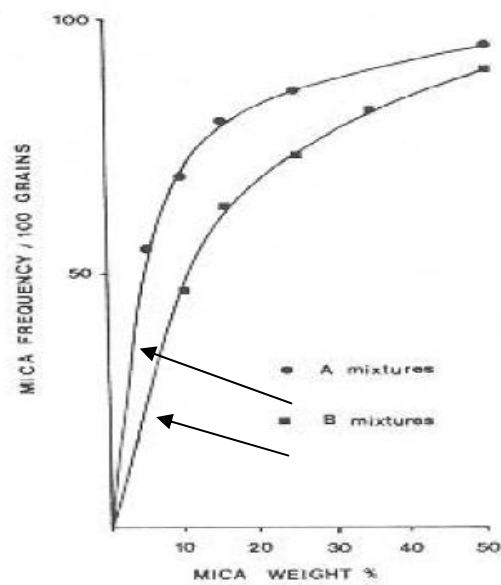


Figure 2.26 Mica weight percentage versus mica frequency per 100 grains for muskovite-quartz (A) and biotite-quartz (B) mixtures (Harris et al., 1984a)

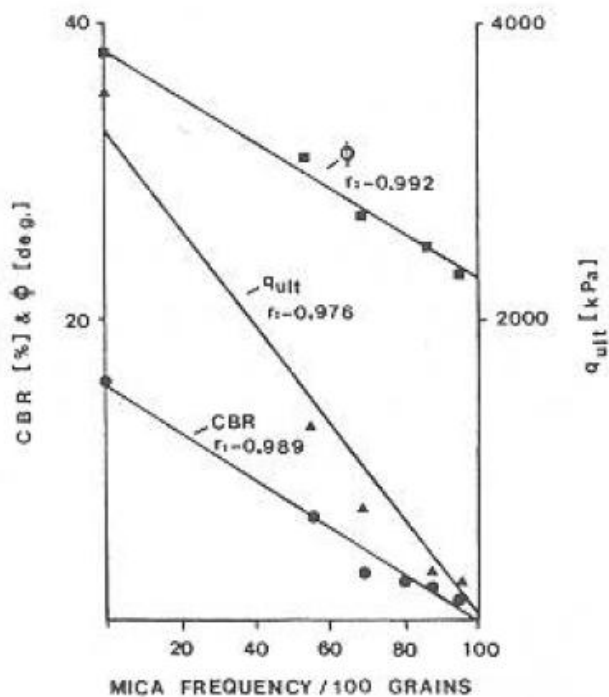


Figure 2.27 Shear strength (ϕ), bearing capacity (q_{ult}), CBR of mica-quartz sand mixtures vs. mica frequency per 100 grains (Harris et al., 1984a)

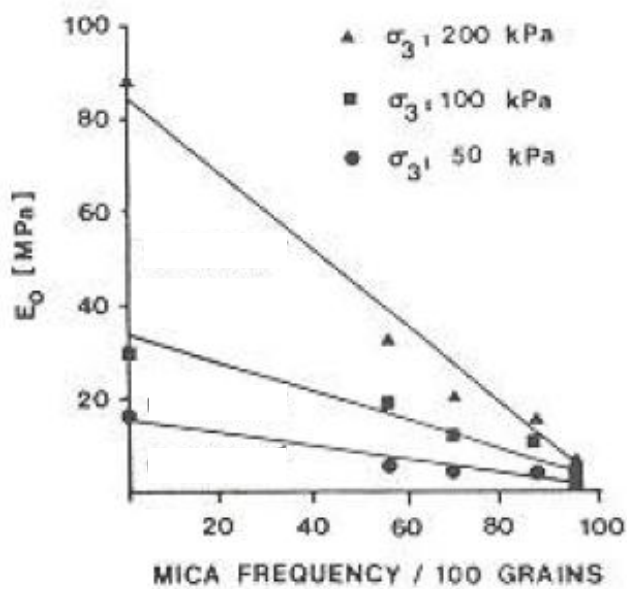


Figure 2.28 Initial tangent axial compression modulus (E_0) of mica-quartz mixtures, at different confining pressures (σ_3), vs. mica frequency per 100 grains of medium sand mixtures (Harris et al., 1984a)

Lee et al. (2007) and Santamarina & Cho (2004) explain mica effect on the sand behavior with bridging concept. In this concept, when size of the mica grains are equal to or larger than size of the sand grains ($D_{50\text{-mica}}/D_{50\text{-sand}} \geq 1.0$), mica grains create bridges among sand grains, and increase the global void ratio. When the global void ratio increases, the strength of sand decreases while compressibility of the sand increases. According to the Lee et al. (2007), bridging properties of mica grains are affected by size and orientation angle of mica grains. The bridging property of mica flakes decreases as orientation angle increases. The most effective orientation angle for bridging is 0° , and mica flakes have the least bridging affect at 90° orientation angle (Figure 2.29). On the other hand, bridging property of the mica flakes increases with increase of the size ratio of mica to sand grains (Figure 2.30). Lee et al., (2007) reached to the conclusion at end of the experimental study that the mica flakes cause an increase in global void ratio via bridging effect. When the global void ratio of the sand increases, compressibility of the sand increases and internal friction angle decreases, as shown in Figure 2.31 through Figure 2.33. Consequently, stiffness and strength of the sand decrease with increasing mica content.

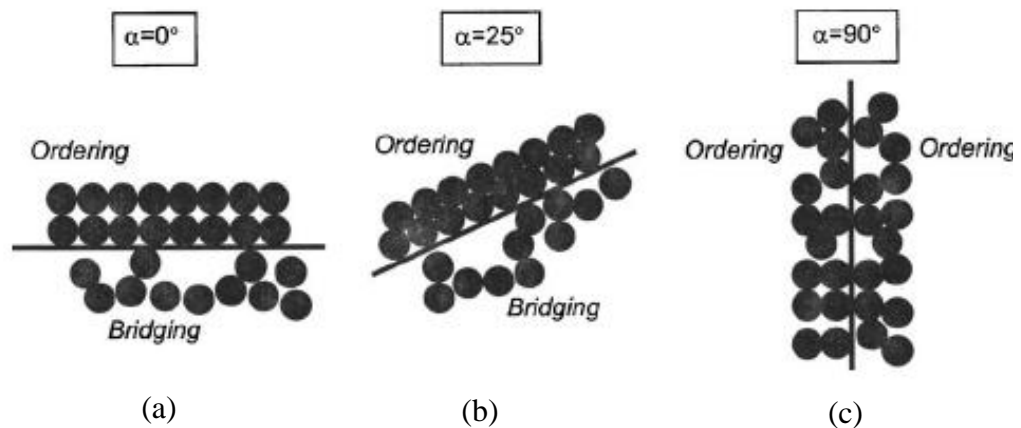


Figure 2.29. Possible mica-sand ordering patterns depending on orientation angle (Lee, et al. 2007)

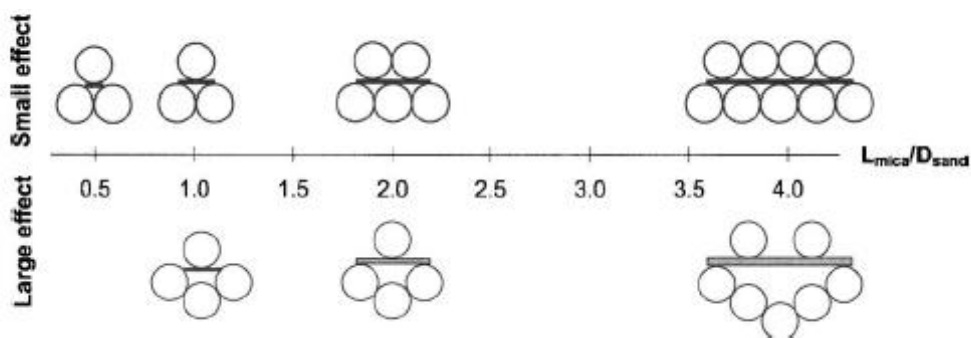


Figure 2.30. Bridging and ordering effects of mica plates (Lee, et al. 2007)

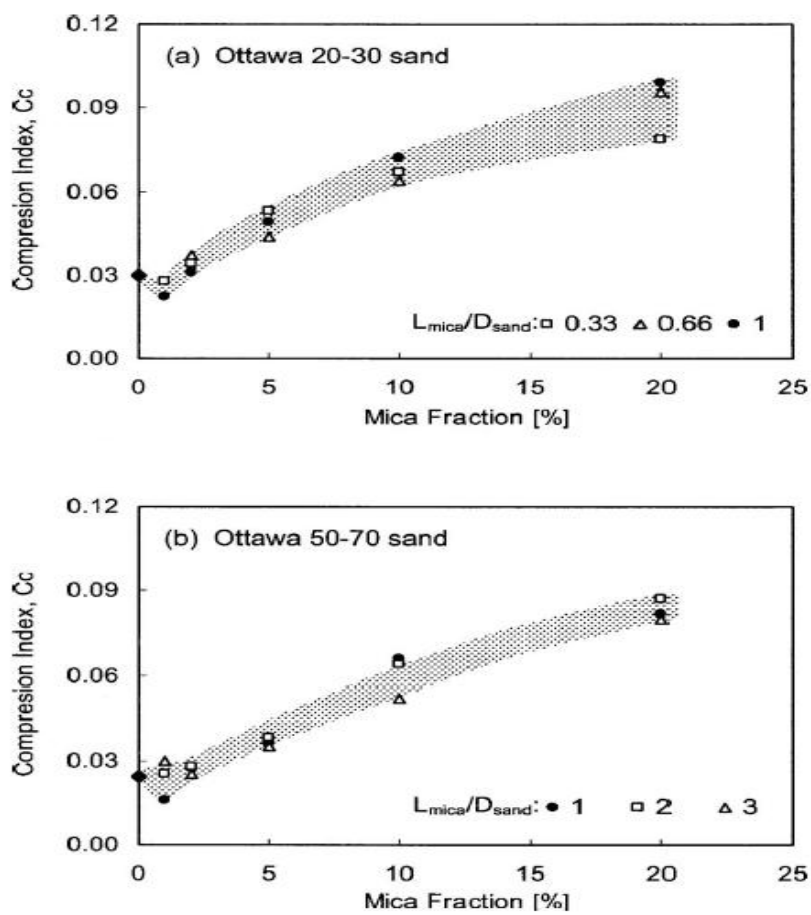


Figure 2.31 Values of compression index C_c versus mica content for different values of size ratio (D_{mica} / D_{sand}) : a) mixtures with Ottawa 20–30 sand; b) mixtures with Ottawa 50–70 sand (Lee, et al. 2007)

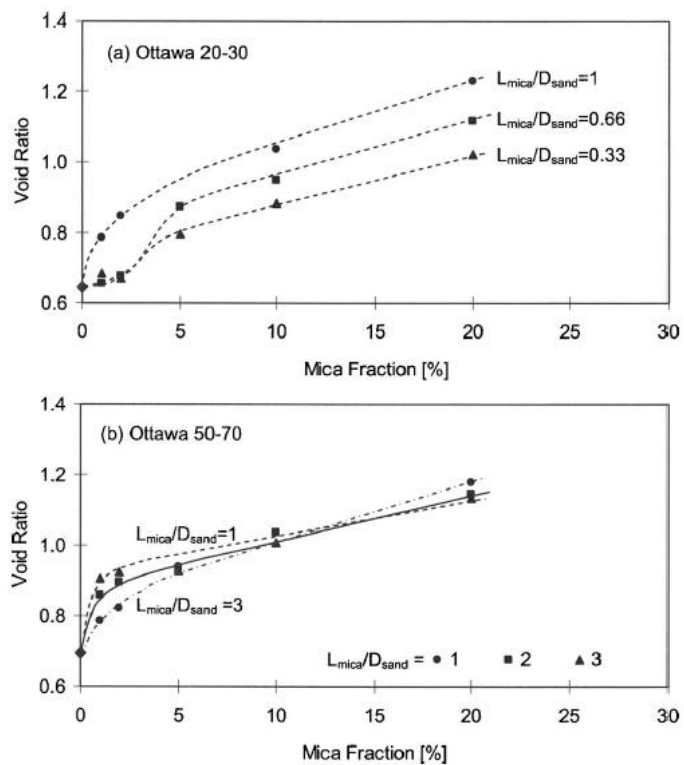


Figure 2.32 Void ratio versus percentage mica for mixtures of sand (Lee, et al. 2007)

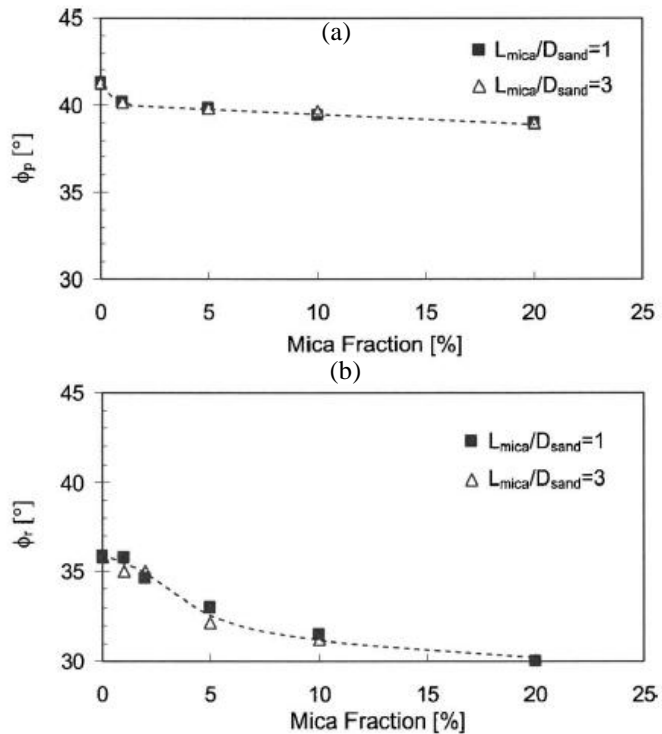


Figure 2.23 Friction angle versus mica content for mixtures with different size ratios: a) peak friction angle b) residual friction angle (Lee, et al. 2007)

CHAPTER THREE

THE STUDY AREA AND FIELD INVESTIGATIONS

3.1 Geological and Earthquake Characteristics of zmir

zmir province, which is the third biggest city in terms of population, industrial and financial capacity needs comprehensive earthquake engineering studies in order to reduce the seismic risk it carries. The local soil properties, regional geology and tectonics play a key role in earthquake risk of zmir. In this section, the tectonic structure of the Old Gediz Delta and its vicinity is briefly presented along with its geological structure and local soil characteristics.

3.1.1 General Tectonics of the Region

Tectonic sources affecting zmir are tectonic sources of part of the Western Anatolia tectonic system, one of the major active tectonic region in Türkiye. The rate of North-South directional extension is approximately 30-40 mm/year in the region. The main evidence of this motion is the current seismic activity. E-W directional major graben systems are the cause of the current geomorphology. These major grabens are named as Bakırçay, Simav, Gediz, Küçük Menderes, Büyük Menderes and Gökova grabens (Patton, 1992; Taymaz et al., 1991; Westaway, 1990). The major grabens and fault systems in central Western Anatolia can be seen in Figure 3.1. Although majority of the active faults were developed as normal faults along the boundaries of the graben systems with dip angles varying between 45° ~ 70° , zmir also presents a unique example to the presence of strike-slip active faults that are believed to control the activity of normal faults around the city (Bozkurt & Sözbilir, 2004; Emre et al., 2005; Özkaymak & Sözbilir, 2008; engör, 1982; Uzel et al., 2011).

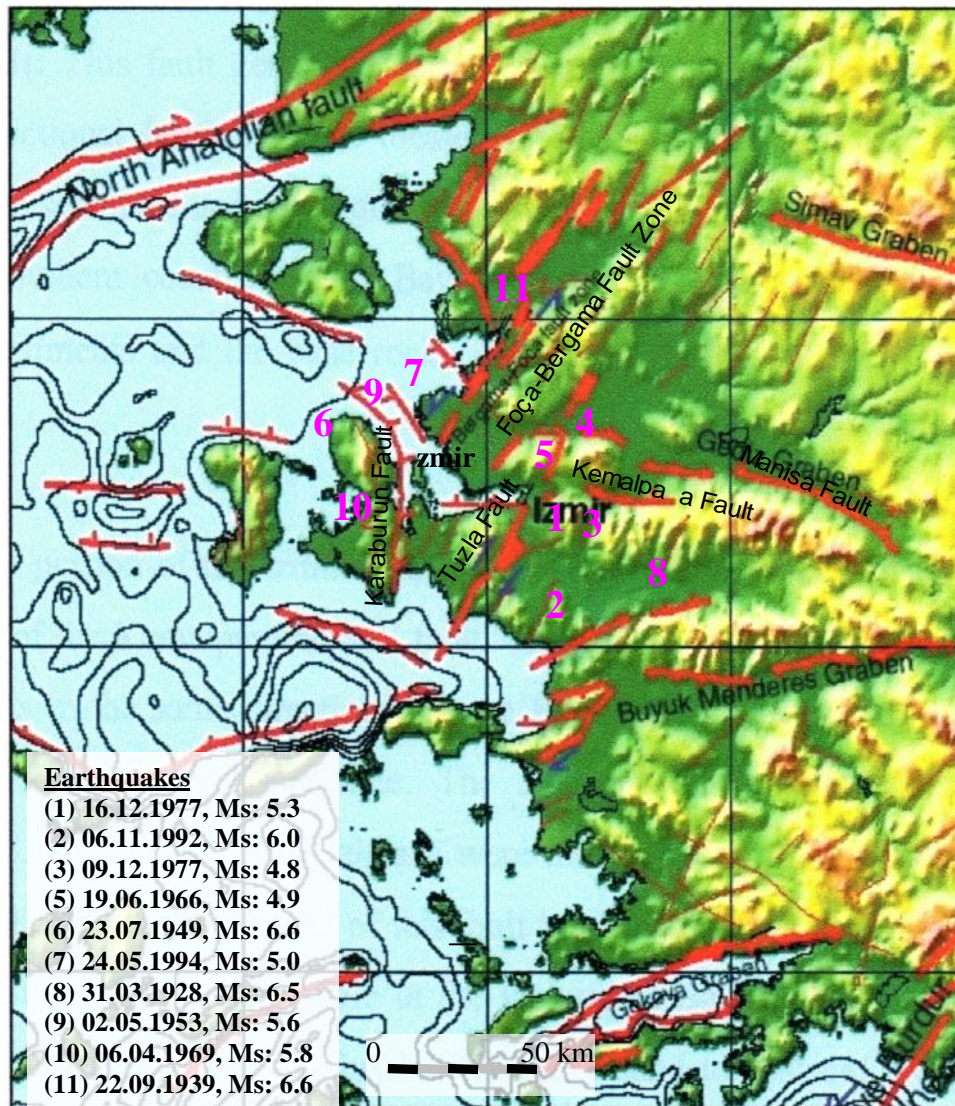


Figure 3.1 Major grabens and fault systems in the central Western Anatolia, and epicenters of the major earthquakes during instrumental period (RADIUS, 1999)

Western Anatolia has been subject to tensile forces. Normal faults were formed as a result of tensile forces in the region. (Barka & Reilinger, 1997; Emre & Barka, 2000; Mc. Kenzie, 1978; Sözbilir, 2001). In general, İzmir and its neighborhood are graded as the first-degree earthquake zone (DBYBHY, 2007; RADIUS, 1999).

There are three different tectonic zones nearby İzmir. These regions are Menderes massif in the East, İzmir-Ankara suture zone in the middle and Karaburun zone in the west. These tectonic zones can be seen in Figure 3.2. Menderes massif and Karaburun zone has been a stable platform for carbonate sedimentation since Triassic

to the end of the Campanian. During the first deformation taking place with the transportation of the platform into the basin in terms of naps between ages of Maestrihtian and Danien while flysh sedimentation was occurring, the Bornova Complex was thrust over the Menderes metamorphic units by the help of large scale tectonic movements (Dewey & engör, 1979; Sözbilir et al., 2008). This deformation was in terms of sheared zones appearing as fish flake like shapes that were commonly present in the Bornova Complex. It is estimated that, this deformation period occurred in the late Eocene era and at the same time period main metamorphism of Menderes massif was developed (Seyito lu et al., 1992; Sözbilir et al., 2009; engör et al., 1985). The Bornova Complex was elevated in Miocene age and owing to its internal structure it was sheared along NE-SW direction. In this age areas lakes were formed in lower elevations as a result of the paleogeography of

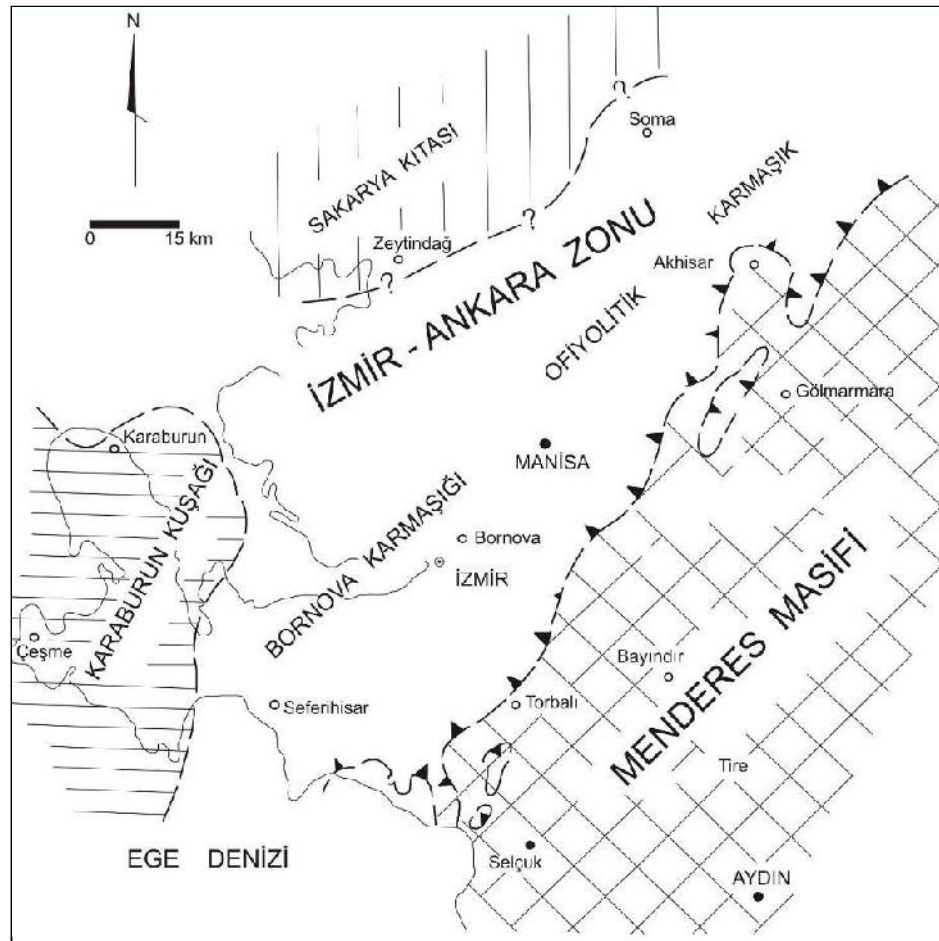


Figure 3.2 Tectonic zones of İzmir and its vicinity (Erdoğan & Güngör, 1992)

region (Kaya, 1981; Yılmaz, 1997). In the second stage of the Neotectonic era, stress caused West Anatolia to get shifted towards South Aegean Subducted zone. As a result of this mechanism, West-East directed faults risen and present horst–graben morphology were formed (Akyol et al., 2006; Özkaymak et al., 2011; engör, 1987; Uzel & Sözbilir, 2008). The graben system elongating between the Gediz Valley and Kemalpa a towards the zmir Bay through Bornova is the most significant component of the regional tectonism. The thermal water outbreaks along the south of zmir Bay are indications to the activity of the faults at the south. There are also similar faults in on the north side of the Bay Area. The active fault systems nearby zmir are shown in Figure 3.3.

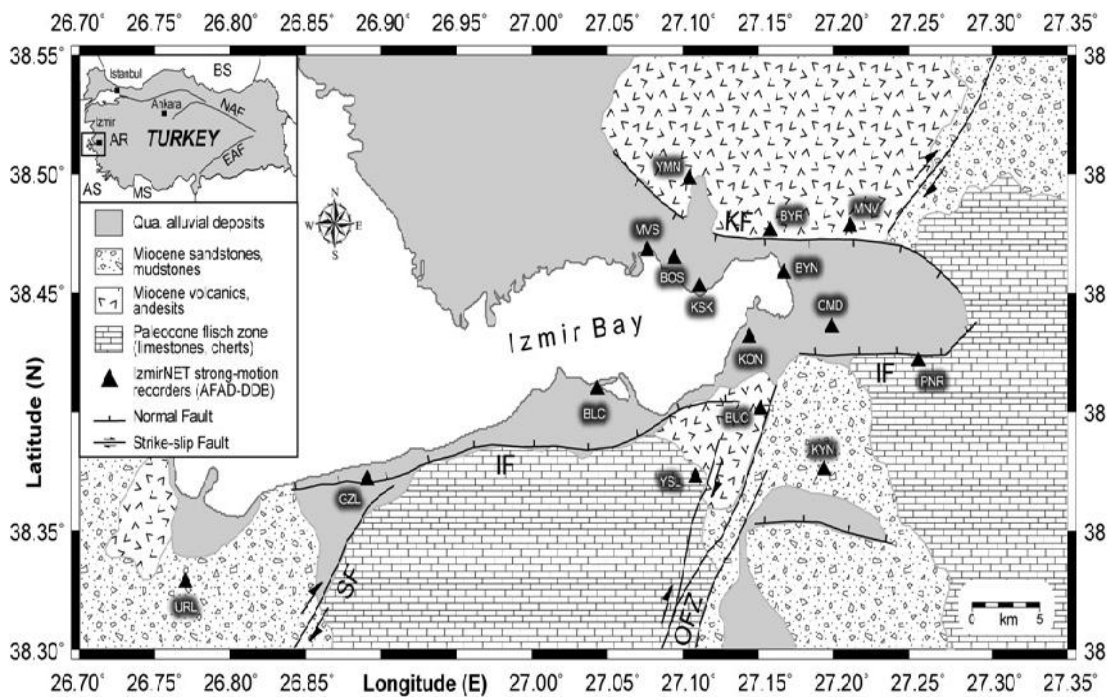


Figure 3.3 Active fault map of zmir and its vicinity (Sözbilir et al., 2008 and 2009; Uzel et al., 2011)

F: zmir Fault, KF: Kar ıyaka Fault, SF: seferihisar Fault, OFZ: Orhanlı-Tuzla Fault zone, AR: Aegean Region, AS: Aegean Sea, BS: Black Sea, EAFZ: East Anatolia Fault Zone, MS: Mediterranean Sea, NAFZ: North Anatolia Fault Zone

3.1.2 Historical Earthquakes Affecting the Old Gediz River Delta

There are some records of historical destructive earthquakes. The oldest earthquake took place in the year AD 17. This earthquake caused catastrophic damage 10 ancient cities including present time zmir, Manisa, and Aydın (Türkelli

et al., 1994a; Türkelli et al., 1994b). The 1688, 1739, 1778, 1873, 1880, 1928, 1939, 1949, 1974 earthquakes also caused life losses and damages. A list of major earthquakes in zmir and its vicinity are given Table 3.1. Following some major earthquakes, settlement of the ground surface and building damages were reported in the coastal region of the Old Gediz River Delta such as Kar ıyaka, Bostanlı, and Mavi ehir (Ambraseys & Finkel, 1995; Türkelli et al., 1995; Kuruo lu, 2004). Larger portion of the damages in the 1688 zmir Earthquake was in the coastal area of zmir (Ambraseys & Finkel, 1995). Ambraseys & Finkel, (1995) reported that some portion of the Gediz River Delta submerged following the 1739 zmir Earthquake. The 1880 Menemen- zmir Earthquake caused heavy damages in Kar ıyaka and Bornova region (Türkelli et al., 1995; Türkelli et al., 1994a). Structural damages during the 1974 zmir Earthquake occurred in the Akkum Apartment Building as reported by Ergünay et al. (1974), and Kuruo lu (2004). The building is on the Kar ıyaka coastline. In 1977 two medium scale earthquakes (M=5.3) with their epicenters very close to the city center caused damage in 40 buildings injuring 20 people (Dadak & Tolay, 2002). Locations of the affected buildings are in Kar ıyaka, Alsancak, Hatay, Buca, Gültepe, Gürçe me, and Yeni ehir districts (Kuruo lu, 2004). Another earthquake is the 1992 Do anbey-Seferihisar Earthquake. The earthquake caused damages in the towns of Do anbey, Seferihisar, Ürkmez and Gümüldür. These earthquakes did not cause major damage in zmir, but it was strongly felt in alluvial sites (Türkelli et al., 1995; Kuruoglu, 2004). Figure 3.1 and Table 3.1 shows epicenters of the major instrumented period earthquakes.

3.1.3 General Geology of zmir and Its Vicinity

The base of the zmir and its vicinity consists of Upper Cretaceous-Paleocene sandstone-shale alternations, a geological formation inside zmir-Ankara Zone; Seyito lu & Scott, 1996; Sözbilir, 2002). The Miocene gravelstone units overlay with angular discordance above the basement units. Thickness of the gravelstone unit is 40-45 m. Upper level of the unit contains siltstone, claystone, marn, sandstone and gravelstone conglomerates. Andesite and tuff overlay these units. Alluvium unit,

which also contains blocks and gravels discordantly cover the above mentioned geological formations. The general geological map of zmir and its vicinity is given in Figure 3.4 (Erdo an, 1990; Özer et al., 2001; Seyito lu & Scott, 1991).

Table 3.1 Major earthquakes in neighborhood of zmir (KOERI, 2003; Kuruo lu, 2004)

Period	Date	Latitude	Longitude	I ₀ Intensity (MSK scale)	Ms (Magnitude)	Location
Historical Earthquakes	AD 17	38.40	27.50	IX	6.9	zmir, Manisa, Aydin
	110	37.00	26.00	IX	6.9	zmir, Efes
	177	38.40	27.10	IX	6.9	zmir, Sakız Island
	688	38.40	27.00	IX	6.9	Izmir
	20.03.1389	38.40	26.30	IX	6.9	Izmir, Sakız Island
	10.07.1688	38.40	27.20	X	7.5	zmir
	04.04.1739	38.40	27.20	IX	6.9	zmir
	03- 05.07.1778	38.40	27.20	IX	6.9	zmir
	01.02.1873	37.75	27.00	IX	6.9	Sisam Island, zmir
	29.07.1880	38.60	27.10	IX	6.9	Menemen, zmir
	03.04.1881	38.25	26.10	X	7.5	Sakız Island, zmir
	25.10.1889	39.30	26.30	IX	6.9	Midilli & Sakız, zmir
During Instrumental Period	31.03.1928	27.35	27.35	IX	6.5	Torbah- zmir
	22.09.1939	26.93	26.93	IX	6.6	Dikili- zmir
	23.07.1949	26.27	26.27	IX	6.6	Karaburun-Izmir
	06.04.1969	26.41	26.41	VIII	5.9	Karaburun-izmir
	01.02.1974	27.2	27.2	VII	5.5	zmir
	16.12.1977	27.19	27.19	VII	5.3	zmir
	06.11.1992	26.99	26.99	VII	6	Do anbey- zmir
	10.04.2003	26.83	26.83	VII	5.6	Urla- zmir

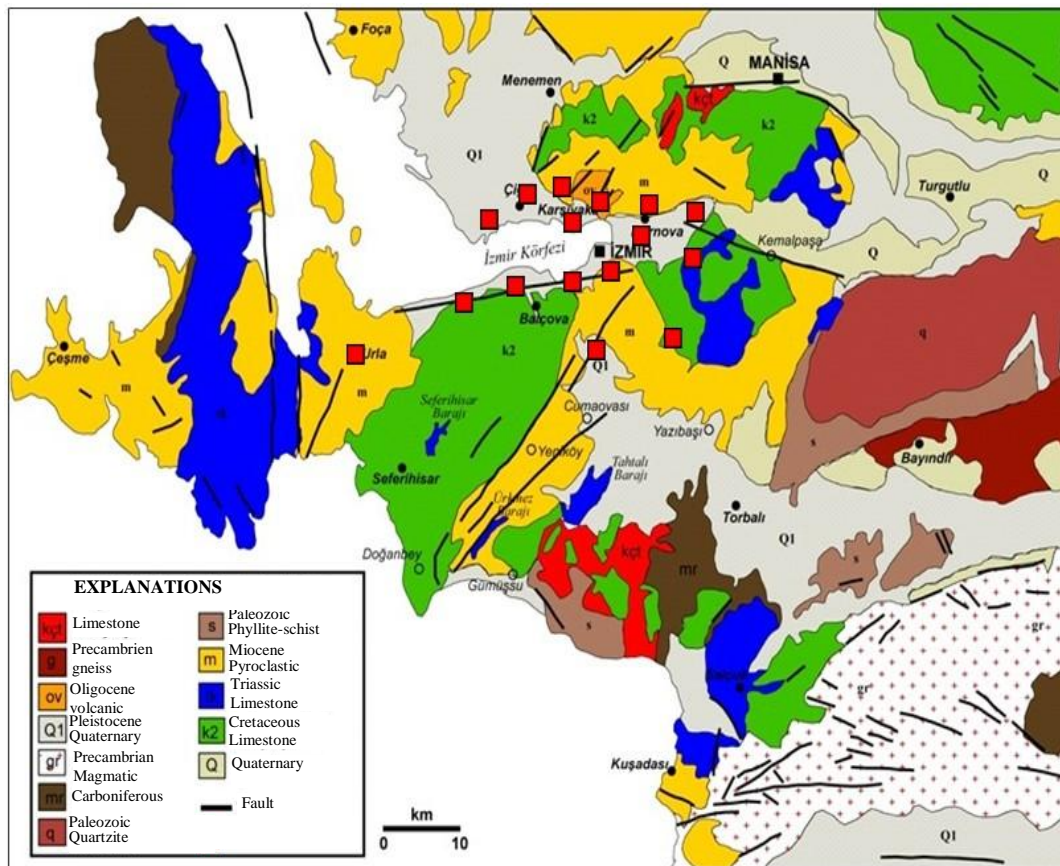


Figure 3.4 General geological map of Izmir and its vicinity (106G159, 2011)

3.1.4 Alluvial Geomorphology

Fundamental characteristics of geomorphological units in the neighborhood of Izmir were formed by crustal movements in the Neotectonic period when volcanism was severely occurring. Firstly, Izmir-Ankara Suture Zone was broken and extensions in the NE-SW and NW-SE directions occurred. Then, Menderes massif rose and basins between rising blocks were filled by Miocene lakes. Starting at the end of the Miocene, new broken elements were formed in the E-W direction while valleys between the blocks were deepening. This faulting and breaking process formed the present morphology.

Terrestrial unit, which was formed by continuous tectonic movement, was covered by alluvial sediments along the coast of Izmir Bay since Pliocene. While

coarse-grained materials were transported by rivers from mountains to plains, the deposited materials rose together with mountain blocks by tectonic movements. On the other hand, finer materials were deposited in the middle part of the plains.

Eroded materials, which were formed by afterward abrasions of rising blocks, were transported to lower basins. These abraded lands can be observed on the northern hills of Kar ıyaka and Bornova. There are sediments, which consist of limestone fragments and coarse volcanic blocks, in the northern part of the zmir Bay. This unit can be seen only on the northern part of the Bay and explains why the thickness of the Bornova plain progressively gets deeper towards south (Kayan, 2000). There is not any major river throughout Bornova plain, so Bornova is not a typical delta plain. However, there are three major streams flowing towards to the sea. Alluvial sediments have been formed by these streams (Kayan 2000).

The Old Gediz River Delta is on the northwestern part of Kar ıyaka - Bostanlı region. Delta was formed by sedimentation of alluvial deposits, which were transported by Gediz River in the Quaternary period. The Gediz River flowed into the sea in the northwestern part of zmir Bay until the late nineteenth century. After the late nineteenth century, the Gediz River was shifted to its present bed. The Figure 3.5 shows the Old and New Gediz River Delta regions. The continental brown, stiff to very stiff clays below 30~40 m depth are generally over-consolidated in this region. The Quaternary aged alluvial soils of Old Gediz River Delta were deposited over such continental soils. These sedimentary deposits are generally normally consolidated or under-consolidated. Continental deposits are underlain by andesitic and flysch bedrock. The complex geological and geomorphological structure of the delta caused horizontal discontinuities on the stratification of soils even at close distances (Kayalar, 1991; Özden, 2000; Kuruo lu, 2004).



Figure 3.5 Region of the the New and Old Gediz River Delta (106G159, 2011)

3.2 In Situ Sounding and Laboratory Test Data

The project named as “İzmir Metropolü ile Alia a ve Menemen İlçelerinde Güvenli Yapı Tasarımı için Zeminin Sismik Davranı larının Modellenmesi – Modeling of Seismic Behavior of Soils for Safe Structural Design in İzmir Metropolitan Area and Alia a, Menemen Towns (106G159, 2011)” and sponsored by TÜB TAK commenced in 2006. Whithin the scope the project, many strong ground motion stations were placed in İzmir. Many boreholes were drilled during the project. The boreholes provided new knowledge pertaining to the depth of bedrock, information about geological properties and fault systems of the region. Bedrock elevations as obtained from deep boreholes are illustrated in Figure 3.6 for İzmir Bay Area.

In this dissertation, the boreholes drilled in the Old Gediz River Delta were utilized. Utilized boreholes were approximately 20 meter depth, except the 12-MV borehole. The depth of the 12-MV borehole was 270 m. In this study, soils within the first 20 m from the ground level were interested due to scope of the dissertation.

In the field, the Standard Penetration Test was performed at 1.5 meter intervals. Ground water table (GWT) was measured in the boreholes. Disturbed and undisturbed soil samples were recovered. They were used in the laboratory testing program including cyclic triaxial tests.



Figure 3.6 Boreholes and bedrock elevations, in zmir (106G159, 2011)

3.3 Geotechnical Properties of Old Gediz River Delta Soils

Geotechnical characteristics of soil layers in the area have been examined by many researchers (Güz, 1970; Kayalar, 1991; Özkan & Çalı an, 1991; Özden, 2000; Kuruoglu, 2004), and geotechnical companies. Reports prepared by academic institutions (Dokuz Eylül, Ege, and Celal Bayar University), and dissertations of doctoral, and master of science studies (Alper, 2008; Baysal, 2006; Kuruo lu, 2004; Durmu , 2006) also provided significant information about the subject.

Probably, the doctoral dissertation of Kuruo lu (2004) is one of the most comprehensive studies about soil properties of the northern coast of zmir Bay soils. The other comprehensive study about Gediz River Delta Soils is the above mentioned TÜB TAK sponsored research project. Based on the data and information acquired from such previous studies, three soil profiles are determined. The soil profile given in Figure 3.7 is a rather comprehensive one covering the profiles of Figure 3.8 as obtained from shallow borings realized under the supervision of this author. Index and engineering properties of the study area soils are given in Table 3.2 and Table 3.3.

Table 3.2 Index and engineering properties of Kar ıyaka Coastline Soils (Kuruo lu, 2004)

Index Properties	Depth	-No.4	- No.200	w _L	w _P	I _p	w _n	γ _n	G _s	USCS
	(m)	(%)	(%)	(%)	(%)	(%)	(%)	(kN/m ³)	-	-
	0.0-8.0	68-100	4-44		NP		22-40	18.5	2.62	SM
	8.0-19.0	90-100	70-100	56-85	23-49	15-43	43-62	16.5	2.60	MH
	19.0-25.0	51-99	6-41		NP		12-36	18	2.61	SM
	25.0-35.0	89-100	24-77	54-91	24-35	22-59	14-32	19	2.65	SC/CH
	35.0-40.0	91-100	36-79	55	26	29	21-43	19	2.70	CH
	40.0-47.0	40-45	1-5	-	-	-	19-25	21	2.65	GC
	47.0-51.0	96-100	51-66	45	25	20	14-32	20	2.65	CH
	51.0-54.0	-	-	-	-	-	22-28	21	2.65	GC

(Table 3.2 continued)

Engineering Properties	Depth	SPT-N	c_u	q_u	$c_{u, \text{field vane}}$	ϕ
	(m)	-	(kN/m^2)	(kN/m^2)	(kN/m^2)	($^\circ$)
	0.0-8.0	3-42	-	-	-	30
	8.0-19.0	1-9	10-20	20-40	15-20	26
	19.0-25.0	9-50	-	-	-	30
	25.0-35.0	16-50	80-120	160-240	-	30
	35.0-40.0	19-35	-	-	-	30
	40.0-47.0	31-50	-	-	-	34
	47.0-51.0	33-50	-	-	-	30
	51.0-54.0	50	-	-	-	34

Table 3.3 Index and engineering properties of Bostanlı-Mavi ehir Soils (Kuruo lu, 2004)

Index Properties	Depth	-No.4	- No.200	w_L	w_P	I_p	w_n	γ_n	G_s	USCS
	(m)	(%)	(%)	(%)	(%)	(%)	(%)	(kN/m^3)	-	-
	0.0-5.0	100	90-100	53-75	29-34	24-38	42-59	17.5	2.70	CH
	5.0-8.0	100	9-42		NP		19-32	18	2.65	SM
	8.0-22.5	100	81-100	56-84	26-34	27-43	49-68	17	2.70	CH
	22.5-30.0	56-60	9-32	44-50	21-26	22-25	27-43	18.5	2.65	SC
	30.0-45.0	94-100	50-77	39-43	17-19	21-26	16-23	20	2.70	CL
	45.0-55.0	70-80	40-45		NP		19	20	2.65	SM

Engineering Properties	Depth	SPT-N	c_u	q_u	$c_{u,T}$	ϕ
	(m)	-	(kN/m^2)	(kN/m^2)	(kN/m^2)	($^\circ$)
	0.0-5.0	2	10-20	20-40	20-25	28
	5.0-8.0	10-15	-	-	-	30
	8.0-22.5	2-8	20-60	40-120	30-35	28
	22.5-30.0	29-49	-	-	-	30
	30.0-45.0	13-38	100-150	200-300	-	32
	45.0-55.0	23-50	-	-	-	34

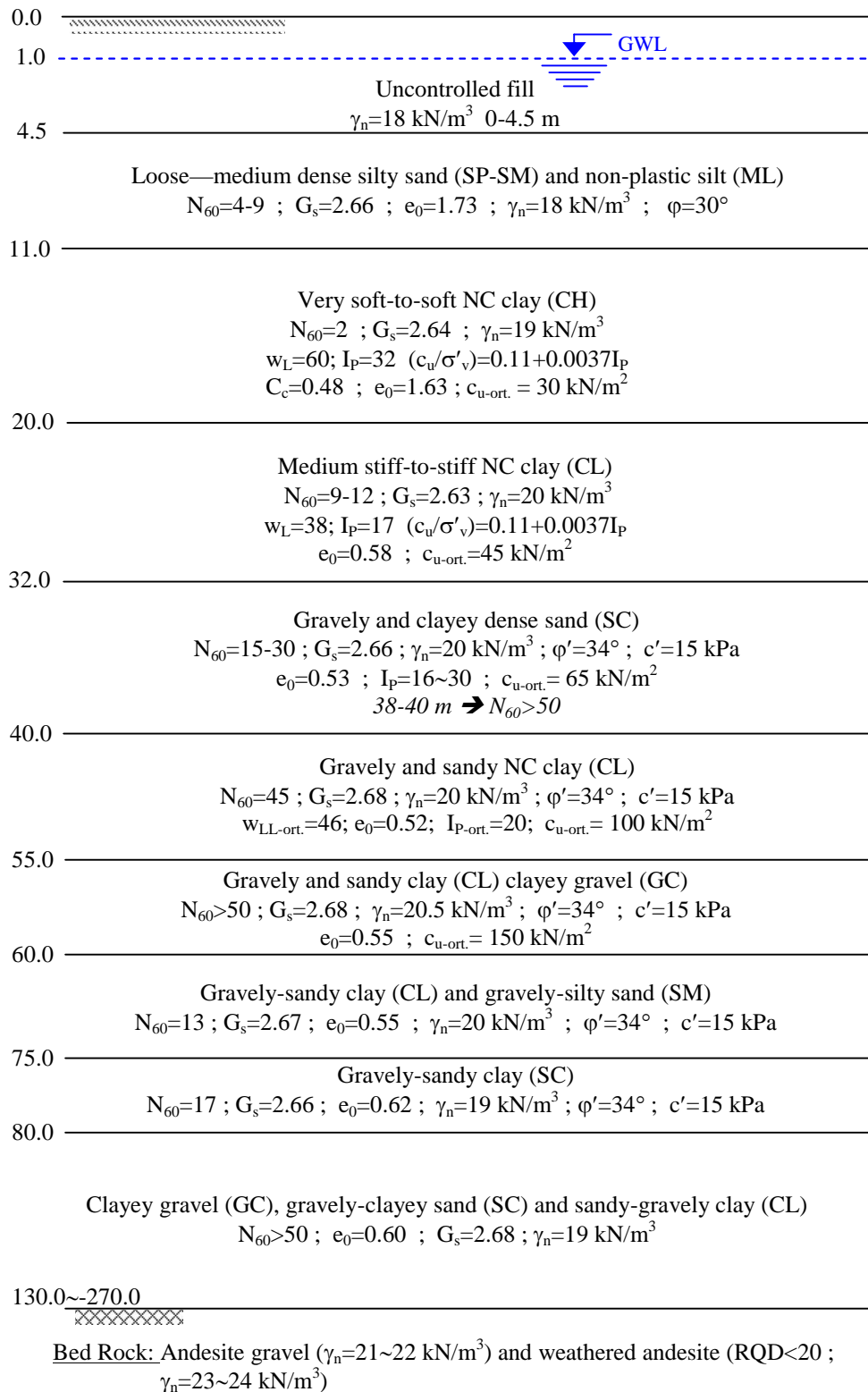
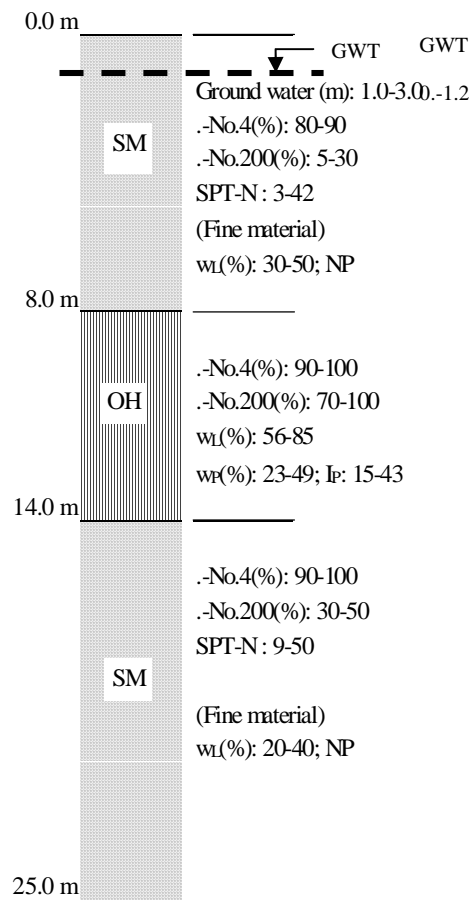


Figure 3.7 Generalized soil properties and soil profile for Old Gediz River Delta soils (106G159, 2011)

Kar ıyaka Coastline Region



Bostanlı - Mavi ehir Region

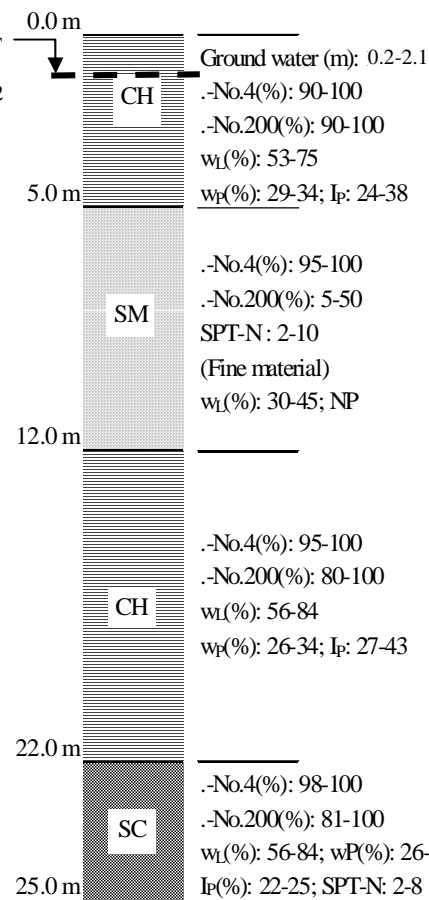


Figure 3.8 Geotechnical profile for the Kar ıyaka coastline and Mavi ehir-Bostanlı regions

According to the literature and laboratory test data, the Old Gediz River Delta contains liquefiable sandy soils. Such soil layers contain varying amounts of fine content (i.e. silts and clays). The Old Gediz River Delta soils are also noticeable in terms of shiny mica flakes, which originate from the parent rocks present along side the river bed. It was determined by means of X-Ray Diffraction (XRD) and flotation techniques during this dissertation study that the ratio of mica flakes by weight vary between 5% and 25%.

CHAPTER FOUR

TESTING MATERIALS AND EXPERIMENTAL METHODS

4.1 Materials

Five different types of materials were utilized in the testing program of this dissertation. The No.1 and No.2 materials can be identified as sands without mica and fines materials. No.1 sand was recovered from Gediz River Bed near Hasanlar Village of Menemen Whereas No.2 sand was obtained from sample of boreholes, which were drilled in Mavi ehir (Site-1), Bostanlı (Site-2) and Kar ıyaka (Site-3) regions. No.3 and No.4 materials are platy mica grains of various sizes. No.3 material was supplied by Kaltun Madencilik A. . (Çine) as ground mica mineral. The mica grains named as No.4, on the other hand, belong to study area boreholes. It was obtained by means of physical separation using flotation technique. Silty sand (SM) samples of the Old Gediz River Delta were used for this purpose. The No.5 material is the unsieved and unseparated silty sand obtained from the 12-MV borehole (from the depth interval of 7.50~8.00 meter).

Alluvial sandy materials for the test program were generally obtained from the Standard Penetration Test (SPT) spoon. Each SPT spoon sample weighs less than 500 gr. This is not enough to prepare the test sample in triaxial device. Because of this reason, the sandy samples were reconstituted. The average grain size distribution of the reconstituted alluvial delta sand (AS sand) can be seen in Figure 4.1 as named “Average grain size distribution of delta sand”. The Figure 4.1 shows also the upper and lower bounds for the grain size of the alluvial sandy materials. The bounds cover the literature data and test results of this study.

Non-platy and platy grains were separated by means flotation technique. Separation process of mica and sand materials with flotation technique is not highly efficient when the particles size is coarser than 0.250 mm and finer than 0.100 mm (Geredeli &

Özbayo lu, 1995; Bilir et al., 1997). Because of this reason, firstly reconstituted alluvial delta sand was sieved through 0.212 mm and 0.075 mm sieves. Then sieved delta sand was used in separation process to obtain mica and sand grains materials in high purity. The separated platy grains mainly consist of mica minerals. The grain size distribution of the separated platy mica grains and sand (without mica) is given in Figure 4.1.

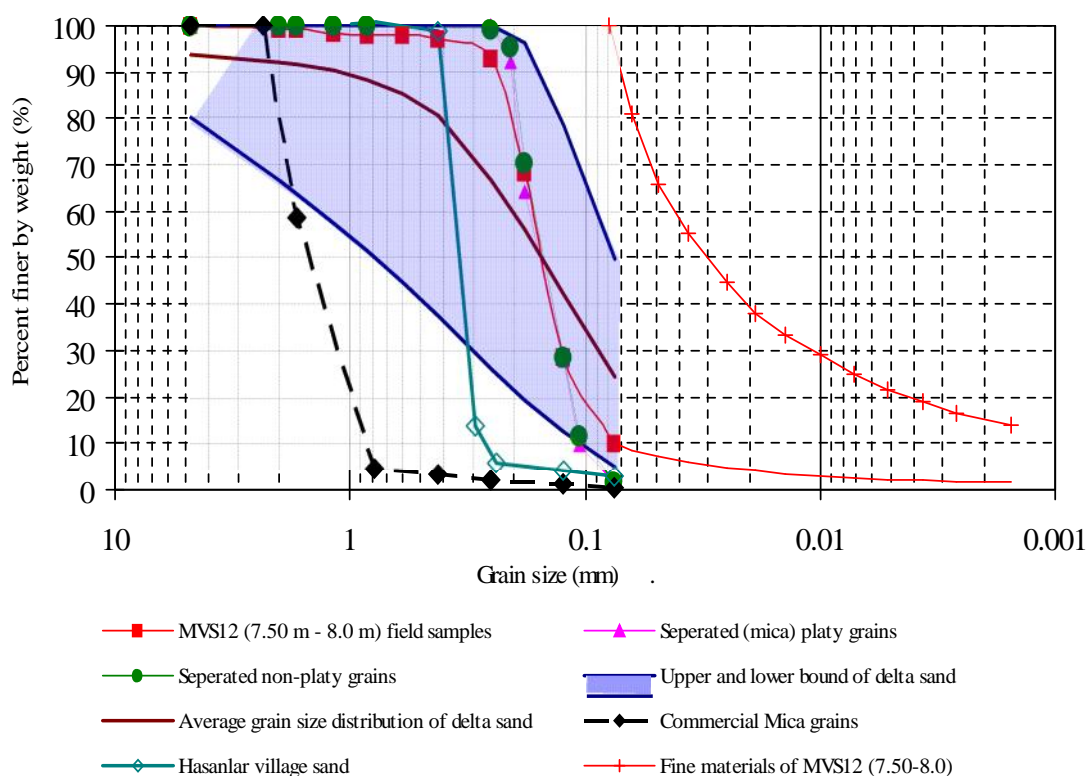


Figure 4.1 Grain size distribution curves of test materials

The granular soils are classified according to their grain shape. The typical categorizations for the shape of the granular soils are given in Figure 4.2. The shape of the test materials can be seen in Figure 4.3. In the Figure 4.3 (a) and (d) are separated alluvial delta sand (No.2), (b) and (e) are Gediz River Bed sand near the Hasanlar Village (No.1), (c) and (f) are 12-MV borehole samples obtained at 7.50-8.00 meter depth (No.5), (g) is separated mica grains (No.4), (h) is commercially supplied mica grains (No.3). As seen Figure 4.3, the mica grains (g and h) are platy shaped. Alluvial

(No.2, No.5) and Gediz River bed sands (No.1) are angular shaped according to categorization of the Figure 4.2.

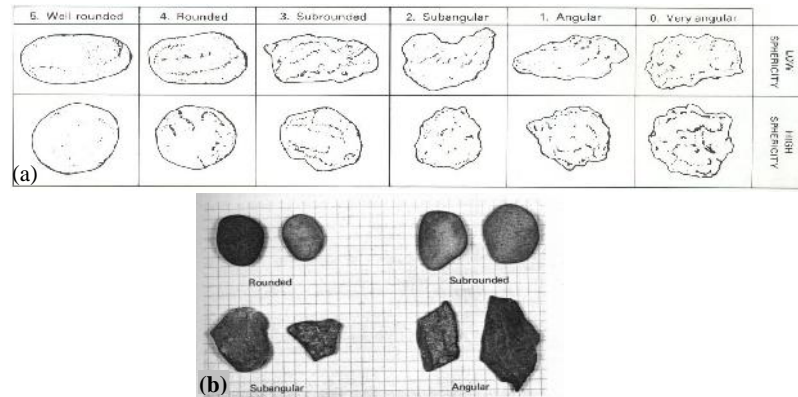


Figure 4.2 (a) Categories of roundness for grains of low and high sphericity (Petijohn, 1973), (b) Typical shapes of sand grains (Holtz et al., 2011).

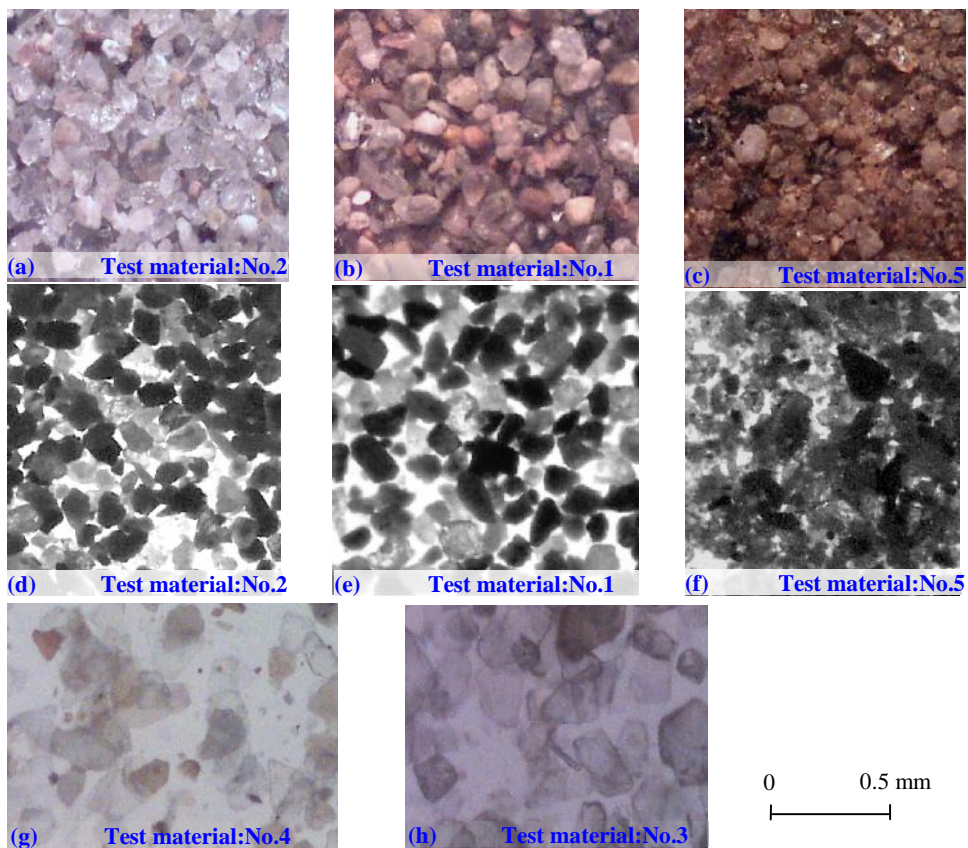


Figure 4.3 Images of test materials, (a), (d) Separated sand (No.2), (b), (e) Gediz River sand (No.1), (c), (f) 12-MV (7.50m-8.0m) boreholes sandy sample (No.5), (g) Separated mica (No.4), (h) Commercially supplied mica (No.3)

The index properties and physical characteristics of the test materials are given in Table 4.1.

Table 4.1 The physical characteristics and index properties of the test materials

	Hasanlar Village Sand (No.1)	Separated Delta Sand (No.2)	Commercially Supplied Platy Grains (No.3)	Separated Delta Platy Grains (No.4)	Fines Materials (NP)	12-MV (7.5m-8.0m) Boreholes Samples (No.5)
Specific Gravity, G_s	2.67	2.67	2.81	2.80	2.69	2.67
Coefficient of Uniformity, C_u	1.34	1.67	2.01	1.64	39.7	2.30
Coefficient of Curvature, C_c	1.02	0.98	0.90	0.89	2.70	1.33
Mean Diameter, D_{50} (mm)	0.35	0.15	1.46	0.16	0.029	0.15
Maximum Dry Unit Weight (gr/cm^3)	1.46	1.54	0.82	1.23	1.17	1.75
Minimum Dry Unit Weight (gr/cm^3)	1.05	1.23	0.29	0.45	0.77	1.17
Minimum Void Ratio, e_{\min}	0.83	0.74	2.42	1.28	1.28	0.53
Maximum Void Ratio, e_{\max}	1.55	1.16	8.53	5.19	2.46	1.29
Percent of Fine Materials (%)	< 2.0	< 2.0	< 2.0	< 2.0	100	10.6
w_L (%)	-	-	-	-		37
w_P (%)	-	-	-	-	NP	NP
USCS	SP	SP	SP	SP	ML	SP-SM

Mineralogical compositions of the test materials and alluvial sandy soil deposits were determined in X-Ray diffraction (XRD) tests (Barden & Sides, 1971; Ogunsanwo, 1988). Mineralogical compositions of the materials are presented in Table 4.2.

Table 4.2 Mineralogical composition of the test materials

Gediz River Hasanlar village sand:	Quartz, Anorthite, Illite
Platy Mica grains supplied from Kaltun A .	: Muscovite, Quartz, Illite
Separated non-platy materials	: Quartz, Anorthite, Muscovite, Illite, Dolomite
Separated platy materials	: Muscovite, Quartz, Anorthite
Fine Materials	: Quartz, Muscovite, Biotite, Albite, Illite, Anorthite, Zeolite, Kaolinite, Dolomite
12-MV (7.50m - 8.00 m) sample :	Quartz, Muscovite, Anorthite, Magnesium, Biotite

Mainly determined minerals in the Old Gediz River Delta sandy soils are Quartz, Muscovite, Anorthite, Zeolite, Kaolinite, Calcit, Dolomite, Albite, Biotite, Nimitite, Sanadine, Clinoclore, Coesite.

4.2 Experimental Methods

4.2.1 Standard Penetration Test (SPT)

The Standard Penetration Test (SPT) was performed at 1.5 meter intervals in the boreholes. During drilling process, soil samples were continuously cored out. The core soil samples were covered with plastic cover and then they are placed in the borehole cases. Inner diameter of the core sampler was 70 mm. Diameter of the boreholes was about 100 mm. The SPT machine was equipped with Safety Hammer. The SPT machine was able to lift the hammer and drop automatically. In the tests, standard sampler was used. Drilling machine equipped with SPT equipment can be seen in Figure 4.4.a and 4.4.b.



Figure 4.4 (a) Drilling machine equipped with SPT apparatus (b) Split-barrel sampler (SPT spoon) with soil sample inside

Before the Standard Penetration Test, the borehole was cleaned by means of water pumping in the boreholes. After the cleaning of the borehole, the equipment in the borehole was gently pulled out avoiding development of sucking inside the borehole. Further 20 minutes was spend in order to allow for full dissipation of any excess pore water pressure that might have occurred during drilling and cleaning processes. Then, SPT split-spoon sampler with the rigs was gently lowered down the borehole and Standard Penetration Test was performed according to the ASTM D1586.

In this dissertation, utilized eight boreholes (12-MV , ESK-4, 24-MV , ESK-1, 06-BOS, ESK-2, 10-KSK, ESK-3), which were drilled in three different sites (Mavi ehir, Bostanlı, Kar ıyaka), are in the Old Gediz River Delta Locations and global coordinates of the eight boreholes and sites are given in Figure 4.5 and Table 4.3, respectively.



Figure 4.5 Locations of the three investigated sites and eight boreholes utilized in the study

Table 4.3 Global coordinates of the boreholes

Borehole		Global Coordinate		SITE
No	Name	UTM - X	UTM - Y	
2	12-MV	506764	4257908	Site-1 (Mavi ehir)
86	ESK-1	506764	4257908	
80	24-MV	506725	4258256	
89	ESK-4	506725	4258256	
4	06-BOS	508252	4257591	Site-2 (Bostanlı)
87	ESK-2	508252	4257591	
1	10-KSK	509736	4256323	Site-3 (Kar ıyaka)
88	ESK-3	509736	4256323	

4.2.2 Index and Physical Properties of Test Materials

Specific gravity of test materials was determined in accordance with ASTM D854. Maximum and minimum dry unit weights (minimum and maximum void ratios) of the sand samples were determined following ASTM D4253 and D4254, respectively. Maximum and minimum dry unit weights of the fine materials were found using the method proposed by Lade et al. (1998). Plastic limit was determined in accordance with ASTM D4318. The fall-cone test method as described in BS 1377 was used to determine liquid limit of fine fractions. Sieve and hydrometer tests were conducted as described in ASTM D422 to determine the grain size distribution of test materials.

4.2.3 Determination of Internal Frictional and Repose Angles of Tested Materials

In order to find out shear strength parameters of the sand, drained monotonic triaxial test was used. Beside this test, natural angle of repose was measured for loose sand samples as sketched in Holtz et al., (2011) and shown in Figure 4.6. Drained monotonic triaxial tests were conducted in accordance with JGS 0524-2000.



Figure 4.6 Determination of repose angle

4.2.4 Triaxial Tests

During the test program, monotonic and cyclic triaxial tests were conducted on consolidated and saturated sand-mica mixtures as well as sandy alluvial deposit samples. The consolidated-drained monotonic triaxial compression tests were conducted on samples to determine internal frictional angles of tested samples. Load controlled undrained cyclic triaxial test was used to determine the cyclic strength (liquefaction resistance) and post liquefaction volumetric strain following liquefaction of the samples.

4.2.4.1 Triaxial Test Apparatus

Two triaxial test apparatus were used in the test program. One of them is the DTC-367S model Seiken brand. The other apparatus is made by Controls-Wykeham Farrance including test software.

4.2.4.1.1 Tests in DTC-367S Seiken Apparatus. The diameter and height of the test specimens are 50 mm and 100 mm, respectively. The apparatus is equipped with a pneumatic actuator. The apparatus can perform cyclic triaxial test under load control and monotonic triaxial test under strain control. Both the loading stage and data acquisition system are manually controlled. The general view of the apparatus is shown in Figure 4.7. Apparatus is in Ege University soil mechanics laboratory.

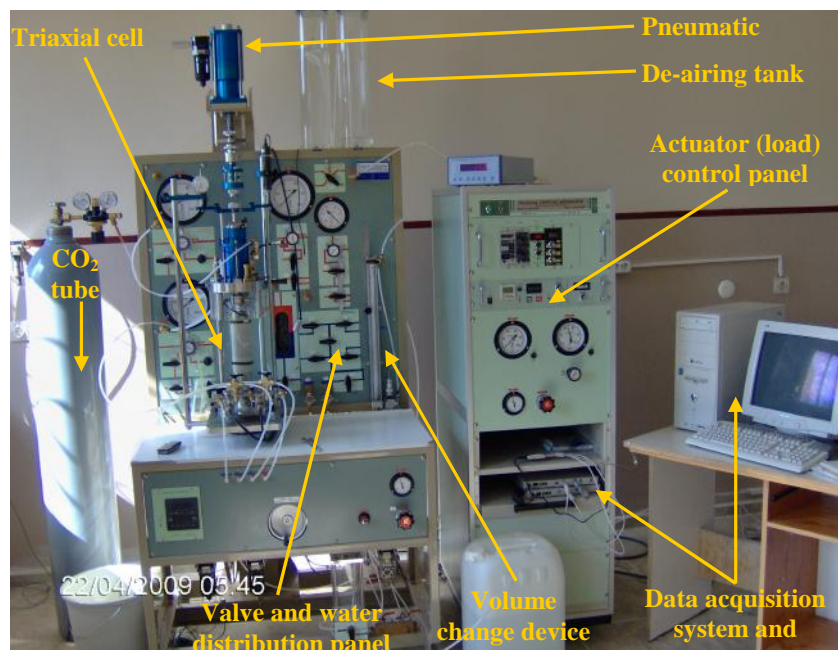


Figure 4.6 Seikan brand triaxial test set-up

4.2.4.1.2 Tests in Controls–Wykeham Farrance Apparatus. The diameter and height of the test specimens are 70 mm and 140 mm, respectively. The apparatus is equipped with a pneumatic actuator. The apparatus can perform cyclic and monotonic triaxial test by load/stress and deformation/strain control. Both the loading stage and data acquisition system are controlled by the computer. The general view of the test set-up is shown in Figure 4.8. The testing system is in the soil mechanics laboratory of Dokuz Eylül University.

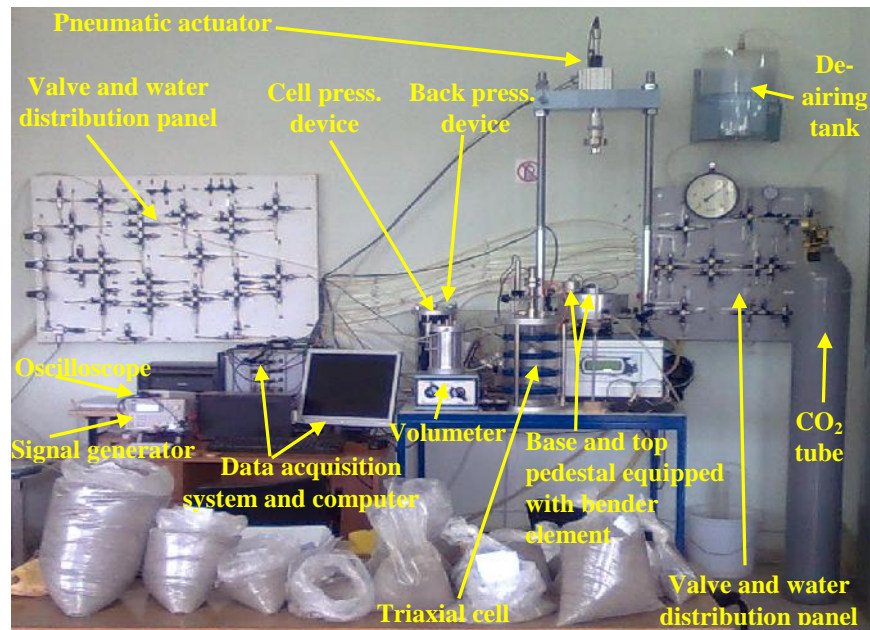


Figure 4.8 Controls-Wykeham Farrance brand triaxial test set-up

4.2.4.2 Sample Preparation for Triaxial Tests

Two different sample preparation methods were used in the testing program. The first method is the air pluviation and the second method is the moist placement (Ishihara, 2003; Ladd, 1977; Mulilis et al., 1975). Air pluviation method was used for samples, which were prepared on Seiken brand apparatus. The size ratio of mica grains and sand grains (D_{mica}/D_{sand}) in samples, which were prepared with air pluviation, is 4.17. In this method, mica grains were supplied commercially (No.3 mica) and sand grains were obtained from Gediz River bed near by Hasanlar Village (No.1 sand). The moist placement method was used for samples, which were prepared on Controls brand apparatus. The size ratio of mica grains and sand grains (D_{mica}/D_{sand}) in samples (No.2 sand and No. 4 mica) which were prepared with moist placement is 1.07. The mica and sand grains that were used in moist placement technique were supplied from boreholes using flotation technique. D_{mica} and D_{sand} are average diameters of mica and sand grains, respectively.

As illustrated in Figure 4.9, The cylindrical rubber membrane is attached to the base pedestal using o-ring (Figure 9.a, b, c, d) and the mould is first placed around the pedestal of the apparatus (Figure 9.e, f). Then, the membrane is stretched-out to the inner face of the split mold, which is attached to the base pedestal (Figure 9.g). Then, porous stone and filter paper are placed on the base pedestal (Figure 9.h). After the porous stone and filter paper are placed, any one of the sample preparation methods (i.e. air pluviation or moist tamping) is employed as described below.

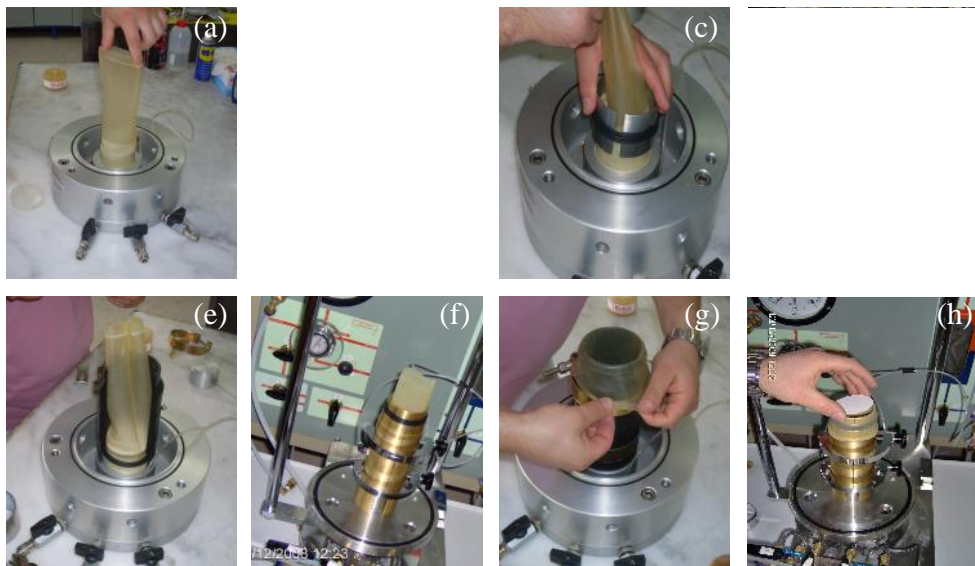


Figure 4.9 Attached the rubber membrane and placed split mold on the base pedestal

4.2.4.2.1 Air Pluviation Method. Oven-dried and weighed sand-mica mixture is filled in a bottle with a nozzle 8.0 mm in diameter. Then, sand was rained thru nozzle at a constant height of approximately 7.0-8.0 cm to obtain loose ($D_r \cong 30\%$) samples (Figure 10.a). After the sand is rained, the specimen top is adjusted (Figure 10.b). Rubber membrane is attached on the specimen cap. Then, rubber membrane is sealed using an O-ring (Figure 4.10.c).

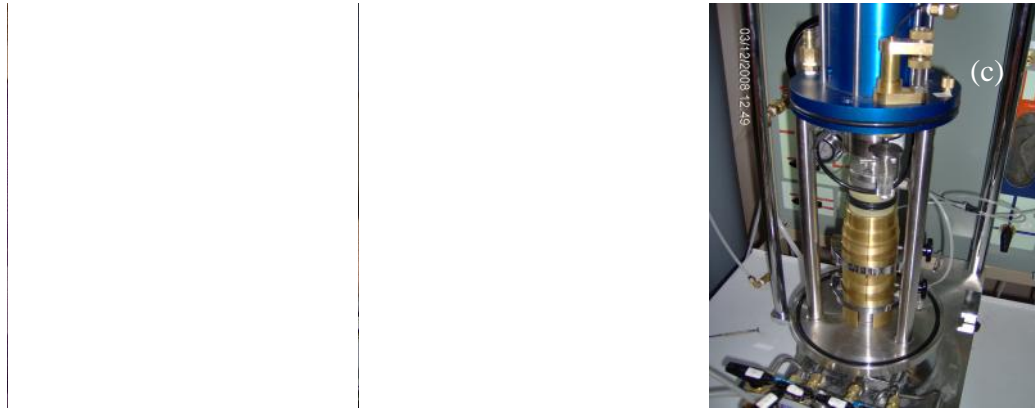


Figure 4.10 Sample preparations using air-pluviation method

4.2.4.2.2 Moist Placement (Tamping) Method. Firstly and similarly as in the case of air pluviation method, membrane is stretched into the mold, which is attached to the base pedestal. Required amount of oven-dried mixture is weighed in six equal portions. Each portion is mixed with 5% de-aired water. Then, each portion of the slightly moist mixture is strewed with fingers to a predetermined height in six lifts as shown in Figure 4.11. At each lift stage, tamping is gently applied with a small flat-bottom tamper. After all the portions are placed in the mold, the top cap is enclosed by the membrane like in air pluviation method.

After the sample placement using one of the above-explained methods and before removing the split mold, 20 kPa negative pressure is applied inside the specimen to obtain a self-standing specimen (Figure 4.12).

After removing the split mold carefully to avoid disturbance to the specimen, height and diameter of the sample are measured with 0.01 mm accuracy. Diameter is measured at least three different points at top, middle, and bottom of the samples. Also height of the sample is measured at least three different points.

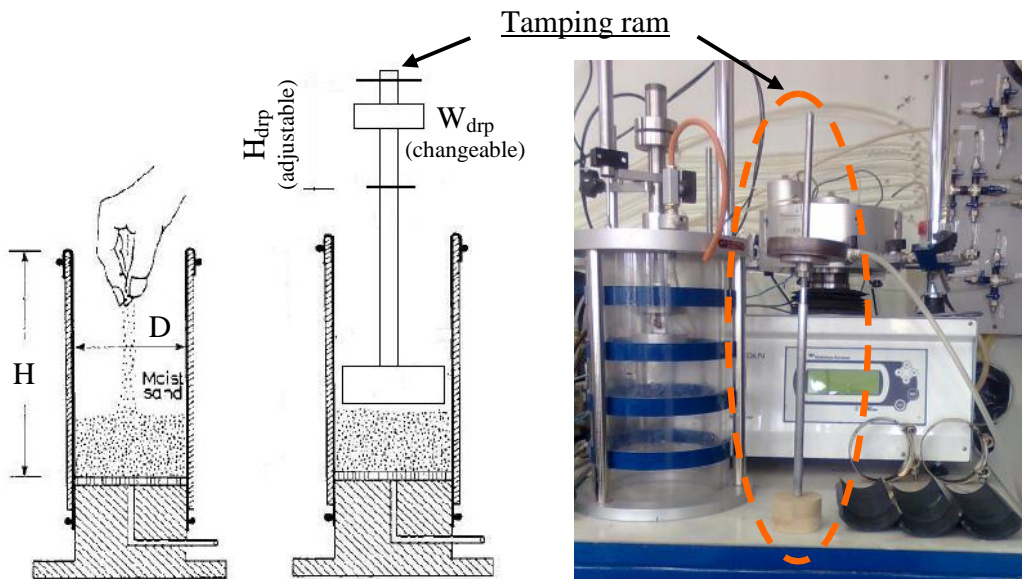


Figure 4.11 Moist placement method (moist tamping)



Figure 4.12 Applying vacuum inside the specimen and measuring the specimen dimensions

After measuring sample dimensions, triaxial cell is assembled with base plate and filled with water to apply confining pressure. The vacuum inside the specimen is decreased step by step while increasing the confining pressure step by step until the desired value (20 kPa) is reached (each step is 2 kPa). While increasing the confining pressure, differential pressure between the outside and inside of the specimen is kept about 20 (± 2) kPa.

As the confining pressure reaches the 20 kPa, carbon dioxide (CO₂) gas regulator is set at low pressure as much as possible (less than 7 kPa). Adjusted carbon dioxide gas is connected to the base drainage valve of the samples. End of the hosepipe that is connected to the top drainage valve of samples is plunged into water in the bucket, which is used for the exit of air pushed out by carbon dioxide gas. Output of the carbon dioxide gas is observed as bubbles from the hosepipe into the bucket. The amount of carbon dioxide bubbles must be equal or less than one bubble in one second in order to protect the samples structure from any disturbance of gas flowing. When the carbon dioxide gas flow is enough, de-aired water is sent into the specimen slowly. At any time in the flowing process of the carbon dioxide and de-aired water, internal pressure of the specimen is kept less than 7 kPa.

After the sample preparation, degree of saturation of the sample was checked as stated by Skempton (1954). A soil element under undrained condition is subjected to equal increases in total stress $\Delta\sigma_3$ in each direction, resulting in an immediate increase Δu_3 in pore pressure. Effective stress in each direction increases as $(\Delta\sigma_3 - \Delta u_3)$. Reductions in the volume of the soil skeleton and in volume of pore space occur as $C_s V (\Delta\sigma_3 - \Delta u_3)$ and $C_v n V \Delta u_3$, respectively (V , n , C_s and C_v are volume of the soil element, porosity, compressibility of the soil skeleton and pore fluid, respectively, under an isotropic effective stress). When the soil particles and fluid (water) are assumed to be incompressible, the reduction in volume of the soil skeleton must be equal to the reduction in volume of the pore space as $C_s V (\Delta\sigma_3 - \Delta u_3) = C_v n V \Delta u_3$. If $1/[1 + n(C_v/C_s)] = B$ is defined as pore pressure coefficient, increase in pore pressure can be written as $\Delta u_3 = B \Delta\sigma_3$. Therefore, B is formulated as in Equation 4.1. Relation between degree of saturation and B value is illustrated in Figure 4.13 by Skempton (1954).

$$B = \frac{\Delta u}{\Delta \sigma'_{confining}} \quad (4.1)$$

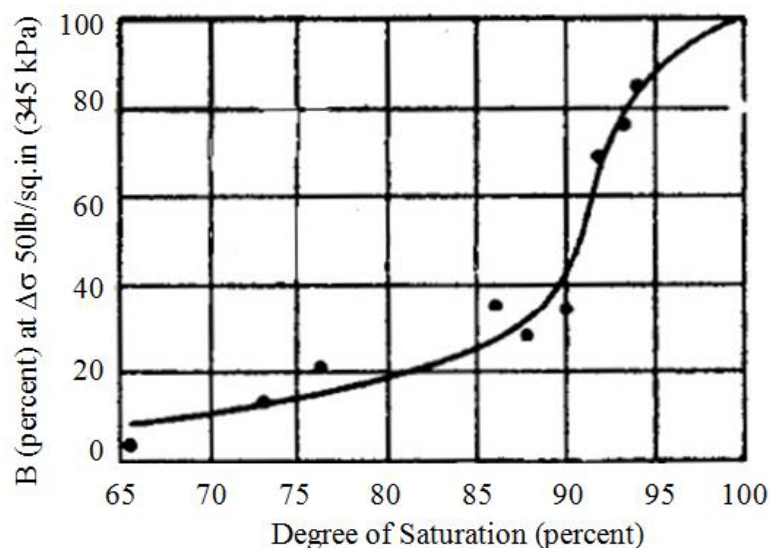


Figure 4.13 Relation between degree of saturation and B value (Skempton, 1954)

After the first increment of confining pressure under (50 kPa) undrained condition is applied, B value is equal or higher than 0.92, back pressure is applied. If the B value is lower than 0.92, the confining pressure is decreased to the initial level and flowing of the de-aired water is continued. When the B value exceeds 0.92, back pressure is applied. The back pressure is increased step by step. In each step, pressure increment is 30 kPa. Increments of the back pressure are applied at least 30 minutes or longer. When the back pressure reaches to 300 kPa and B value becomes equal or higher than 0.97, samples are consolidated isotropically under desired effective confining pressure.

4.2.4.3 Monotonic Triaxial Tests

Monotonic triaxial tests were performed on samples with mica to sand size ratio of $D_{\text{mica}}/D_{\text{sand}}=1.07$. Dimensions of the samples were 70 mm and 140 mm in diameter and height respectively. Monotonic test samples were isotropically consolidated under 50 kPa, 100 kPa and 200 kPa effective confining pressures. Following the consolidation, they were tested as strain controlled under drained condition in accordance with JGS 0524-2000.

4.2.4.4 Load Controlled Cyclic Triaxial Strength Tests

Load controlled cyclic triaxial strength test was conducted on $D_{\text{mica}}/D_{\text{sand}}=1.07$ and $D_{\text{mica}}/D_{\text{sand}}=4.17$ sand mica mixtures. Diameter and height of samples were 70 mm and 140 mm for $D_{\text{mica}}/D_{\text{sand}}=1.07$ and 50 mm and 100 mm for $D_{\text{mica}}/D_{\text{sand}}=4.17$ respectively. The samples were isotropically consolidated under 100 kPa effective confining pressure. Tests were conducted as load controlled. Dynamic loading was axial compression and axial extension with a sinusoidal shape. Loading frequency was 0.1 Hertz. The tests were terminated once 10% axial deformation level was reached. After the termination of the cyclic loading, post liquefaction volumetric strains were measured. Load controlled cyclic triaxial strength tests were conducted as described in ASTM D5311 standard.

4.2.5 Separation Method of Platy and Non-Platy Grains

Firstly, mineralogical structure of the platy grains was determined with thin section in the Gemology Laboratory of Dokuz Eylül University (Figure 4.14). It was determined during microscopic investigation of the thin section (Figure 4.15 and Figure 4.16) that the platy grains consist of biotite and muscovite mica minerals. It was determined that mica grains mainly consist of muscovite mineral (Figure 4.16) by means of microscopic investigation.



Figure 4.14 A sample of thin section Gediz River Delta sandy soils

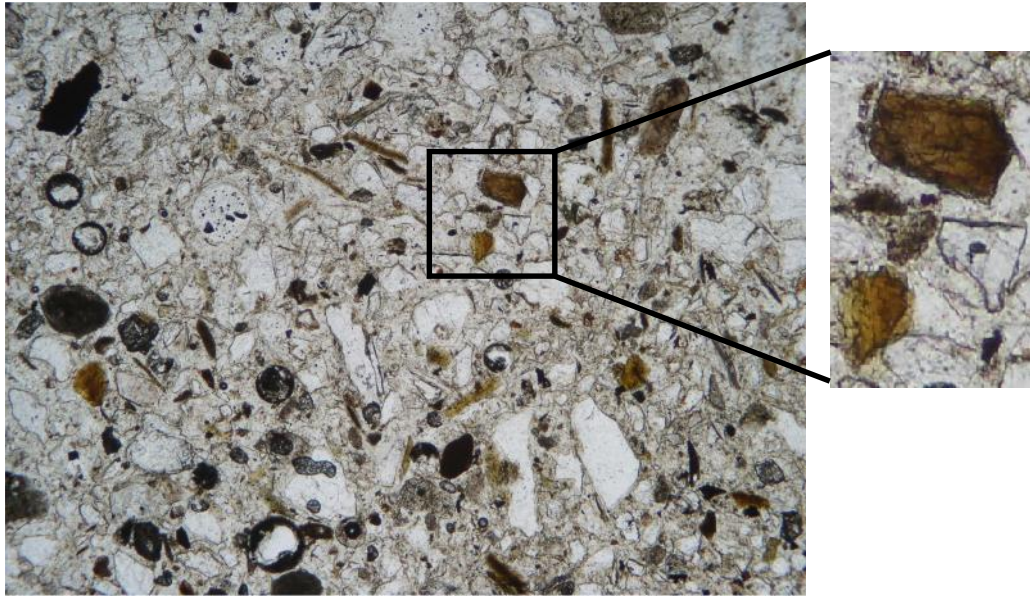


Figure 4.15 View of the thin section under the microscope with Plane-Polarized Light (PPL). The Biotite mica mineral is shown in detailed view

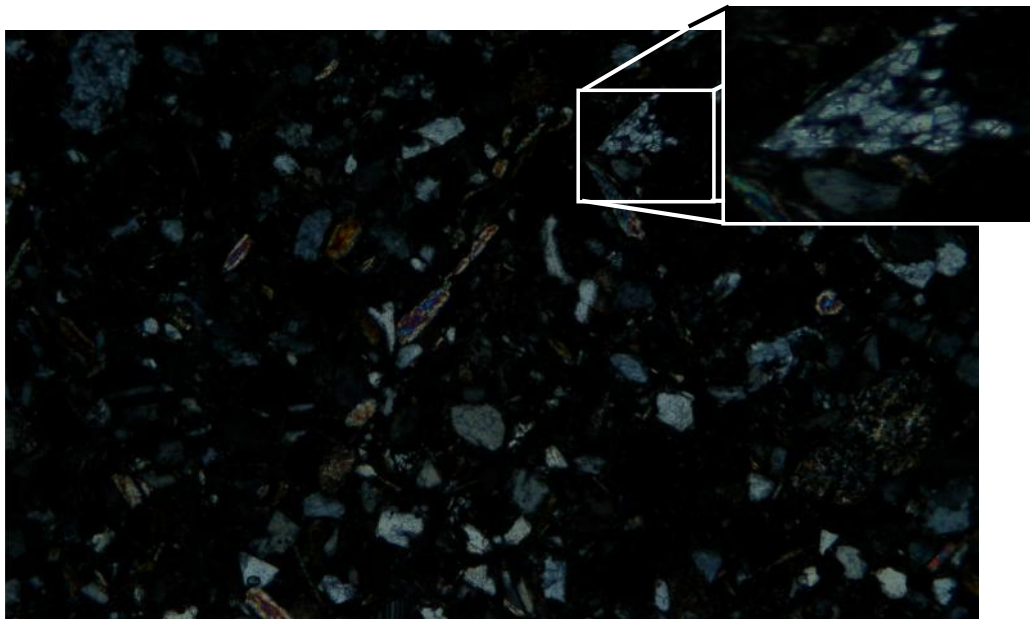


Figure 4.16 View of the thin section under the microscope with Crossed Polars (XPL). The muscovite mica mineral is shown in detailed view

There are few methods for the separation of mica grains. One of the methods is electrostatic separation (Iuga et al., 2004). Firstly, this method was used in the Electrostatic Separation Laboratory of Dokuz Eylül University. Unfortunately, mica minerals could not be separated at desired efficiency. The electrostatic separation machine can be seen in Figure 4.17.



Figure 4.17 Electrostatic separation machine

The other method is flotation technique to separate mica minerals (Geredeli & Özbayo lu, 1995; Bilir et al., 1997). Mica mineral was separated at intended efficiency using flotation technique as described Geredeli & Özbayo lu (1995). Flotation studies were carried out in the Flotation Laboratory of the Dokuz Eylül University.

In the flotation technique, properties of mineral surfaces were altered to a hydrophobic or hydrophilic condition with chemical additive materials. That is, the surface of mineral grains are either repelled or attracted by water. Condition of the created pulp (slurry) provides attachment of pre-determined mineral particles to air bubbles. The air bubbles carry the selected minerals to the surface of the pulp, pre-determined mineral, which is in the froth phase, is skimmed off and collected in a can.

Other minerals remain submerged in the pulp. The flotation process is sketched in Figure 4.18.

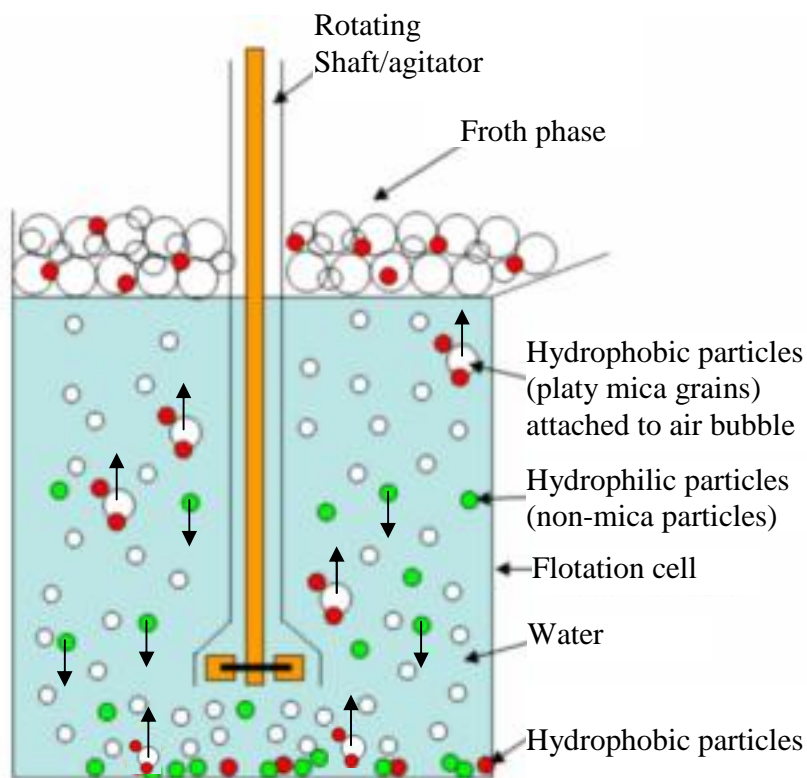


Figure 4.18 Schematic diagram of the flotation process in a froth flotation cell

In the flotation process, grain size distribution of soil materials was in the range of 0.075 mm to 0.212 mm. If the grain size is coarser or finer than these sizes, the platy and non-platy grains cannot be separated with high purity.

Armac-T chemical compound was used in order to alter mica surfaces to a hydrophobic, and Downford chemical compound was used for altering surfaces of non-mica particles to a hydrophilic condition. NaOH was used as pH regulator. pH value of flotation slurry was set at 9.5. During the process, mica minerals were carried to the slurry surface by air-bulbs and they are skimmed in a pot. Froth flotation cell and skimming of the mica minerals can be seen in Figure 4.19.



Figure 4.19 Flotation process and separated mica and non-mica minerals

4.2.6 X-Ray Diffraction (XRD) Tests

When an X-ray hits a crystal, it diffracts in a pattern characteristic of the structure. Since most minerals have unique diffraction patterns, mineralogical structures can be identified using a database of diffraction patterns. A powder X-ray diffractometer consists of an X-ray source (usually an X-ray tube), a sample stage, a detector and a system to vary angle θ . The X-ray is focused on the sample at an angle θ , while the detector opposite the source reads the intensity of the X-ray as it receives at 2θ away from the source path. The incident angle is then increased over time while the detector angle always remains 2θ above the source path (Figure 4.20). Most modern machines use transducers that produce an electrical signal when exposed to radiation. These

detectors are often used as photon counters, so intensities are determined by the number of counts in a certain amount of time. Diffraction patterns (number of counts) are plotted in 2 .

XRD test is widely used to determine mineral content and several other properties of materials. For this purpose, The International Centre for Diffraction Data (ICDD) (www.icdd.com, 2010) was established at 1941. In this dissertation, data of ICDD and methods of Aydal (1990) were used.

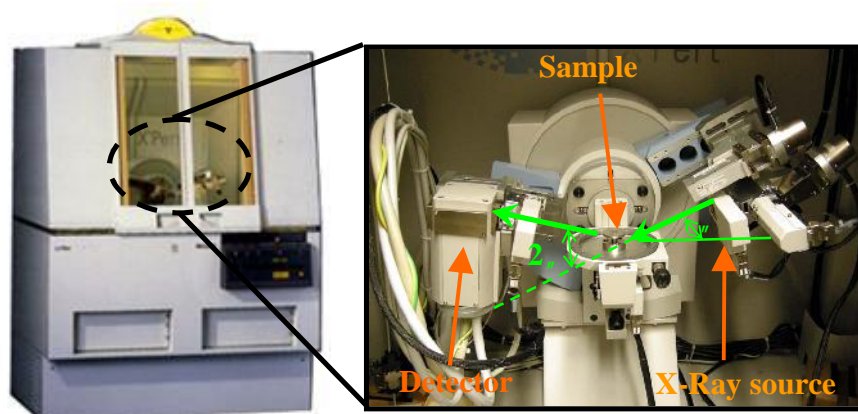


Figure 4.20 X-Ray diffractometer

XRD tests were conducted in zmir Yüksek Teknoloji University Metallurgy (YT-mam) Laboratories. The XRD apparatus was Philips X'Pert Pro diffractometer as shown in Figure 4.20.

In XRD tests, all materials were grinded and sieved from No.200 sieve. Then, the mixtures at certain mica contents (0%, 5% 10%, 20%, 56%, 100%) were prepared. Separated mica and non-mica materials obtained from flotation process were used to prepare the mixtures. XRD apparatus was set as given in Table 4.4. After set up, prepared mixtures were tested, including Old Gediz River Delta samples without changing condition and set up of the apparatus.

Table 4.4 X-RD test properties and conditions

Scan Axis	: Gonio	K-Alpha1 [Å]	: 1.54060
Start Position [°2Th.]	: 5.0167	K-Alpha2 [Å]	: 1.54443
End Position [°2Th.]	: 79.9597	K-Beta [Å]	: 1.39225
Step Size [°2Th.]	: 0.0330	K-A2 / K-A1 Ratio	: 0.50000
Scan Step Time [s]	: 10.0348	Generator Settings	: 40 mA, 45 kV
Scan Type	: Continuous	Diffractometer Type	: 0000000080920022
PSD Mode	: Scanning	Diffractometer Number	: 0
PSD Length [°2Th.]	: 2.12	Goniometer Radius [mm]	: 240.00
Offset [°2Th.]	: 0.0000	Divergence Slit Type	: Fixed
Measurement Temperature [°C]	: 25.00	Divergence Slit Size [°]	: 0.4785
Incident Beam Monochromator	: No	Specimen Length [mm]	: 10.00
Dist. Focus-Diverg. Slit [mm]	: 91.00	Spinning	: No
Anode Material	: Cu		

Count values at $2\theta=8.82^\circ$ of mixtures were used to correlate mica content and count value. The correlation between mica content and count value was used to determine mica content of the field samples. The count values (for $2\theta=8.82^\circ$) of test samples and correlations are given in the following chapter.

4.2.7 Bender Element Test

Bender element test is one of the foremost experiments used in determining shear wave velocity, thereby to determine small-strain shear modulus (G_{\max}), which is considerably important in terms of earthquake geotechnical engineering. G_{\max} is employed in the design of foundations under dynamic loads, modeling of dynamic behavior of soils and, quality control of improved soils (Lee & Santamarina, 2005).

Bender element test is conducted by means of an oscilloscope (or a computer utilized as an oscilloscope), a signal generator and two piezoelectric tips (assembled in a way that is inside the sample) on lower and upper caps of the test sample,. Piezoelectric materials convert electric voltage applied on them into bending deflection or vice versa. Electric voltage is applied on one of the piezoelectric tip via signal generator and the applied electric voltage generates bending deflection in the piezoelectric element (Figure

4.21). Depending on the design of piezoelectric element, bending deflection on the bender element generates shear or pressure wave within the soil. Piezoelectric tip that generates shear or pressure wave is called transmitter. Shear or pressure wave produced at one end progresses within the soil and reaches the other tip which is called the receiver. Wave generates a bending deflection in the receiver. Consequently, bending deflection is converted to electric voltage by the receiver.

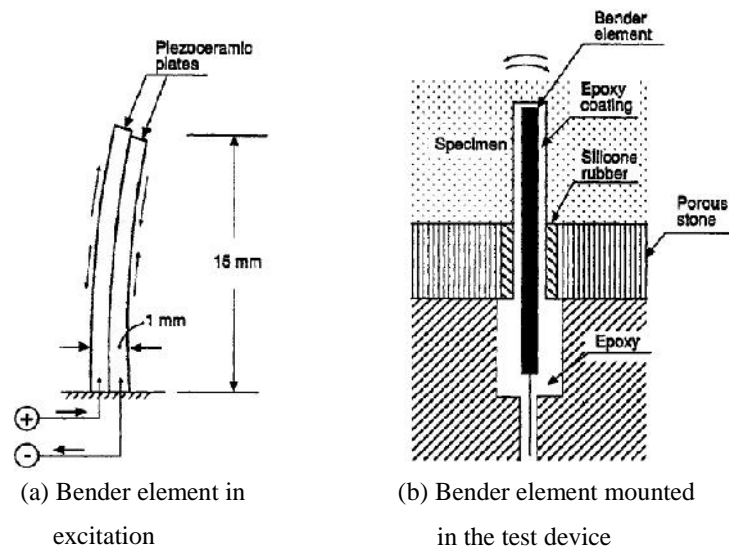
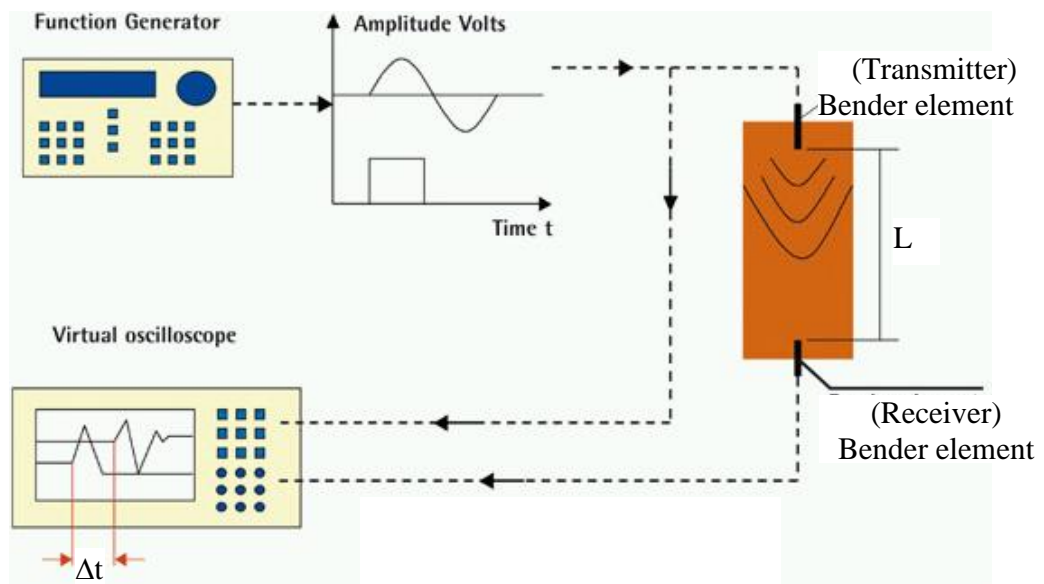


Figure 4.21 Details of bender element (Ishihara, 2003)

The signal is created by voltage excitation produced by the signal generator. Produced signal is simultaneously send to the oscilloscope and transmitter tip. Signal, which is send to the oscilloscop, directly reaches to the oscilloscop. Signal, which is send to the transmitter, passes through the samples then reaches to the oscilloscop (Figure 4.22). A time difference occurs between two signals, which are reached to the oscilloscop. This time difference is the traveling time of the wave within the soil. Wave velocity within the soil is found by dividing the distance between bender elemet tips to the time difference (travelling time).

The moist tamping method was employed on all samples prepared for bender element tests. All samples were saturated before the bender element test and isotropically consolidated. The amplitude of the signal used in the bender element test was 20 mV.



$$V_s = L / \Delta t$$

L: Length of transmitter to receiver

Δt : Time lag

ρ : Density (ρ : saturated unit weight / acceleration of gravity)

$$G_{\max} = V_s^2 \cdot \rho$$

V_s : Shear wave velocity

G_{\max} : Maximum shear modulus

Figure 4.22 Schematic diagram of the bender element test devices.

CHAPTER FIVE

TEST RESULTS

5.1 Mica Content of Old Gediz River Delta Sandy Soils

Mineralogical structure of natural platy grains was explored at first hand. For this purpose, thin sections were prepared and analyzed in Gemology laboratory of Dokuz Eylül University. As a result of these analyses, it was detected that platy grains mainly consist of mica mineral. After the determination of mineralogical structure of platy grains, mica grains were separated using flotation technique, as presented in Chapter 4. Then mica contents of sandy field samples were determined using X-Ray Diffraction (XRD) analyses.

After determination of platy mica grains in the field samples, various methods (examination of thin section, separation using materials of various with difference of specific gravities, electrostatic separation, flotation technique, X-Ray Fluorescence test, and X-Ray Diffraction test) were employed to separate and to determine mica content of field samples. The most efficient results were obtained with flotation technique as described in the previous chapter. X-Ray Diffraction test was utilized to determine mica content of the field samples.

In order to determine mica content of samples, mixtures presented in Table 5.1 were prepared by mixing separated mica and non-mica materials. The XRD tests were performed on prepared mixtures. Analyses of XRD tests showed that there was a linear correlation between XRD count values and mica percentage of samples. Then, using this correlation, mica content of sandy field samples was determined. The linear regression by means of least squares method is given in Figure 5.1 and Equation 5.1. The peak value of mica mineral at $2\theta=8.815^\circ$ was used in developing this correlation since the highest ($2\theta=26.566^\circ$) peak value of mica mineral overlapped with one of the peak of quartz mineral.

Table 5.1 Prepared mica - sand mixtures and XRD count values

Sample No	Mica content of prepared mixtures (%)	Count values at $2\theta=8.815^\circ$
1	0	247
2	5	733
3	10	1420
4	20	2297
5	38	5260
6	56	6657
7	77	6830
8	100	9985

$$MC = 9.84 \times 10^{-3} X_{cv} \quad (5.1)$$

MC: Mica Content (%); X_{cv} : XRD count value

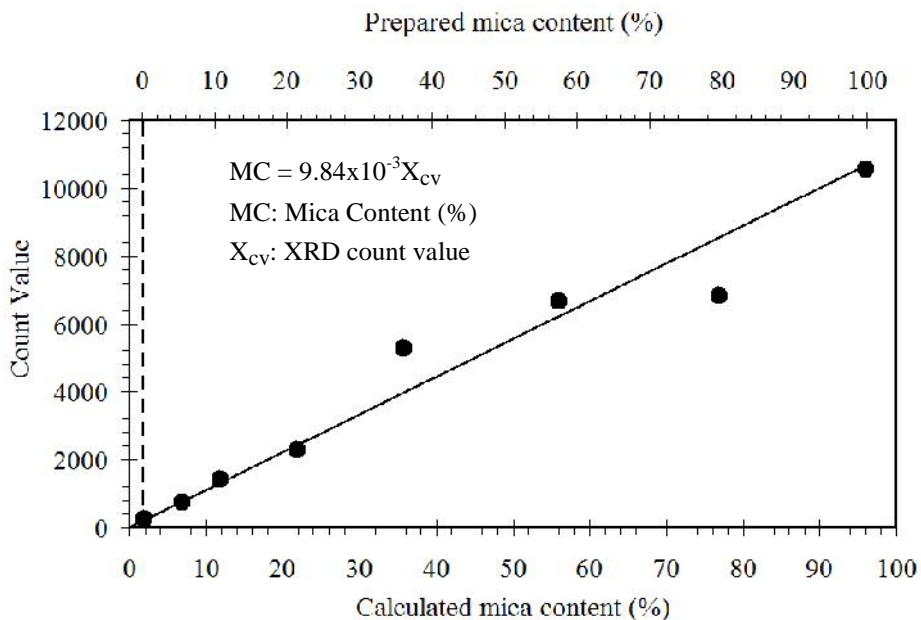


Figure 5.1 Relation of mica content and XRD count values of prepared mixtures

XRD count values of the field samples (for $2\theta=8.815^\circ$) are presented in Table 2. Variation of mica content by depth pertaining to 12-MV , 10-KSK, and 06-BOS

boreholes are calculated using Equation 5.1. Mica content of investigated site soils are presented in Table 5.2 and Figure 5.2. When Table 5.2 is examined, relation between depth and mica content of site soils can be seen. Linear correlations, established by means of the least squares method, between depth and mica content (MC) of regional soils are presented in Figure 5.2. Equation 5.2, 5.3 and 5.4 represent variation of mica content with depth for Site-1, Site-2 and Site-3 soils, respectively.

Table 5.2 XRD tests results and mica content of field samples

Boreholes								
SITE-1			SITE-2			SITE-3		
12-MV & ESK-1			06-BOS & ESK-2			10-KSK & ESK-3		
Depth	Count Value	Mica Content	Depth	Count Value	Mica Content	Depth	Count Value	Mica Content
(m)		(%)	(m)		(%)	(m)		(%)
5.4	539	5.3	12.0	741	7.3	4.7	742	7.3
7.1	524	5.2	13.3	963	9.5	7.4	823	8.1
8.7	1031	10.1	25.5	897	8.8	9.7	1044	10.3
10.2	1602	15.8				10.5	1108	10.9
13.0	1966	19.3				11.3	742	7.3
16.3	2229	21.9				16.5	996	9.8
25.0	2697	26.5				18.8	2082	20.5
						22.5	1443	14.2
						26.3	1798	17.7

$$MC=2.2z - 8.5 \quad z \leq 12.4 \text{ m} \quad (\text{Site-1}) \quad (5.2)$$

$$MC=0.6z + 12.0 \quad z > 12.4 \text{ m} \quad (\text{Site-1})$$

$$MC=0.046z + 7.7 \quad (\text{Site-1}) \quad (5.3)$$

$$MC=0.52z + 4.4 \quad (\text{Site-2}) \quad (5.4)$$

Where z is the depth in meter, MC is the mica content in percent by weight.

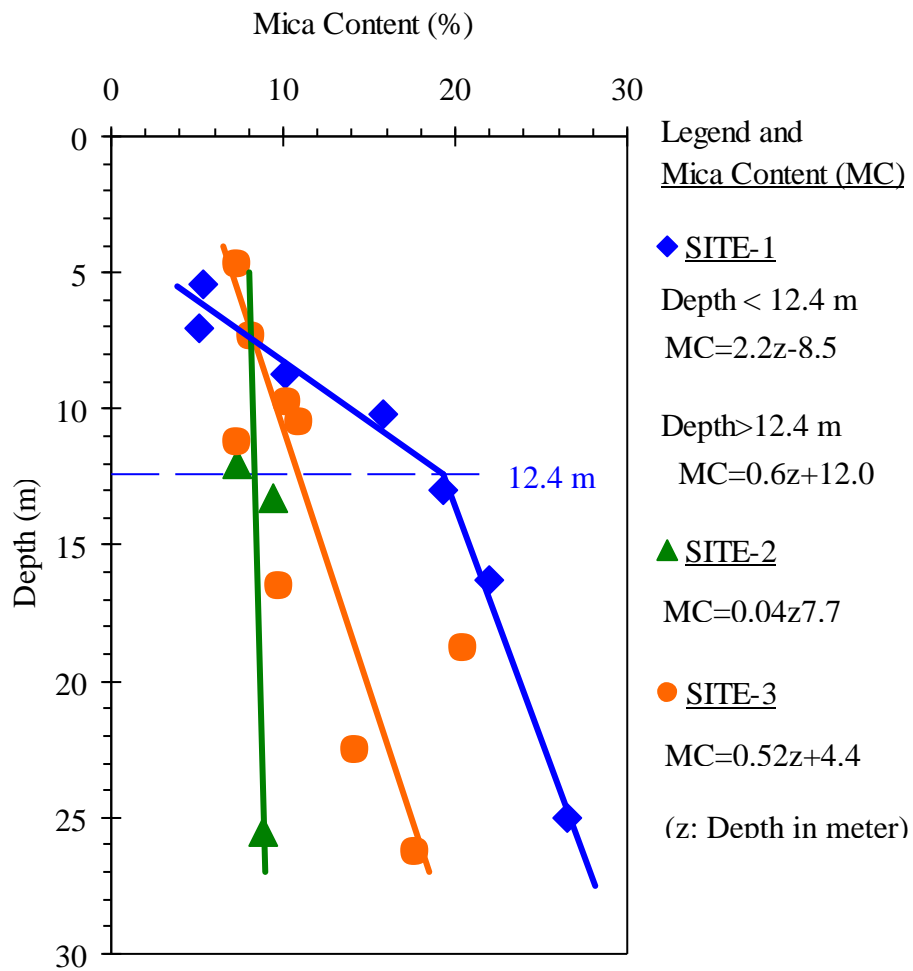


Figure 5.2 Variation of mica content of field samples with depth at Gediz River Old Delta

In the light of performed analyses, it was determined that the average mica content is about 12%. The mica content of the Old Gediz River Delta is between 5%~25% within in the liquefaction depth interval (0 m - 20 m) for silty sand layers.

5.2 Standard Penetration Test Results

Standard Penetration Tests were performed in eight boreholes, which were shown in Figure 4.5 as described in previous chapter. Uncorrected blow counts of the standard penetration tests are given in Table 5.3, where, percent of coarse and fine materials are also presented.

Table 5.3. Standard Penetration Test results and index properties of SPT samples

Test (Point) No	Depth (z) (m)	SPT-N (Blow Counts) (15 ^{cm} -45 ^{cm})	Sand & Fine Material (<4.75 ^{mm}) (%)	Fines Content (<0.075 ^{mm}) (%)	Gravel (%)	Sand (%)	GWT (m)	Borehole		SITE
								Name	No	
1	8.3	13	100.0	42.5	0.0	57.5	0.5	12-MV	2	SITE-1
2	7.7	19	99.6	12.9	0.4	86.8	0.7	ESK-1	86	
3	20.3	22	70.1	19.2	29.9	50.9				
4	4.7	22	99.7	16.7	0.3	83.1	0.5	24-MV	80	
5	6.3	23	98.2	11.8	1.8	86.4				
6	18.3	16	93.9	24.0	6.1	69.8				
7	21.3	12	95.6	35.5	4.4	60.1				
8	1.7	9	88.9	32.1	11.1	56.8				
9	4.7	17	98.6	17.0	1.4	81.6	0.7	ESK-4	89	
10	6.3	13	94.1	19.0	5.9	75.2				
11	7.7	31	99.5	14.5	0.5	85.0				
12	9.3	23	98.1	6.75	2.0	91.3				
13	10.7	13	89.1	6.9	10.9	82.2				
14	7.8	14	100.0	43.3	0.0	56.8	2.1	06-BOS	4	SITE-2
15	10.8	22	100.0	49.7	0.0	50.2				
16	13.8	12	97.3	40.1	2.7	57.8				
17	9.3	13	100.0	41.2	0.0	58.9	2.1	ESK-2	87	
18	10.7	13	100.0	47.9	0.0	52.4				
19	1.8	15	81.3	22.4	18.7	58.9	1.0	10-KSK	1	SITE-3
20	3.3	12	92.2	10.6	7.8	81.6				
21	4.8	18	90.0	15.0	10.0	75.0				
22	6.3	16	99.3	15.0	0.7	84.3				
23	7.8	14	98.2	28.6	1.8	69.6				
24	9.3	20	89.4	8.8	10.6	80.6				
25	10.8	17	98.0	10.0	2.0	88.0				
26	15.4	12	97.1	47.2	2.9	50.0				
27	19.8	8	99.8	31.3	0.2	68.5				
28	21.3	11	98.0	30.0	2.0	68.0				
29	23.3	19	100.0	48.0	0.0	52.0				
30	24.3	21	99.7	48.5	0.3	51.2				
31	25.8	14	97.0	42.0	3.0	55.0				
32	27.3	18	96.6	37.0	3.4	59.6				
33	6.3	20	100.0	43.6	0.0	56.5	1.0	ESK-3	88	
34	9.3	12	100.0	42.9	0.0	57.2				
35	20.3	34	78.0	18.2	22.1	59.7				

SPT blow counts were normalized in order to eliminate the overburden stress, fines content, rod length, borehole diameter, sampling method and energy ratio effects. Corrections of SPT blow counts were made according to NCCER (1997) and Youd & Idriss (2001) (see Chapter 4). Mica content (MC) of the tested soil samples were determined using Equations 5.2, 5.3 and 5.4. Size ratio of the mica and sand grains ($D_{\text{mica}}/D_{\text{sand}}$) is found as 1.07 (Figure 4.1 and Table 4.1). Corrected SPT blow counts, correction coefficients and calculated mica content of the tested samples are given in Table 5.4.

Table 5.4 Corrected (normalized) SPT blow counts and Mica content of SPT samples

Test (Point) No	Depth (z) (m)	Correction Coefficients						$(N_1)_{60cs}$	Mica Content (%)	
		C_N	C_E	C_B	C_R	C_S	α			β
1	8.3	1.10			0.95		5.0	1.20	21	10.1
2	7.7	1.12			0.95		1.8	1.04	23	8.8
3	20.3	0.71			1.00		3.5	1.07	20	23.9
4	4.7	1.43			0.85		2.9	1.06	31	2.5
5	6.3	1.25			0.95		1.5	1.03	30	5.6
6	18.3	0.75			1.00		4.2	1.11	17	22.7
7	21.3	0.70			1.00		5.0	1.20	15	24.5
8	1.7	2.00			0.75		4.8	1.17	21	2.5
9	4.7	1.41			0.85		3.0	1.06	25	2.5
10	6.3	1.23			0.95		3.4	1.07	20	5.6
11	7.7	1.12			0.95		2.3	1.04	37	8.8
12	9.3	1.03			0.95		0.1	1.01	23	12.4
13	10.7	0.96			1.00		0.1	1.01	13	15.5
14	7.8	1.04			0.95		5.0	1.20	22	8.1
15	10.8	0.91			1.00		5.0	1.20	29	8.2
16	13.8	0.82			1.00		5.0	1.20	17	8.4
17	9.3	0.97			0.95		5.0	1.20	19	8.2
18	10.7	0.91	1.0	1.0	1.00	1.0	5.0	1.20	19	8.2
19	1.8	1.98			0.75		4.0	1.10	28	5.4
20	3.3	1.58			0.80		1.1	1.02	17	6.2
21	4.8	1.36			0.85		2.5	1.05	24	6.9
22	6.3	1.21			0.95		2.5	1.05	22	7.7
23	7.8	1.10			0.95		4.6	1.14	21	8.5
24	9.3	1.02			0.95		0.5	1.02	20	9.3
25	10.8	0.95			1.00		0.9	1.02	17	10.0
26	15.4	0.80			1.00		5.0	1.20	17	12.4
27	19.8	0.71			1.00		4.8	1.17	11	14.7
28	21.3	0.69			1.00		4.7	1.15	13	15.5
29	23.3	0.66			1.00		5.0	1.20	20	16.5
30	24.3	0.65			1.00		5.0	1.20	21	17.0
31	25.8	0.63			1.00		5.0	1.20	16	17.8
32	27.3	0.61			1.00		5.0	1.20	18	18.6
33	6.3	1.21			0.95		5.0	1.20	33	7.7
34	9.3	1.02			0.95		5.0	1.20	19	9.3
35	20.3	0.70			1.00		3.3	1.07	29	15.0
$\gamma_{\text{water}}=10 \text{ kN/m}^3$					$\gamma_{\text{n-soil}}=18.0 \text{ kN/m}^3$					
$P_a=100 \text{ kPa}$					$\gamma_{\text{sat}}=19.5 \text{ kN/m}^3$					

Influence of platy mica grains on corrected (normalized) SPT blow counts can be seen in Figure 5.3. Mica content affects SPT blow counts linearly. The linear relationship between mica content and corrected SPT blow counts can be written as in Equation 5.5 obtained using least squares method (Equation 5.5).

$$(N_1)_{60cs} = -0.43MC + 25.71 \quad (5.5)$$

Any increase (ΔMC) in mica content of sandy soils reduces $(N_1)_{60cs}$ by $(\Delta(N_1)_{60cs})$ as seen Figure 5.3. $\Delta(N_1)_{60cs}$ can be calculated using Equation 5.6 and 5.7.

$$(N_1)_{60cs} + \Delta(N_1)_{60cs} = -0.43(MC + \Delta MC) + 25.71 \quad (5.6)$$

$$\Delta(N_1)_{60cs} = -0.43\Delta MC \quad (5.7)$$

The equivalent corrected blow count for Old Gediz River Delta sandy soils can be estimated by using Equation 5.8.

$$(N_1)_{60cs \text{ (without mica)}} = (N_1)_{60cs} - 0.43\Delta MC \quad (5.8)$$

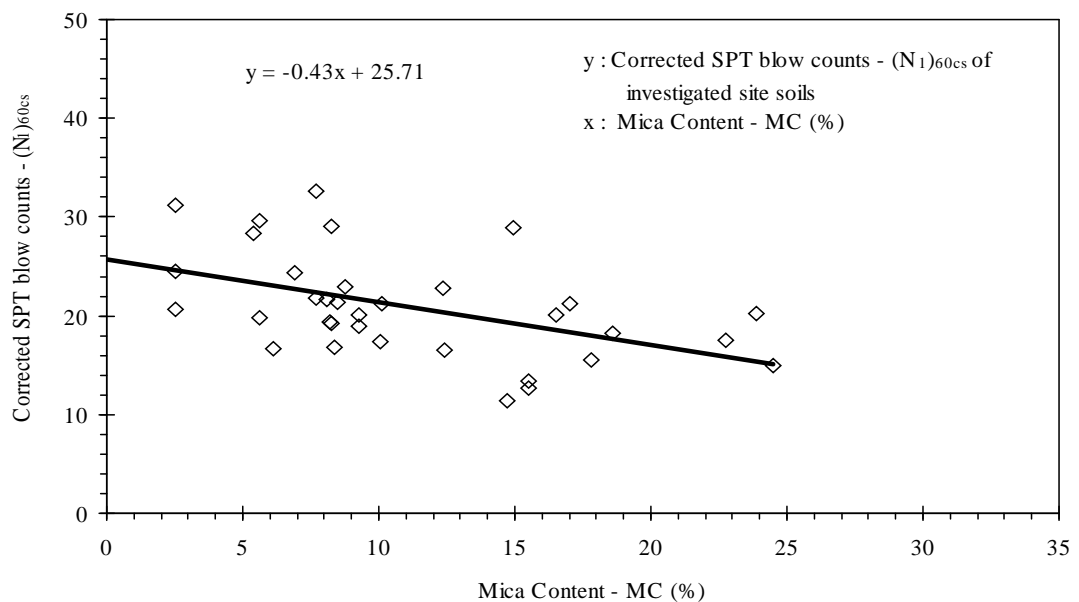


Figure 5.3 Relation of mica content and corrected (normalized) SPT blow counts of Old Gediz River Delta sandy soils

According to Equation 5.5, the estimated SPT blow count normalized with respect to an effective stress level of 100 kPa is estimated approximately 26 when MC is 0% for the depth interval of 2.0~20.0 m. This can be seen in Figure 5.3 for MC=0%.

The necessary horizontal acceleration a_{max}/g for liquefaction can be calculated according to modified Seed & Idriss method (NCEER, 1997; Youd & Idris, 2001) for $(N_1)_{60cs}=26$. Equation 5.9 expresses the case where $F_s=1$.

$$CSR = (CRR_{7.5})MSF \quad (5.9)$$

Equation 2.20 and 2.22 are substituted in Equation 5.9 and the equation arranged according to (a_{\max}/g) can be written as:

$$\frac{a_{\max}}{g} = \frac{\dagger'_{vo}}{\dagger_{vo}} \frac{CRR_{7.5}}{r_d} \frac{10^{2.24}}{M_w^{2.56}} \quad (5.10)$$

In the Equation 5.10, \dagger'_{vo} and \dagger_v were calculated for the case where $\gamma_{\text{sat}}=19.5$ kN/m^3 , $\gamma_w=10.0$ kN/m^3 and ground water level = 0.5 m. r_d and M_w found using according to Equation 2.18 and 2.22, respectively. $CRR_{7.5}$ depends on $(N_1)_{60cs}$. $(N_1)_{60cs}$ was taken as 26 for clean sand and $(N_1)_{60cs}$ was calculated using Equation 5.5 for other mica contents. a_{\max}/g values corresponding to liquefaction initiation are presented in Figure 5.4. As one can notice in Figure 5.4, $(a_{\max}/g)_n$ decreases with mica content (MC) for all earthquake magnitudes (M_w).

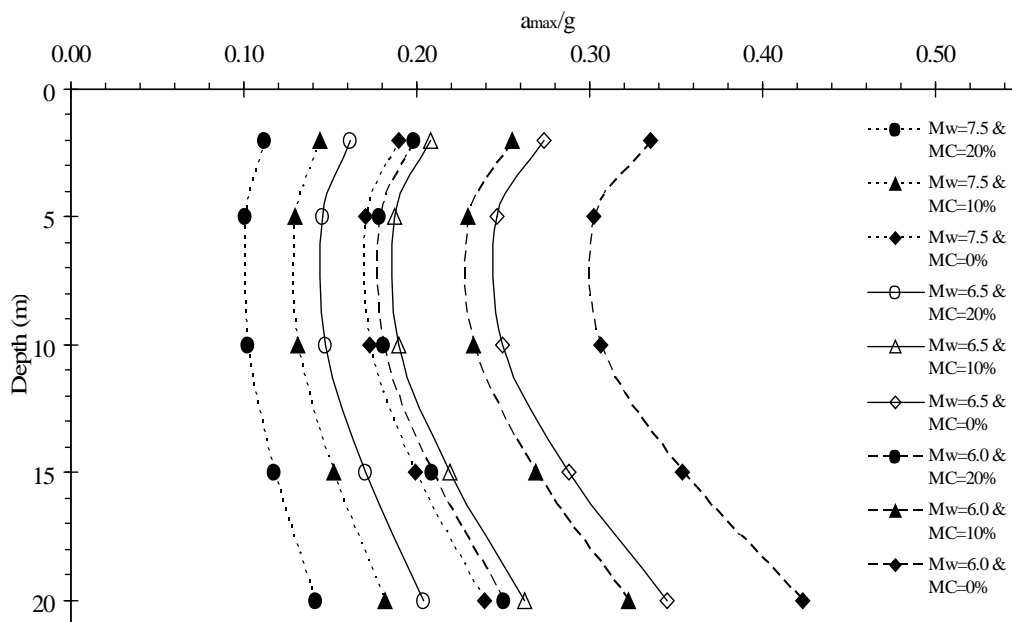


Figure 5.4 Effect of the mica content on liquefaction susceptibility of Old Gediz River Delta sandy soils.

5.3 Minimum and Maximum Void Ratios of Sand-Mica Mixtures

Sand and mica were mixed at different percentages by weight. Accordingly, prepared mixtures are given in Table 5.5, along with their maximum and minimum void ratios. The specific gravity, dry unit weight and D_{mica}/D_{sand} ratios are also given in the same table.

Table 5.5 Maximum and minimum void ratios of the test mixtures

D_{sand}/D_{mica}	Mica Content (%)	$G_{sand}:2.665$		$G_{mica}:2.805$		e_{min}	e_{max}
		G_s	$\gamma_{max-dry}$	$\gamma_{min-dry}$	e_{min}		
			(gr/cm^3)	(gr/cm^3)			
1.07	0.0	2.67	1.54	1.23	0.741	1.163	
	1.5	2.67	1.54	1.22	0.725	1.184	
	2.5	2.67	1.56	1.21	0.713	1.205	
	5.0	2.67	1.56	1.18	0.703	1.257	
	10.0	2.68	1.54	1.12	0.736	1.368	
	15.0	2.69	1.53	1.10	0.757	1.453	
	20.0	2.69	1.50	1.06	0.771	1.502	
4.17	0.0	2.67	1.46	1.045	0.825	1.550	
	2.0	2.67	1.44	1.03	0.859	1.592	
	5.0	2.67	1.42	0.99	0.878	1.701	
	10.0	2.68	1.40	0.90	0.909	1.993	
	15.0	2.69	1.35	0.90	0.990	2.000	
	20.0	2.69	1.32	0.86	1.044	2.130	

(D_{mica} : Average diameter of mica grains in mixture, D_{sand} : Average diameter of sand grains in mixture, G : Specific gravity, γ : Unit weight, e_{min} and e_{max} : minimum and maximum void ratios)

Coefficients of uniformity of sand and mica materials are less than 2.0 (Table 4.1). Grain size distributions of the materials are uniform. Therefore, the relevance of grain size distribution on packing density is not pronounced. Variation of extreme void ratios as a function of mica content is plotted in Figure 5.6a and 5.6b. One can notice that both e_{max} and e_{min} increase with mica content. This increasing trend is more visible for e_{max} . There is also a similar trend when D_{mica}/D_{sand} ratio is considered. Extreme void ratio variation is larger for mixtures with $D_{mica}/D_{sand}=4.17$. The above explained variations of extreme void ratios can be better followed in Figure 5.7 where $I_e=e_{max} - e_{min}$ is plotted with respect to mica content.

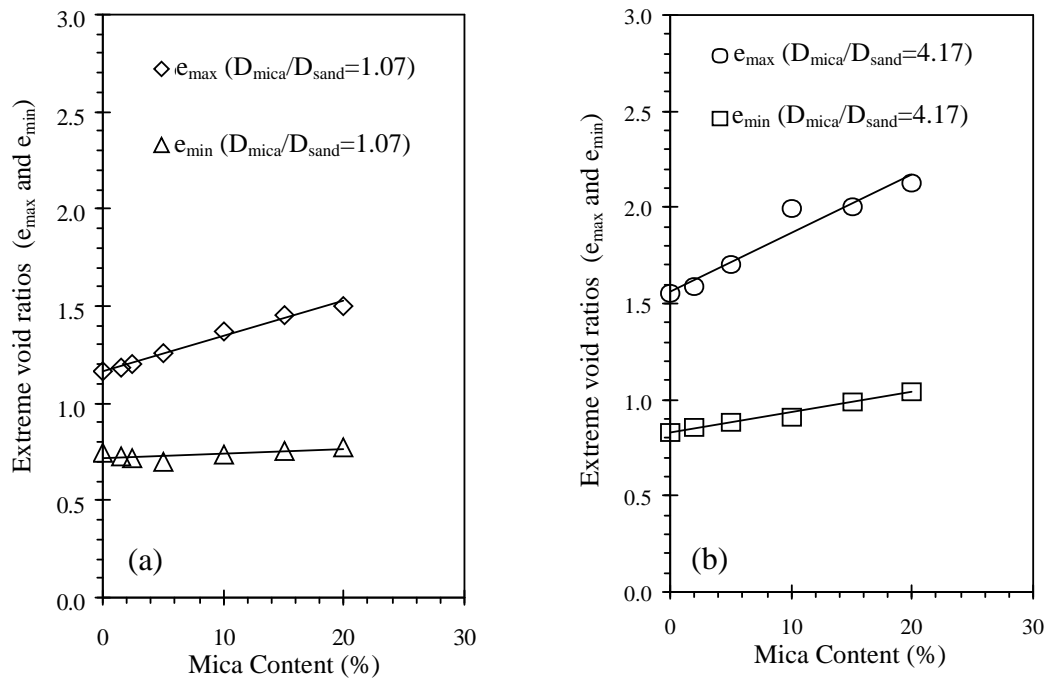


Figure 5.6 Extreme void ratios of sand-mica mixtures (a) separated materials using flotation technique (b) Gediz River bed sand with commercially supplied mica materials

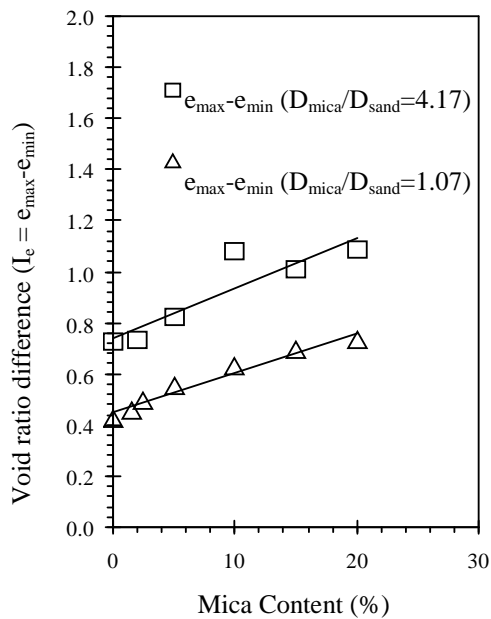


Figure 5.7 Extreme void ratios of sand-mica mixtures (a) separated materials using flotation technique (b) Gediz River bed sand with commercially supplied mica materials

Similar observations can be found in Cho et al. (2006), Guimaraes (2002), Lee et al. (2007) and Santamarina & Cho (2004). Platy mica grains bridge over gaps over

among sand grains generating relatively large voids. Such voids around mica grains increase the maximum and minimum void ratios. Change in e_{\max} is greater than the change in e_{\min} . This indicates that in the loose state mica grains can generate more gaps than they do in the dense state. Some unstable mica bridges are probably collapsed in dense state. Maximum and minimum void ratio test results showed that mica grains are more effective when the sand samples are in loose state.

5.4 Internal Friction Angles of Sand Mica Mixtures

In order to study influence of mica grains on shear strength parameters of sand-mica mixtures, monotonic triaxial tests were performed under consolidated drained (CD) test condition. Consolidation pressures of 100, 150, 200 kPa were applied to test specimens. Testing program is summarized in Table 5.6. Test results are presented in Figures 5.8 thru 5.15 in terms of stress–strain and volumetric strain versus axial strain curves.

Table 5.6 Monotonic triaxial test specimens

Mica Content (MC) (%)	1.5											
Set No:	1			2			3			4		
Relative Density (D_r) (%)	41.9			57.5			67.6			81.0		
	42.1	42.1	41.5	57.1	58.3	57.1	68.2	67.8	66.8	80.1	81.6	81.3
Cell Pressure (σ_3) (kPa)	100	150	200	100	150	200	100	150	200	100	150	200
Mica Content (MC) (%)	10											
Set No:	5			6			7					
Relative Density (D_r) (%)	43.4			54.1			78					
	43.4	43.3	43.5	54.5	54.0	53.8	77.7	78.1	78.2			
Cell Pressure (σ_3) (kPa)	100	150	200	100	150	200	100	150	200			
Mica Content (MC) (%)	20											
Set No:	8			9			10					
Relative Density (D_r) (%)	43.5			60.5			77.6					
	44.3	42.9	43.0	60.2	60.8	60.5	78.4	77.5	76.9			
Cell Pressure (σ_3) (kPa)	100	150	200	100	150	200	100	150	200			

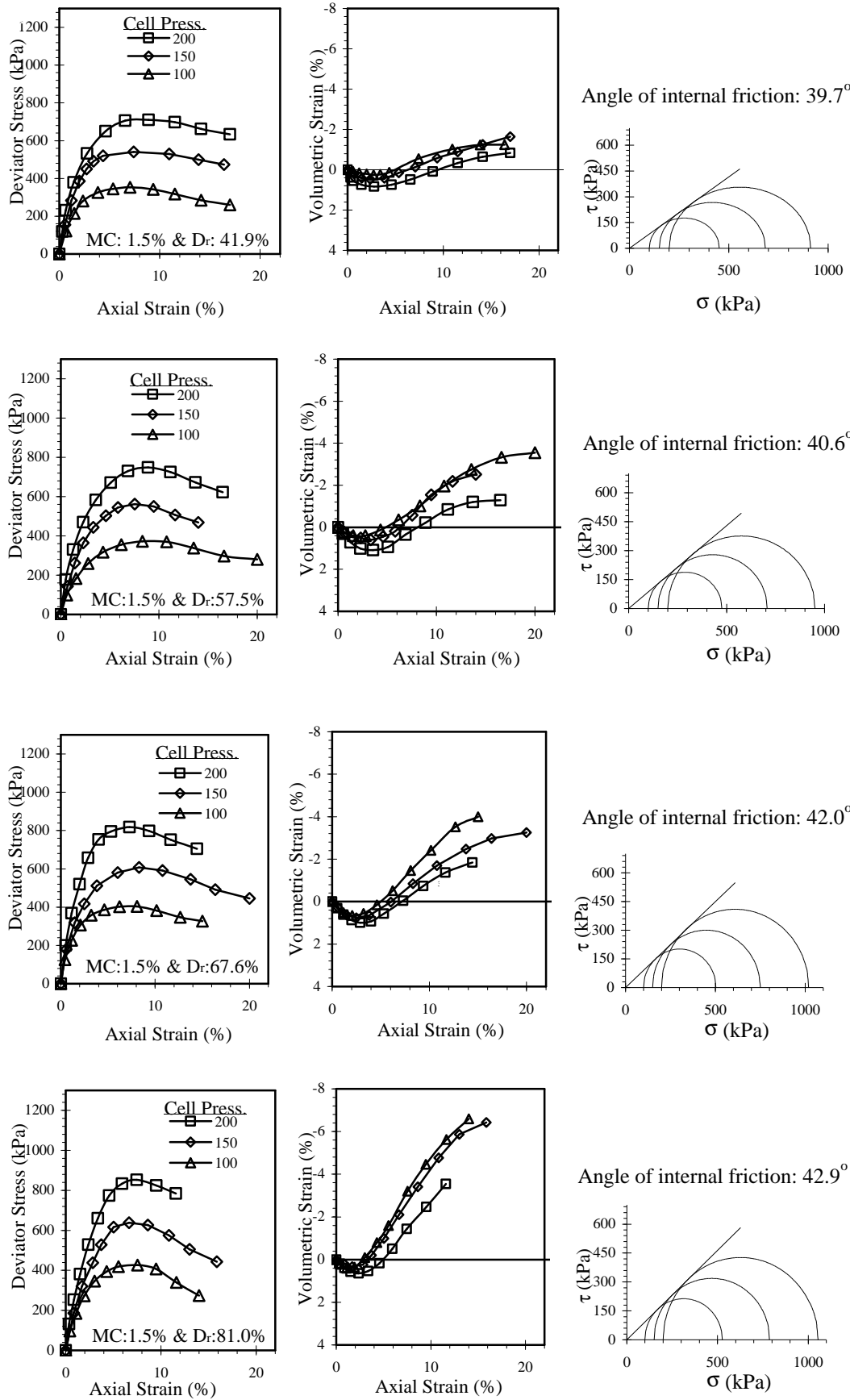


Figure 5.8 Triaxial compression tests results of clean sand (MC=1.5%)

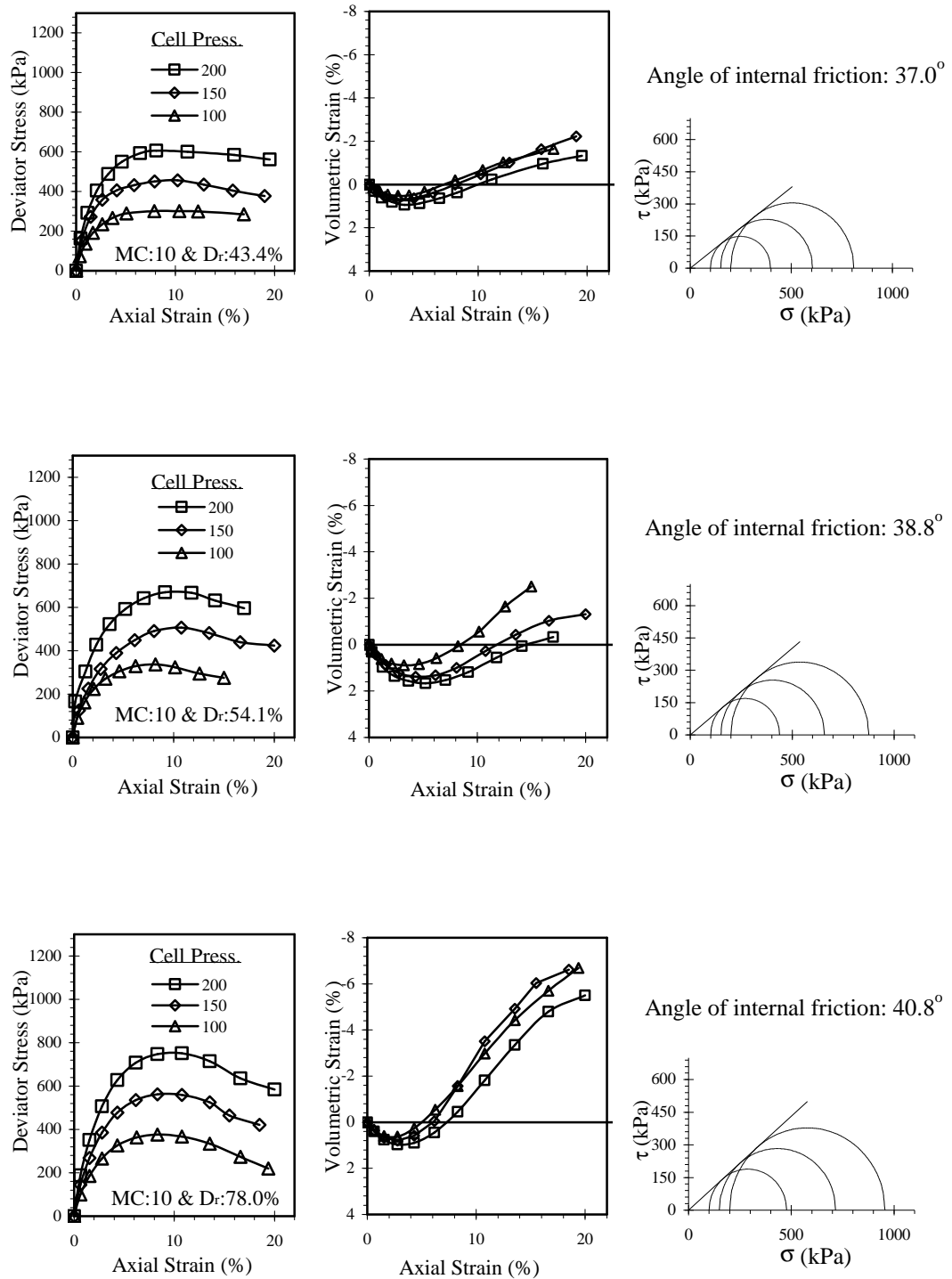


Figure 5.9 Triaxial compression tests results of sand – 10% mica mixtures

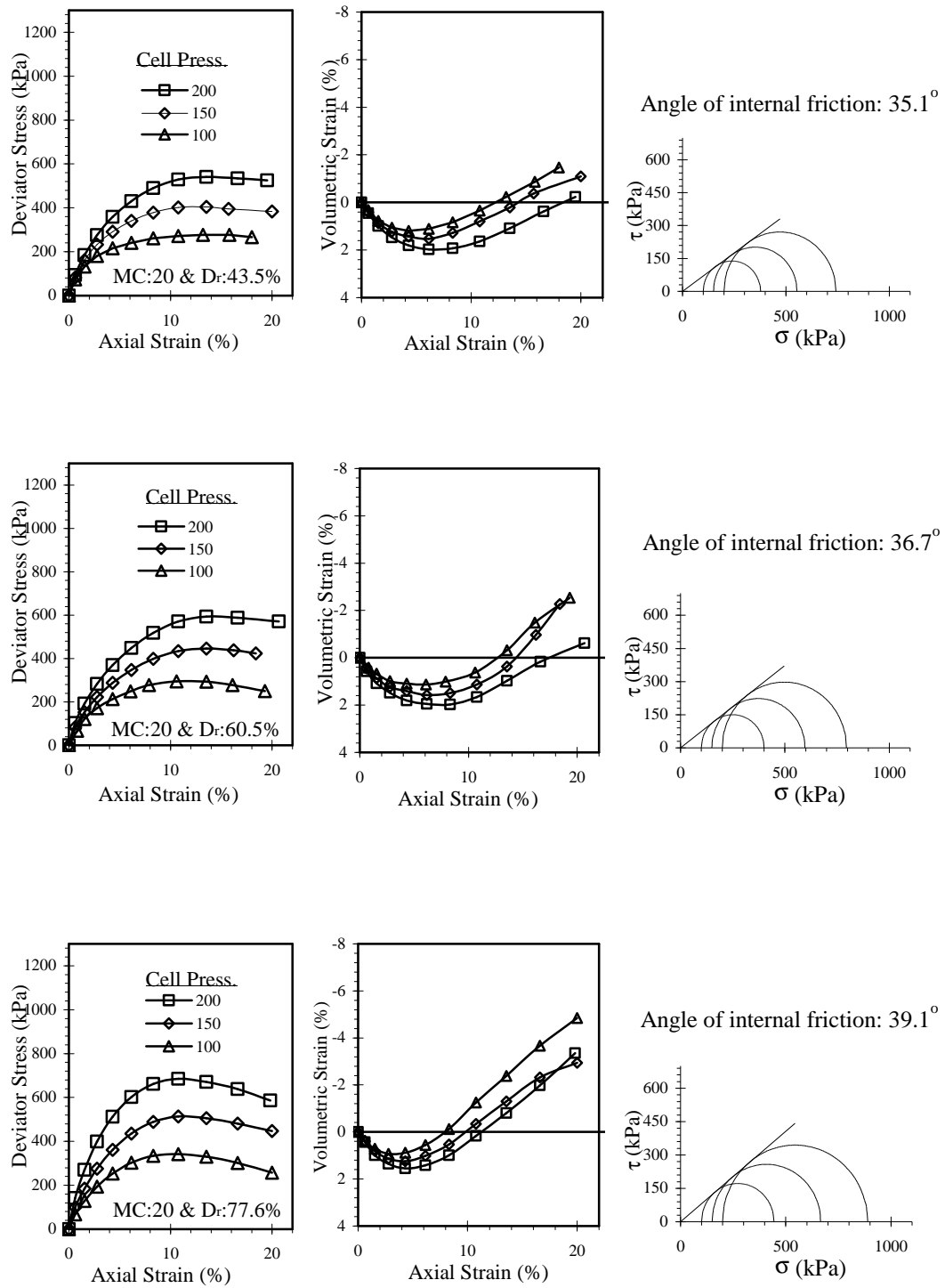


Figure 5.10 Triaxial compression tests results of sand – 20% mica mixtures

In addition to triaxial compression tests, loose deposition of sand piles by means of air pluviation method were also performed in order to determine repose angles of sand–mica mixtures. Mixtures were prepared at mica contents of 1.5%, 5%, 10% and 20%. Nozzle of the pluviation cap was 5 mm and pluviation height was 3.0 cm. Repose angle of the sand–mica mixtures were measured with a protractor (Figure 4.6). Densities of air–pluviated sand-mica mixtures were determined using a cylindrical container. The sands were pluviated into the container from same height (3 cm). Then void ratio and relative densities of the pluviated sands were determined measuring weight and volume of the sand. Relative densities of the air-pluviated 1.5%, 5%, 10% and 20% sand-mica mixtures were found as 27.8%, 27.0%, 26.0 and 24.8, respectively.

Angle of friction (ϕ) values of the sand-mica mixtures are presented in Table 5.7 and Figure 5.11. The friction angles determined by means of triaxial compression tests are slightly higher than repose angles. Friction angle of the sand decreased with increasing mica content (Figure 5.11). For example, 20% mica content caused $\sim 5.0^\circ$ decrease in friction angle at 42% relative density ($D_r=42\%$) and $\sim 3.5^\circ$ for $D_r=78\%$. Decrease of the friction angle with mica content and relative density is illustrated in Figure 5.12.

Table 5.7 Angle of internal friction of sand–mica mixtures

Angles of Repose			Triaxial test results					
Mica Content (%)	D_r (%)	ϕ ($^\circ$)	Mica Content (%)	D_r (%)	ϕ ($^\circ$)	ϕ ($^\circ$)	ϕ ($^\circ$)	ϕ ($^\circ$)
1.5	27.8	36.8	1.5	41.9	57.5	67.6	81.0	
	27.8	37.4		39.7	40.6	42.0	42.9	
5	27.0	35.9	10	43.4	54.1	78.0		
	27.0	35.7		37.0	38.8	40.8		
10	26.0	34.4	20	43.4	60.5	77.6		
	26.0	34.7		35.1	36.7	39.1		
20	24.8	32.4						
	24.8	32.2						

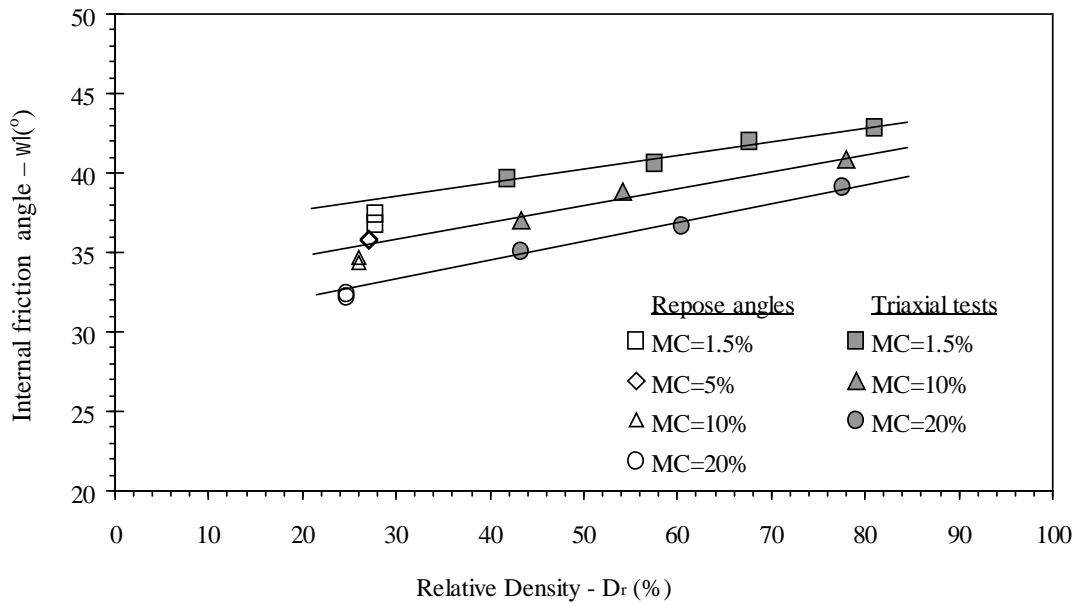


Figure 5.11 Internal frictional angles of sand–mica mixtures as obtained in drained triaxial tests

Harris et al. (1984a) and Lee et al, (2007) explored mica effects on shear strength of sand. Unfortunately, relative density information is not available in aforementioned studies. Test results of Harris et al. (1984a) and Lee et al, (2007) on sand-mica mixtures are given in Figure 5.12. Results of this study are also given in the same figure.

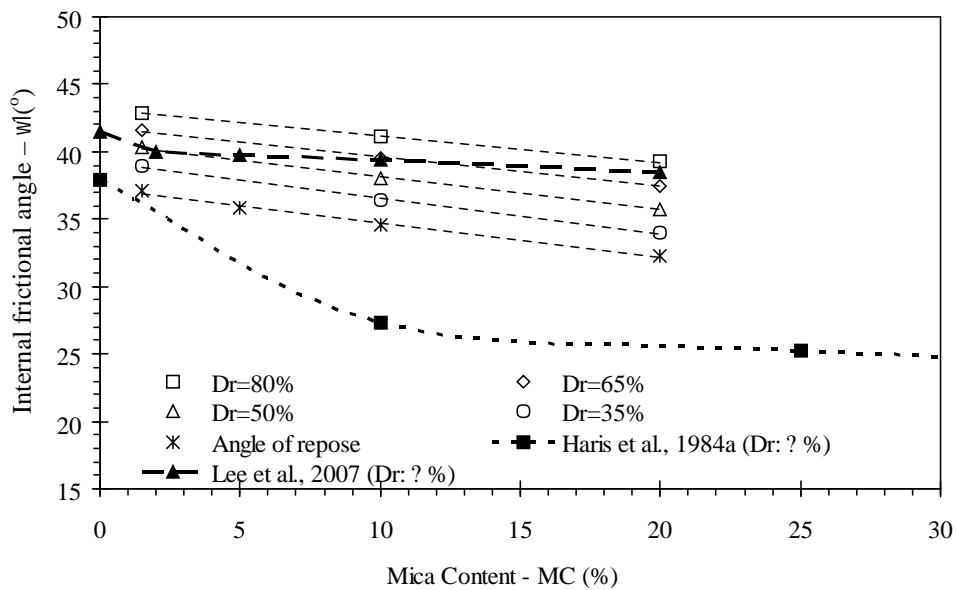


Figure 5.12 Variation of internal frictional angle with mica content

5.5 Shear Wave Velocity of Sand Mica Mixtures (Bender Element Tests)

Maximum shear modulus (G_{\max}), which is a major parameter in dynamic soil response analyses, is obtained at small deformation amplitudes. To this end, at small deformation levels ratio of shear stress to shear deformation ($G_{\max}=\tau_{\min}/\chi_{\min}$) is calculated or shear modulus is attained by calculating shear wave velocity ($G_{\max}=V_s^2 \cdot \rho$). Deformation of samples during cyclic loading should be measured at micro levels with high accuracy to be able to calculate shear modulus for small strain levels. Unfortunately, deformations at micro levels cannot be measured thoroughly with deformation dials or transducers. Therefore, as a common tendency, shear modulus at small strain level is determined through measurement of shear wave velocity.

One of the techniques for the determination of shear wave velocity in laboratory is the “bender element” test. This method is based on producing shear wave at one end of the sample via piezoelectric materials that generates micro amplitude vibrations and perceiving waves by means of sensors mounted at the other end of the sample (Shirley & Hampton, 1978). The most essential critics that can be directed to bender element technique is the possible ambiguity in the determination of arrival time of shear wave on receiver sensor and interference of P-waves, which reach towards sample boundaries during vibration of wave-generating tip.

Grain shape effects on shear wave velocity were explored by some researchers. Cho et al. (2006) conducted a series bender element tests on rounded and crushed sands. According to Cho et al (2006), shear wave velocity increase with roundness. The test results of the Cho et al. (2006) are given in Figure 5.13.

Lee et al. (2007) explored effects of mica grain size on shear wave velocity of sand. In the study, mica grains in different sizes were used. Bender element tests were conducted on samples, which were prepared in conventional oedometer cell as they were vertically loaded. Unfortunately, void ratios or densities of the samples cannot be inferred from the study. Nevertheless, mica effect on the sand samples is

obvious in the study (Figure 5.14). As seen in Figure 5.14, shear wave velocity decreases with mica content for all mica grain sizes.

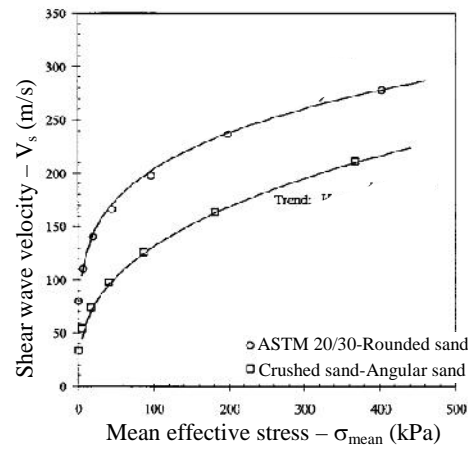


Figure 5.13 Roudness effect on the shear wave velocity (Cho et al. 2006)

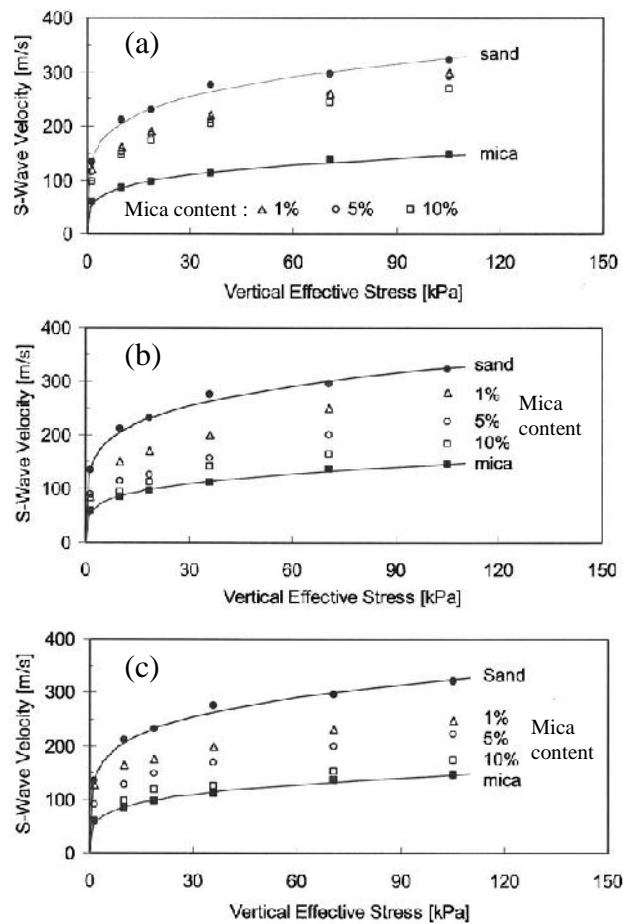


Figure 5.14. Mica grain size effects on shear wave velocity. (a), (b) and (c) are $D_{mica}/D_{sand}=0.33$, $D_{mica}/D_{sand}=1.0$ and $D_{mica}/D_{sand}=3.0$, respectively (Lee et al., 2007)

Shear wave velocities of soil samples at different mica contents, prepared at relative density values between loose and dense-very dense states, were measured via bender element tests as part of this study. Samples were set up at 1.5, 10 and 20% mica contents for $D_{\text{mica}}/D_{\text{sand}}=1.07$. One of the recorded signals from bender element tests and measured shear wave velocity (V_s) are presented in Figure 5.15. Reduced test data can be seen in Figure 5.16 thru 5.18.

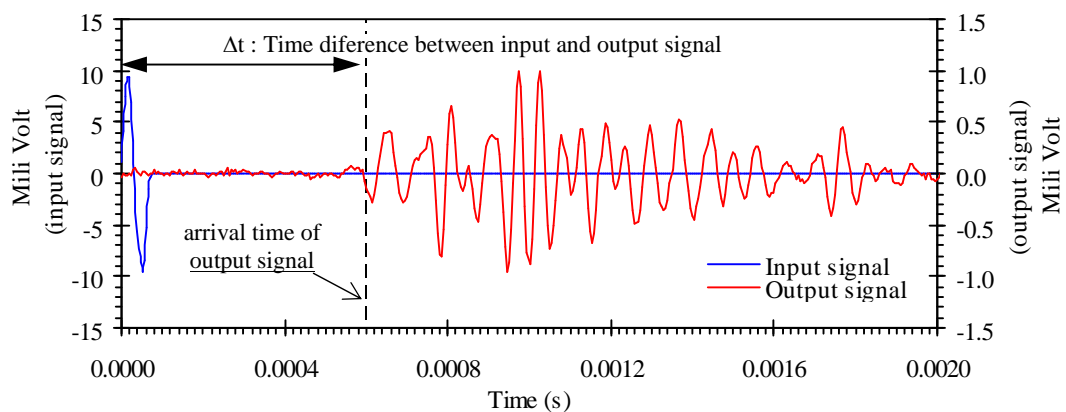


Figure 5.15 Recorded signal during bender element test

Shear wave velocity (V_s) decreases with mica content, whereas it increases with confining stress and relative density. The effect of grain shape on dynamic behavior of soil was observed in bender element tests. For instance, as seen in Figure 5.16, there is high correlation between V_s and void ratio for certain confining pressure and mica content pairs. The effect of mica content on V_s can be better observed in shear-wave velocity – mica content graphs (Figure 5.17). For instance, at 55% relative density, shear wave velocity of 1.5%, 10% and 20% mica contents were determined as 250 m/s, 210 m/s and 185 m/s, respectively (Figure 5.17) for 100 kPa cell pressure. For all relative densities, shear wave velocities decreased with mica content. As mica content increases from 1.5% to 20%, shear wave velocities for all densities decrease at on approximate rate of 20-30%.

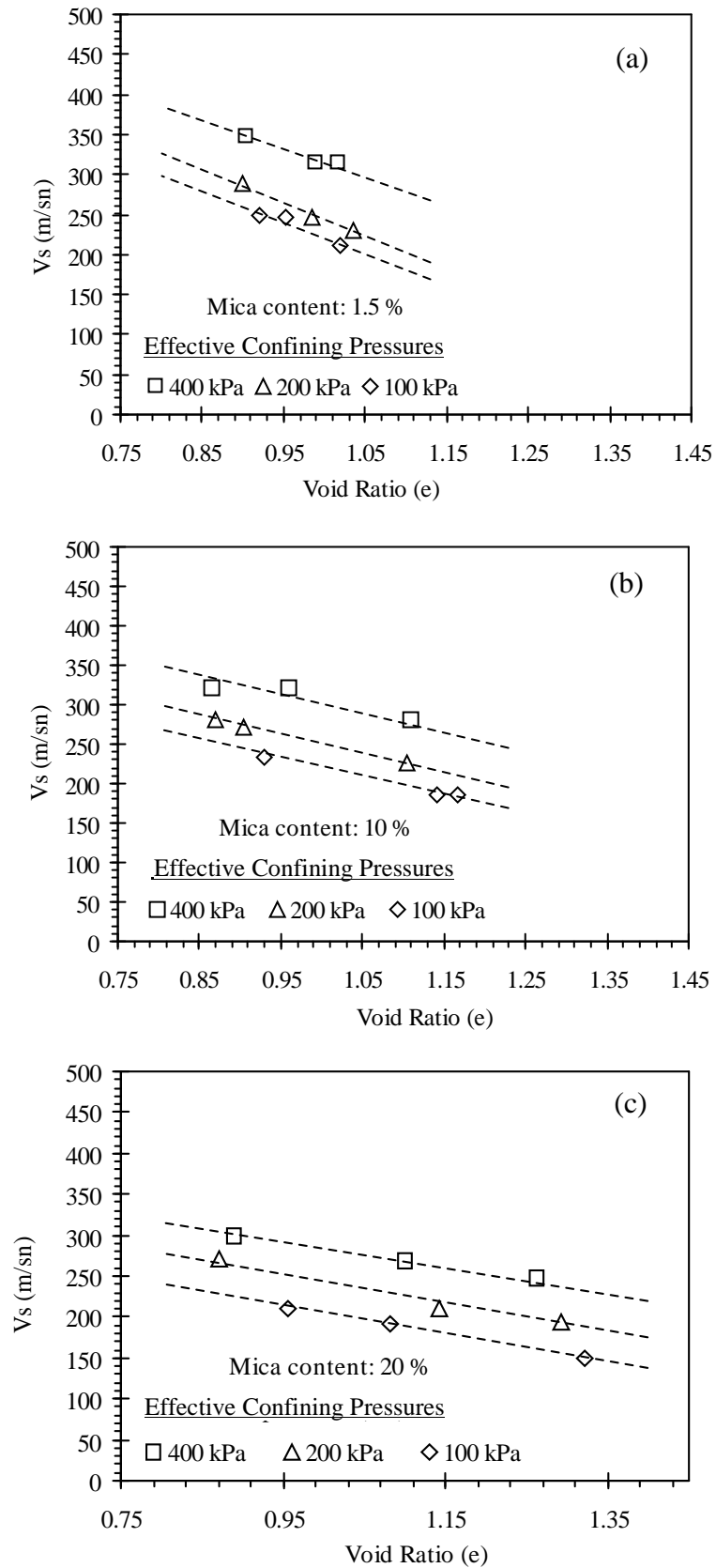


Figure 5.16 Relationship between shear wave velocity and void ratio for different cell pressures and mica content

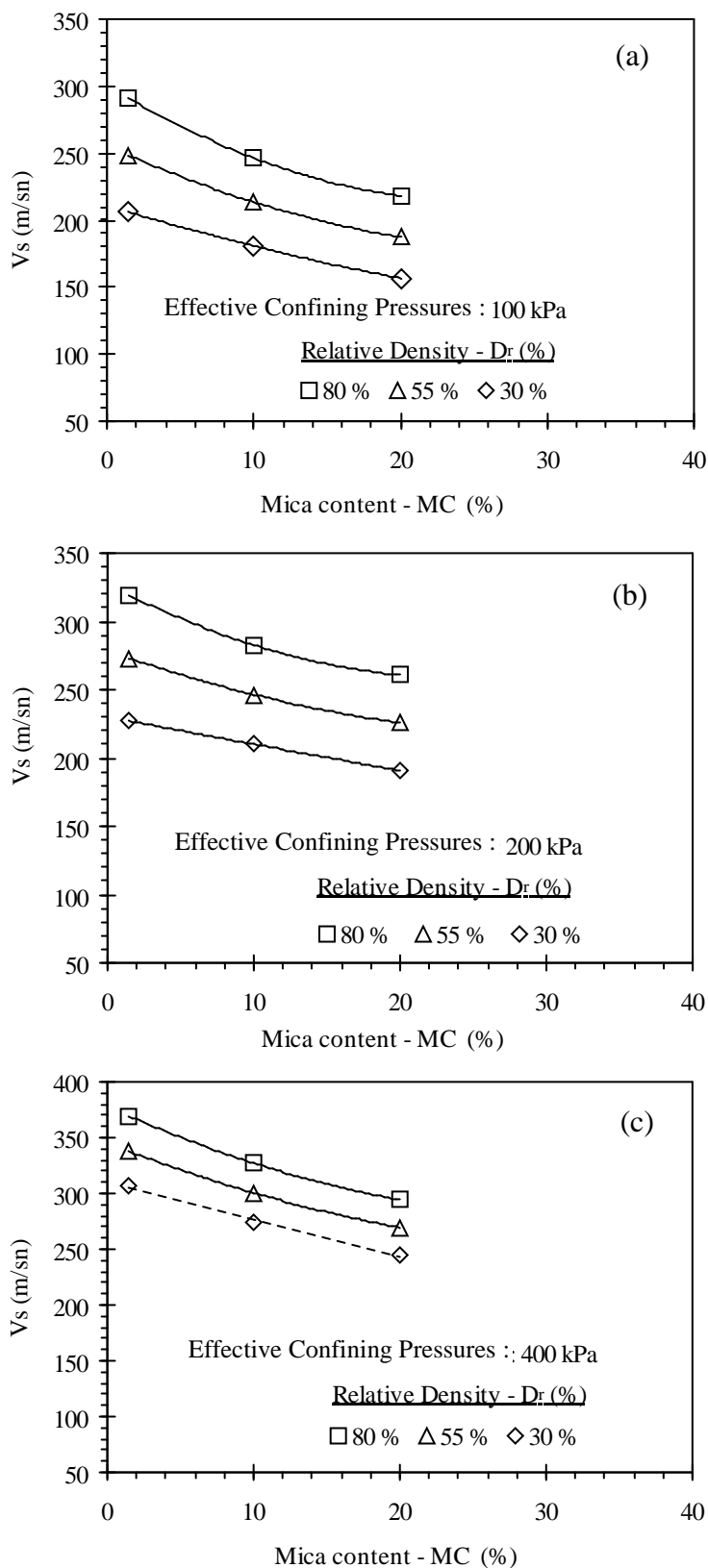


Figure 5.17 Relationship between shear wave velocity and mica content for different relative density levels and cell pressures (derived from Figure 5.16)

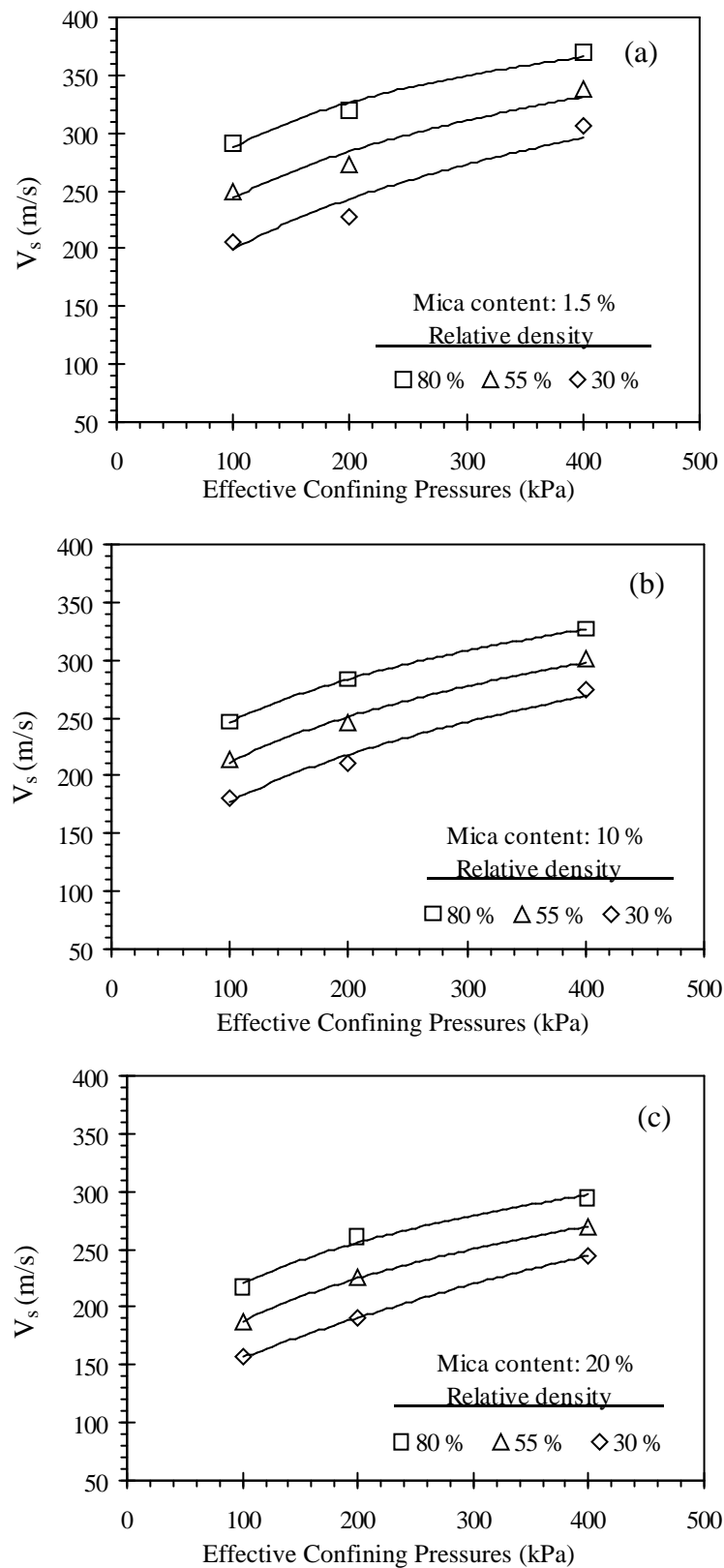


Figure 5.18 Relationship between shear wave velocity and cell pressure (σ_3) for different mica content and relative density (derived from Figure 5.16)

5.6 Post-Liquefaction Volumetric Strains

Induced excess pore water pressure in a soil layer due to earthquake loading is gradually dissipated following the earthquake. Dissipation of excess pore water pressure causes volume change in soil layers and this appears as settlement on soil surface. One of the important consequences of liquefaction is the settlement of ground surface. Surface settlements due to post liquefaction volume change are affected by layer thickness, relative density of soil prior to earthquake, and grain size distribution. In this study, volumetric strains following liquefaction were measured for shear strain levels larger than 8%. In general degree of post-liquefaction settlement is controlled by shear strain level until it reaches 7~8%. Beyond this level, however, volumetric strains become independent of shear strain as shown in Figure 5.19 (Ishihara & Yoshimine, 1992).

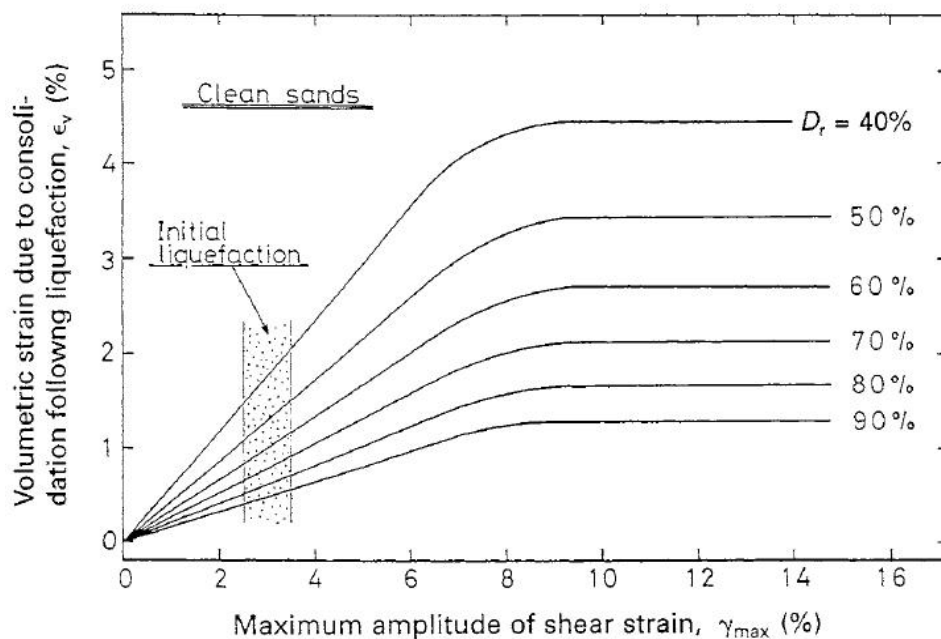


Figure 5.19 Post-liquefaction volumetric strains–shear strain relationships (Ishihara & Yoshimine, 1992)

Post-liquefaction volumetric strains of sands were experimentally researched by various academicians (Askari et al. 2010; Chien et al., 2000; Ishihara & Yoshimine, 1992; Lee & Albaisa, 1974; Nagase & Ishihara, 1988; Seed et al., 1984; Tatsuoka et

al., 1974; Tokimatsu & Seed, 1987; Ueng et al., 2009; Yoshimi et al., 1975). Findings of those studies are summarized in Figure 5.20 where volumetric strains obtained at large shear strain amplitudes are plotted as a function of increasing relative density. As one would expect, volumetric strain decreases with relative density. Fine content causes an increase in post liquefaction volumetric strain according to Askari et al., (2010) (Figure 5.20) and Chien et al., (2000) (Figure 5.20 and Figure 5.21).

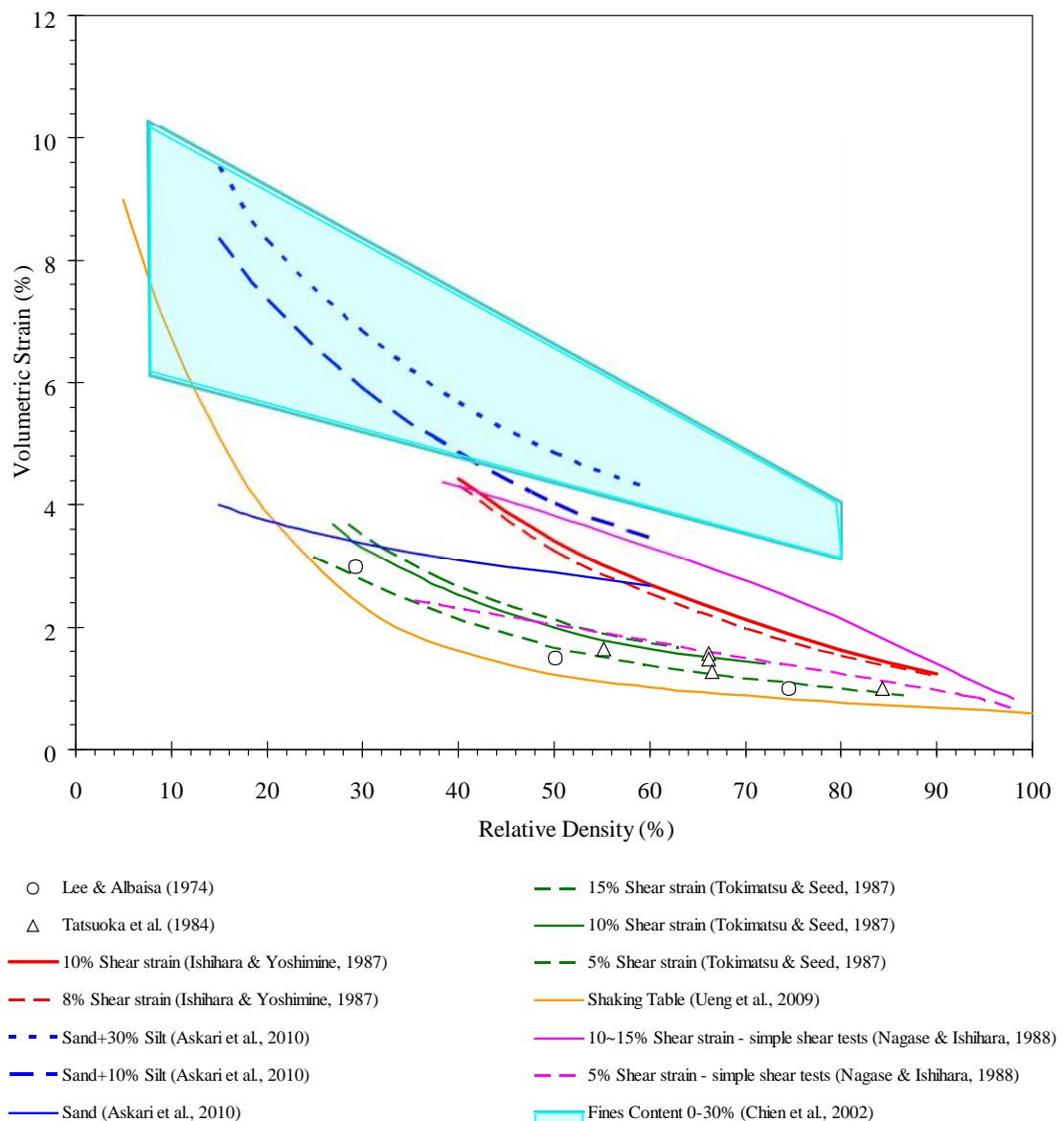


Figure 5.20 Post-liquefaction volumetric strain for large shear strain deformation levels

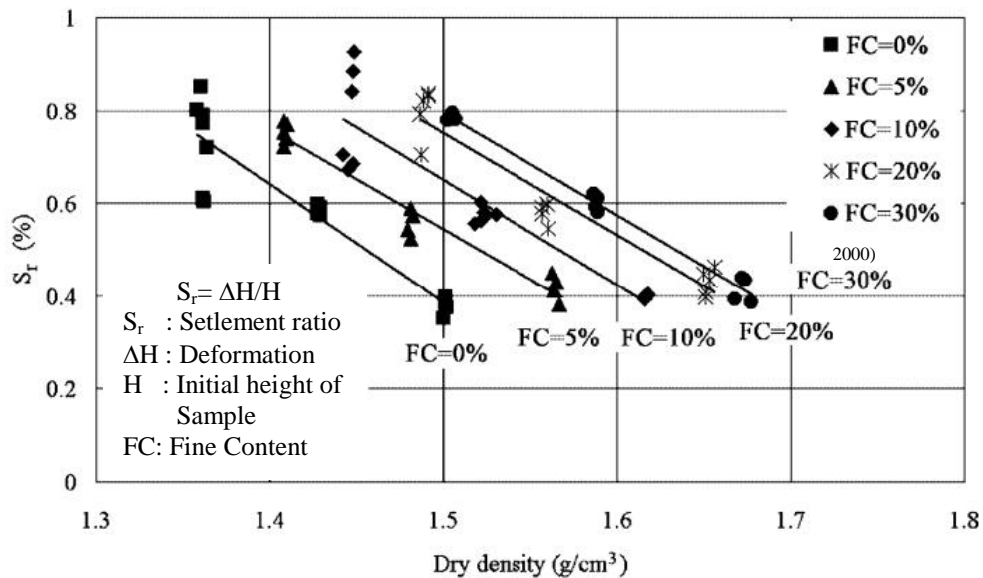


Figure 5.21 Influence of the fine content on post-liquefaction volumetric strain (Chien et al., 2000)

Platy grains increase the void ratio and compression index of sandy materials by means of bridging mechanism (Cho et al., 2006; Lee et al., 2007). Volume changes of samples were measured in cyclic strength tests in order to determine the effect of mica grains on post liquefaction volumetric strain of Old Gediz River Delta sandy soils. Volume changes of samples were measured following the completion of undrained cyclic loading. Cyclic tests were terminated after the development of large axial strains (>8%).

Test results given in Figure 5.22 represent large deformation behavior of sand–mica mixtures as a result of volumetric strains measured at shear strains of 8% and larger. Test results belonging to field samples containing 10% non-plastic fine materials and 7.5% mica grains by weight are given in Figure 5.23. Relation of post-liquefaction volumetric strain at large strain levels to mica content and non-plastic fine material is illustrated in Figure 5.24 and 5.25 respectively. The curves in Figure 5.24 and 5.25 are derived from Figure 5.22 and 5.23.

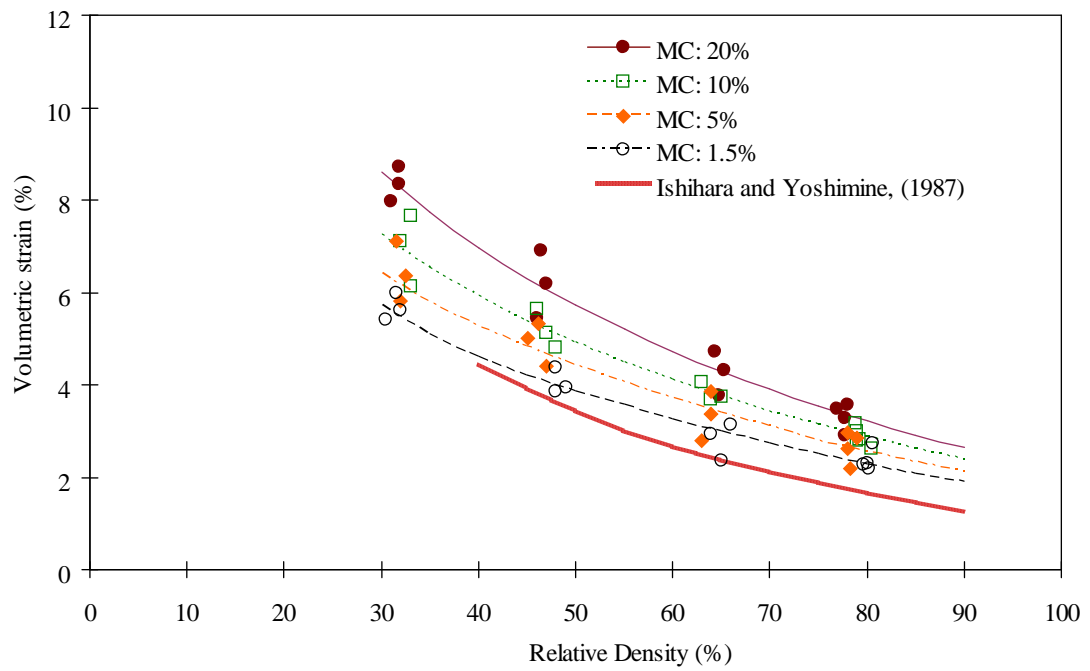


Figure 5.22 Post-liquefaction volumetric strain (ϵ_v) of clean sand-mica mixtures ($\epsilon_{axial} > 8\%$)

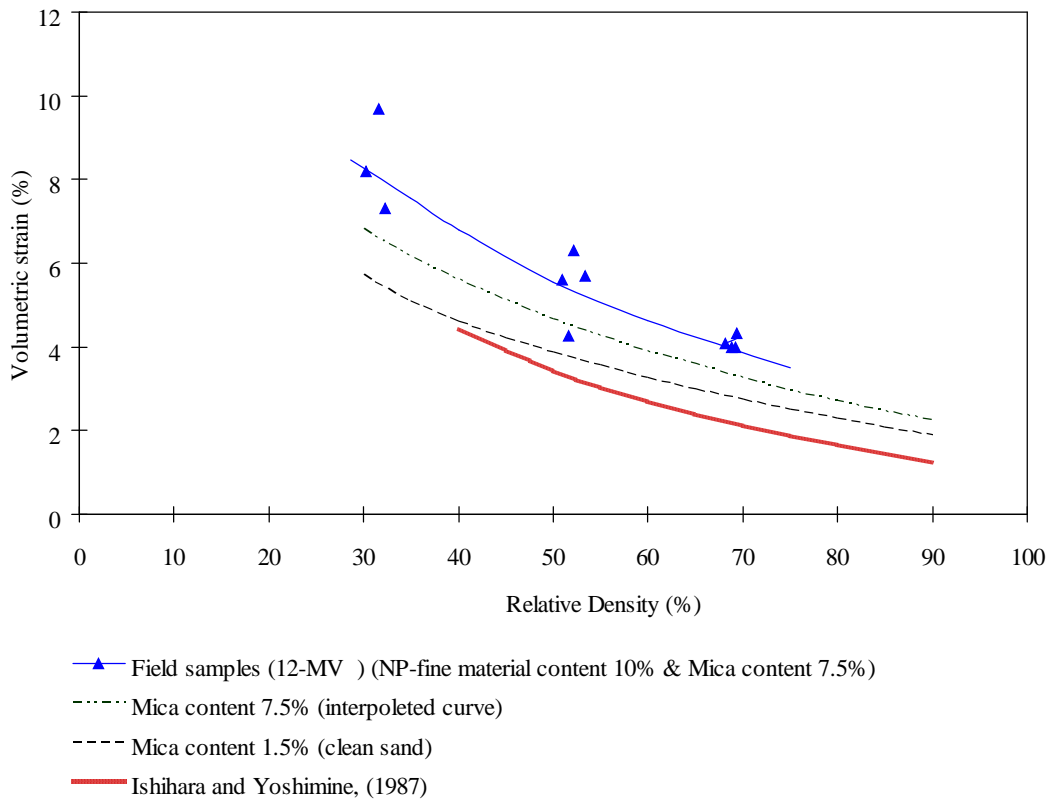


Figure 5.23 Post-liquefaction volumetric strain (ϵ_v) of 12-MV field samples containing 7.5% mica and 10% non-plastic fine materials ($\epsilon_{axial} > 8\%$)

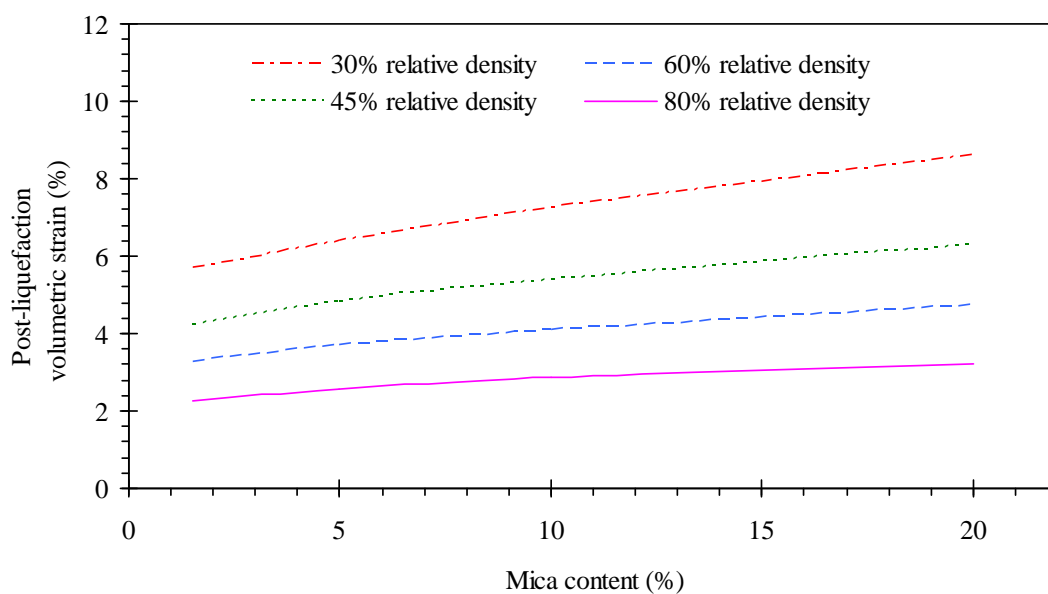


Figure 5.24 Relation between mica content and post-liquefaction volumetric strain of Old Gediz River Delta sands

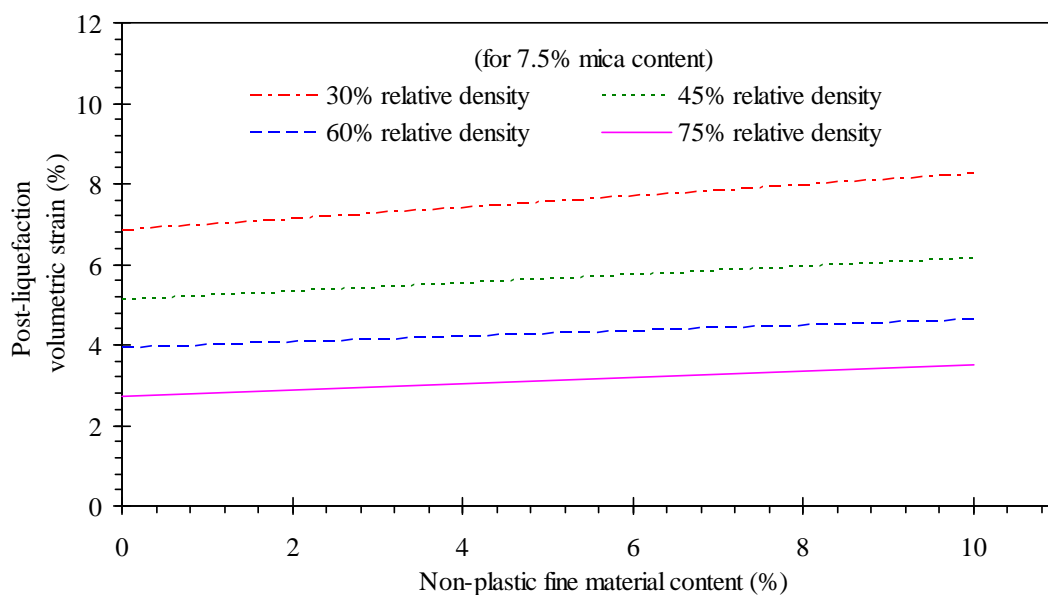


Figure 5.25 Relation between non-plastic fine materials and post-liquefaction volumetric strain of Gediz River Old Delta sands

It is comprehended from Figure 5.22 and 5.24 that the post-liquefaction volumetric strains increase with mica content. For instance, volumetric strains are determined as $\varepsilon_v=7.0\%$, 5.9% , 5.25% , 4.6% for 20% , 10% , 5% and 1.5% mica content respectively while relative density is 40% (Figure 5.22 and 5.24).

When post-liquefaction volumetric strain curve of clean sand (without fine materials) for 7.5% mica content is compared with that of field samples containing 7.5% mica and 10% non-plastic fine material (Figure 5.23 and 5.25), it can be seen that non-plastic fine material causes an increase in post-liquefaction volumetric strain of the Old Gediz River Delta sand at large strain level. For instance, volumetric strains corresponding to $D_r=40\%$ are determined as 5.6% and 6.8% for clean sand with 7.5% mica content (i.e. not including fines fraction) and 12-MV field sample, respectively.

As seen in Figure 5.22 through 5.25, variations in volumetric strains decrease with increasing density. The effect of mica and non-plastic fine materials on post-liquefaction volumetric strain of dense sand behavior is small compared to loose and medium dense samples.

When tests results are compared with those given in literature (Figure 5.26), one may notice that ε_v-D_r curves stay above the Ishihara-Yoshimine clean sand curve. Post-liquefaction volumetric strains of clean sands are slightly higher than sands given in the literature. Therefore, Ishihara-Yoshimine (1987) curve constitutes the lower bound for the study area. On the other hand, results of the 12-MV field samples containing 10% non-plastic material are compatible with the literature.

As seen from test results, mica grains and non-plastic fine material considerably modified the post-liquefaction volumetric strains characteristics of sandy soils at large axial strain levels. This behavior is compatible with the expected response of the sand-mica mixture, which is under the control of bridging effect of mica grains (Lee et al., 2007). According to Lee et al. (2007), platy mica grains cause an increase in the void ratio of the sand material by generating bridges among rounded grain. Mica grains become more effective on sand characteristics when the sample is loose. An increase in relative density of the samples causes a decrease in mica grains influence on sand behavior. One may notice in Figure 5.22 and 5.23 that volumetric strain- relative density curves get closer as the density increases. This indicates that bridging effect of mica grains is shaded with an increase in the relative density of

sand samples. In other words, in loose samples more bridges are formed among sand grains.

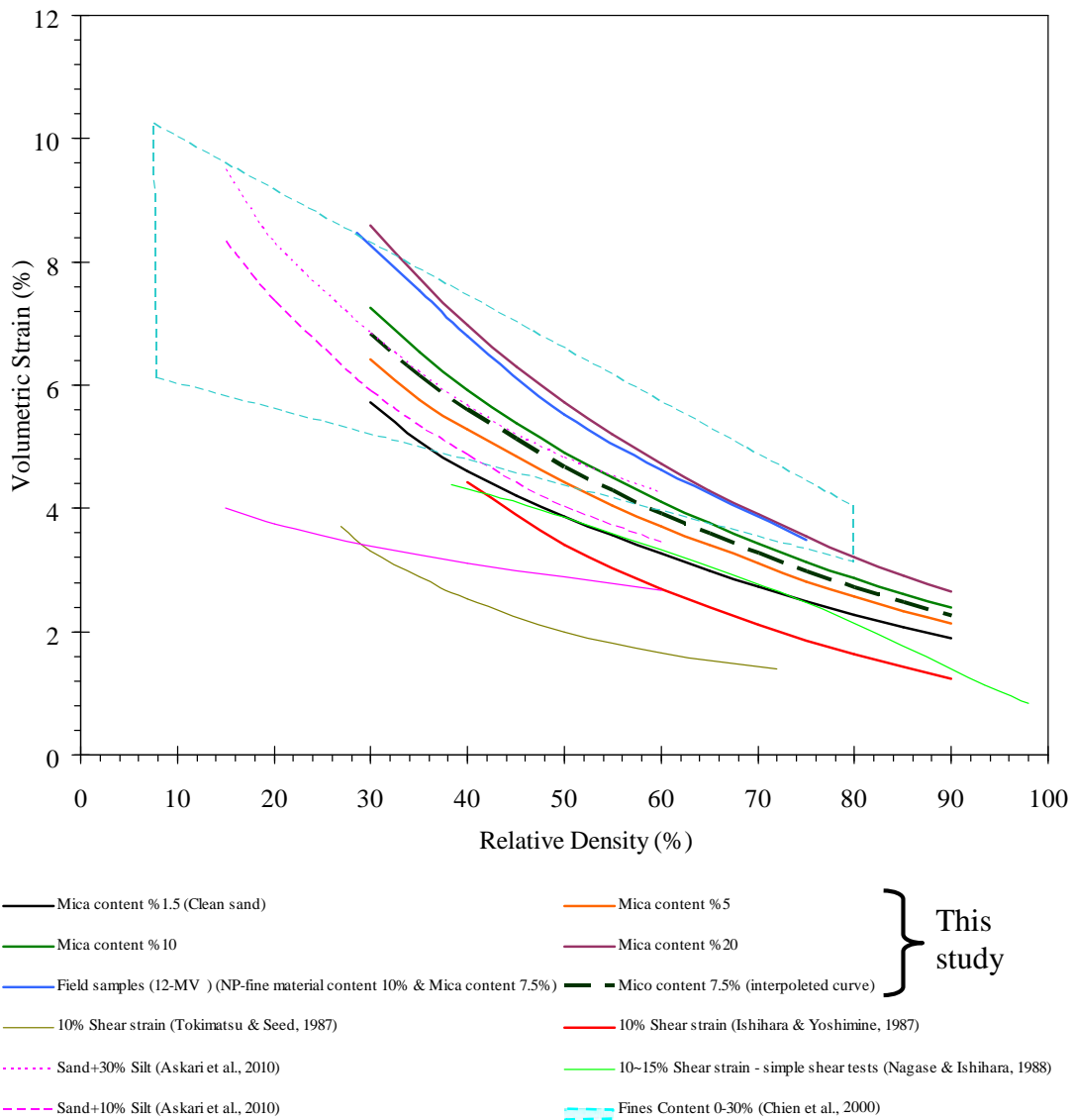


Figure 5.26 Comparison of test results with literature

Post-liquefaction volumetric strain of the Old Gediz River Delta sand sample containing non-plastic fine material is higher than that of the clean sand sample with same relative density containing same amount of mica. Fine material causes an increase in the post-liquefaction volumetric strain potential and a decrease in stability of the sand. When grain size distributions of fines and coarse materials are close to each other, fine grains can locate between contact points of coarse grains. Such fine

grains between the contact points of coarse grains cause a decrease in the number of contact points. Therefore, stability of the materials decrease and compression potential of the materials increase. Consequently, fine materials at certain content can cause a decrease in stability and cause an increase in compressibility potential of coarse materials (Thevanayagam, 2007a; Monkul & Yamamuro, 2011). Chien et al. (2000) explored effects of fine contents on post liquefaction settlement in an experimental study. In the study, it is reported that post liquefaction settlement increases with fine material ratio for certain relative densities. This effect was also observed for the 12-MV (7.50 m- 8.0 m) samples containing 10% non-plastic fine materials.

5.7 Cyclic Strength (Liquefaction) Test Results

Cyclic triaxial tests commenced in 1960s (Seed & Lee, 1966) and it was accepted as a standard technique to determine cyclic shear strength of soils against liquefaction (ASTM-D5311, JGS-T542). The undrained dynamic loading creates stress conditions on a plane of 45° through the sample, which is the same as those produced on the horizontal plane in the ground during earthquakes. Due to this correspondence, the cyclic triaxial tests provide a means to assess the resistance of sands to liquefaction. The stress conditions at each stage of cyclic loading are illustrated in Figure 5.27. When the axial stress is applied, the shear stress induced on the 45° plane is half of the axial deviator stress. The normal stress equal to half of the axial stress is also induced on this plane. The compressive stress on the 45° plane mostly transmitted to pore water without inducing any change in the existing effective confining stress (Ishihara, 2003).

Special attention is paid to Skempton's B value while performing cyclic triaxial test since $B \geq 0.97$ is desired in order to achieve the above-mentioned condition in the test. The consolidation pressure of samples was selected as 100 kPa to represent average effective consolidation stress in the liquefaction depth (0 m – 20 m). Besides, the Old Gediz River Delta soils contain liquefiable silty fine sands in this depth interval.

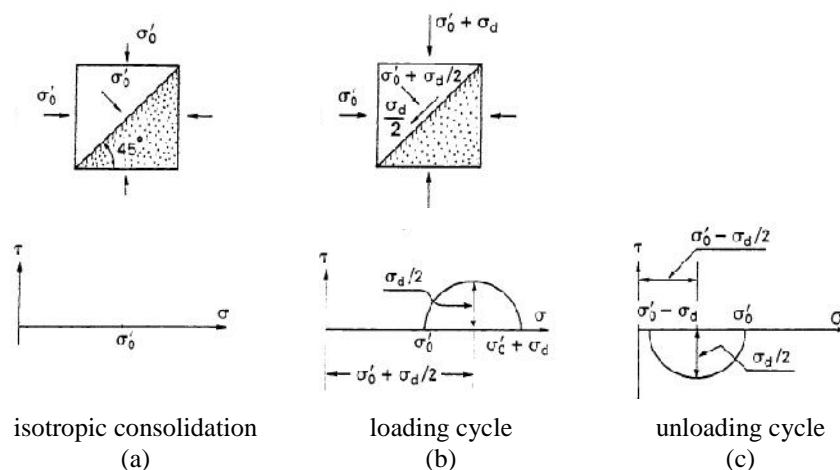


Figure 5.27 loading stages in a saturated soil sample in cyclic triaxial test (Seed & Lee, 1966)

In generally, when strains reach 5% level, soils are failed and they flow. Therefore, in the literature, 5% double amplitude axial strain level in cyclic triaxial test is considered as the threshold strain level in defining cyclic strength (Mulilis et al., 1975; Seed, 1979; Ishihara, 2003). However, there is not a consensus in the definition of cyclic strength in the literature about number of cycles, which provide 5% double amplitude axial strain at a certain cyclic stress ratio. In this study, definition of Seed (1979) is followed in evaluation of test results. In study of Seed (1979), magnitude of cyclic stress ratio required to produce 5% double amplitude axial strain at 15th cycle was defined as the cyclic strength.

Cyclic strength of the sand–mica mixtures and samples containing non-plastic fines were determined in cyclic triaxial tests. The test results are presented in Figure 5.28 through Figure 5.32, which show the relationship between the cyclic stress ratio (cyclic deviator stress divided by twice the initial effective confining pressure) and the number of cycles required to cause 1%, 2%, 5% and 10% double amplitude axial strain at different densities. Also, the required cyclic stress ratio ($CSR_{5\%-15th}$) for 5% double amplitude axial strain at 15th cycle is noted on the figures. In the evaluation of the test results, $CSR_{5\%-15th}$ values are considered as cyclic strength of the test samples. Details of the cyclic triaxial tests can be found in appendices. Relative density ratio on the figures stands for the density of test samples at the beginning of the cyclic loading following the consolidation stage. Similarly, axial and volumetric strains are also defined using the dimensions of samples prior to cyclic loading.

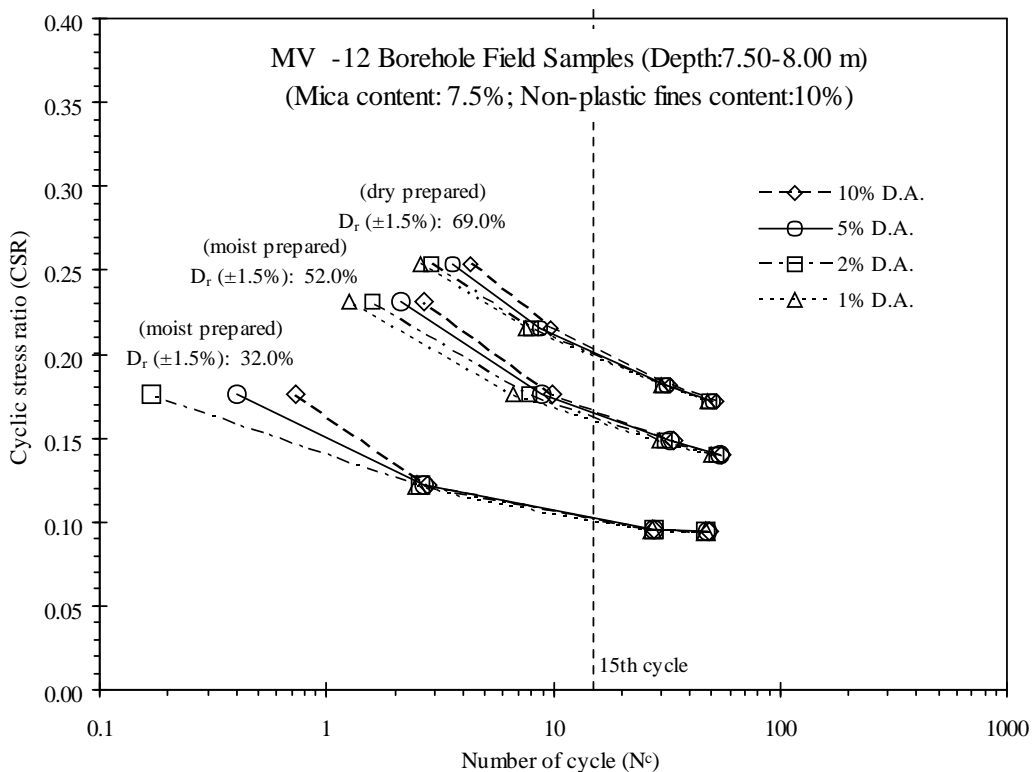


Figure 5.28 Cyclic stress ratio (CSR) versus number of cycles (N_c) for 1%, 2%, 5%, 10% double amplitudes (D.A.) and different relative densities for MV -12 borehole field samples (Mica content:7.5 %, non-plastic fines content: 10%)

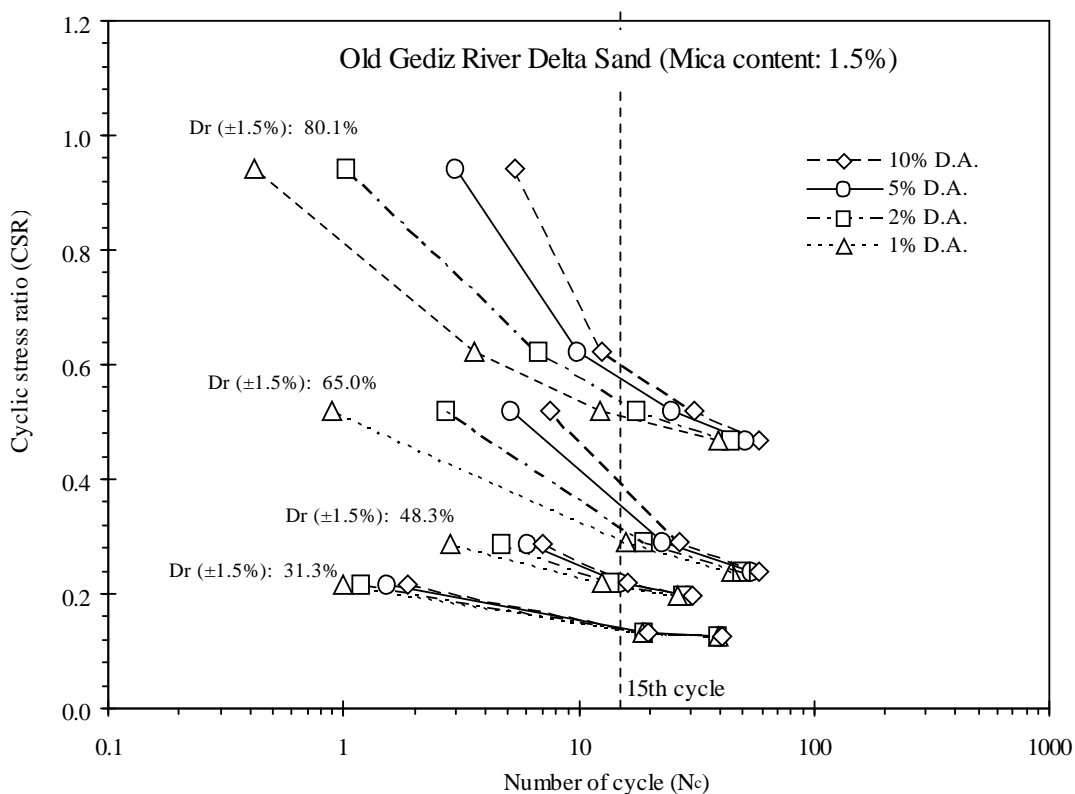


Figure 5.29 Cyclic stress ratio (CSR) versus number of cycles (N_c) for 1%, 2%, 5%, 10% double amplitudes (D.A.) and different relative densities for Old Gediz River Delta sand with 1.5% mica

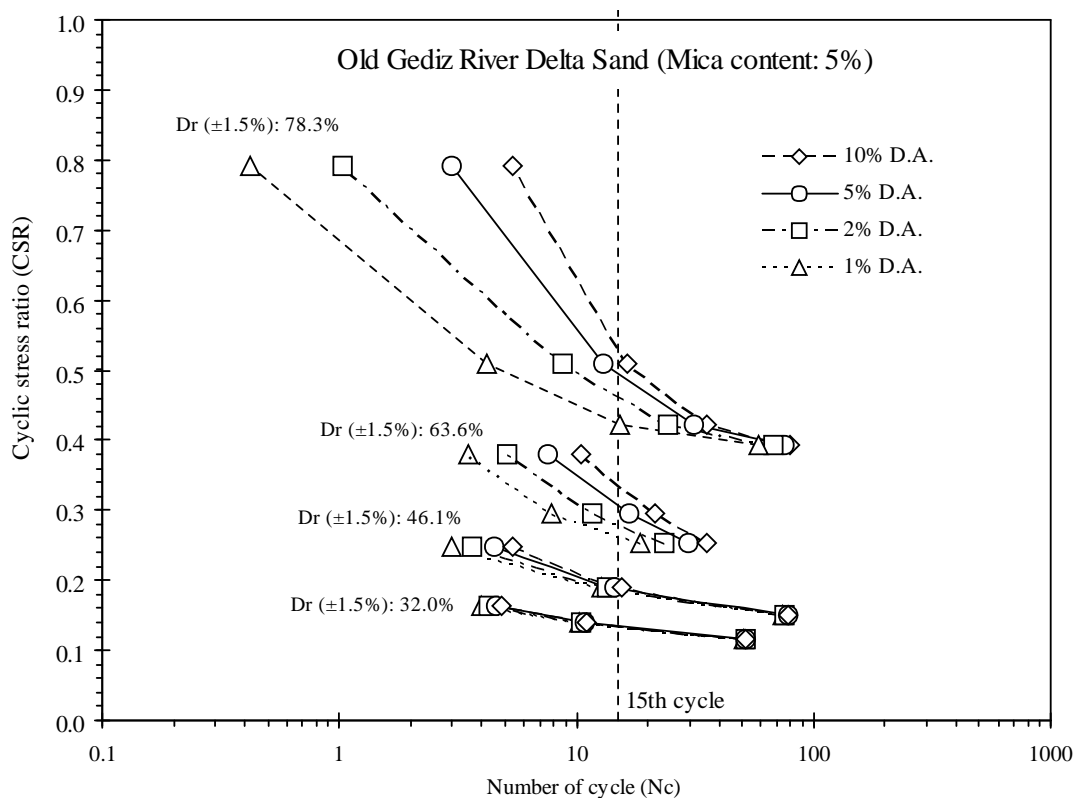


Figure 5.30 Cyclic stress ratio (CSR) versus number of cycles (N_c) for 1%, 2%, 5%, 10% double amplitudes (D.A.) and different relative densities for of Old Gediz River Delta sand with 5% mica

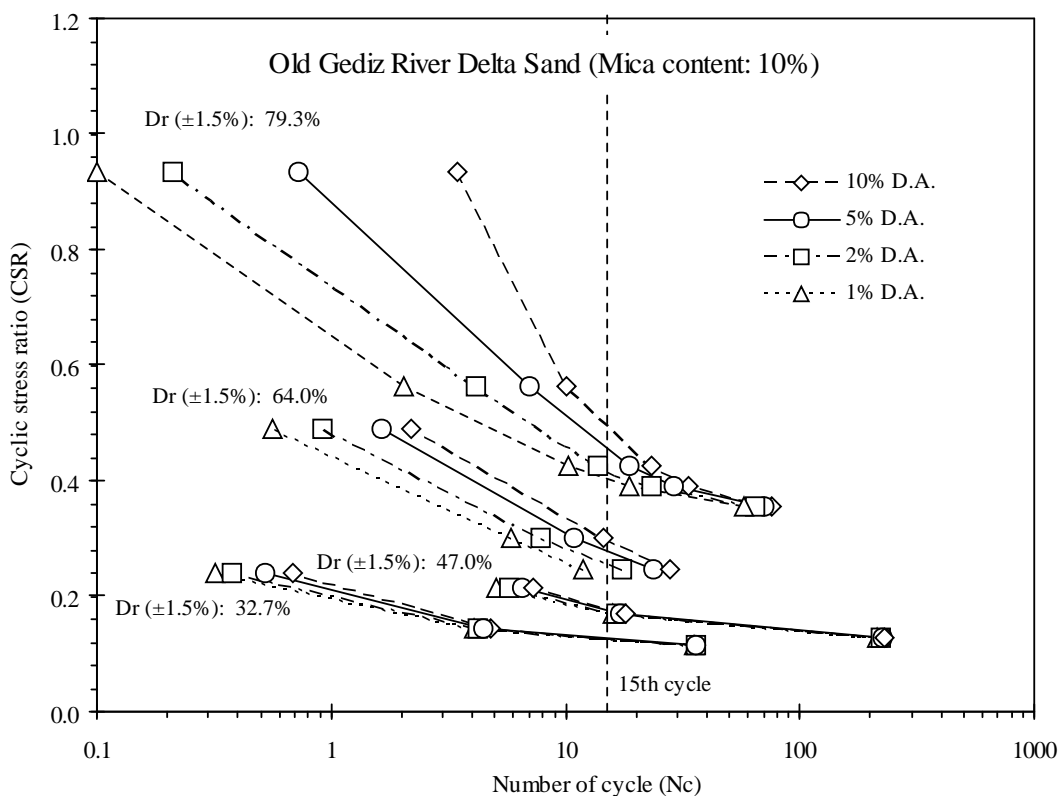


Figure 5.31 Cyclic stress ratio (CSR) versus number of cycles (N_c) for 1%, 2%, 5%, 10% double amplitudes (D.A.) and different relative densities for Old Gediz River Delta sand 10% mica

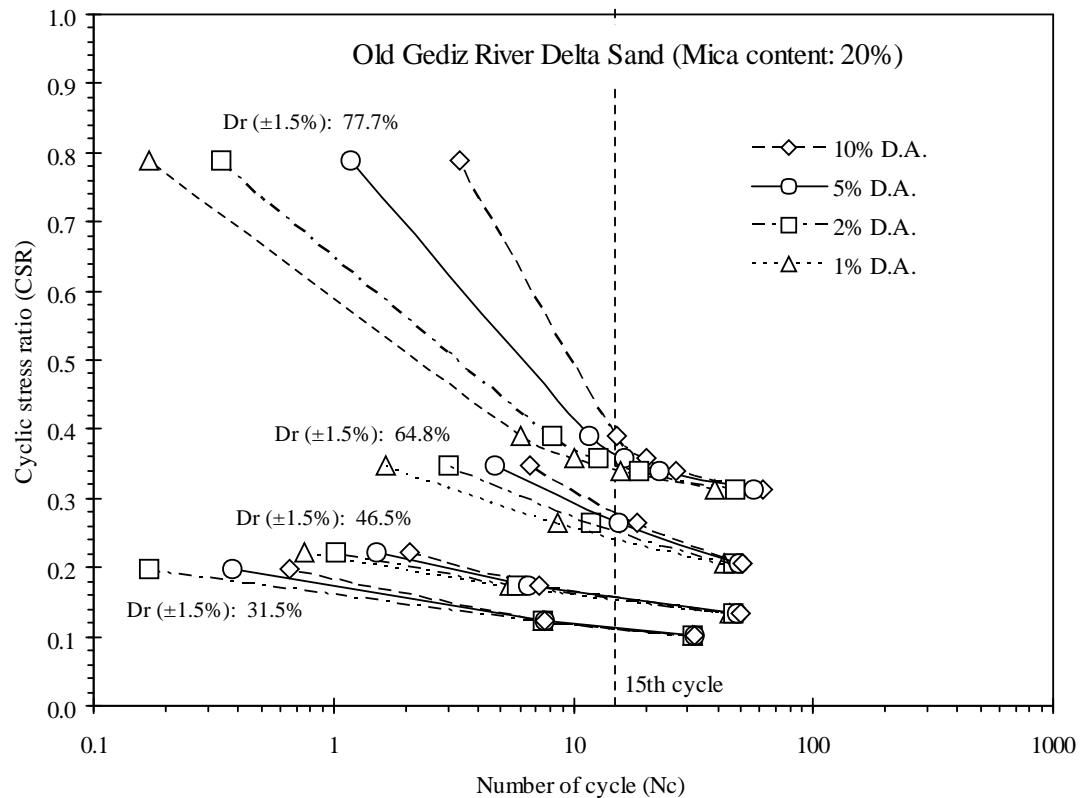


Figure 5.32 Cyclic stress ratio (CSR) versus number of cycles (N_c) for 1%, 2%, 5%, 10% double amplitudes (D.A.) and different relative densities for Old Gediz River Delta sand with 20% mica

Cyclic stress ratio versus required number of cycles to cause 5% DA axial strain for the tested samples with various mica content are plotted in Figure 5.33 for different densities. The cyclic stress ratio (CSR) required to cause 5% DA axial strain for 15th cycle versus mica content are also plotted in Figure 5.34 for different densities. For all densities, DA axial strain curves are shifted down as mica content increased (Figure 5.33). Therefore, the cyclic stress ratio required to cause 5% DA axial strain for certain number of cycles decreased with mica content. The same effect of mica grains can be seen in Figure 5.34, where required CSR decreased with mica content for all densities.

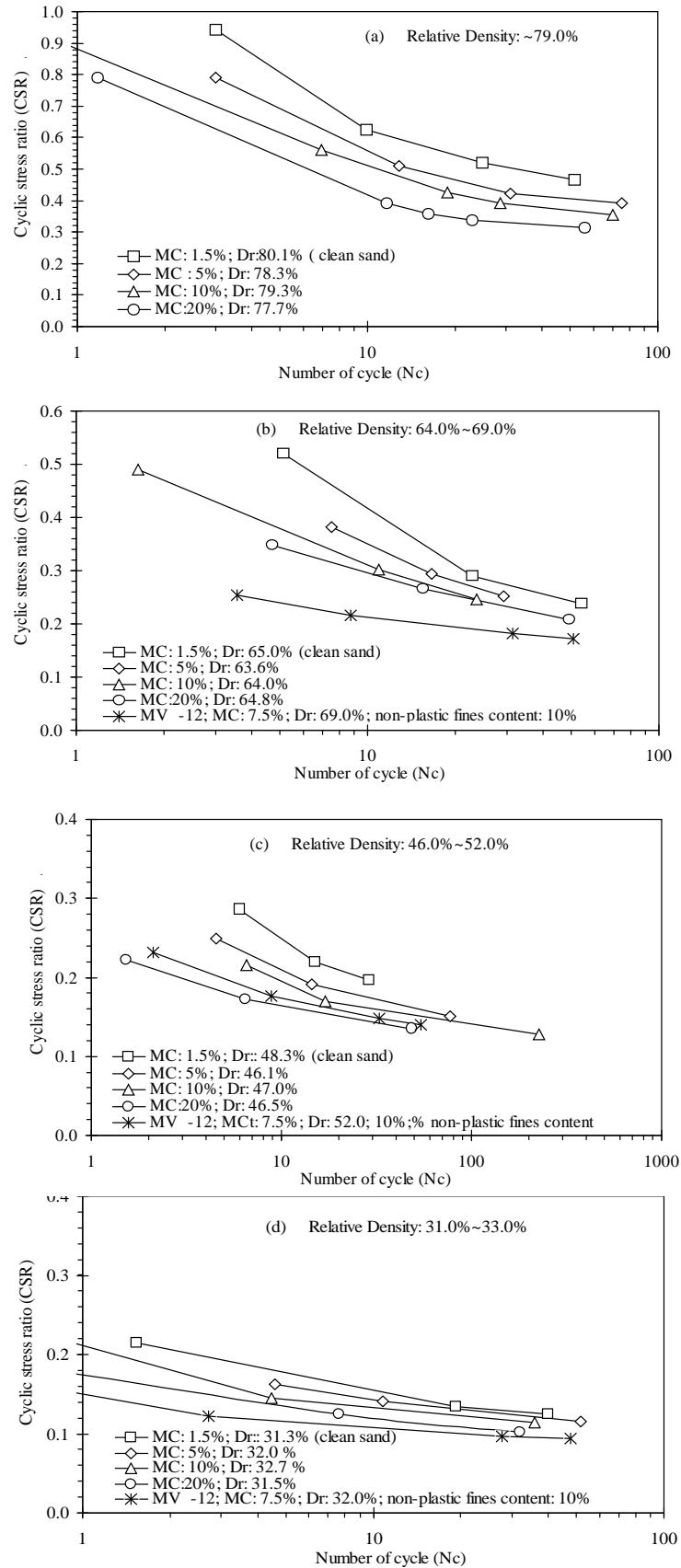


Figure 5.33 The cyclic stress ratio (CSR) required to cause 5% DA axial strain for 15th cycle versus mica content

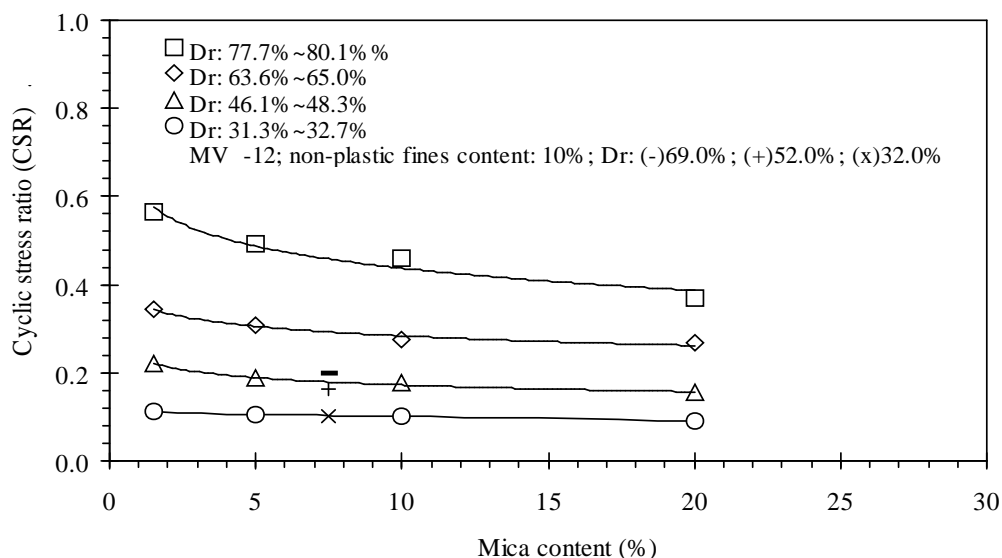


Figure 5.34 the cyclic stress ratio (CSR) required to cause 5% DA axial strain for 15th cycle as a function of mica content

The cyclic shear strength (cyclic stress ratio required to produce 5% double amplitude axial strain at 15th cycle) was plotted against relative density in Figure 5.35. Mica content reduces cyclic shear strength of the sand. The lowest cyclic shear strength belongs to 12-MV sample containing 7.5% mica and 10% non-plastic fines. It appears that non-plastic fines further decrease cyclic shear strength of the sand.

In Figure 5.36 and 5.37, cyclic triaxial test results of this study are compared with literature. In Figure 5.36, cyclic stress ratio versus required cyclic number for 5% double amplitude axial strain curves are compared with literature obtained test samples prepared by means of moist tamping method. Monterey sand (Mulilis, 1975), which was prepared using moist vibration method was considered as moist tamping by Ishihara (2003). The sands, which are prepared by means of moist tamping and moist vibration methods, exhibit similar behavior (Ladd, 1977). This can be seen when data by Ladd (1977) are examined (Figure 5.36). In this respect, when cyclic stress ratio versus required number of cycle for 5% DA axial strain curves of Old Gediz River delta sands are compared with Ladd (1977) and Monterey sand (Mulilis, 1975) for same density levels, Old Gediz River Delta sand exhibit similar behavior with Ladd (1977) at medium dense relative density condition. On

the other hand, CSR– N_c curves for 5%DA of Old Gediz River Delta sand lies fairly low from Monterey sand (Mulilis, 1975). If the air pluviated MV -12 sample ($Dr \sim 69.0$) is compared with air pluviated Monterey sand ($Dr = 70\%$), it is seen that cyclic strength of the air pluviated MV -12 samples is lower than that of Monterey sand like moist tamping samples.

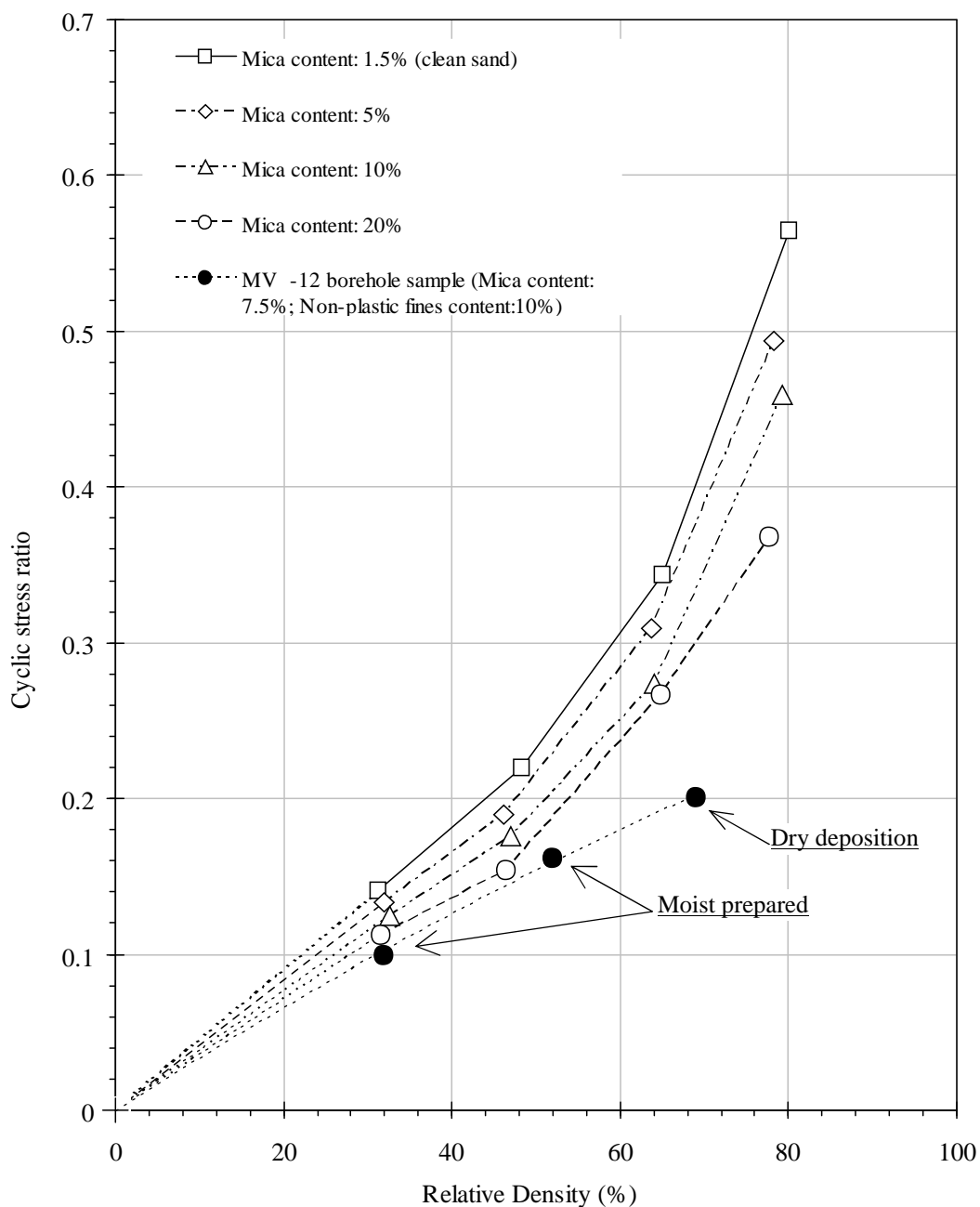


Figure 5.35 Cyclic stress ratios (required 5% D.A. at 15th cycle) versus relative density for 1.5%, 5%, 10%, 20% mica contents.

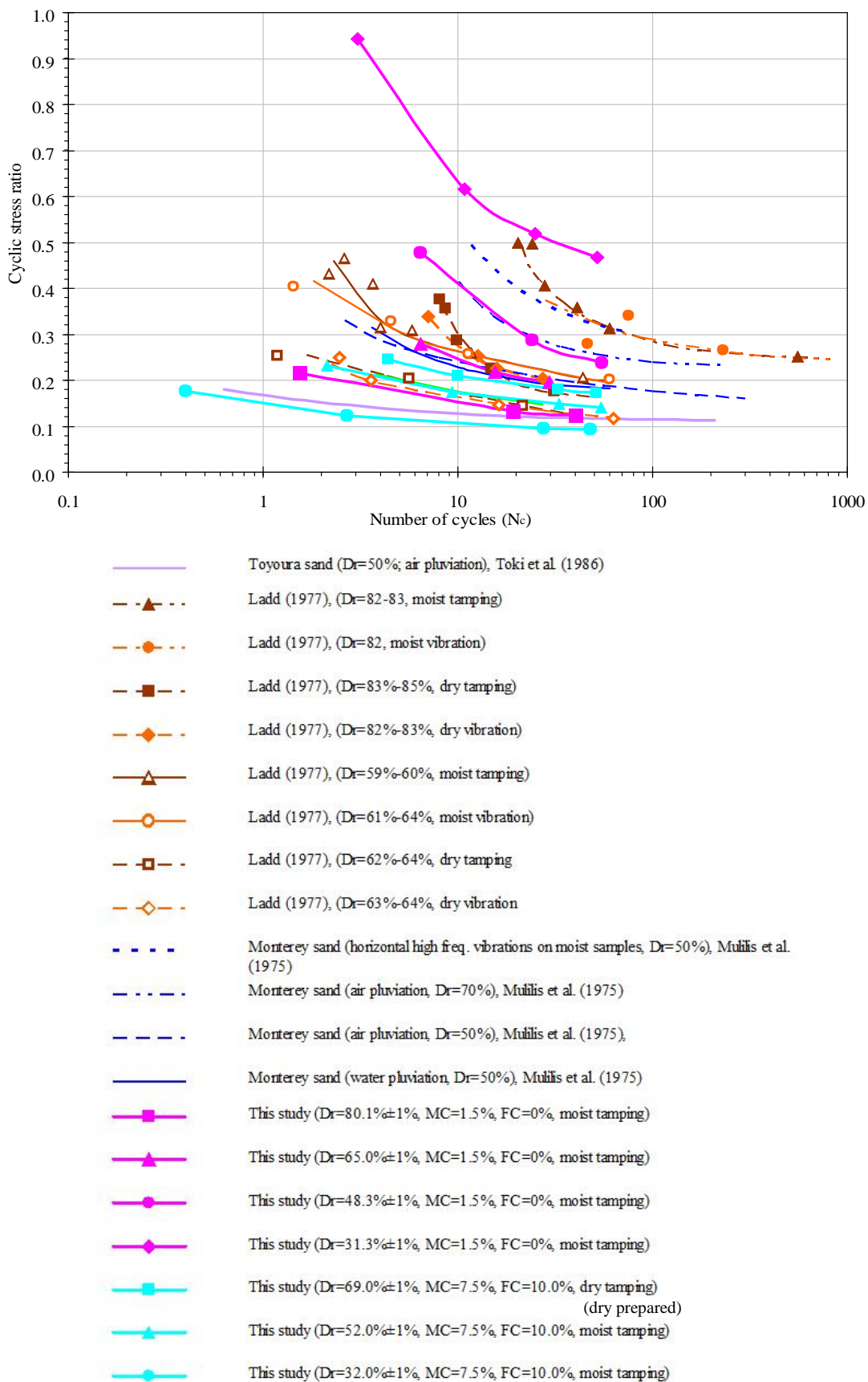


Figure 5.36. Comparison of the cyclic triaxial test results with the literature which are prepared using moist tamping (vibrating) and air pluviation methods

In the Figure 5.37, CSR- N_c curves of Old Gediz River Delta sand for 5%DA strain level are compared with remolded and frozen samples. 5%DA curves of the Old Gediz River Delta sands are located below the frozen samples except freshly deposited soils.

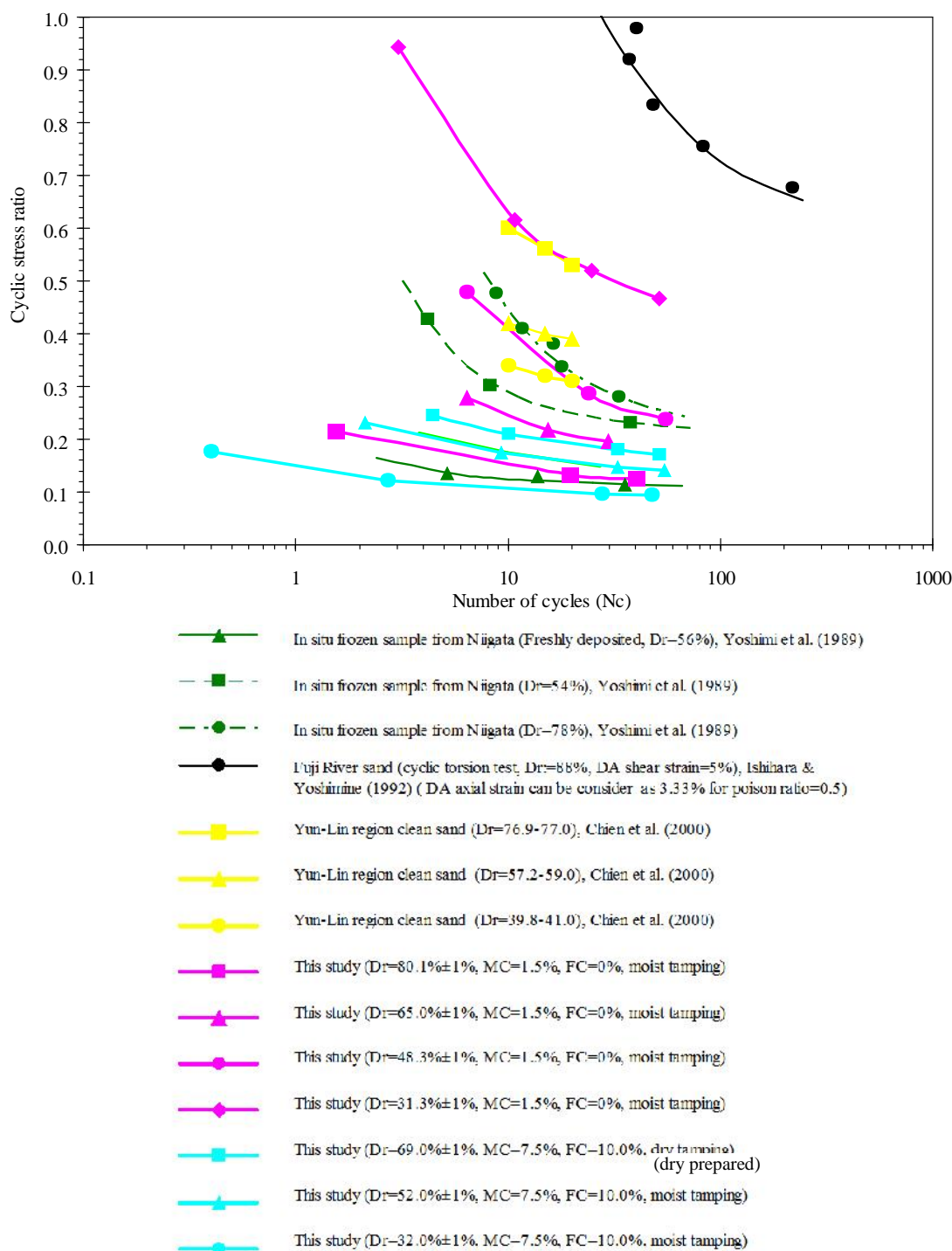


Figure 5.37. Comparison of the cyclic triaxial test results with frozen and field samples of the literature

Cyclic resistance data determined in Laboratory dynamic tests are related to field data by converting the relative densities of the test specimens to equivalent penetration resistance, and the resistance of sandy soils against liquefaction is analyzed by means of the methods that are based on field test data (i.e. Standard Penetration, Cone Penetration or Shear-Wave Velocity test data). For this purpose, several relationships between relative density (D_r) and N are available in the literature. Similar relationships are also available for (q_c) or V_s data. Some of the most commonly used methods are already introduced in Chapter 2. Cyclic strength of test samples are related to corrected Standard Penetration field resistance using the method of Tokimatsu and Seed (1987) as explained in the second chapter of the thesis (Figure 2.9). Cyclic resistance ratios versus equivalent $(N_1)_{60}$ values of tested samples are plotted in Figure 5.38.

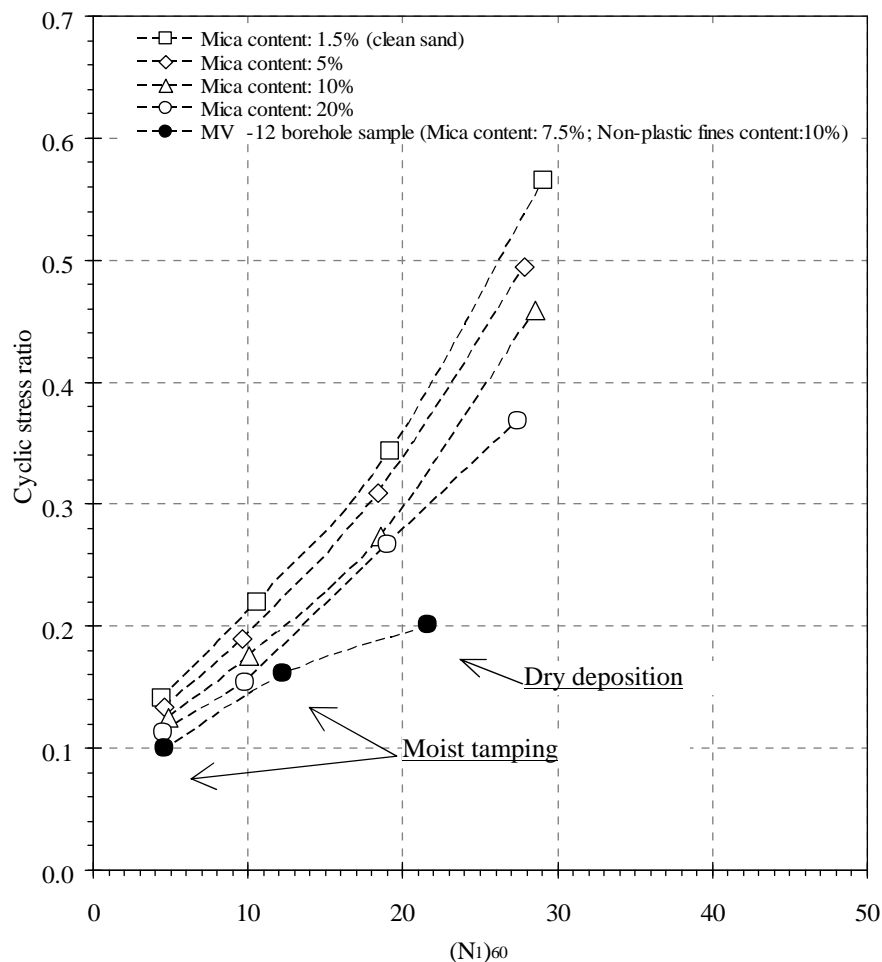


Figure 5.38 Cyclic resistance ratio (required 5% D.A. at 15th cycle) versus equivalent $(N_1)_{60}$ values for 1.5%, 5%, 10%, 20% mica contents and the MV - 12 sample

Mica grains increases void ratio of the host material (i.e. fine sand in this thesis). Besides this effect, mica may also change orientation of the sand grains and may cause a reduction in the number of contacts among sand grains. Consequently, mica grains cause a changing in sand properties as shown in Figure 5.3 and Equation 5.8 that SPT resistance is reduced as mica content increases. Therefore, direct use of D_r - $(N_1)_{60}$ correlations may be misleading since they do not include specific parameters to account for the presence of mica flakes. In this manner, the mica effect on $(N_1)_{60}$ of Figure 5.38 is eliminated using Equation 5.8. When Equation 5.8 is applied on $(N_1)_{60}$ values of Figure 5.38, Figure 5.39 is obtained. As one may notice in Figure 5.39, CSR- $(N_1)_{60}$ pairs for each mixture are located in a narrow band showing that mica effect on liquefaction resistance is pronounced as mica content exceed 10 %.

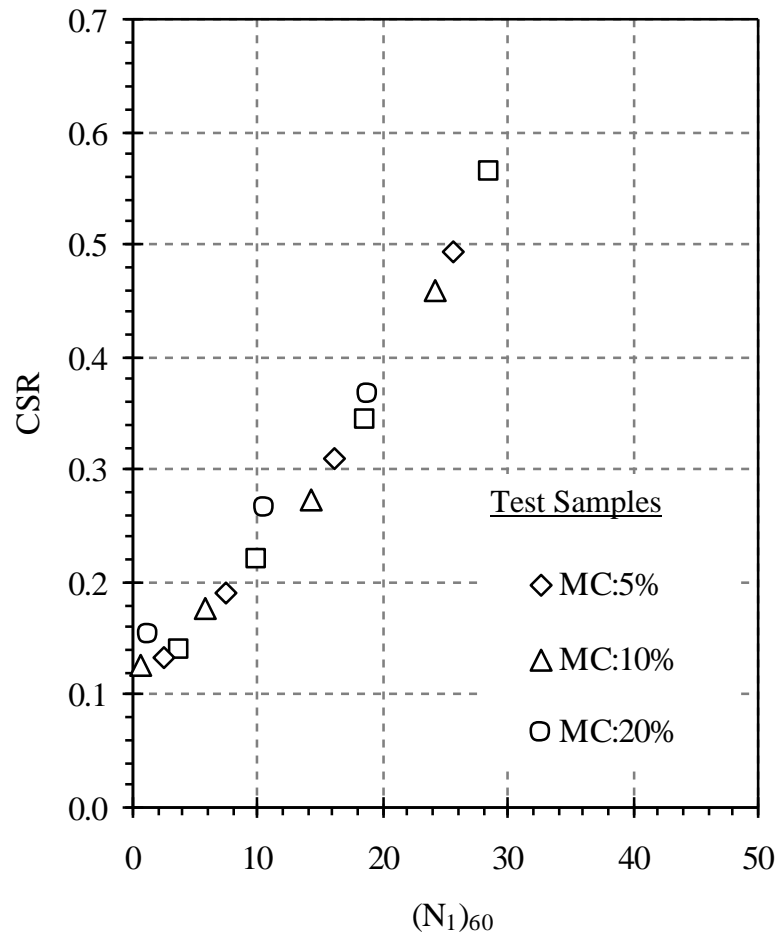


Figure 5.39 Cyclic resistance ratios (required 5% D.A. at 15th cycle) versus equivalent $(N_1)_{60}$ values for clean (without mica) Old Gediz River Delta sand. (The $(N_1)_{60}$ values is obtained using of Equation 5.8 and Figure 5.38)

Figure 5.38 and 5.39 curves are replotted in the following (Figure 5.40) along with the curves of other liquefaction evaluation methods based on Standard Penetration resistance.

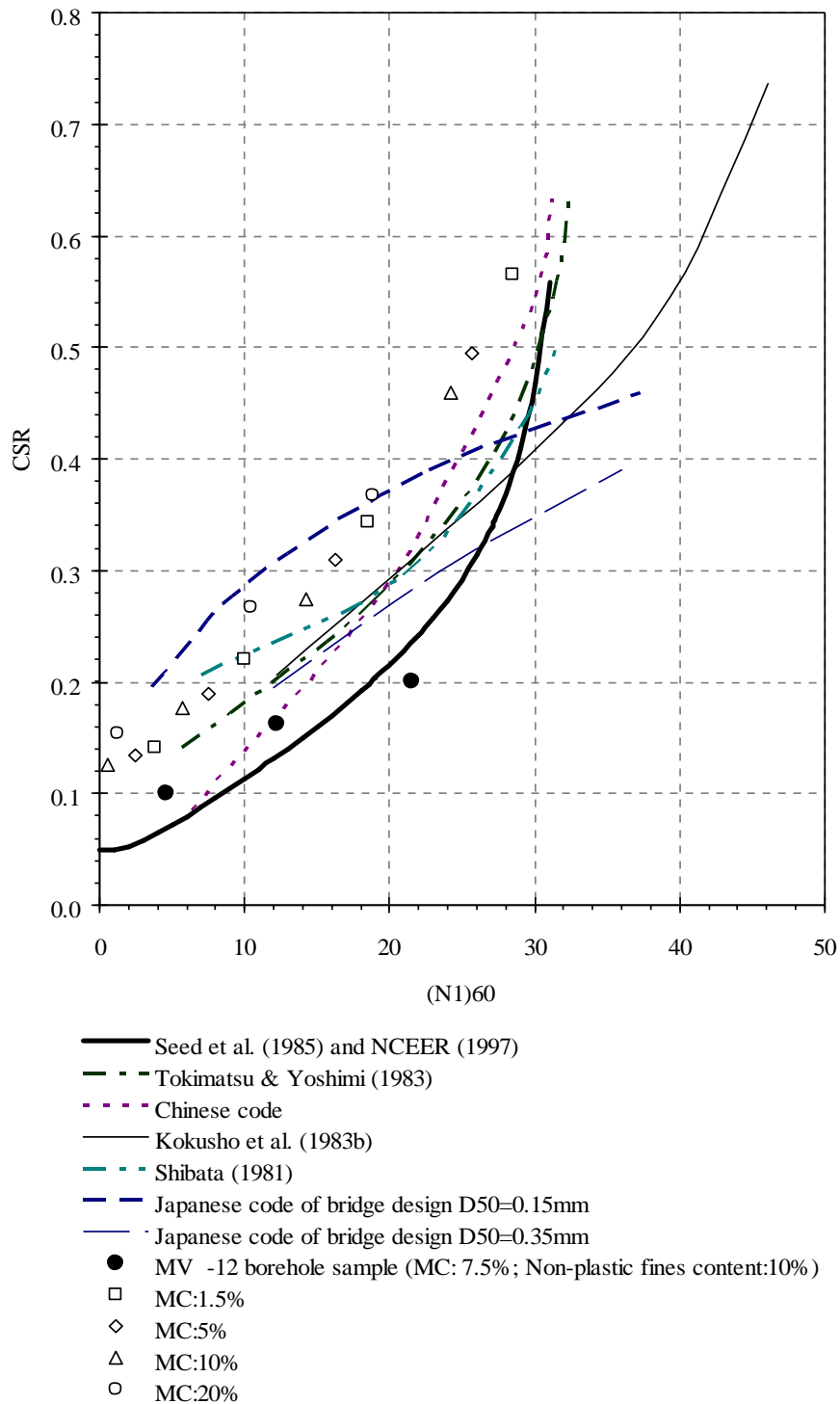


Figure 5.40 Cyclic resistance ratios of tested samples and methods for evaluation of the cyclic strength of sands based on the normalized SPT-N value

The global void ratio is one of the major parameters that is strongly related to engineering characteristics of the soils. CSR values are plotted with respect to global void ratio in Figure 5.41. One may notice in Figure 5.38, 5.39 and 5.41 that contradictory conclusions may be drawn as liquefaction resistance curves are plotted using conventional $D_r-(N_1)_{60}$ relationships are compared with those obtained using $(N_1)_{60}$ values that reflect mica grain effect being expressed by means of Equation 5.8.

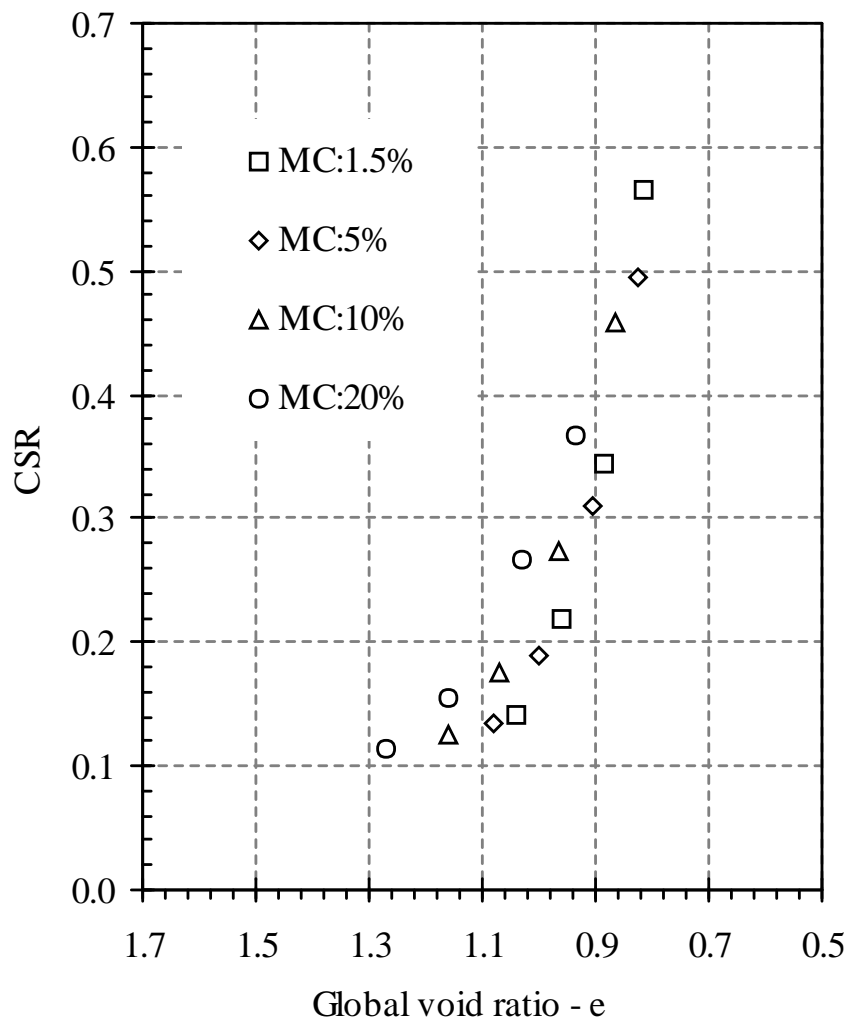


Figure 5.41 Cyclic resistance ratios (required 5% D.A. at 15th cycle) versus global void ratios (e) for 1.5%, 5%, 10%, 20% mica content of Old Gediz River Delta sand

As it is already mentioned in the above paragraphs, mica flakes act in such a manner that they increase the global void ratio of the sand-mica mixture. This is

readily observed on the maximum void ratio as shown in Figure 5.6. In the same figure, however, increasing effect of mica flakes on global void ratio is much less for the minimum void ratio. Therefore, mixtures may exist at the same global void ratio although they exhibit quite different relative densities. It can be seen in Figure 5.38 that liquefaction resistance decreases as mica content increases. However, it is a known fact that it is the global void ratio that governs the soil response for a certain mean effective stress level. One shall also evaluate test data according to the global void ratio in order to check whether sand-mica mixtures having close global void ratios exist although they show different relative densities. It is also necessary to see if such test specimens have close liquefaction resistances when the test results are expressed after the mica grain influence on $(N_1)_{60}$ is corrected or the data is plotted according to the global void ratio. Such a data reduction attempt is made in Figure 5.39 and 5.41, respectively. It is quite remarkable that CRR- $(N_1)_{60}$ curves vary in a narrow band and mica content on liquefaction resistance becomes effective beyond 10%. The CRR- N_{m60} data for MC=20% is shifted towards left of the rest of the data showing a slight increase in liquefaction resistance. This behavior can be seen in Figure 5.41 more clearly.

This effect of mica grains is similar to recent finding on the influence of non-plastic materials on the response of sandy soils (Thevanayagam, 2007a; Thevanayagam, 2007b; Yamamura et. all., 1999; Monkul and Yamamura, 2011). Researchers such as Thevanayagam (2007a) and Yamamura (1999) put forward that silty non-plastic fines decrease strength of sands up to a certain amount and beyond a threshold value of non-plastic fine material cyclic strength of sandy soils increases. Cyclic strength of clean Old Gediz River Delta sand with negligible amount of mica (MC=1.5) and fine materials is higher than 1998-NCEER (Youd & Idris, 2001) curve. The 1998-NCEER (Youd & Idris, 2001) curve represents the lower bound for the cyclic strength of clean delta sands.

CHAPTER SIX

CONCLUSIONS AND RECOMENDATIONS

In this experimental study, the effects of the platy mica grains, on dynamic behavior of the sandy soils within the liquefaction depth of the study area have been researched. Certain dynamic properties with an emphasis on liquefaction resistance of the sandy soils within the liquefaction depth of the survey area were studied. The conclusions and the recommendations of this study are presented herein:

Soil samples that were recovered from the study area were used in the testing program. Apart from the present study, dynamic experimental studies regarding the Old Gediz River Delta are scarce. Therefore, the findings of this study have significant importance since they will be informative and advisory for future researches to be conducted on the sandy soils of the area.

Platy mica content of the soils within the study area was determined down to 20 m from the surface. Soils of the survey area contain platy mica mineral ranging between 5% and 20%. Such mica content for sandy soils may be sufficient to change major engineering properties (such as internal friction angle, settlement potential, liquefaction resistance and SPT blow counts). In order to estimate soil behavior correctly, mica content of the sandy soils were studied in detail. For this purpose, a method based on simple, fast and low-cost XRD analyses results for determining the mica content of the soils was introduced and a correlation to estimate the mica content of sandy soils of the study area was developed.

Influence of platy mica grains on shear wave velocity was observed during bender element tests. For all mica contents, shear wave velocity decrease as relative density and effective confining pressure decreases. It was noticed that shear wave velocity was inversely proportional with mica content.

The mica grains used in the experimental study significantly reduced the liquefaction resistance of clean sand of the Old Gediz River Delta from the relative

density point of view. When compared to clean sand curve of the Seed et al. (1985) method, which is very often used in national and international wise and is considered nearly a standard for liquefaction analyses, two results manifest themselves: (1) Liquefaction resistances of the clean sand in the study area were found to be higher than base clean sand curve in Figure 2.8 (Seed et al. 1985); (2) Liquefaction resistances of field samples (FC=10% and MC=7.5%) are very close to clean sand curve in Figure 2.8 (Seed et al. 1985). Comparisons for different mica contents show that mica effects decreases cyclic strength of the sand (Figure 5.35 and 5.40).

Mica grains have significant effect on packing density of the sand. Influence of mica grains on certain strength and compressibility characteristic of sandy soils was studied by previous researchers. However, relative density effect on variation of friction angle, compressibility index, maximum and minimum void ratios with respect to mica ratio was not taken into consideration. In this research, it was found that the change in maximum void ratio with increasing mica amount was higher than it was found for minimum void ratio. This may be explained with the bridging mechanism of the mica grains resulting in the generation of larger size voids among sand grains for loose samples. As the density of the sand increases bridges collapse and influence mica grains on sand behavior diminishes. This fact is also observed in monotonic triaxial tests and post-liquefaction volumetric strain measurements where variations in frictional angle and volumetric strains are less for denser test samples. As a conclusion, it may put forward that bridging mechanism of mica flakes over the sand particles is a satisfactory explanation of the influence of mica grains on soil behavior provided that the relative density of the soil is taken into consideration along with other parameters such as mica content and size ratio (D_{mica}/D_{sand}).

On the other hand, when the global void ratio is considered, it seems that effect of the mica grains disappears. Moreover, when Figure 5.41 is examined, it seems that mica grains slightly increase cyclic strength. This may be explained that when two different sands which have different mica content (for instance 1.5% and 20%) are considered, more tamping energy is required in order to bring the mixture with higher mica content to the same global void ratio. Bridges that form over the sand

grains may collapse and mica flakes get into the voids inhibiting the movement of the sand grains during cyclic loading. More research including image processing to observe grain orientation is needed to clarify this aspect of the thesis.

At the end of the liquefaction tests, pore water pressure dissipated once the drainage valves of the samples were opened, and the volume of the drained pore water was measured. Liquefaction tests ended after reaching 10% strain level. Therefore, volume change measurements were made for large strains and volume changes presented in this study represent large strain levels. It is understood that post-liquefaction volumetric strains increase with mica and non-plastic fines content. When the density exceeds 70%, volumetric strain reduces as expected. As shown by these results, as the density increases, the difference between volumetric strain values decreases (Figure 5.20 and 5.21). Effects of mica content in dense samples are lower as compared with loose and medium dense samples. It is observed that the non-plastic fine material increases the volume change of the sand in comparison with the clean sand sample at the same density. Therefore, for micaceous sand and especially sand of the study area (i.e. Old Gediz River Delta), available methods in the literature for estimating post liquefaction volumetric strain may be considered as the lower limit.

It should be kept in mind that all of the statements made above and the conclusions reached so far depend on the test results obtained on re-constituted sand-mica mixtures with sand to mica grain size ratio of nearly equal to unity. At this point, the effect of specimen preparation method (i.e. wet tamping versus air or water raining) and mica size on bridge formation is not completely covered in the thesis. Therefore, it is recommended for future research that undisturbed frozen samples shall be recovered in the field and a testing program shall be pursued so that investigations at micro and macro scales could be made to find out ordering of sand-mica grains and corresponding cyclic strength. Such a study is also expected to provide correlation factors between liquefaction resistance of natural undisturbed micaceous sandy soils and reconstituted laboratory test specimens. Sand-mica mixtures at different size ratios shall also be studied in future test studies.

REFERENCES

- 106G159. (2011). zmir Metropolü ile Alia a ve Menemen ilçelerinde güvenli yapı tasarımı için zeminin sismik davranı larının modellenmesi. (2011 in reviewed as completed). *Earthquake Research Center of Dokuz Eylöl University (DAUM) and TÜB TAK*. TÜB TAK Project No: 106G159, zmir.
- Akıncı, A., Eyido an, H, Göktürkler, G., Akyol, N., & Ankaya, O. (2000). zmir ili çevresinin depremselli i ve deprem tehlikesinin incelenmesi. *Batı Anadolu'nun Depremselli i Sempozyumu (BADSEM), Bildiriler Kitabı*, ISBN: 975-585-148-8, 231-238, zmir.
- Akyol, N., Zhu, L., Mitchell, B. J., Sözbilir, H., & Kekovalı, K. (2006). Crustal Structure and Local Seismicity in Western Anatolia. *Geophysical Journal International*, 166 (3), 1259-1269.
- Alper, . Y. (2008). *A geotechnical earthquake engineering investigation for soils of south eastern coast of zmir Bay*. Master Thesis, Graduate School of Natural and Applied Sciences of Dokuz Eylöl University, zmir, Türkiye.
- Altın, S. (1993). 6 Kasım 1992 zmir Depremi sonuçları üzerine bir irdeleme. *n aat Mühendisleri Odası Teknik Dergisi*, 731-742.
- Ambraseys, N. N. (1988). Engineering seismology. *Earthquake Engrg. and Struct. Dynamics*, 17, 1-105.
- Ambraseys, N. N., & Finkel C. F. (1995). *The seismicity of Turkey and adjacent areas-a historical review 1500-1800*. stanbul: Eren Yayıncılık.
- Andrus, R. D., Stokoe, K. H., & Roesset, J. M. (1991). Liquefaction of gravelly soil at Pence Ranch during the 1983 Borah Peak, Idaho Earthquake. *Proceedings*,

First International Conference on Soil Dynamics and Earthquake Engineering, Karlsruhe, Germany.

- Andrus, R. D., & Stokoe, K. H. (1997). Liquefaction resistance based on shear-wave velocity. *Proc. NCEER Workshop on Evaluation of Liquefaction Resistance of Soils. T.L. Youd and I.M. Idriss, eds., National Center for Earthquake Engrg. Research, Buffalo, N.Y., 89-128.*
- Arango, I. (1996). Magnitude scaling factors for soil liquefaction evaluations. *J. Geotech. Engrg., ASCE, 122 (11), 929-936.*
- Ario lu, E., Ario lu, M. B., & Girgin C. (2003). Arias iddeti ile sıvıla ma analizi. *Beton Prefabrikasyonu, 65 (66), 11-19.*
- Askari, F., Dabiri, R., Shafiee, A., & Jafari, M. K. (2010). Effect of non-plastic fines content on cyclic resistance and post liquefaction of sand-silt mixtures based on shear wave velocity. *JSEE, 12 (1), 13-24.*
- ASTM (2005). *Annual Book of ASTM Standards. American Society for testing and materials Vol. 04.08, Philadelphia, USA.*
- Aydal, D. (1990). Cevherdeki toplam demir yüzdesinin Xrd-floresans radyasyon iddeti yardımıyla kantitatif olarak bulunması. *Maden Tetkik ve Arama Dergisi, 111, 133-152.*
- Ba cı, G., (2000). zmir ve çevresinin deprem riski. *Batı Anadolu'nun Depremselli i Sempozyumu (BADSEM) Bildiriler Kitabı, ISBN: 975-585-148-8, 239-248, zmir.*
- Barden, L., & Sides, G. (1971). Sample disturbance in the investigation of clay structure. *Geotechnique, 21 (3), 211-22.*

- Barka, A., & Reilinger, R. (1997). Active Tectonics of the Eastern Mediterranean region deduced from GPS, Neotectonic and Seismicity data. *Annelis de Geofisica*, 40 (3), 587-610.
- Baysal, B. (2006). Mavi ehir zmir bölgesi zeminlerinin geomekanik özelliklerinin belirlenmesi ve bölgede yapılacak yapıların zemin iyile tirme çalı malarına örnek bir uygulama. *M. Sc.. Thesis, Graduate School of Natural and Applied Sciences of Celal Bayar University, Manisa, Turkey.*
- Bilir, K., Öteyaka, B., Uçba , Y., Bozkurt, R., & Süer, Ü. (1997). Modifiye flotasyon kolonunda iri taneli feldspatların zenginle tirilmesi. 2. *Endüstriyel Hammaddeler Sempozyumu*, 253-261.
- Bokhtair, M., Muqtadir, A., & Ali, M. H. (1999). Stress-path dependent behaviour of micaceous sand. *Journal Of Civil Engineering The Institution of Engineers, Bangladesh*, 27 (2), 129-141.
- Bokhtair, M., Muqtadir, A., & Ali, M. H. (2000). Effect of mica content on stress - deformation behaviour of micaceous sand. *Journal Of Civil Engineering The Institution of Engineers, Bangladesh*, 28 (2), 155-167.
- Bouckovalas, G. D., Andrianopoulos, K. I., & Papadimitriou, A. G. (2003). A critical state interpretation for the cyclic liquefaction resistance of silty sands. *Soil Dynamics and Earthquake Engineering*, 23, 115-125.
- Bozkurt, E., & Sözbilir, H. (2004). Tectonic evolution of the Gediz Graben: Field evidence for an Episodic, two-stage extension in Western Turkey. *Geological Magazine*, 141, 63-79.
- BS 1377 (1990). *British Standards*. British Standards Institution, London, UK.

- Candan, O. (1994). Ala ehir kuzeyinde (Menderes Masifi, Demirci–Gördes Asmafisi) gözlenen metagabrolarm petrografisi ve metamorfizması. *Türkiye Jeoloji Bülteni*, 37, 29-40.
- Casagrande, A. (1940). Characteristics of cohesionless soils affecting the stability of slopes and earth fills, *Contributions to Soil Mechanics, Boston Society of Civil Engineers*, 257-276
- Castro, G. (1975). Liquefaction and cyclic mobility of saturated sands. *Journal of the Geotechnical Engineering Division, ASCE*, 101 (GT6), 551-569.
- Castro, G., & Poulos, S. J. (1977). Factors affecting liquefaction and cyclic mobility. *Journal of the Geotechnical Engineering Division, ASCE*, 106 (GT6), 501-506.
- Castro, G. (1995). Empirical methods in liquefaction evaluation. *Primer Ciclo d Conferencias Internacionales*, Leonardo Zeevaert, Universidad Nacional Autonoma de Mexico, Mexico City.
- Cho, G. C., Dodds, J., & Santamarina, J. C. (2006). Particle shape effects on packing density, stiffness and strength: natural and crushed sands. *Journal of Geotechnical and Geoenvironmental Engineering, ASCE*, 132 (5), 591-602.
- Chien, L. K., Oh, Y. N., & Chang, C. H. (2000). Evaluation of liquefaction resistance and liquefaction induced settlement for reclaimed soil. *Twelfth World Conference on Earthquake Engineering*. Paper No. 0386 Auckland, New Zealand.
- Chinese Building Code. (1974). *Earthquake resistant design code for industrial and civils buildings*. TJ11-74, Pechino: Chine Build. Publ. House.
- Christian, J. T., & Swiger, W. F. (1975). Statistics of liquefaction and SPT results. *ASCE, Journal of the Geotechnical Engineering Division*, 101 (GT11), 1135-1150.

- Çatal, H. H., Photo:1999, (2011, December, 10). *17 A ustos 1999 Körfez Depreminde yapısal hasar görüntüleri*. <http://kisi.deu.edu.tr/huseyin.catal/>
- Dadak, A., & Toloy, S. (2002). zmir ili ve çevresinde ya anmı depremler üzerine literatür ara tırması. *Final Project No. GEOBP0204, Supervisors: Gürkan Özden & Mehmet Kuruo lu, Dokuz Eylül University, Faculties of Engineering, Civil Engineering Department, Geotechnics Division, zmir, Turkey.*
- Das, B. M. (1992). *Principles of soil dynamics*. ISBN: 0-534-93129-4. Boston: PWS-Kent Publishing Company.
- DBYBHY (2007). *Deprem bölgelerinde yapılacak binalar hakkında yönetmelik*. Ankara: T.C. Bayındırlık ve skan Bakanlı ı.
- Dewey, J. F., & engör, A. M. C. (1979). Aegean and surrounding regions: complex multiplate and continuum tectonics in a convergent zone. *Geol. Soc. Am. Bull.*, 1 (90), 84-92
- Durmu , E. (2006). Konak (zmir) ilçesi zeminlerinin geoteknik özellikleri ve davranı analizleri., *M. Sc.. Thesis, Graduate School of Natural and Applied Sciences of Celal Bayar University, Manisa, Turkey.*
- Emre, Ö., & Barka, A. (2000). Gediz Grabeni - Ege Denizi arasının (zmir yöresi) aktif fayları, *Batı Anadolu'nun Depremselli i Sempozyumu (BADSEM), zmir, Bildiriler Kitabı*, ISBN: 975-585-148-8, 131-132.
- Emre, Ö., Özalp, S., Do an, A., Özaksoy, V., Yıldırım, C., & Gökta , F. (2005). zmir ve yakın çevresinin diri fayları ve deprem potansiyelleri. *MTA Genel Müdürlü ü, Rapor No: 10754*, 1-80.

- Erdo an, B. (1990). zmir-Ankara Zonu'nun, zmir ile Seferihisar arasındaki bölgede stratigrafik özellikleri ve tektonik evrimi. *Türkiye Petrol Jeologları Derne i (TPJD) Bülteni*, 2, 1-20.
- Erdo an, B., & Güngör, T. (1992). Menderes Masifi Kuzey kanadının stratigrafisi ve tektonik evrimi. *Türkiye Petrol Jeologları Derne i (TPJD) Blt.*, 4 (1), 9-34.
- Ergünay, O., Bayülke, N., & Genço lu, S. (1974). *1 ubat 1974 zmir Depremi Raporu*. Ankara: T.C. mar ve şkan Bakanlığı 1 Deprem Ara tırma Dairesi.
- Finn, L. W. D, Dennison, J. P., & Bransby, P. L. (1971). Sand liquefaction in triaxial and simple shear tests, *Journal of the Soil Mechanics and Foundations Division. ASCE*, 97 (SM4), 639-659.
- Finn, L. W. D., Lee, K. W. & Martin, G. R. (1977). An Effective Stress Model for Liquefaction. *Journal of the Geotechnical Engineering Division, ASCE*, 103 (GT6), 517-533.
- Georgiannou, V. N. (2006). The undrained response of sands with additions of particles of various shapes and sizes. *Geotechnique*, 56 (9), 639-649.
- Geredeli, A., & Özbayo lu, G. (1995). Simav feldspatının flotasyonu. *Endüstriyel Hammaddeler Sempozyumu*. 71-81, zmir, Türkiye.
- Gibbs, H. J., & Holtz, W. G. (1957). Research on determining the density of sand by spoon penetration testing. *Proc. 4th Int. Conf. On Soil Mech. and Found. Engrg.* 1, 35-39.
- Guimaraes, M. (2002) Crushed stone fines and ion removal from clay slurries-fundamental studies. *PhD dissertation, Georgia Institute of Technology, Georgia*.

- Güz, H. (1970). İzmir Körfezi'nde Deniz Bostanlığı Lagüna sedimanlarının geoteknik özellikleri. *İstanbul Mühendisleri Odası Türkiye İstatistik Mühendisleri V. Teknik Kongresi*, Rapor No: 6, Ankara.
- Halder, A., & Tang, W.H. (1981). Statistical study of uniform cycles in earthquakes. *Journal of the Geotechnical Engineering Division, ASCE*, 107 (GT5), 577-589.
- Harris, W. G., Parker, J. C., & Zelazny, L. W. (1984a). Effects of mica content on engineering properties of sand. *Soil Science Society of America Journal*, 48, 501-505.
- Harris, W. G., Zelazny, L. W., Parker, J. C., Baker J. C., Weber, R. S., & Elder, J. H. (1984b). Engineering properties of soils as related to mineralogy and particle-size distribution. *Soil Science Society of America Journal*, 48, 978-982.
- Hight, D. W., Georgiannou, V. N., Martin, P. L., & Mundegar, A. K. (1998), *Flow slides in micaceous sand. Problematic soils. Yanagisawa, E., Moroto, N., and Mitachi, T., eds.*, Rotterdam, Balkema.
- Holtz, R. D., Kovacs, W. D., & Shean, T. C. (2011). *An Introduction to Geotechnical Engineering*, Second Edition, ISBN: 978-0-13-249634-6, New York: Pearson.
- Horn, H. M., & Deere, D. U. (1962). Frictional characteristics of minerals. *Geotechnique*, 12 (4), 319-335.
- Lateral spreading due to liquefaction. *University of Washington*. (June 22, 2011). <http://www.ce.washington.edu/~liquefaction/html/what/what2.html>.
- ICDD. *The International Centre for Diffraction Data*. (July 16, 2010). www.icdd.com.

- Idriss, I. M. (1999). An update to the Seed-Idriss simplified procedure for evaluating liquefaction potential. Presentation notes. *Workshop, new approaches to liquefaction analysis*, Transportation Research Board, Washington, D.C.
- Ishihara, K. (1985). Stability of natural deposits during earthquakes. *Proceedings of the Eleventh International Conference on Soil Mechanics and Foundation Engineering*, San Francisco
- Ishihara, K. (1993). Liquefaction and flow failure during earthquake. *33-rd Rankine lecture, Geotechnique*, 43 (3), 351-415.
- Ishihara, K. (2003). *Soil behavior in earthquake geotechnics. 2. Press*, ISBN: 0-19-856224-1, New York: Oxford University Press.
- Ishihara, K., & Cubrinovski, M. (1998). Problem associated with liquefaction and lateral spreading during earthquake. *Geotechnical Earthquake Engineering and Soil Dynamics III, ASCE, Geotechnical Special Publication*, 75 (1), 301-312.
- Ishihara, K., & Li, S. (1972). Liquefaction of saturated sand in triaxial torsion shear test. *Soils and Foundations*. 12 (2), 19-39.
- Ishihara, K., & Yoshimine, M (1992). Evaluation of settlements in sands deposits following liquefaction during earthquakes. *Soils and Foundations*, 32 (1), 173-188.
- Ishihara, K., Tatsuoka, F. & Yasuda, S. (1975). Undrained deformation and liquefaction of sand under cyclic stress. *Soils and Foundations*, 15 (1), 29-44.
- Iuga, A., Cuglesan, I., Samuila, A., Blajan, M., Vadan, D., & Dascalescu, L. (2004). Electrostatic separation of muscovite mica from feldspathic pegmatites. *IEEE Transactions On Industry Applications*, 40 (2), 422-429.

- Japan Road Association. (1980). *Design Specifications of Highway Bridges*, Tokyo, Japan.
- JGS (2000). *Standards of Japanese geotechnical society for laboratory shear test (English version)*. The Japanese geotechnical society. Tokyo, Japan.
- Kaya, O. (1981). Miocene reference section for the coastal parts of West Anatolia, *Newsletters of Stratigraphy*, 10, 164-191.
- Kayalar, A. . (1991). Eski Gediz Deltası ve Melez Çayı kıyı sedimanlarının oturma özellikleri ve bu sedimanların üzerindeki yapılarda görülen oturma problemleri. *n aat Mühendisli inde Zemin Sempozyumu, zmir, MO zmir ubesi, Bildiriler Kitabı*, 115-131.
- Kayen, R. E, Mitchell, J. K., Seed, R.B., Lodge, A, Nishio, S., & Coutinho, R. (1992). Evaluation of SPT, CPT, and shear-wave based methods for liquefaction potential assessment using Loma Prieta data. *Proc., 4th Japan-U.S. Workshop on Earthquake-Resistant Des. Of Life-line Fac. And Countermeasures for Soil Liquefaction*, 1, 177-204.
- Kayan, . (2000). zmir çevresinin morfotektonik birimleri ve alüvyal jeomorfolojisi. *Batı Anadolu'nun Depremselli i Sempozyumu (BADSEM)*, zmir, Bildiriler Kitabı, ISBN: 975-585-148-8, 103-111.
- Kayen, R. E., & Mitchell, J. K. (1997). Assessment of liquefaction potential during earthquakes by arias intensity. *Journal of Geotechnical and Geoenvironmental Engineering*, 123 (12), 1162-1174.
- KOERI (2003). *Kandilli Observatory and Earthquake Research Institute*
<http://www.koeri.boun.edu.tr/>

- Kokusho, T., Yoshida, Y., Nishi, K., & Esashi, Y. (1983a). Evaluation of seismic stability of dense sand layer (part 1) – dynamic strength characteristics of dense sand. Report 383025, *Electric Power Central Research Institute*, Japan..
- Kokusho, T., Yoshida, Y., Nishi, K., & Esashi, Y. (1983b). Evaluation of seismic stability of dense sand layer (part 2) – evaluation method by standard penetration test. Report 383025, *Electric Power Central Research Institute*, Japan.
- Kramer, S. L. (1988). Triggering of liquefaction flow slides in coastal soil deposits. *Engineering Geology*, 26 (1), 17-31.
- Kramer, S.L. (1996). *Geotechnical earthquake engineering*. ISBN: 0-13-374943-6, New Jersey: Prentice Hall inc.
- Kuruo lu, M. (2004). Geographic information system (GIS) based database development and evaluation study for soils of northern coast of zmir Bay. *Ph. D. Thesis, Graduate School of Natural and Applied Sciences of Dokuz Eylül University*, zmir, Turkey.
- Ladd, R. S. (1977). Specimen preparation and cyclic stability of sand. *Journal of the Geotechnical Division*. 103 (GT6), 535-547.
- Lade, P. V., Liggio, C. D., & Yamamuro, J. A. (1998). Effects of non-plastic fines on minimum and maximum void ratios of sand. *Geotechnical Testing Journal, GTJODJ*, 21 (4), 336-347.
- Law, K. T., Cao, Y. L., & He, G. N. (1990). An energy approach for assessing seismic liquefaction potential. *Canadian Geotechnical Engineering Journal*, 27 (3), 320-329.

- Lee, J. S., & Santamarina, J. C. (2005). Bender elements: performance and signal interpretation. *Journal of Geotechnical and Geoenvironmental Engineering*. 131 (9), 1063-1070.
- Lee, J. S., Guimaraes, M., & Santamarina, J. C. (2007). Micaceous sands: Microscale mechanisms and macroscale response. *Journal of Geotechnical and Geoenvironmental Engineering*, 133 (9), 1136-1143.
- Lee, K., & Albesia, A. (1974). Earthquake induced settlements in saturated sands. *Journal of ASCE*, 100, 387-405.
- Liao, S., & Whitman, R. V. (1986a). Overburden correction factors for SPT in sand. *Journal of Geotechnical Engineering. ASCE*, 112 (3), 373-377.
- Liao, S. & Whitman, R.V. (1986b). Catalogue of liquefaction and non-liquefaction occurrences during earthquakes. *Res. Rep., Dept. of Civ. Engrg., Massachusetts Insitute of Technology, Cambridge*.
- Liao, S. S. C., Veneziano, D., & Whitman, R.V. (1988). Regression models for evaluating liquefaction probability. *Journal of Geotechnical Engineering. ASCE*, 114 (4), 389-411.
- Liu, A. H., Steward, J. P., Abrahamson, N. A., & Moriwaki, Y. (2001). Equivalent number of uniform cycles for soil liquefaction analysis. *Journal of Geotechnical and Geoenvironmehtal Engineering*, 127 (12), 1017-1025.
- McKenzie, D. P. (1978). Active tectonics of the Alpine-Himalayan Belt: The Aegean Sea and surrounding regions. *Geophys. J. R. Astr. Soc.*, 55, 217-254.
- Meyerhof, G. G. (1957). Discussion on research on determining the density of sands by penetration testing. *Proceedings of the 4th International Conference on Soil Mechanics and Foundation Engineering*, Paper: 3/110, London.

- Monkul, M. M., & Yamamuro, J. A. (2011). Influence of silt size and content on liquefaction behavior of sand. *Canadian Geotechnical Journal*, 48 (6), 931-942.
- Mulilis, J. P., Chan, C. K., & Seed, H. B. (1975). The effects of method of sample preparation on the cyclic stress-strain behavior of sands. *U. S. Nuclear Regulatory Commission Office, Washington, R. No. EERC 75-18.-Jully, California, U.S.*
- Mulilis, J. P., Seed, H. B., Chan, C. K., Mitchell, K., & Arulanandan, K. (1977). Effect of sample preparation on sand liquefaction. *Journal Of The Geotechnical Engineering Division*, 103 (GT2), 91-107.
- Nagase, H., & Ishihara, K. (1988). Liquefaction-induced compaction and settlement of sand during earthquakes. *Soils and Foundations*, 28 (1), 65-75.
- National Research Council (1985). *Liquefaction of soils during earthquakes*. Washington D.C: National Academy Press.
- NCCER-1997. (1997). Edited: Youd, T. L., & Idriss, I. M. Proceeding of the NCEER Workshop on Evaluation of Liquefaction Resistance of Soils. *Technical Report NCEER-97-0022 December 31 1997*. Utah. US.
- Ogunsanwo, O. (1988). Basic geotechnical properties, chemistry and mineralogy of some laterite soils from S.W. Nigeria. *Bulletion of the International Association of Engineering Geology*. Paper No:37. Paris, France.
- Orhan, M., & Ate , A. (2010). Standard Penetrasyon Testi (SPT) ile Saruhanlı (Manisa) İçesi zeminlerinin sıvıla ma potansiyelinin ara tırılması. *AKÜ Fen Bilimleri Dergisi*. 2, 37-49..

- Orhan, M., & Ate , A. (2012). Rölâtif sıklı ın Saruhanlı (Manisa) İçesi zeminlerinin sıvıla masına etkisinin dinamik üç eksenli deneyi ile ara tırılması. *SDU Journal of Technical Sciences*, 2 (1), 26-41..
- Özakcan, A. (2004). zmir'in Mavi ehir ve Manavkuyu Delta sahalarında dinamik zemin davranı ı analizleri. *Final Project No. GEO.BP.04B04, Dokuz Eylül University, Faculties of Engineering, Civil Engineering Department, Geotechnics Division, zmir, Turkey.*
- Özbal, S. (1999). *Herkez ı ı ı kadar çeker, 99 Depremi Gölcük-Adapazarı-8.* Retrieved (December, 2011). from <http://sezayozbal.blogspot.com/2011/11/99-depremi-golcuk-adapazar-8.html>.
- Özden, G. (2000). Marjinal zeminlerde temel problemleri. *ESBA Sempozyumu, zmir, Bildiriler Kitabı*, 1-16.
- Özer, S., Sözbilir, H., Özkar, ., Toker, V., & Sarı, B. (2001). Stratigraphy of Upper Cretaceous-Palaeogene sequences in the southern and eastern Menderes massif (Western Turkey). *International Journal of Earth Sciences*, 89, 852-866.
- Özkan, M. Y., & Çalı an, O. (1991). zmir Körfezi kuzeyinde yer alan alüvyon zeminlerin genel geoteknik özellikleri. *n aat Mühendisli inde Zemin Sempozyumu, zmir, n aat Mühendisleri Odası zmir ubesi, Bildiriler Kitabı*, 207-220.
- Özkaymak, Ç., & Sözbilir, H. (2008). Stratigraphic and structural evidence for fault reactivation: The Active Manisa Fault Zone, Western Anatolia. *Turkish Journal of Earth Sciences*, 17 (3), 615-635.
- Özkaymak, Ç., Sözbilir, H., Uzel, B., & Akyüz, H. S. (2011). Geological and paleoseismological evidence for Late Pleistocene-Holocene activity on the

- Manisa Fault Zone, Western Anatolia. *Turkish Journal of Earth Sciences*, 20 (4), 449-474.
- Patton, S. (1992). Active normal faulting, drainage patterns, and sedimentation in Southwestern Turkey. *Journal of the Geological Society of London*, 149, 1031-1044
- Peacock, W. H., & Seed, H. B. (1968). Sand liquefaction under cyclic loading simple shear conditions. *Soil Mechanics and Foundations Division*, 94 (SM3), 689-708.
- Prakash, S., Guo, T., & Kumar, S. (1998). Liquefaction of silts and silt-clay mixtures. *Geotechnical Earthquake Engineering and Soil Dynamics III, ASCE, GSP No.75*, 337-348.
- RADIUS (1999). Earthquake Scenario and Master Plan for the city of Izmir. *Final Report (Edt. Erdik, M.)*, Bozaziçi University, Istanbul, Turkey.
- Robertson, P. K., & Wride, C. E. (1998). Evaluating cyclic liquefaction potential using the cone penetration test. *Can. Geotech. J.*, 35 (3), 442-459.
- Santamarina, J. C., & Cho, G. C. (2004). Soil behaviour: The role of particle shape. *Proceeding Skempton Conference*. London. 1-14.
- Seed, H. B. (1979). Soils liquefaction and cyclic mobility evaluation for level ground during earthquakes. *Journal of the Geotechnical Engineering Division*, 105 (GT2), 201-253.
- Seed, H. B., & Harder, L. F., (1990). SPT-based analysis of cyclic pore pressure generation and undrained residual strength. *Proc. Seed Memorial Symp., Berkeley*, 2, 351-376.

- Seed, H. B., & Idriss, I. M. (1967). Analysis of soil liquefaction: Niigata Earthquake, *Journal of the Soil Mechanics and Foundations Division, ASCE*, 93 (SM3), 83-108.
- Seed, H. B., & Idriss, I. M. (1969). Influence of soil conditions on ground motions during earthquakes. *Journal of the Soil Mechanics and Foundations Division, ASCE*, 95 (SM1), 99-137.
- Seed, H. B., & Idriss, A. M. (1971). Simplified procedure for evaluating soil liquefaction potential. *Journal of the Soil Mechanics and Foundations Division*, 97 (SM9), 1249-1273.
- Seed, H. B., & Idriss, I. M. (1982). Ground motions and soil liquefaction during earthquakes. *Earthquake Engineering Research Institute Monograph*, Oakland, Calif.
- Seed, H. B., & Lee K. L. (1966). Liquefaction of saturated sands during cyclic loading. *Journal of the Soil Mechanics and Foundations Division, ASCE*, 92 (SM6), 105-134.
- Seed, H. B., Idriss, I. M., & Arango, I. (1983). Evaluation of liquefaction potential using field performance data. *Journal of the Geotechnical Engineering Division, ASCE*, 105 (GT3), 458-482..
- Seed, H. B., Martin, P. P., & Lysmer, J. (1975). The generation and dissipation of pore water pressures during soil liquefaction. *Report No. ERRC 75-26, Earthquake Engineering Research Center, University of California, Berkeley.*
- Seed, H. B., Tokimatsu, K., Harder, L. F., & Chung, R. M. (1985). Influence of SPT procedures in soil liquefaction resistance evaluations. *Journal of the Geotechnical Engineering Division, ASCE*, 111 (12), 1425-1445.

- Seed, H. B., Cetin, K. O., & Moss, R. E. S. (2001). Recent advances in soil liquefaction engineering and seismic site response evaluation. *Proc. 4th Int. Conf. Recent Adv. In Geotech. Earthquake Engrg. Soil Dyn.* Paper SPL-2.
- Seyito lu, G., & Scott, B. C. (1991). late cenozoic crustal extension and basin formation in West Turkey. *Geological Magazine*, 128, 155-166.
- Seyito lu, G., & Scott, B. (1996). The cause of N-S extensional tectonics on Western Turkey: Tectonic escape vs. back-arc spreading vs. orogenic collapse. *Journal of Geodynamics*, 22, 145-153.
- Seyito lu, G., Scott, B. C., & Rundle, C. C. (1992). Timing of Cenozoic extensional tectonics in West Turkey. *Journal of the Geological Society*, 149, 533-538.
- Shibata, T. (1981). Relations between N-value and liquefaction potential of sand deposits. *Proceedings, 16th Annual Convention of Japanese Society of Soil Mechanics and Foundation Engineering*, 621-624.
- Shirley, D. J., & Hampton, L. D. (1978) Shear-wave measurements in laboratory sediments. *J. Acoustical Soc. Am.* 63 (2), 607-613
- Singh, S., Donovan, N. C., & Park, F. (1980). A Re-examination of the effect of prior loadings on the liquefaction resistance of sands. *Proceedings, 8th World Conference on Earthquake Engineering*, Vol:3, stanbul-Türkiye
- Skempton, A. W. (1954). The pore-pressure coefficients A and B. *Geotechnique*, 4 (4), 143-147.
- Skempton, A. W. (1986). Standard penetration test procedures and the effects in sands of overburden pressure, relative density, particle size, aging, and overconsolidation. *Geotechnique*, 36 (3), 425-447.

- Sönmez, H., & Gökçeolu, C. (2005). A liquefaction severity index suggested for engineering practice. *Environmental Geology*, 48 (1), 81-91.
- Sözbilir, H. (2001). Extensional tectonics and the geometry of related macroscopic structures: field evidence from the Gediz Detachment, Western Turkey. *Turkish Journal of Earth Sciences*, 10 (2), 51-67.
- Sözbilir, H. (2002). Geometry and origin of folding in the Neogene sediments of the Gediz Graben, Western Anatolia, Turkey. *Geodinamica Acta*, 15 (5), 277-288.
- Sözbilir, H., Uzel, B., Sümer, Ö., İnci, U., Ersoy, E., Koçer, T., Demirtaş, R., & Özkaymak, Ç. (2008). D-B uzanımlı İzmir Fayı ile KD-uzanımlı Seferihisar Fayı'nın birlikte çalıştığına dair veriler: İzmir Körfezi'ni oluşturan aktif faylarda kinematik ve paleosismolojik Çalışmalar, Batı Anadolu. *Türkiye Jeoloji Bülteni*, 52 (2), 91-114.
- Sözbilir, H., Sümer, Ö., Uzel, B., Ersoy, E., Erkül, F., İnci, U., Helvacı, C., & Özkaymak, Ç. (2009). 17-20 Ekim 2005 Sıvacık Körfezi depremlerinin sismik jeomorfolojisi ve bölgedeki gerilme alanları ile ilişkisi, Batı Anadolu. *Türkiye Jeoloji Bülteni*, 52 (2), 217-238.
- Steinbrugge, K.V. (2010, January, 17). *The earthquake engineering online archive – (Nisee e-library)*. <http://nisee.berkeley.edu/elibrary/Image/S2007>
- Engör, A. M. C. (1982). Ege'nin Neotektonik evrimini yöneten etkenler. *Türkiye Jeoloji Kongresi, Bildiriler Kitabı*, 59-72.
- Engör, A. M. C. (1987). Cross faults and differential stretching of hanging walls in regions of low-angle normal faulting: examples from Western Turkey. In Coward, M.P., Dewey, J.P. and Hancock, P.L. (eds.), *Continental Extensional Tectonics, Geological Society, Special Publ.*, 28, 575-589.

- engör, A. M. C., Görür, N., & Aro lu, F. (1985). Strike-slip faulting and related basin formation in zones of tectonic escape: Turkey as a case study. In Biddle, K. & Christie-Blick, N. (eds.), *Strike-Slip Deformation, Basin Formation and Sedimentation, Soc. of Eco. Paleontologists and Mineralogists, Special Publ.*, 37, 227-264.
- Tatsuoka, F., Sasaki, T., & Yamada, S. (1984). Settlements in saturated sand induced by cyclic undrained simple shear. *Proceedings of the 8th World Conference on Earthquake Engineering, San Francisco*. 3, 95-102.
- Taymaz, T., Jackson, J. A. & McKenzie, D. (1991). Active tectonics of the North and Central Aegean Sea. *Geophysical Journal of Interiour*, 106, 433-490.
- TGM.RSN.86. Gediz Havzası Toprakları. (1974). *TC. Koy Isleri Bakanligi Topraksu Genel Mudurlugu publication and report series no: 86*, Ankara, Türkiye.
- Thevanayagam, S., & Martin, G. R. (2002). Liquefaction in silty soils—screening and remediation issues. *Soil Dynamics and Earthquake Engineering*, 22, 1035-1042.
- Thevanayagam, S., (2007a). Intergrain contact density indices for granular mixes - I: Framework. *Earthquake Engineering And Engineering Vibration*, 6 (2), 123-134.
- Thevanayagam, S., (2007b). Intergrain contact density indices for granular mixes - II: Framework. *Earthquake Engineering And Engineering Vibration*, 6 (2), 135-146.
- Tiwari, B., & Marui, H. (2005). A new method for the correlation of residual shear strength of the soil with mineralogical composition. *Journal Of Geotechnical And Geoenvironmental Engineering*, 131 (9), 1139-1150.

- Toki, S., Tatsuoka, F., Miura, S., Yoshimi, Y., Yasuda, S., & Makihara, Y. (1986). Cyclic undrained triaxial strength of sands for different sample preparation methods. *Soils and Foundations*, 26, 99-116.
- Tokimatsu, K., & Seed, H. B. (1987). Evaluation of settlements in sands due to earthquake shaking. *Journal of Geotechnical Engineering*, 113 (8), 861-878.
- Tokimatsu, K., & Yoshimi, Y. (1983). Empirical correlation of soil liquefaction based on SPT N-value and finer content. *Soils and Foundations*, 23 (4), 56-74.
- Tokimatsu, K., Yoshimi, Y., & Arizumi, K. (1990). Evaluation of liquefaction resistance of sand improved by deep vibratory compaction. *Soils and Foundations*, 30 (3), 153-158.
- Troncoso, J. H. (1990). Failure risks of abandoned tailings dams. *Proceedings International Symposium on Safety and Rehabilitation of Tailings Dams, ICOLD*, Sydney, 82-89.
- Tsuchida, H. (1970). Prediction and countermeasure against the liquefaction in sand deposits. *Abstract of the Seminar in the Port and Harbor Research Institute, Japan*.
- Türkelli, N., Kalafat, D., & nce, . (1994a). 6 Kasım 1992 İzmir Depremi ve Artçı okları. *Deprem Ara tırma Bülteni*, 68, 58-95.
- Türkelli, N., Kalafat, D., Kılıç, K. & Öz, G. (1994b). 28 Ocak 1994 Manisa Depremi ve bölgenin deprem etkinli i, *Deprem Ara tırma Bülteni*, 68, 32-57.
- Türkelli, N., Kalafat, D., Gündo du, O. (1995). 6 Kasım 1992 İzmir (Do anbey) Depremi saha gözlemleri ve odak mekanizması çözümü. *Jeofizik Dergisi*, 9 (1-2), 343-348.

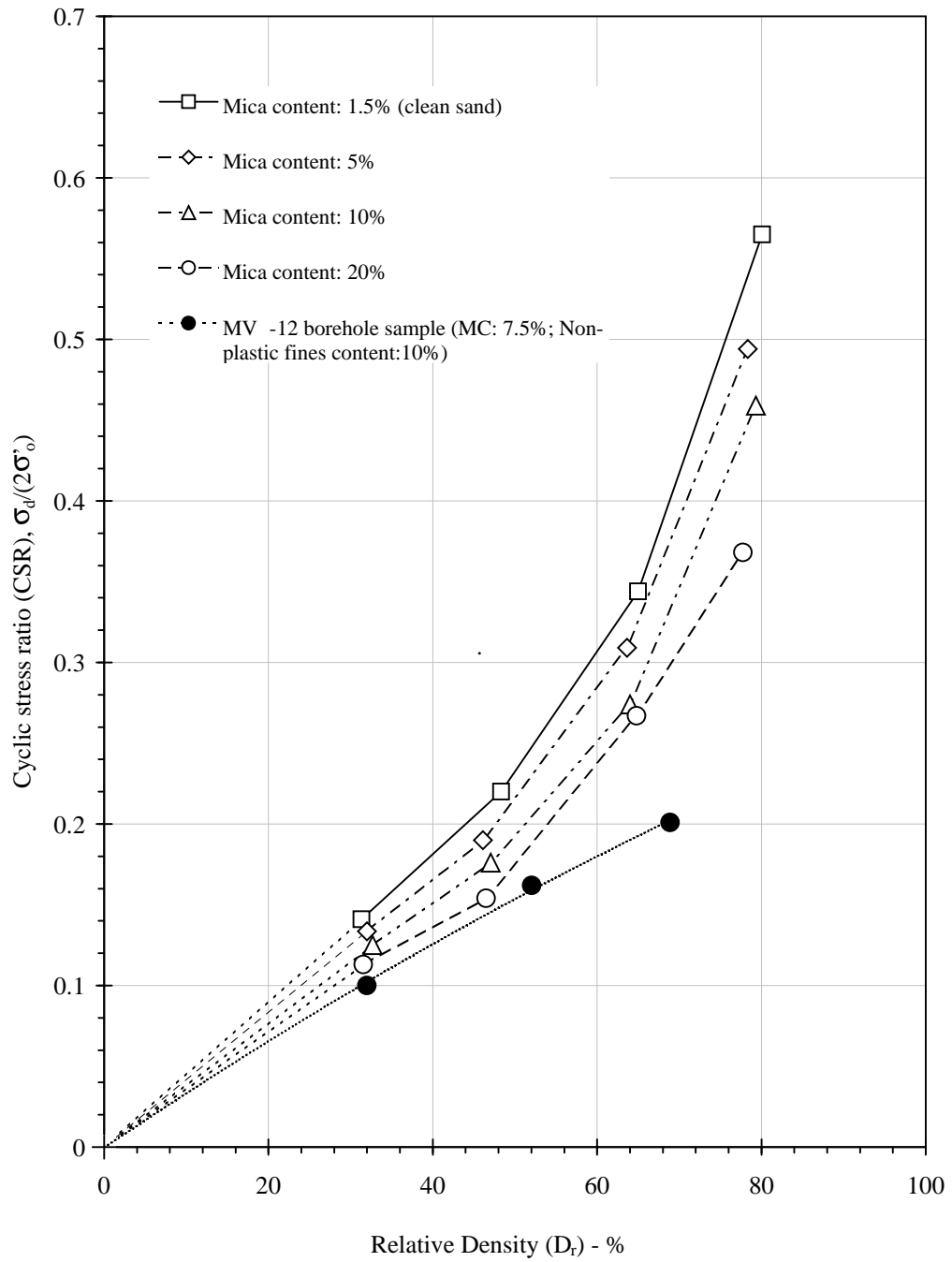
- Ueng, T. S., Wu, C. W., Cheng, H. W., & Chen, C. H. (2010). Settlements of saturated clean sand deposits in shaking table tests. *Soil Dynamics and Earthquake Engineering*, 30, 50-60.
- US Army. (1964). *Photo*. Retrived (June 28, 2010), from <http://libraryphoto.cr.usgs.gov/htmllib/batch74/batch74j/batch74z/ake00138.jpg>, 2010
- Utku, M., Özyalın, ., & Utku, Z. (2001). zmir Depremleri: zmir ve çevresinin deprem riski. *III. zmir ve Çevresi'nin Deprem – Jeoteknik Sempozyumu, zmir*, Puplished in CD.
- Uzel, B., & Sözbilir, H. (2008). The First record of strike-slip basin in Western Anatolia and its tectonic implication: The Cumaovası Basin as an example. *Turkish Journal of Earth Sciences*, 17 (3), 559-591.
- Uzel, B., Sözbilir, H., & Özkaymak, Ç. (2011). Evolution of an actively growing superimposed basin in Western Anatolia: The Inner Bay of zmir. *Turkish Journal of Earth Sciences*, in press.
- Vallejo, L. E., & Mawby, R. (2000). Porosity influence on the shear strength of granular material–clay mixtures. *Engineering Geology*, 58, 125-136.
- Walker, A. J. & Steward, H. E., (1989). Cyclic undrained behavior of nonplastic and low plasticity silts. *Technical Report NCEER-89-0035, National Center for Earthquake Engineering Research, Suny at Buffalo*.
- Westaway, R. (1990). Block rotation in Western Turkey: 1. Observational evidence. *Journal of Geophysical Research*, 95, 19857-19884.

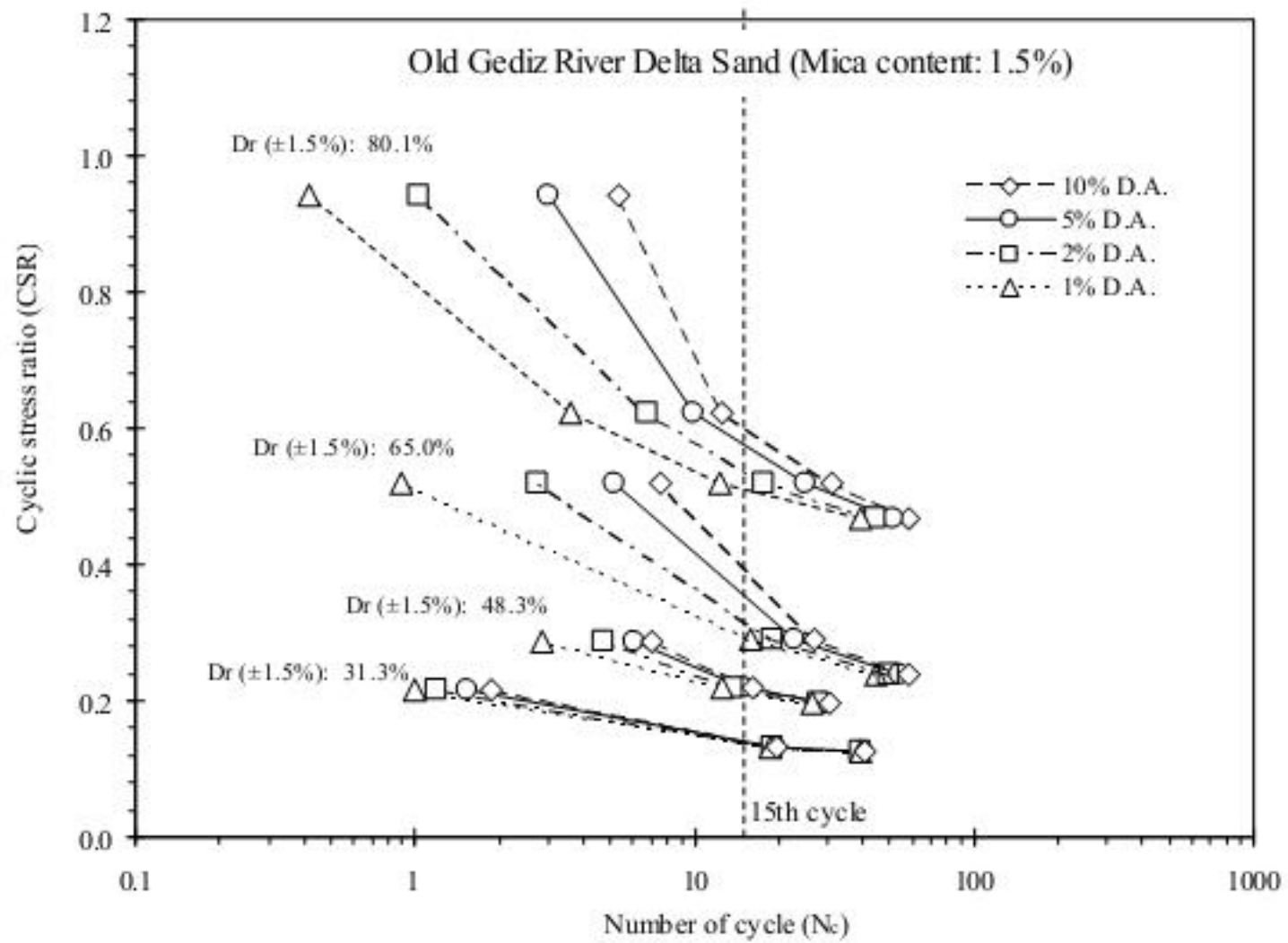
- Xenaki, V. C., & Anthanasopoulos, G. A. (2003). Liquefaction resistance of sand–silt mixtures: an experimental investigation of the effect of fines. *Soil Dynamics and Earthquake Engineering*, 23, 183-184.
- Xia, H., & Hu, T. (1991). Effects of saturation and back pressure on sand liquefaction. *Journal of Geotechnical Engineering*, 117 (9), 1347-1362.
- Yamamuro, J. A., Covert, K. M., & Lade, P. V. (1999). Static and cyclic liquefaction of silty sands. *Proceedings of the Workshop on Physics and Mechanics of Soil Liquefaction*, Balkema.
- Yılmaz, Y. (1997). Geology of Western Anatolia. Schindler, C., & Pfister, M. (eds.), *Active Tectonics of Northwestern Anatolia, The Marmara Polyproject*, vdf Hochschulverlag AG an der ETH Zurich, 31-53.
- Yoshimi, Y., Tokimatsu, K., & Hosaka, Y. (1989). Evaluation of liquefaction resistance of clean sands based on high-quality undisturbed samples. *Soils and Foundation*. 29, 93-104.
- Yoshimi, Y., Tokimatsu, K., Kaneko, O., & Makihara, Y. (1984). Undrained cyclic shear strength of a dense Niigata sand. *Soils and Foundations*, 29 (1), 93-104.
- Youd, T. L. (1984). Recurrence of liquefaction at the same site. *Proceedings, 8th World Conference on Earthquake Engineering*, 3, 231-238.
- Youd, T. L. (1991). Mapping of earthquake-induced liquefaction for seismic zonation. *Proceedings, 4th International Conference on Seismic Zonation, Earthquake Engineering Research Institute, Stanford University*, 1, 111-147.
- Youd, T. L., & Gilstrap, S. D. (1991). Liquefaction and deformation of silty and fine grained soils. *Proceedings, Second International Conference on Earthquake Geotechnical Engineering, Lisbon-Portugal*, 1013-1020.

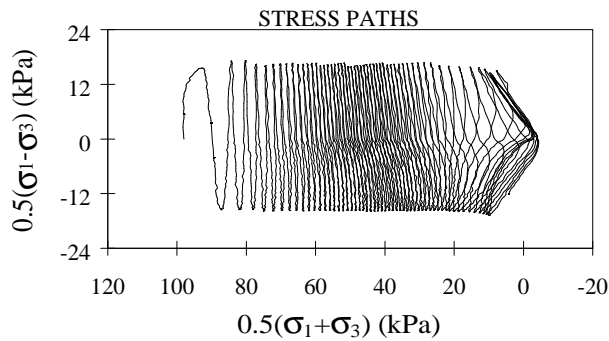
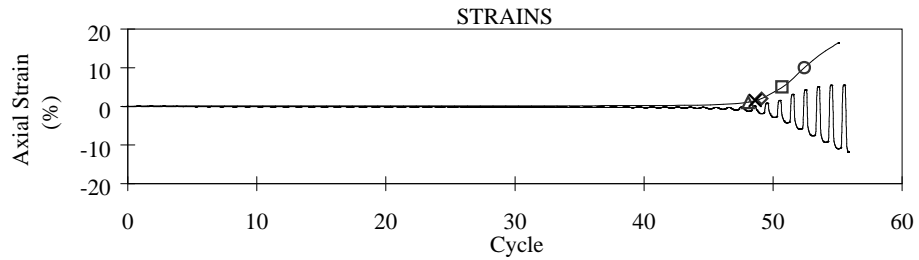
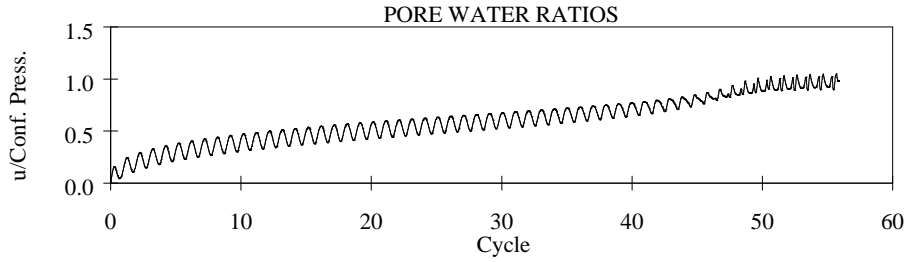
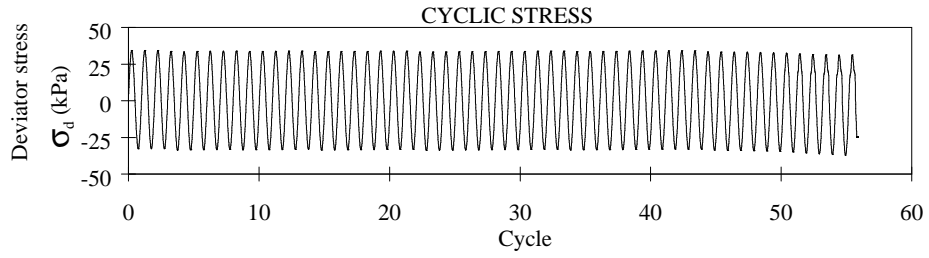
- Youd, T. L., & Noble, S. K. (1997). Liquefaction criteria based on statistical and probabilistic analyses. *Proc. NCEER Workshop on Evaluation of Liquefaction of Soils, Nat. Ctr. For Earthquake Engrg. Res. State Univ. of New York at Buffalo*, 201-215.
- Youd, T. L., & Idriss, I. M. (Ed.). (1997). Proceeding of the NCEER workshop on evaluation of liquefaction resistance of soils. *National Center for Earthquake Engineering Research. Technical Report NCEER-97-0022*, US.
- Youd, T. L., & Idriss, I. M. (2001). Liquefaction resistance of soils: summary report from the 1996 NCEER and 1998 NCEER/NSF workshops on evaluation of liquefaction resistance of soils. *Journal of Geotechnical and Geoenvironmental Engineering*, 127 (4), 297-313.
- Youd, T. L. (1964). *W architecture week, Design and building in depth*. Retrived (March 11, 2012), from <http://www.architectureweek.com/2012/0307/>
- Zlatovic, S., & Ishihara, K. (1997), Normalized behavior of very loose non-plastic soils: Effects of fabric. *Soils and Foundations*, 37 (4), 47-56.

APPENDIXES

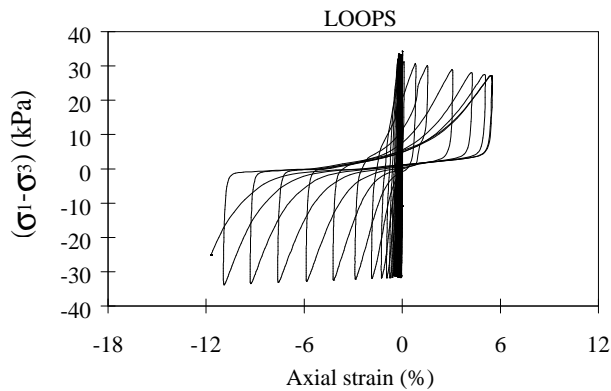
APPENDIX – A
CYCLIC TRIAXIAL TEST RESULTS

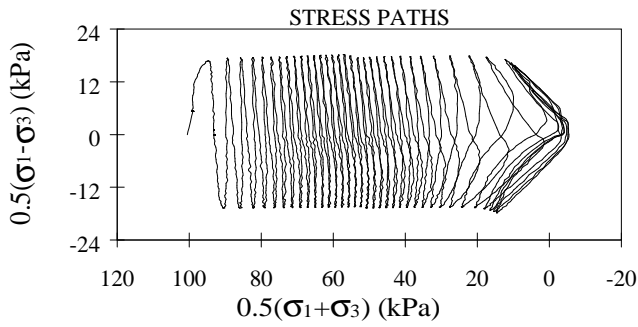
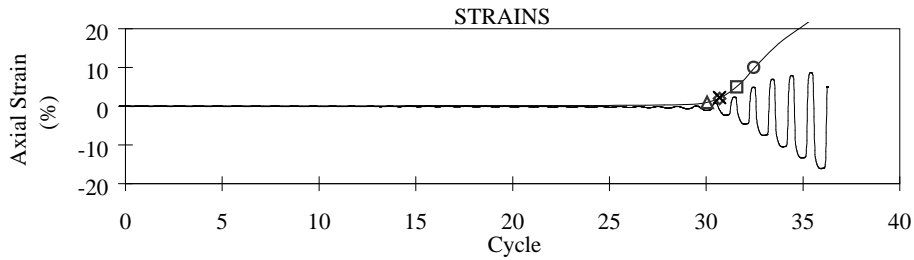
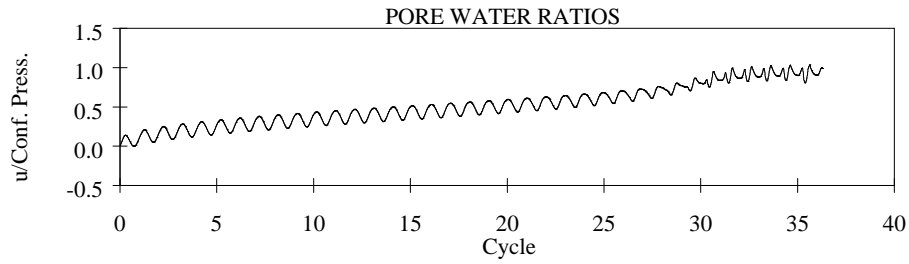
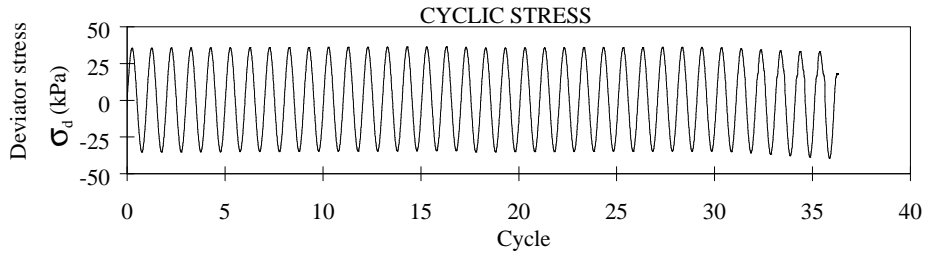




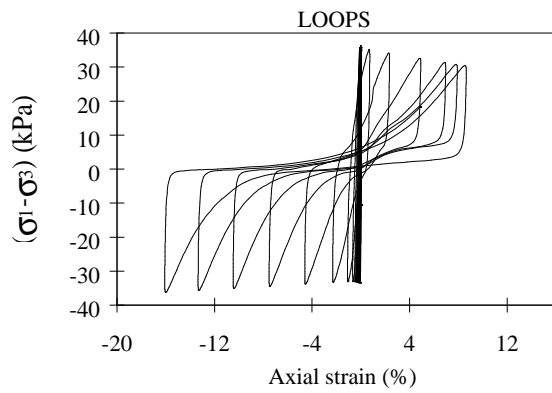


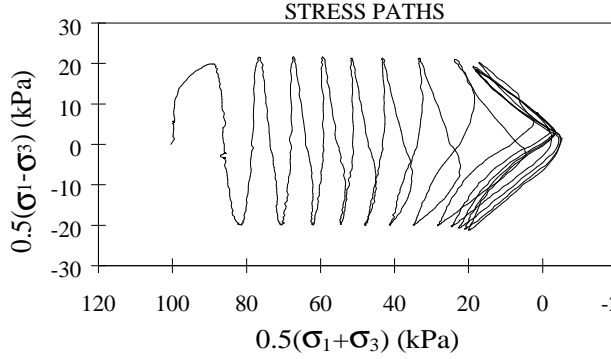
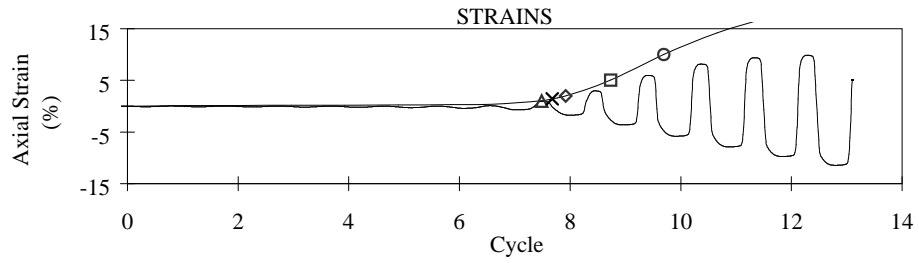
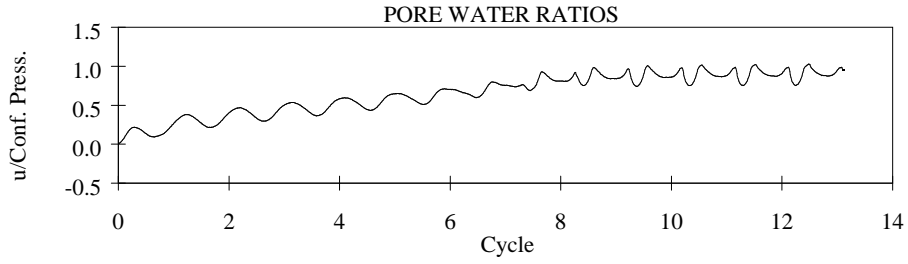
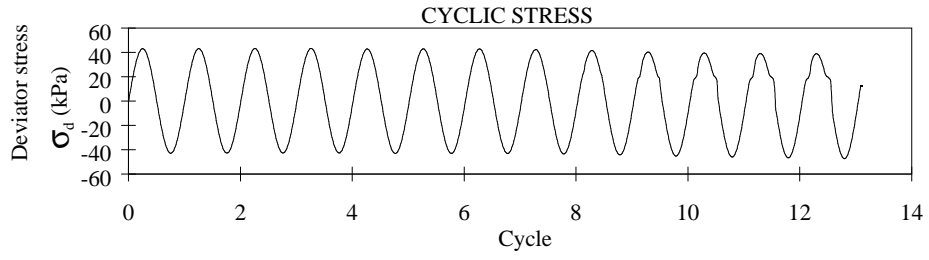
SAMPLE PROPERTIES		MV -A1
Mica Content (%) :		7.5
Non-Plastic Fines Content (%) :		10.0
Relative Density (%) :		68.9
Cyclic Stress Ratio:		0.172
Efective Conf. Press (kPa):		100.0



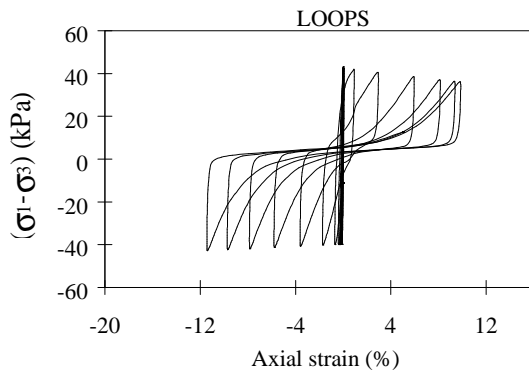


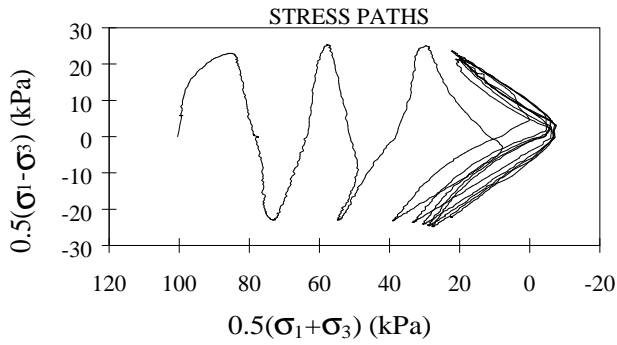
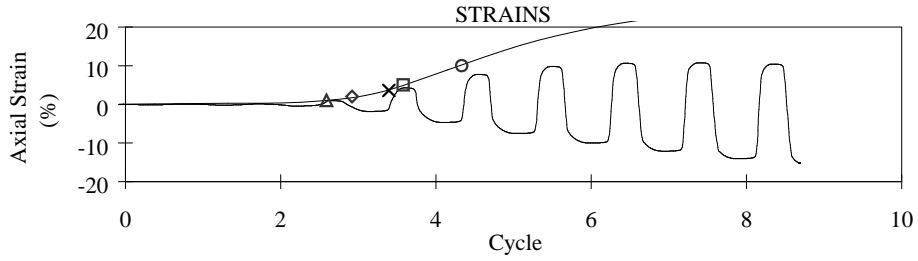
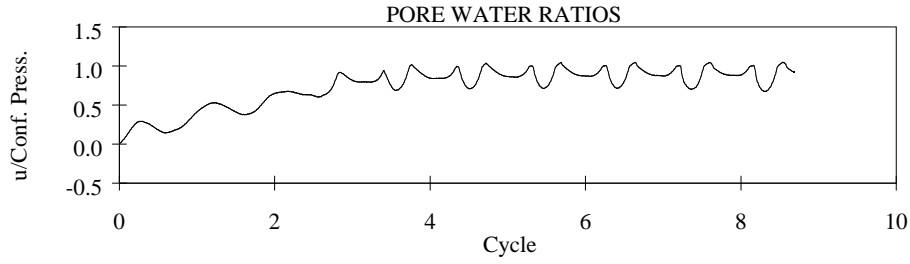
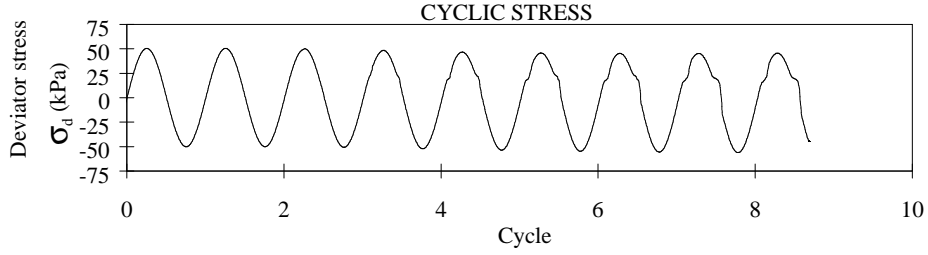
SAMPLE PROPERTIES	MV -A2
Mica Content (%) :	7.5
Non-Plastic Fines Content (%) :	10.0
Relative Density (%) :	69.2
Cyclic Stress Ratio:	0.182
Efective Conf. Press (kPa):	100.0



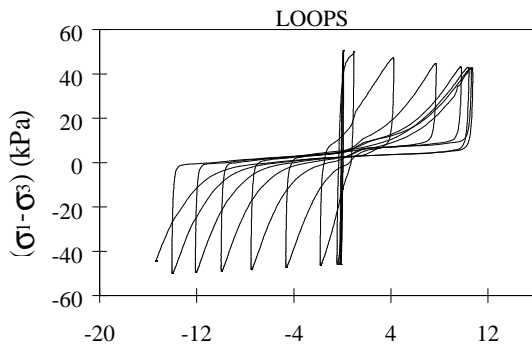


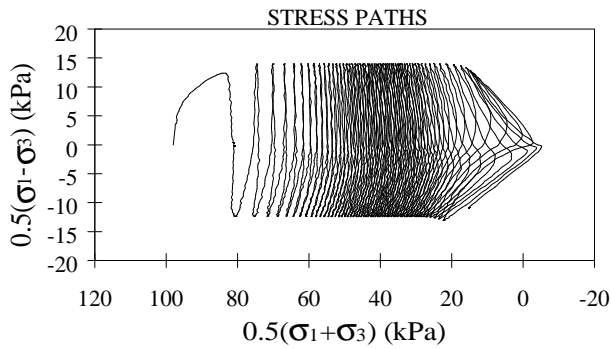
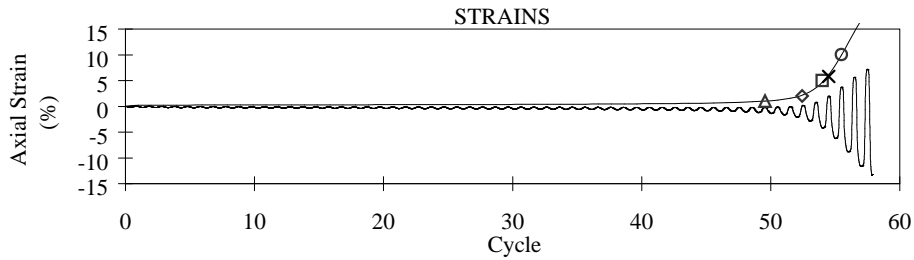
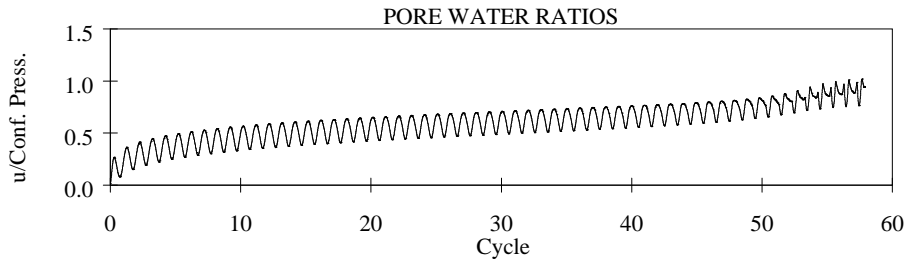
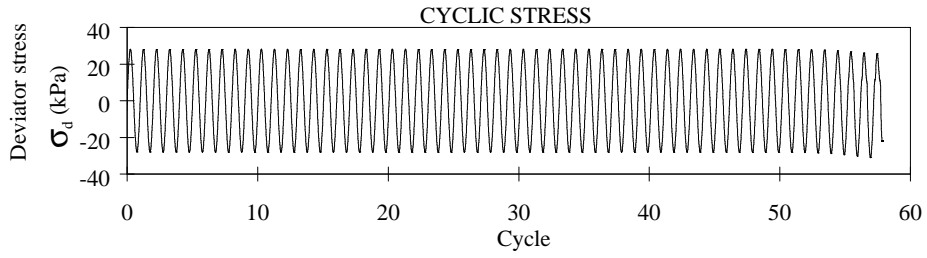
SAMPLE PROPERTIES	MV -A3
Mica Content (%) :	7.5
Non-Plastic Fines Content (%) :	10.0
Relative Density (%) :	68.1
Cyclic Stress Ratio:	0.215
Effective Conf. Press (kPa):	100.3



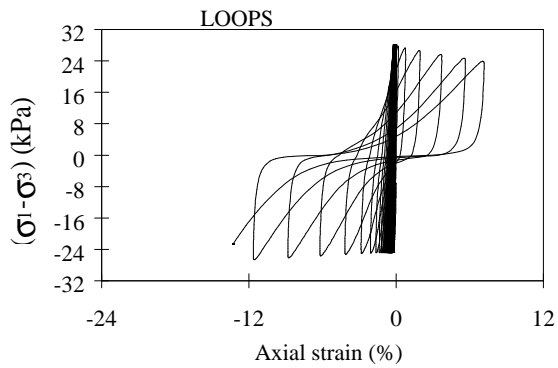


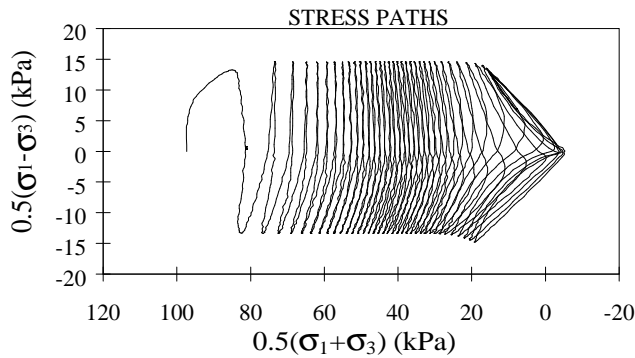
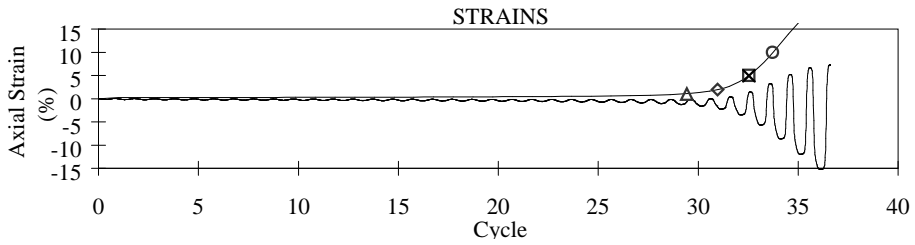
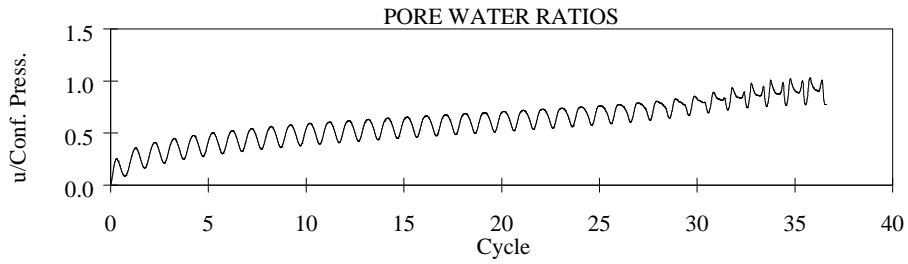
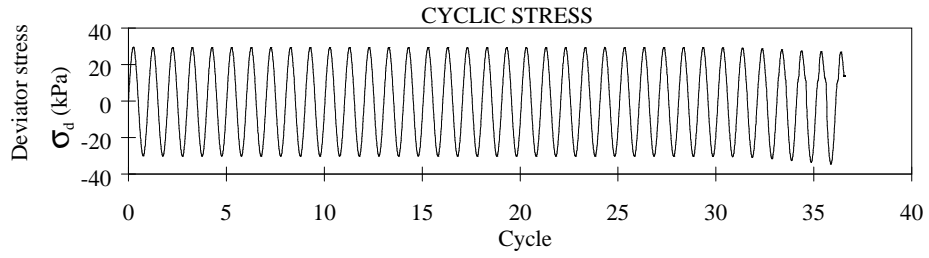
SAMPLE PROPERTIES		MV -A4
Mica Content (%) :		7.5
Non-Plastic Fines Content (%) :		10.0
Relative Density (%) :		69.4
Cyclic Stress Ratio:		0.254
Efective Conf. Press (kPa):		99.5



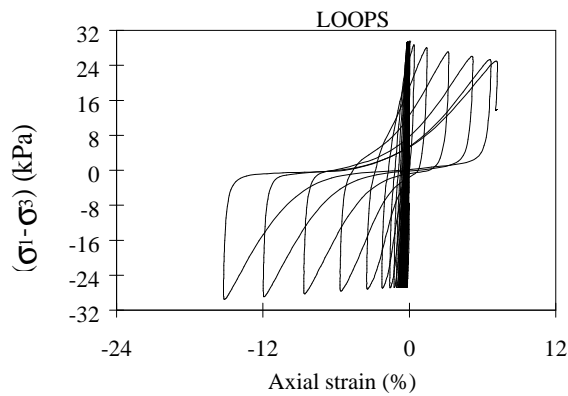


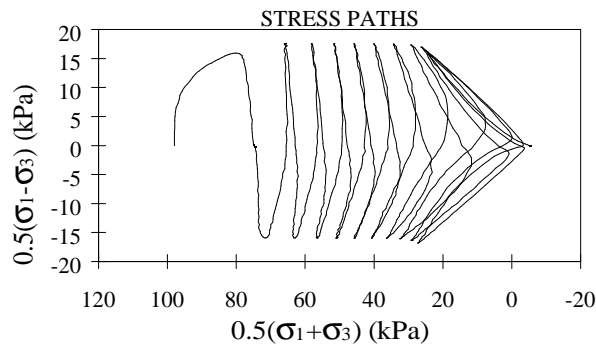
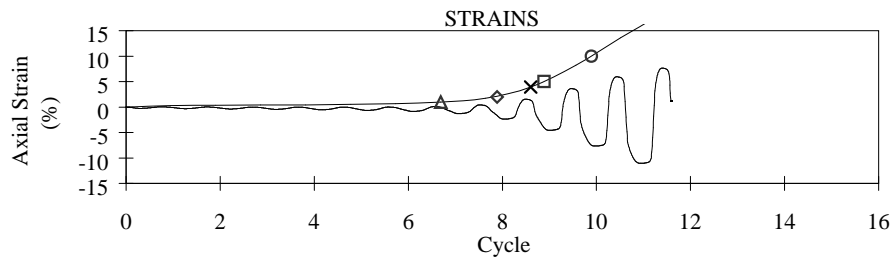
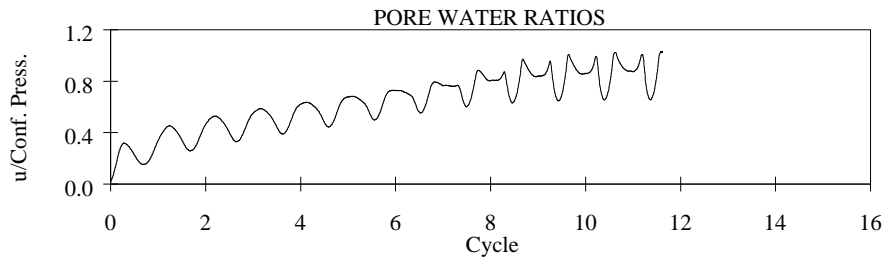
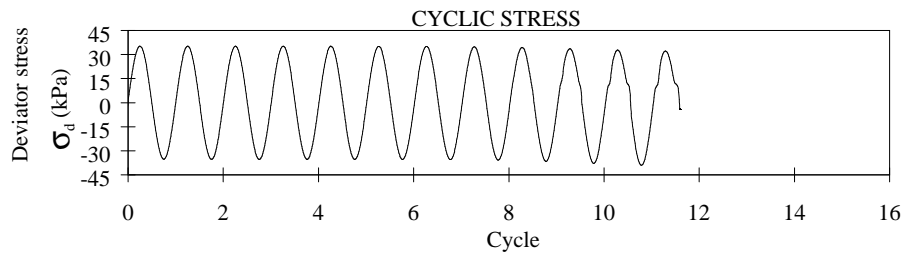
SAMPLE PROPERTIES	MV -B1
Mica Content (%) :	7.5
Non-Plastic Fines Content (%) :	10.0
Relative Density (%) :	51.0
Cyclic Stress Ratio:	0.141
Efective Conf. Press (kPa):	100.0



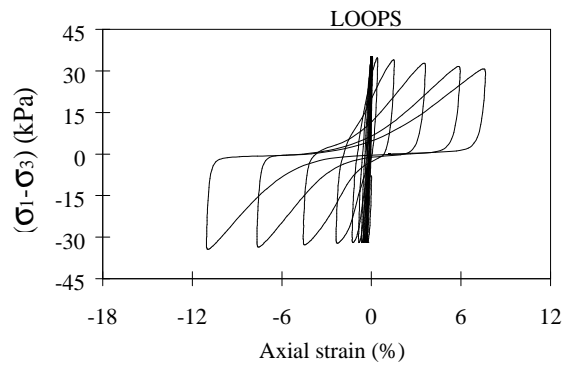


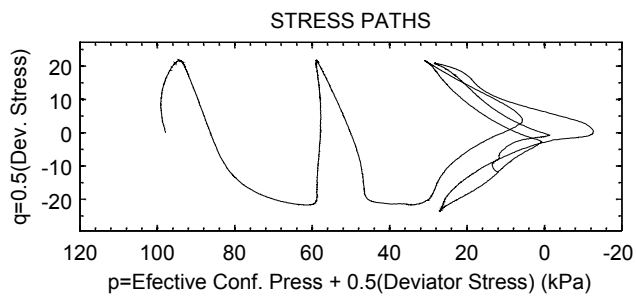
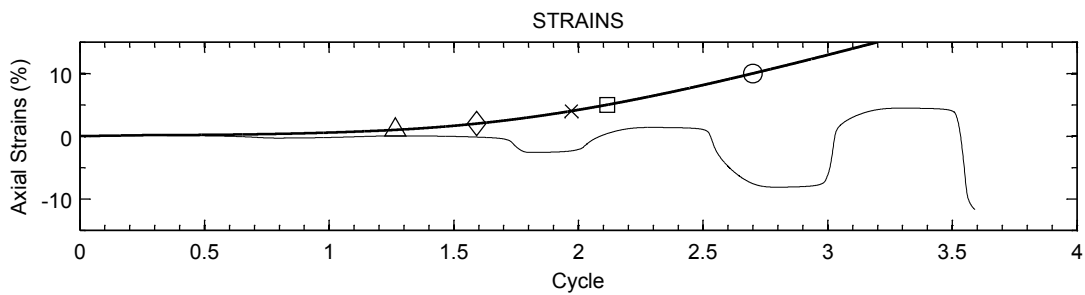
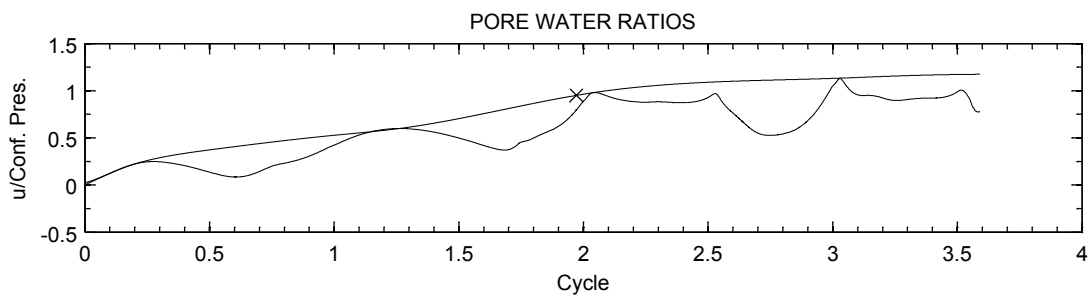
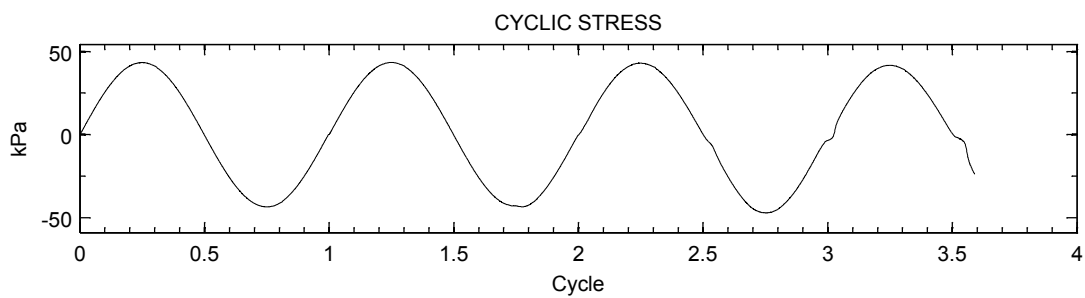
SAMPLE PROPERTIES	MV -B2
Mica Content (%) :	7.5
Non-Plastic Fines Content (%) :	10.0
Relative Density (%) :	52.1
Cyclic Stress Ratio:	0.148
Effective Conf. Press (kPa):	99.7





SAMPLE PROPERTIES	MV -B3
Mica Content (%) :	7.5
Non-Plastic Fines Content (%) :	10.0
Relative Density (%) :	53.4
Cyclic Stress Ratio:	0.176
Effective Conf. Press (kPa):	99.7



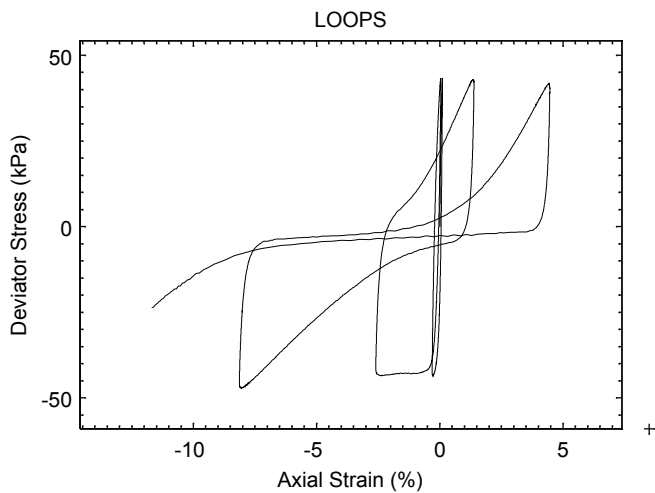


SAMPLE PROPERTIES: MVS-B4

Mica Content (%): 7.5

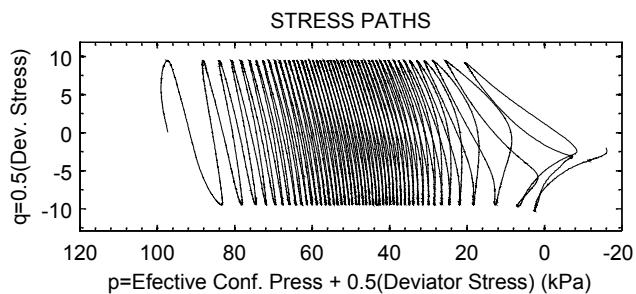
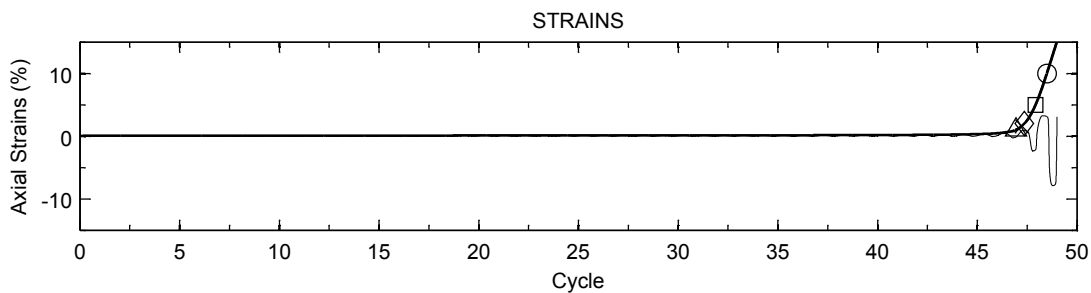
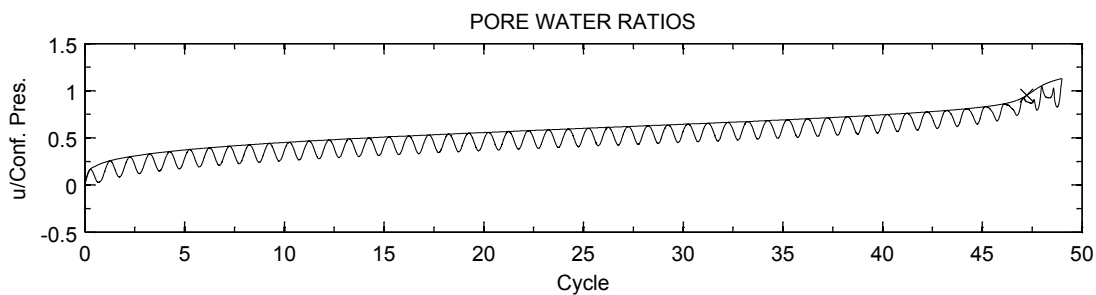
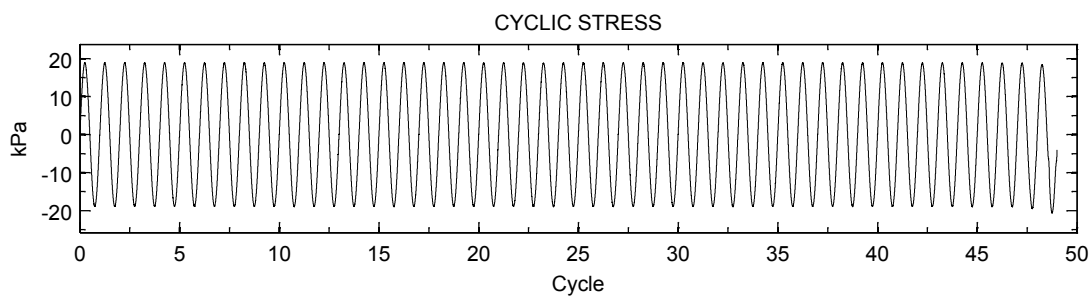
Non-Plastic Fines Content (%): 10

Relative Density (%): 51.6



Cyclic Stress Ratio: 0.231

Efective Conf. Press (kPa): 100

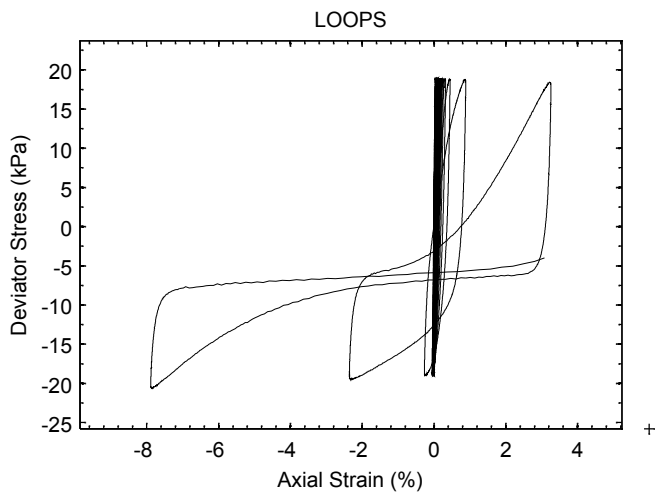


SAMPLE PROPERTIES: MVS-C1

Mica Content (%): 7.5

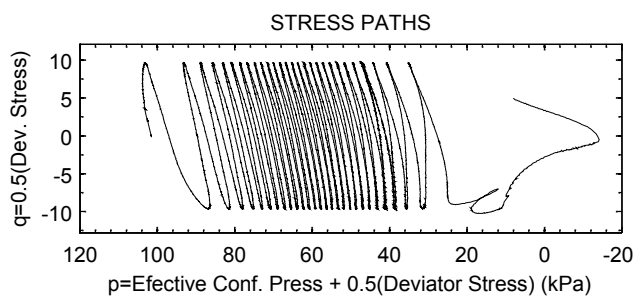
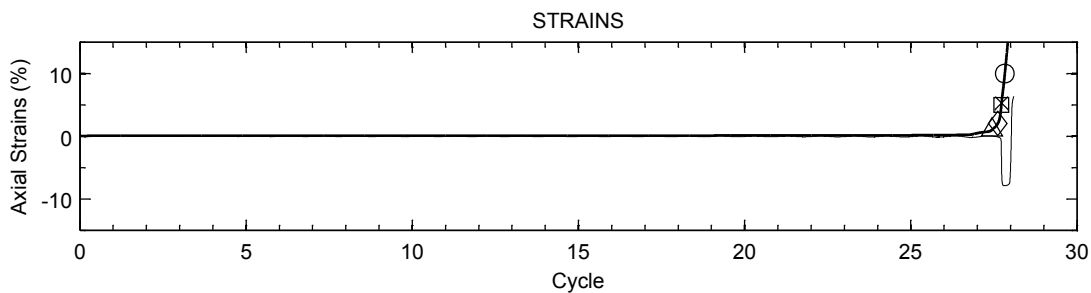
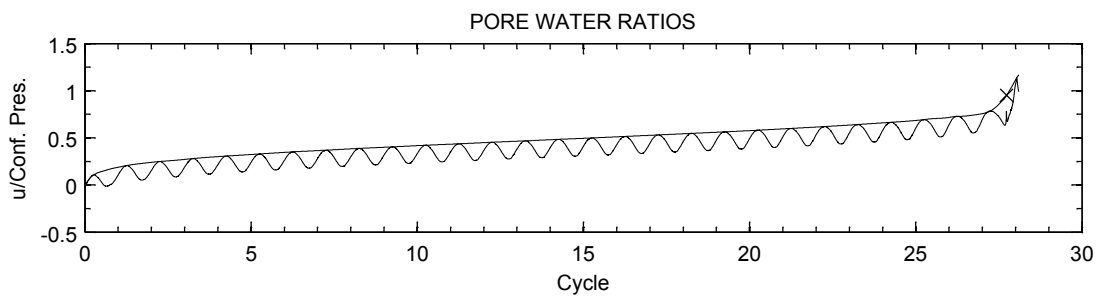
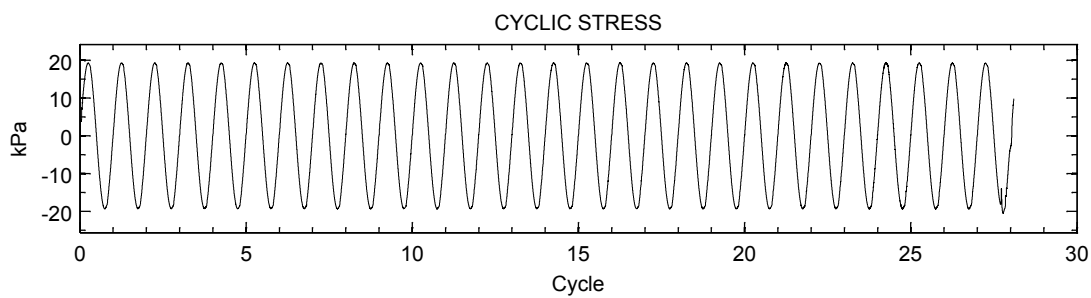
Non-Plastic Fines Content (%): 10

Relative Density (%): 30.45



Cyclic Stress Ratio: 0.094

Efective Conf. Press (kPa): 100.3

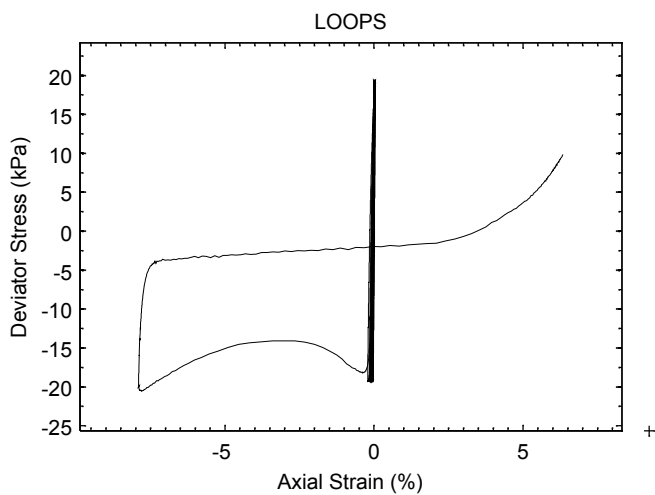


SAMPLE PROPERTIES: MVS-C2

Mica Content (%): 7.5

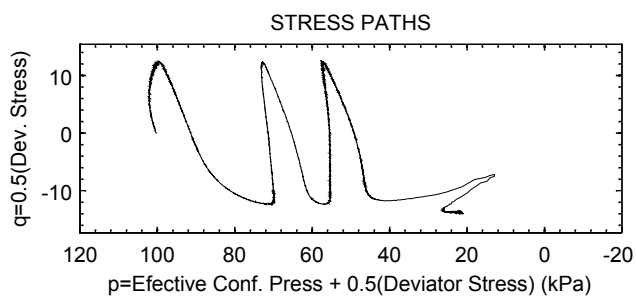
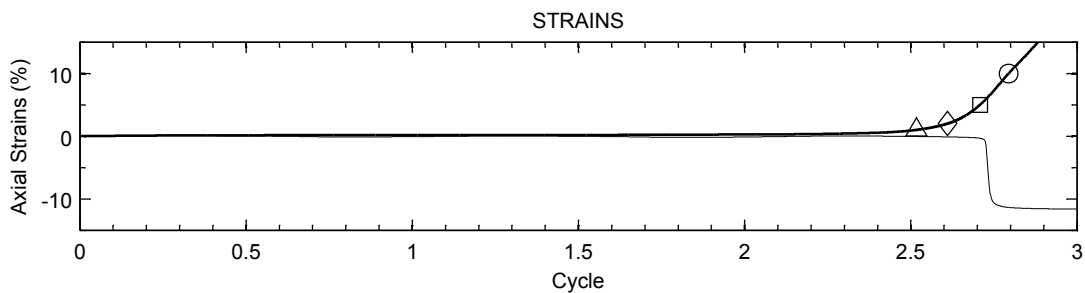
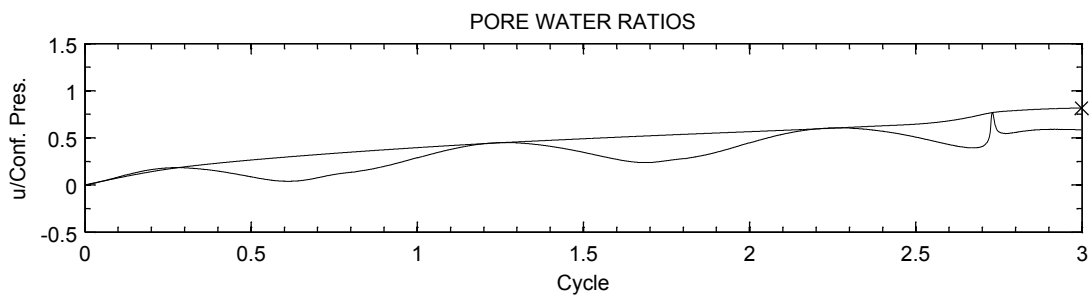
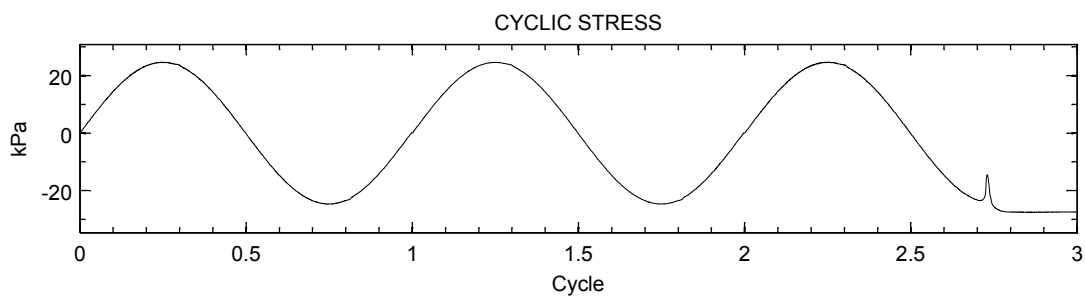
Non-Plastic Fines Content (%): 10

Relative Density (%): 31.65



Cyclic Stress Ratio: 0.096

Effective Conf. Press (kPa): 100.2

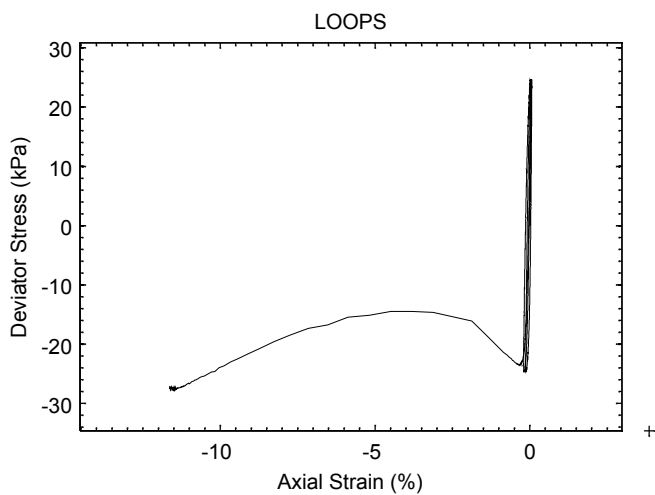


SAMPLE PROPERTIES: MVS-C3

Mica Content (%): 7.5

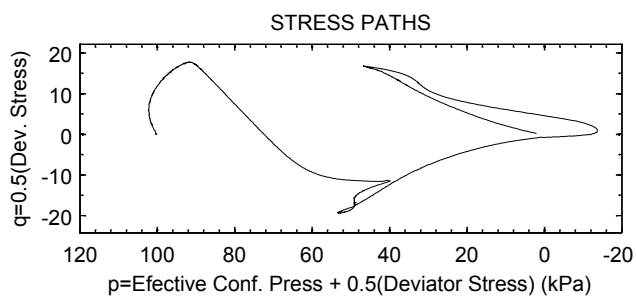
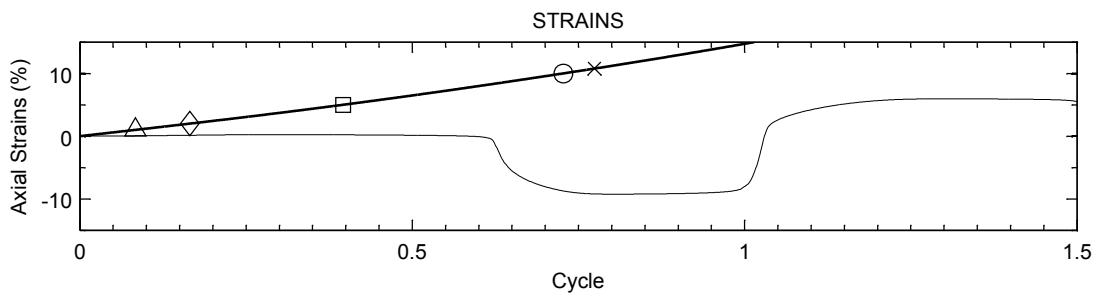
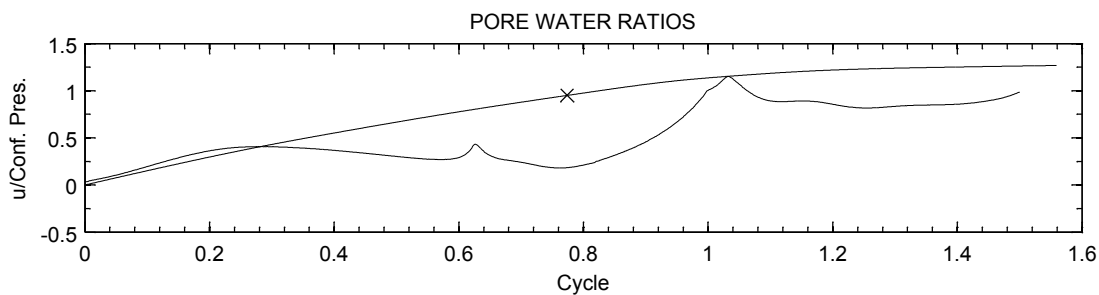
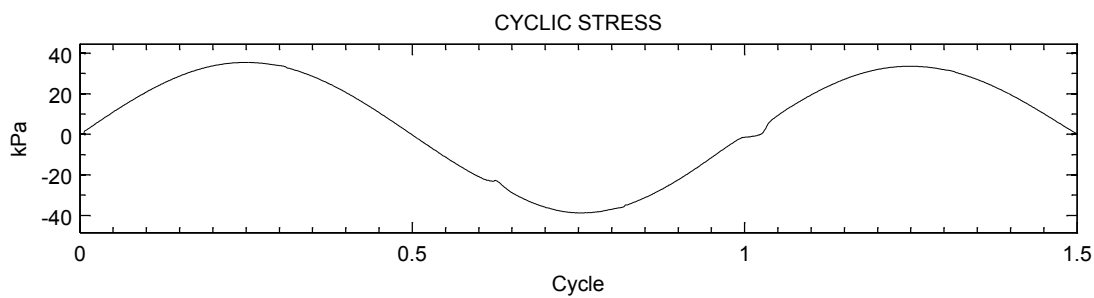
Non-Plastic Fines Content (%): 10

Relative Density (%): 32.35



Cyclic Stress Ratio: 0.122

Effective Conf. Press (kPa): 100.1

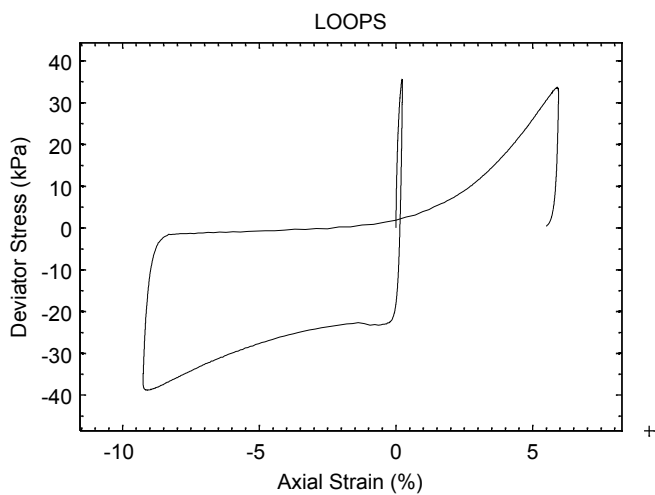


SAMPLE PROPERTIES: MVŞ-C4

Mica Content (%): 7.5

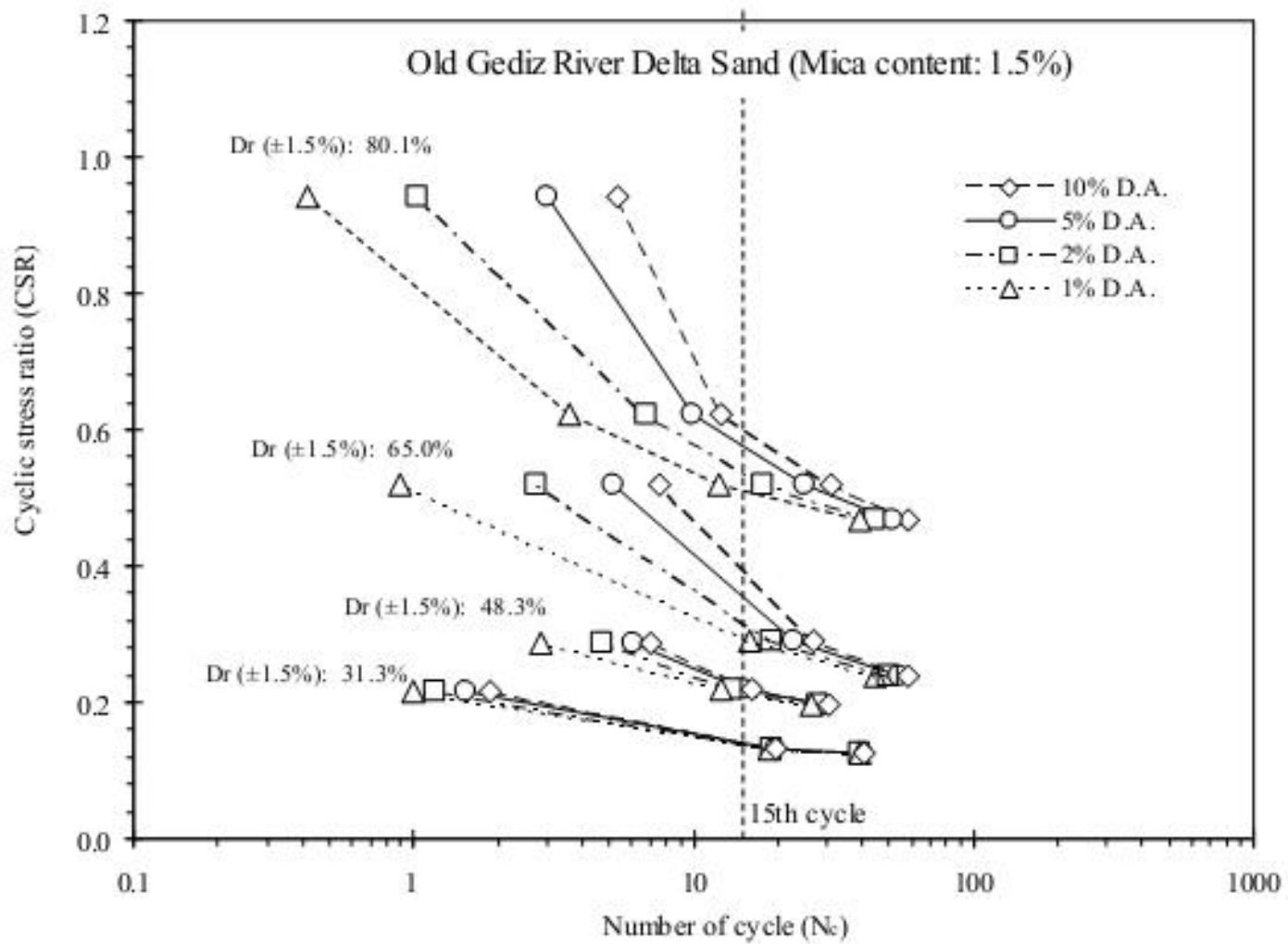
Non-Plastic Fines Content (%): 10

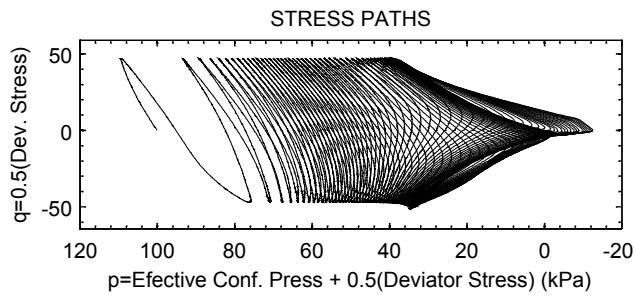
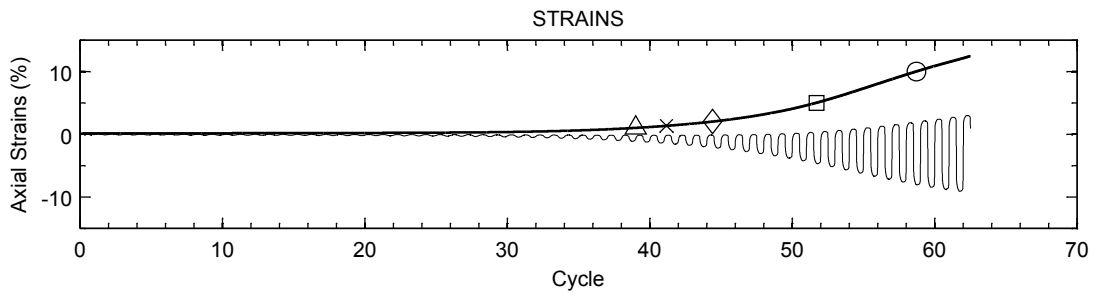
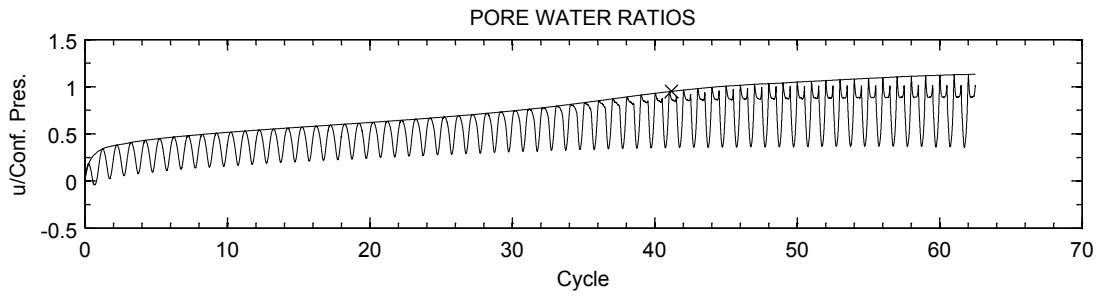
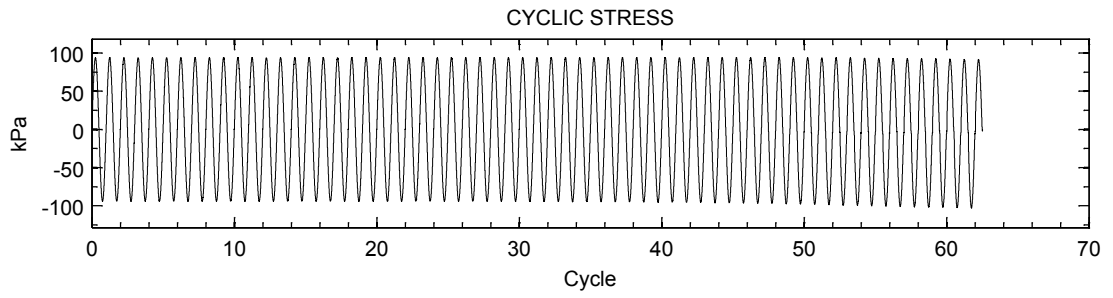
Relative Density (%): 33.55



Cyclic Stress Ratio: 0.176

Efective Conf. Press (kPa): 104



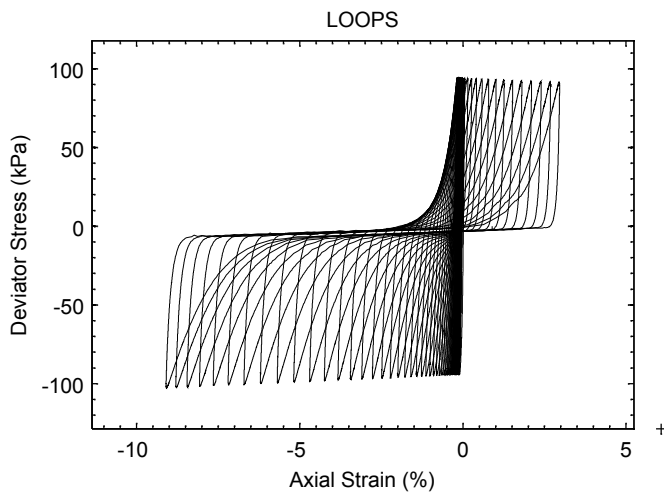


SAMPLE PROPERTIES: MC:1.5-A1

Mica Content (%): 1.5

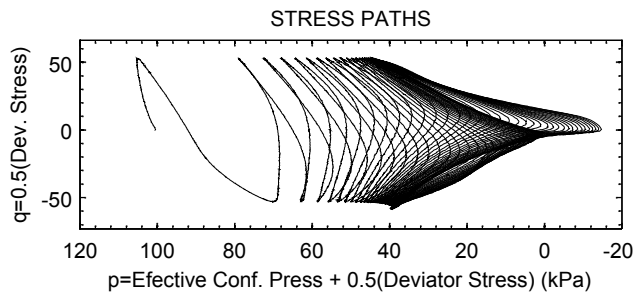
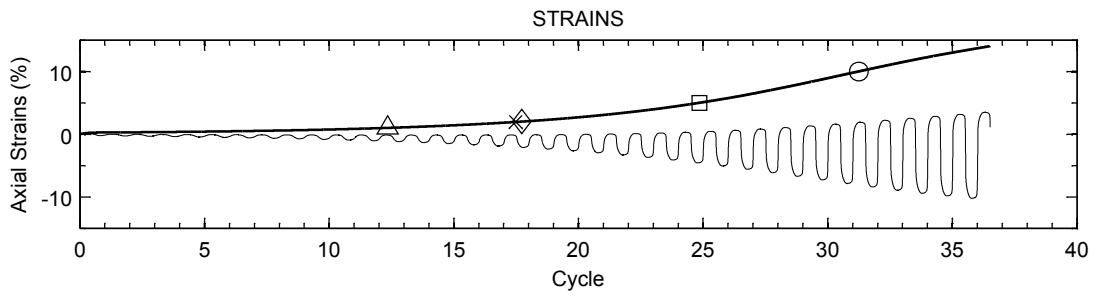
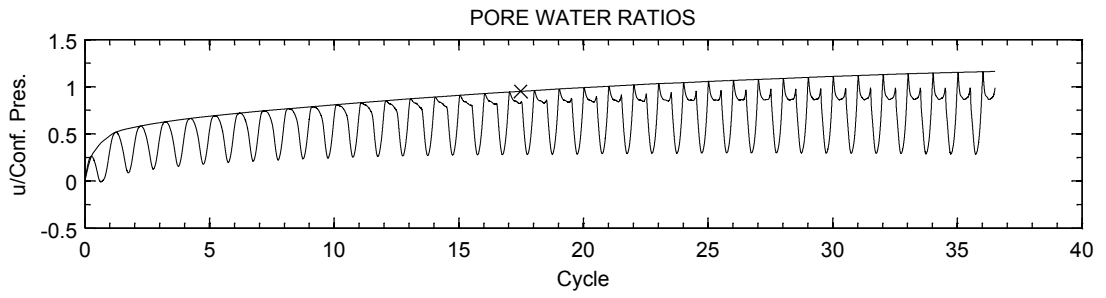
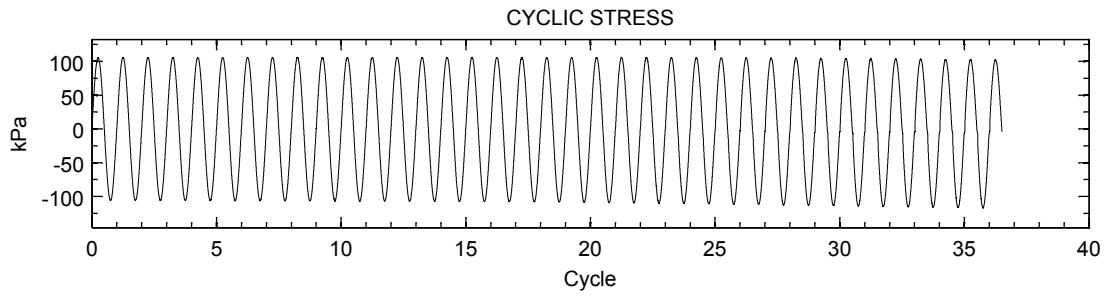
Non-Plastic Fines Content (%): 0

Relative Density (%): 80



Cyclic Stress Ratio: 0.467

Efective Conf. Press (kPa): 100.4

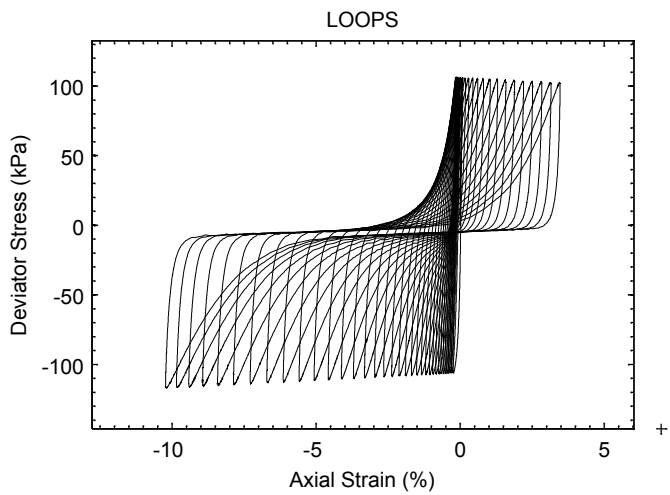


SAMPLE PROPERTIES: MC:1.5-A2

Mica Content (%): 1.5

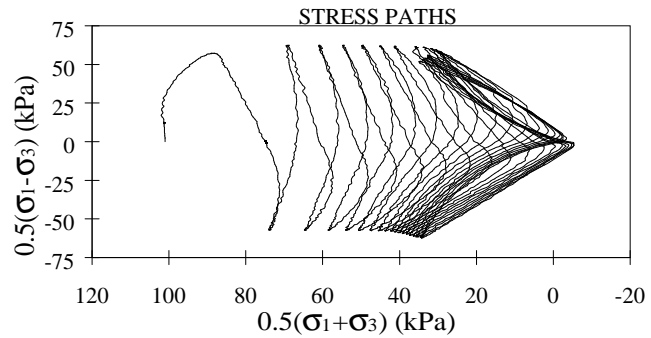
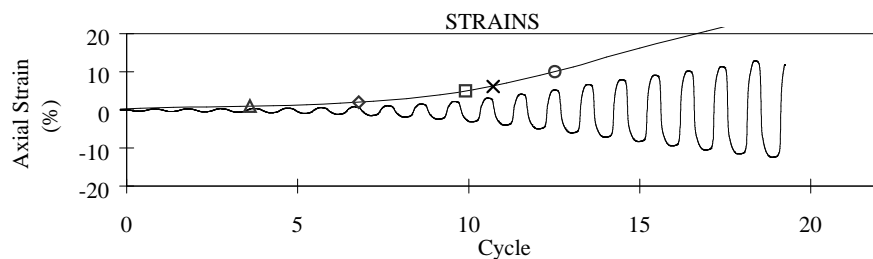
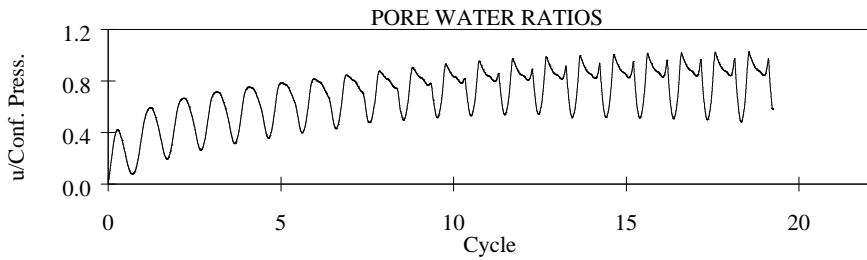
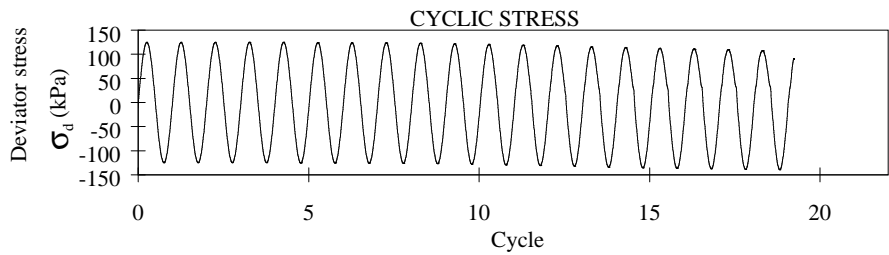
Non-Plastic Fines Content (%): 0

Relative Density (%): 79.6

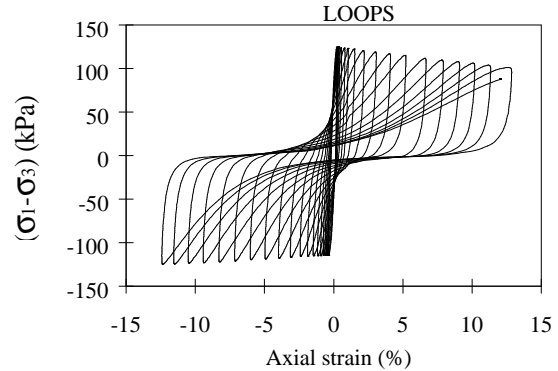


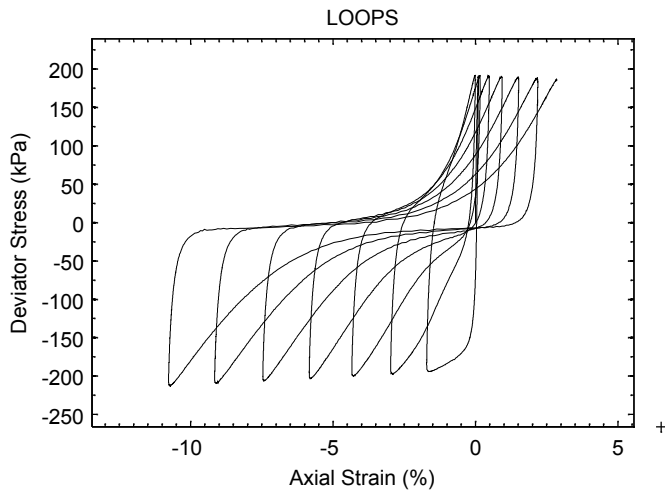
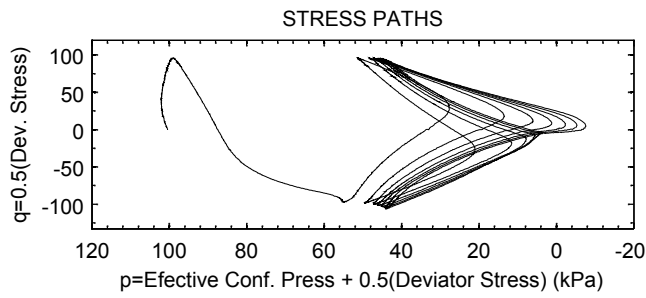
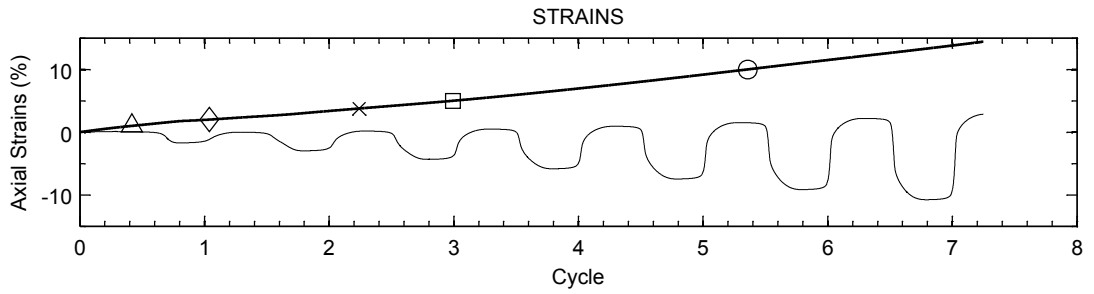
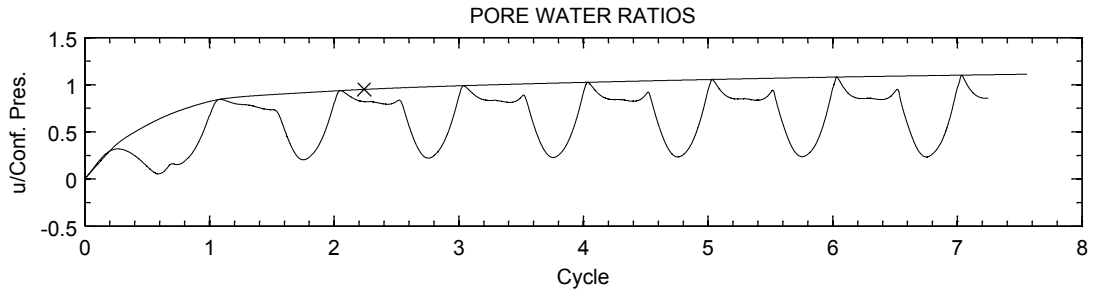
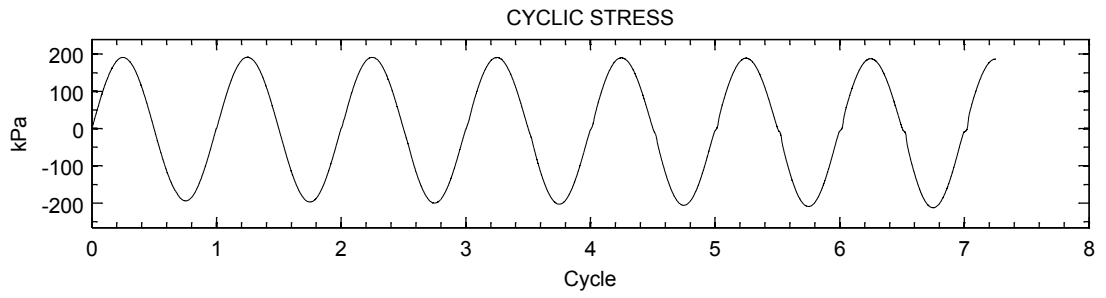
Cyclic Stress Ratio: 0.519

Efective Conf. Press (kPa): 101.6



SAMPLE PROPERTIES	MC1.5-A3
Mica Content (%) :	1.5
Non-Plastic Fines Content (%) :	0.0
Relative Density (%) :	80.6
Cyclic Stress Ratio:	0.624
Effective Conf. Press (kPa):	100.0





SAMPLE PROPERTIES: MC:1.5-A4

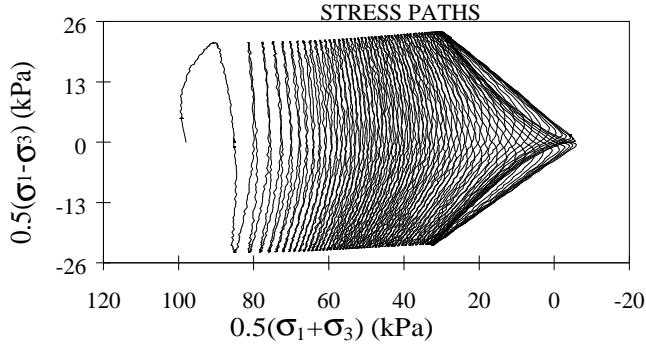
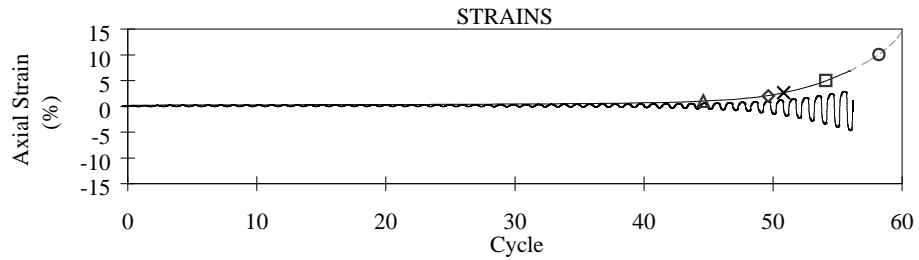
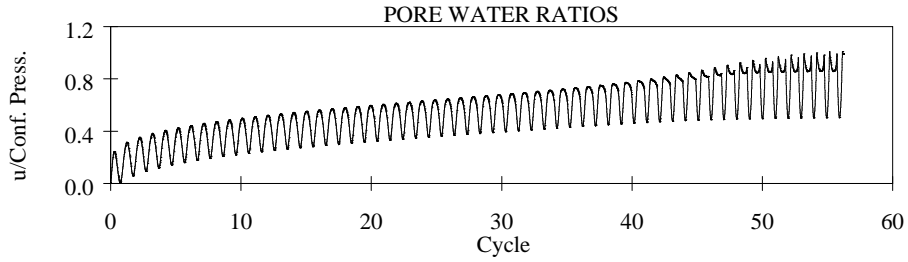
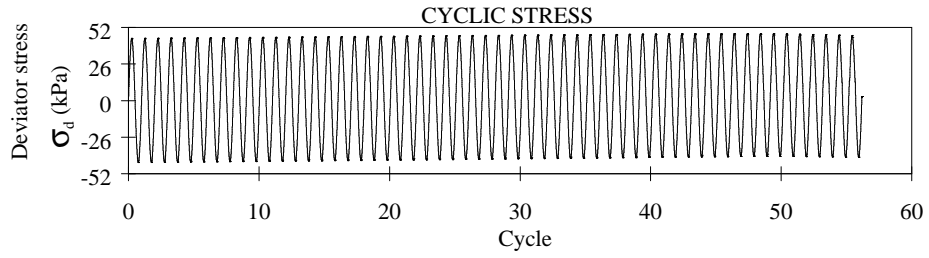
Mica Content (%): 1.5

Non-Plastic Fines Content (%): 0

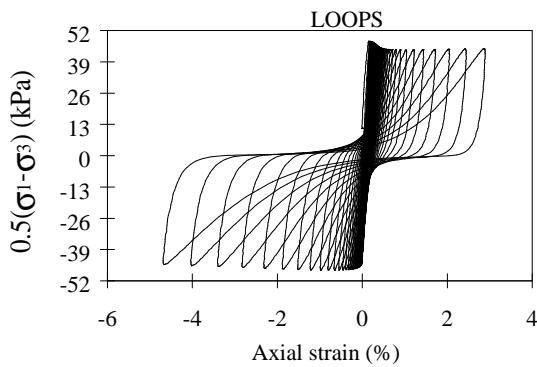
Relative Density (%): 80.2

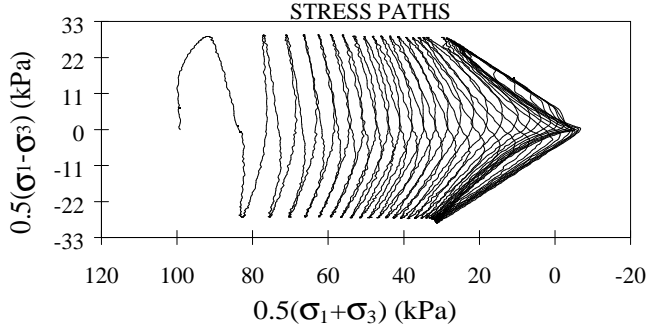
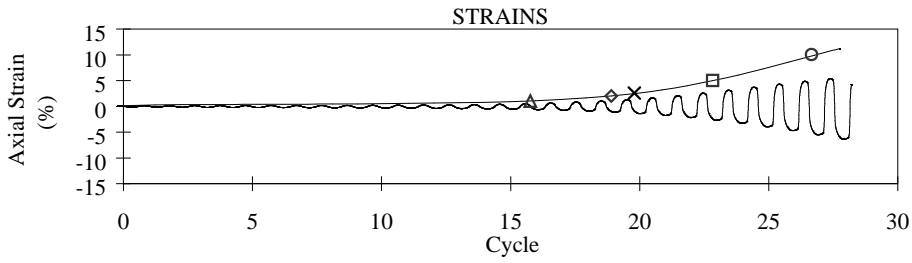
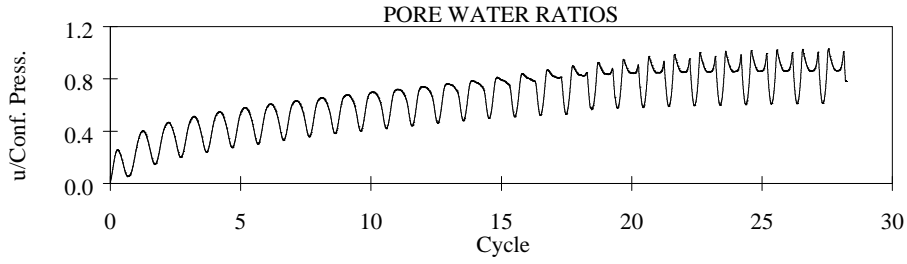
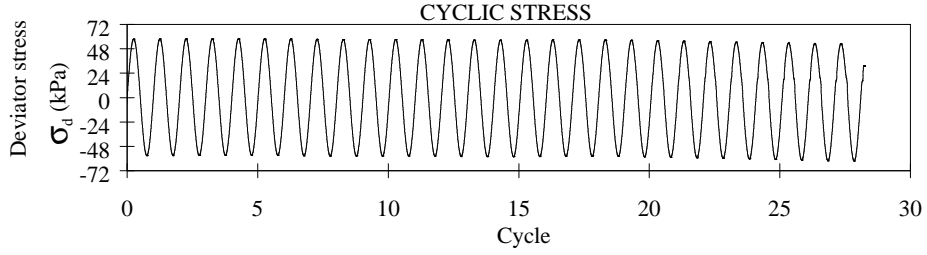
Cyclic Stress Ratio: 0.943

Efective Conf. Press (kPa): 101.1



SAMPLE PROPERTIES		MC1.5-B1
Mica Content (%) :		1.5
Non-Plastic Fines Content (%) :		0.0
Relative Density (%) :		66.0
Cyclic Stress Ratio:		0.238
Effective Conf. Press (kPa):		99.9





SAMPLE PROPERTIES MC1.5-B2

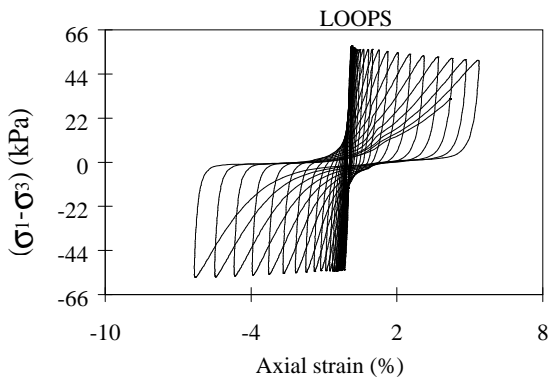
Mica Content (%) : 1.5

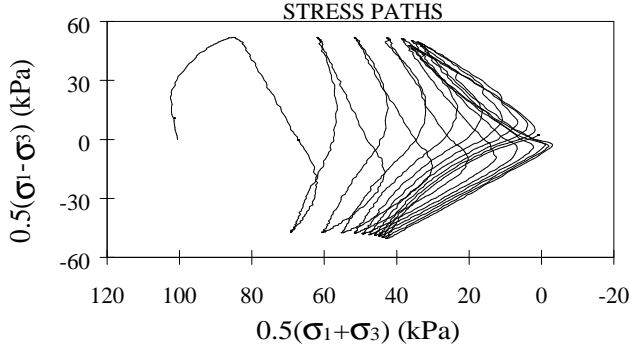
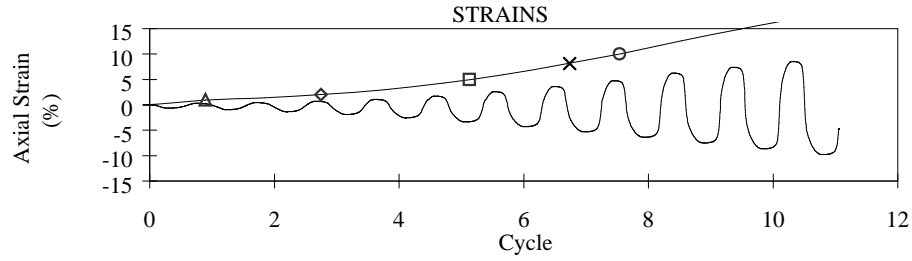
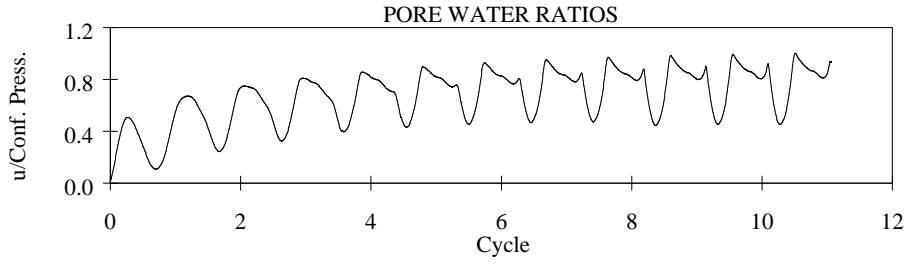
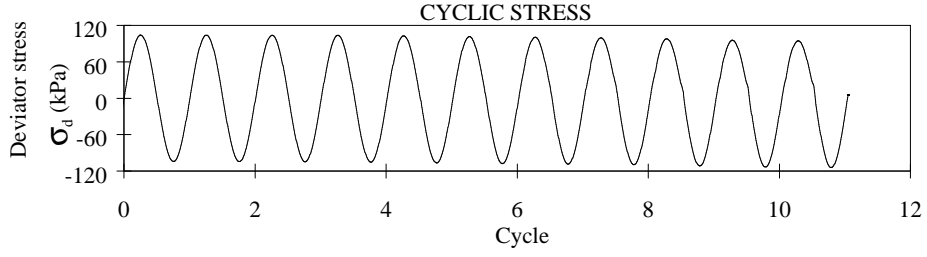
Non-Plastic Fines Content (%) : 0.0

Relative Density (%) : 65.0

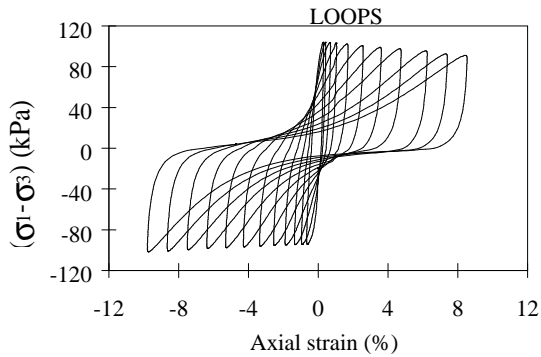
Cyclic Stress Ratio: 0.291

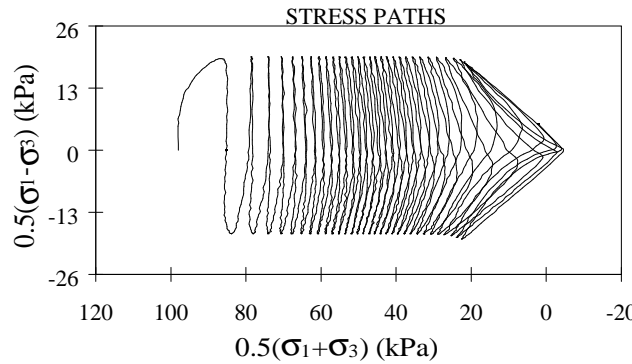
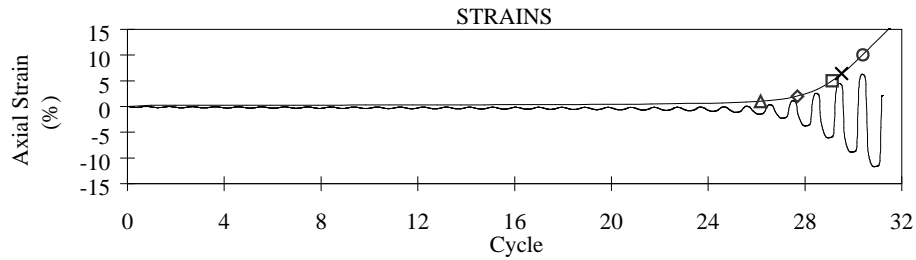
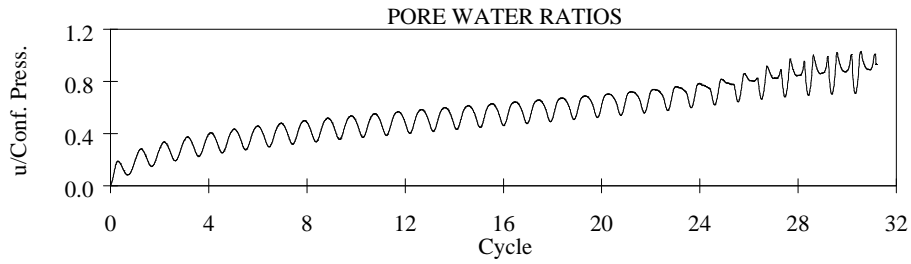
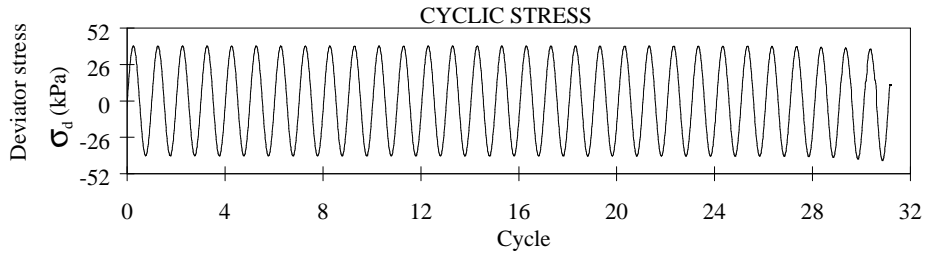
Efective Conf. Press (kPa): 99.6



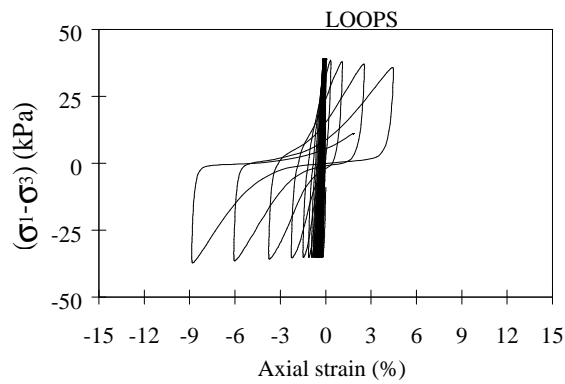


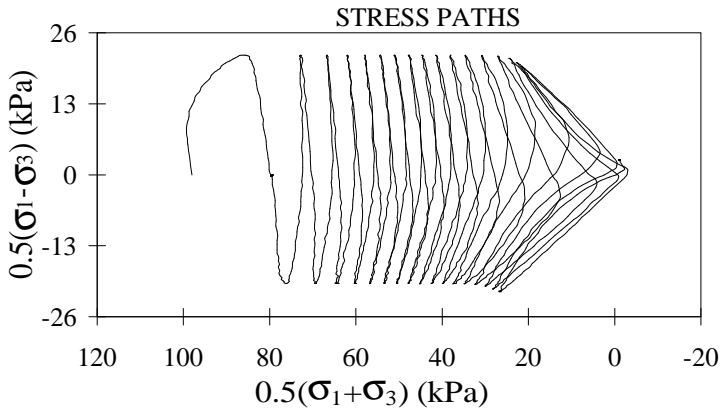
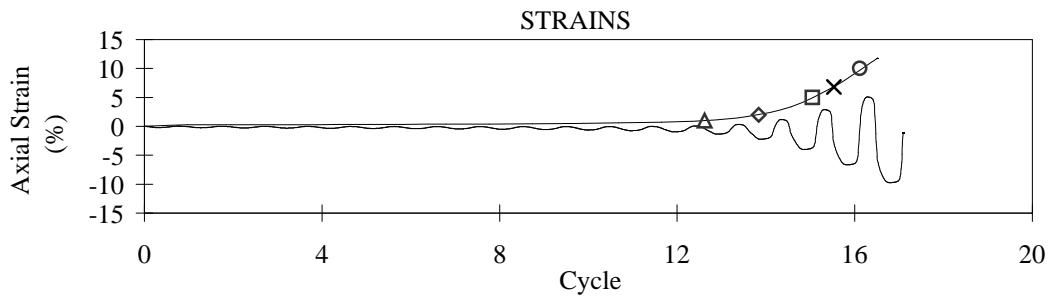
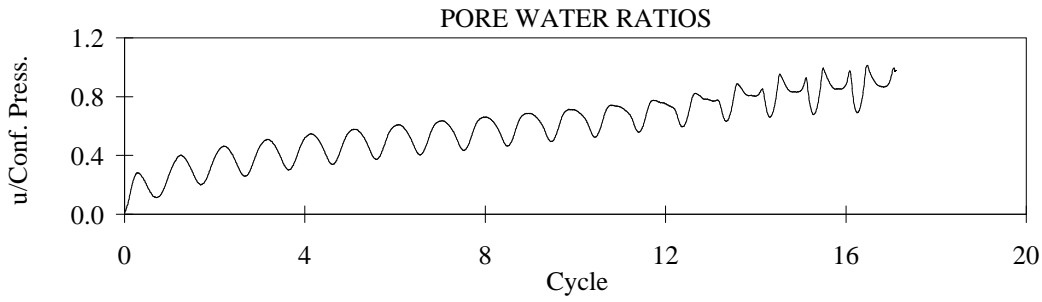
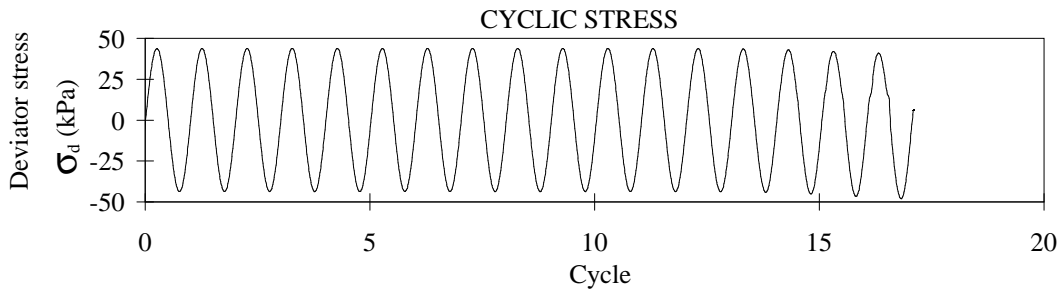
SAMPLE PROPERTIES	MC:1.5-B3
Mica Content (%) :	1.5
Non-Plastic Fines Content (%) :	0.0
Relative Density (%) :	64.0
Cyclic Stress Ratio:	0.520
Efective Conf. Press (kPa):	100.2





SAMPLE PROPERTIES	MC1.5-C1
Mica Content (%) :	1.5
Non-Plastic Fines Content (%) :	0.0
Relative Density (%) :	49.0
Cyclic Stress Ratio:	0.196
Effective Conf. Press (kPa):	99.8





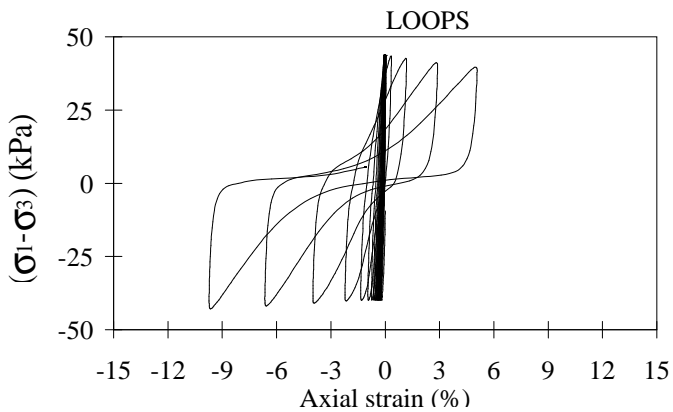
SAMPLE PROPERTIES

MV:1.5-C2

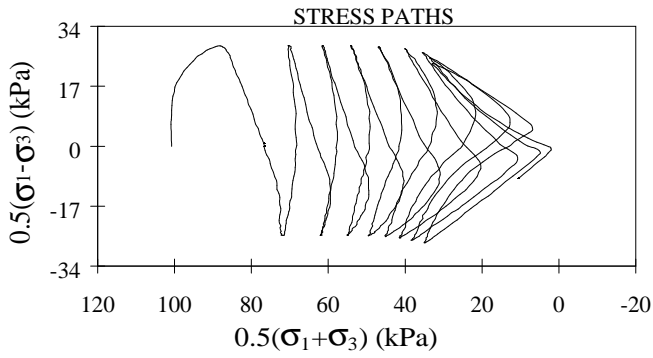
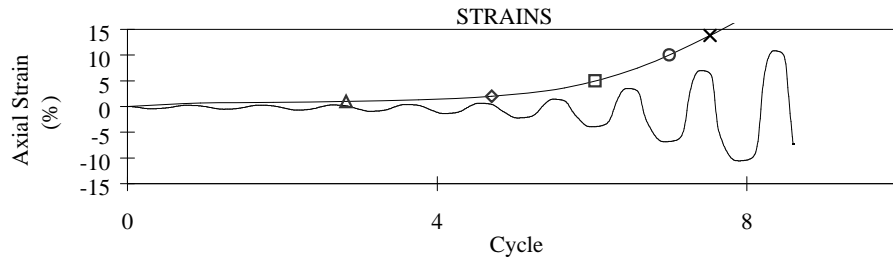
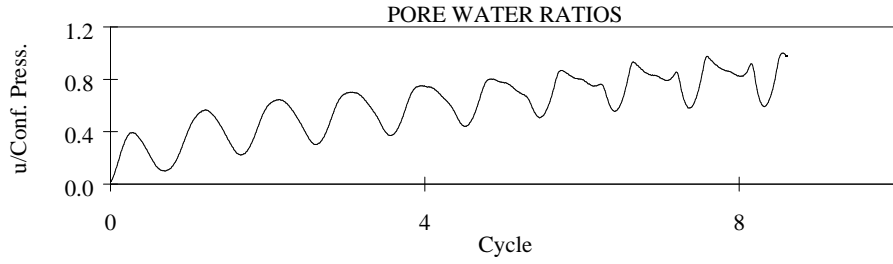
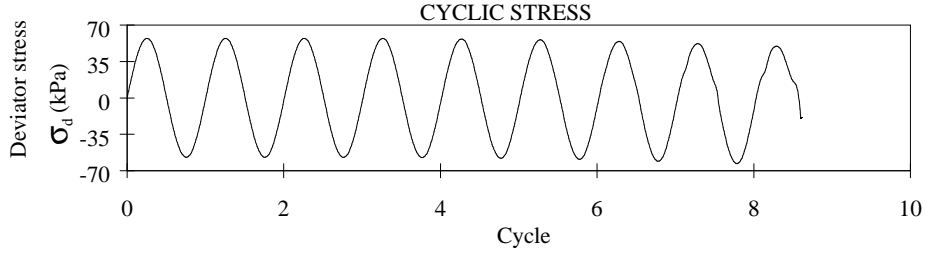
Mica Content (%) : 1.5
 Non-Plastic Fines Content (%) : 0.0
 Relative Density (%): 48.0

Cyclic Stress Ratio: 0.220

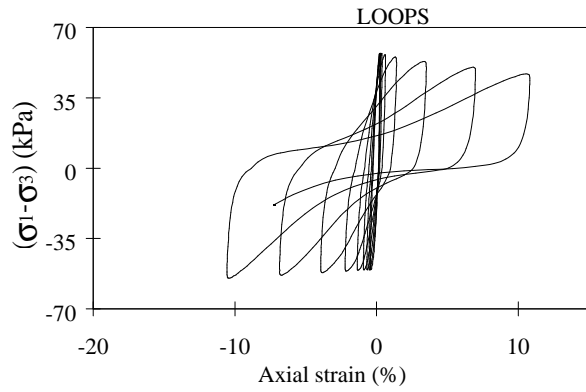
Effective Conf. Press (kPa): 99.5

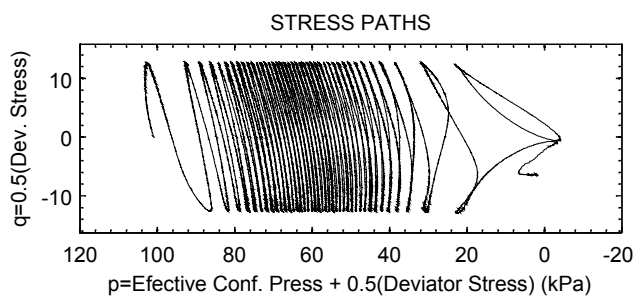
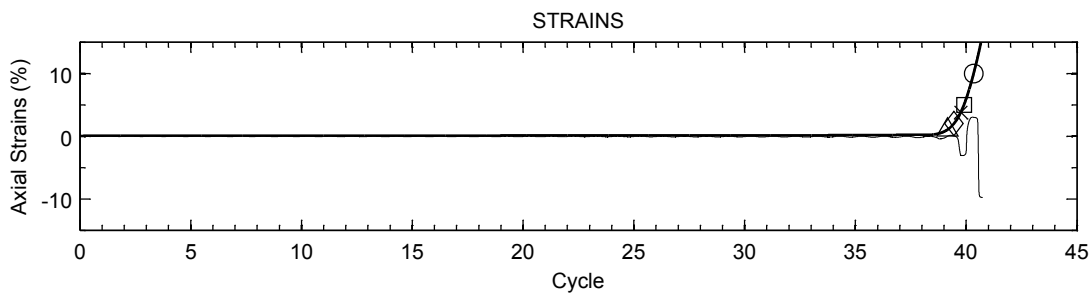
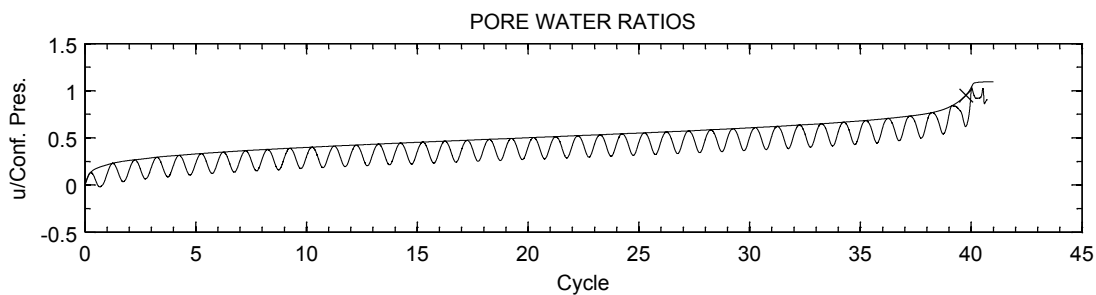
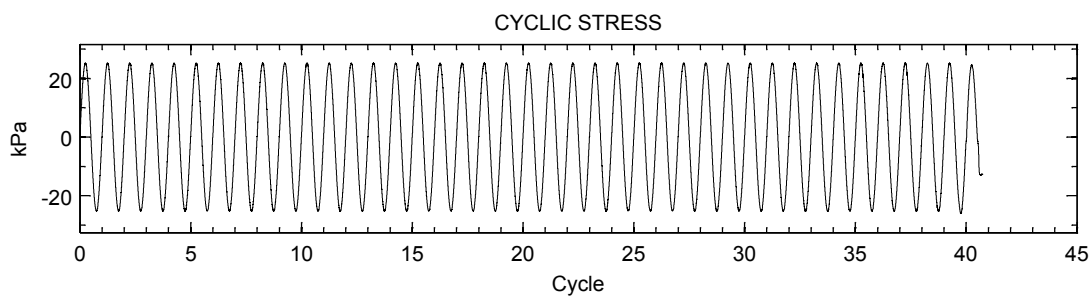


-15 -12 -7 -5 0 5 8 12 15
Axial strain (%)



SAMPLE PROPERTIES		MC:1.5-C3
Mica Content (%) :	1.50	
Non-Plastic Fines Content (%) :	0.00	
Relative Density (%) :	48.0	
Cyclic Stress Ratio:	0.286	
Efective Conf. Press (kPa):	99.80	



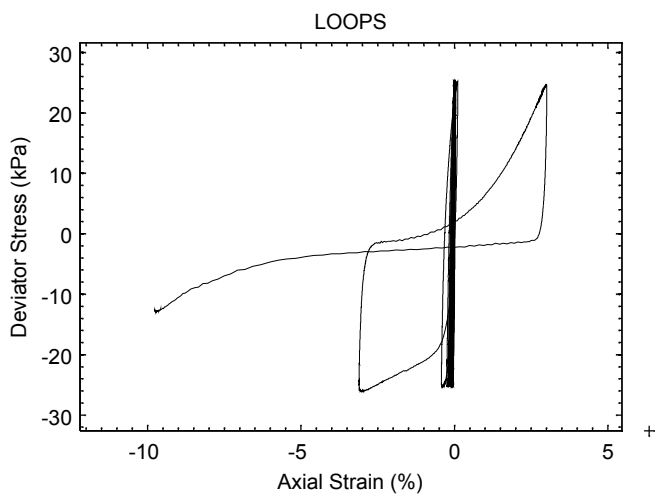


SAMPLE PROPERTIES: MC:1.5-D1

Mica Content (%): 1.5

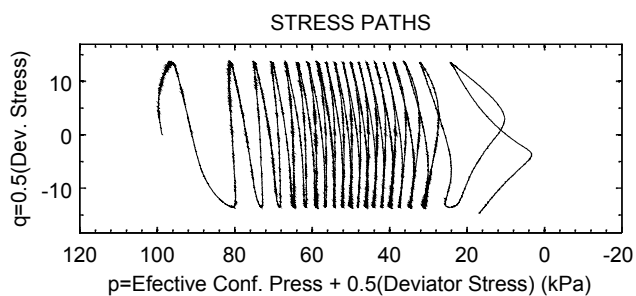
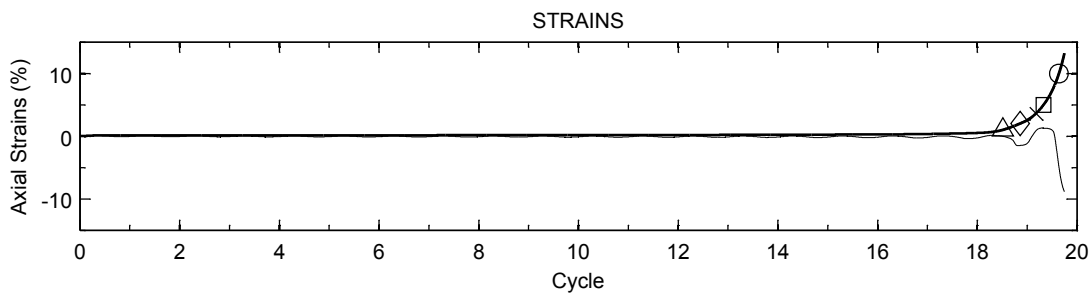
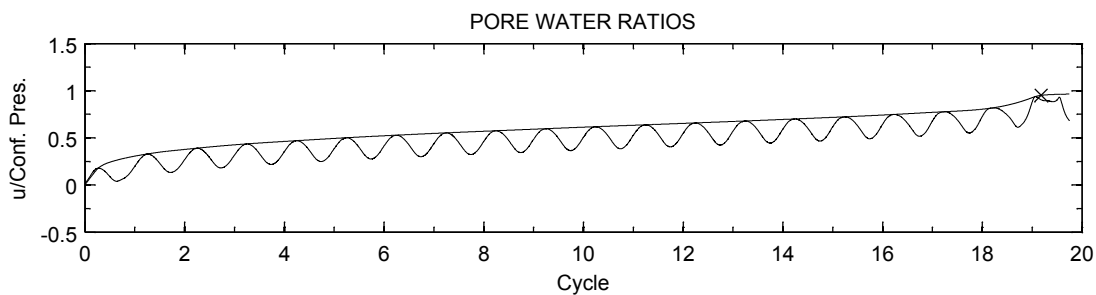
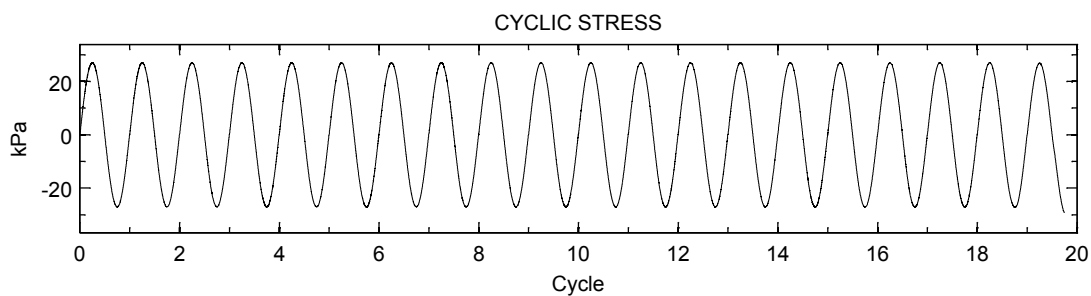
Non-Plastic Fines Content (%): 0

Relative Density (%): 30.5



Cyclic Stress Ratio: 0.125

Effective Conf. Press (kPa): 100.5

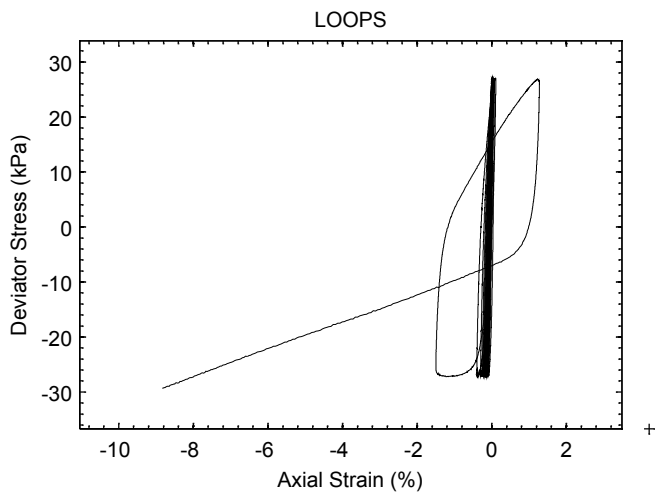


SAMPLE PROPERTIES: MC:15-D2

Mica Content (%): 1.5

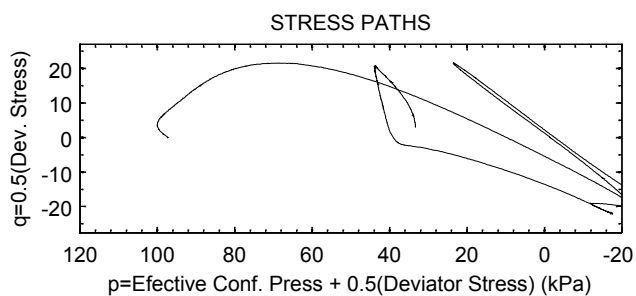
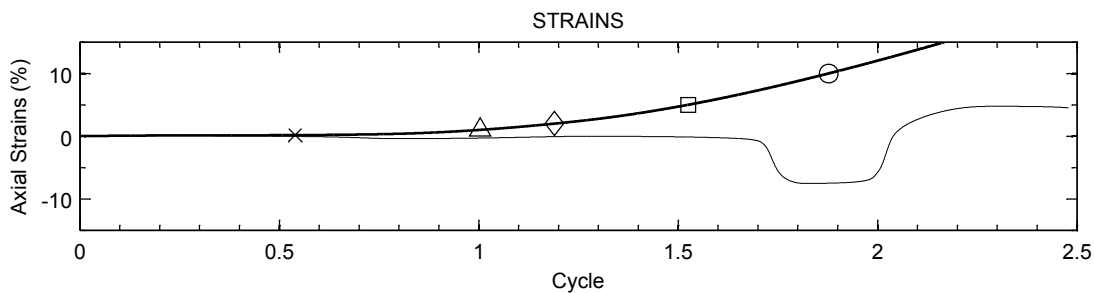
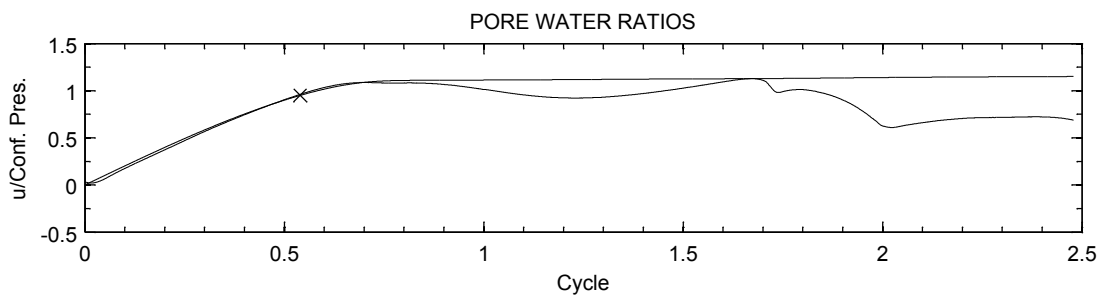
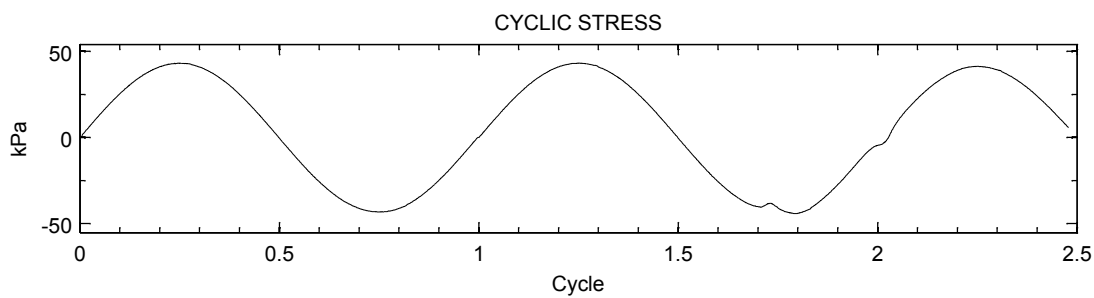
Non-Plastic Fines Content (%): 0

Relative Density (%): 32



Cyclic Stress Ratio: 0.1336

Efective Conf. Press (kPa): 100.3

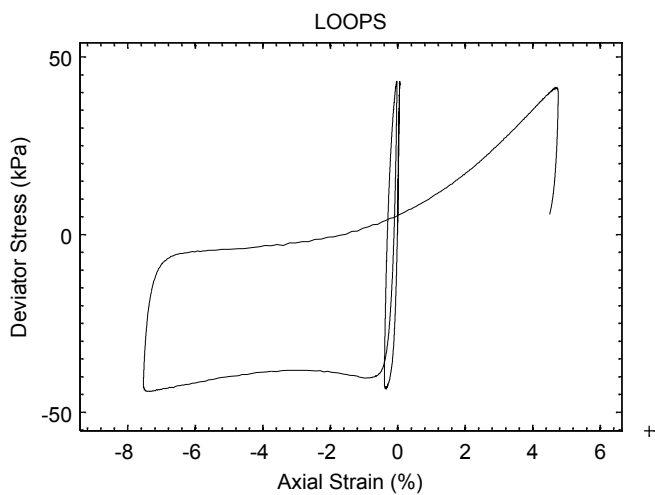


SAMPLE PROPERTIES: MC:1.5-D3

Mica Content (%): 1.5

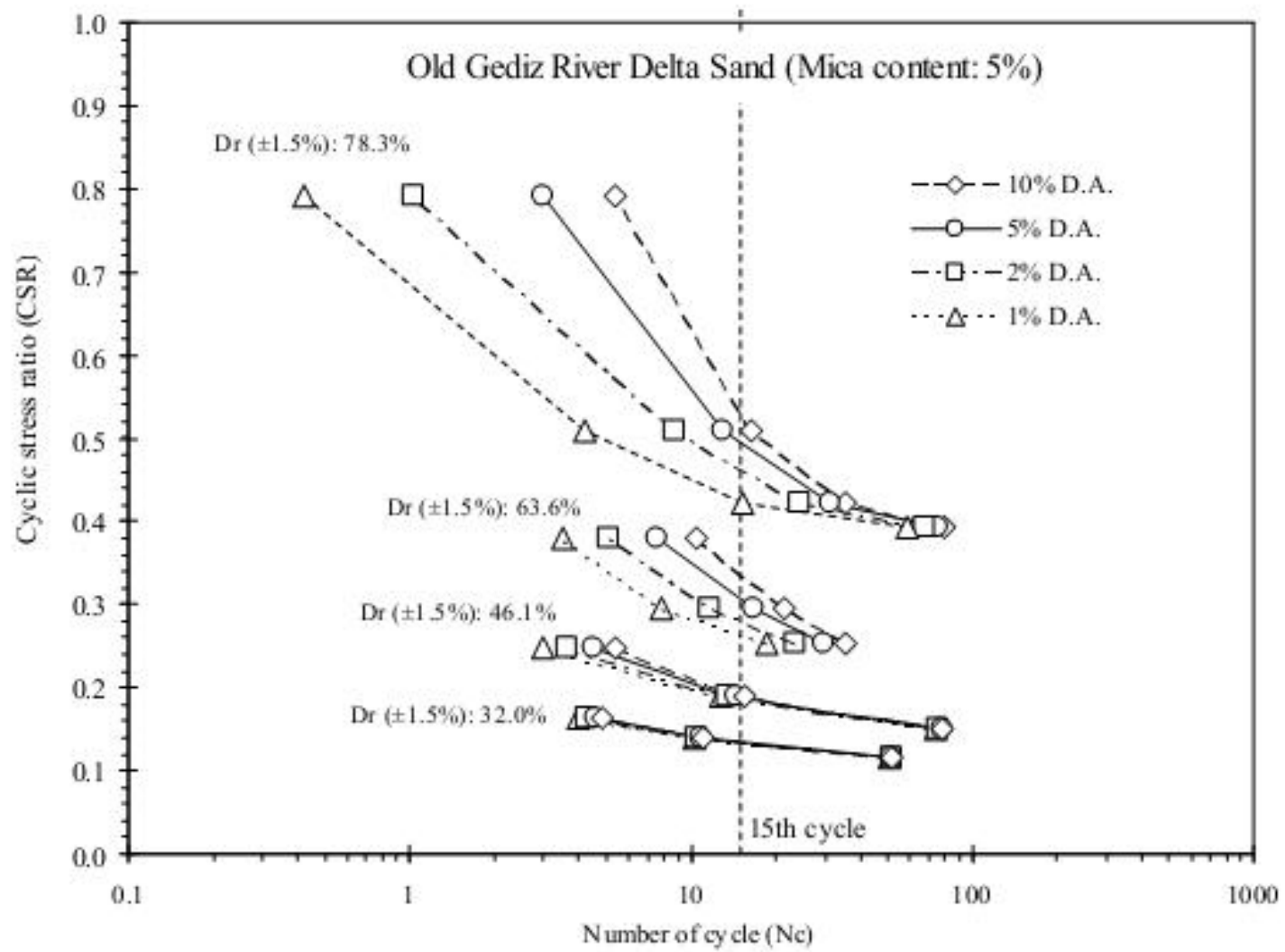
Non-Plastic Fines Content (%): 0

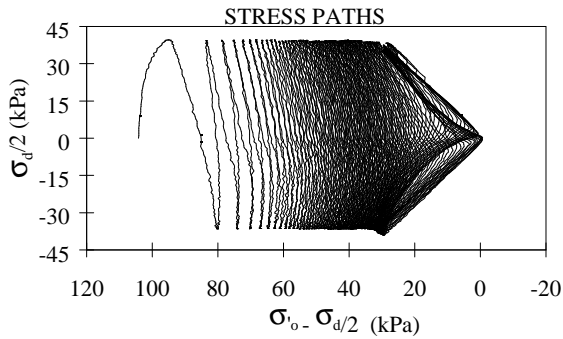
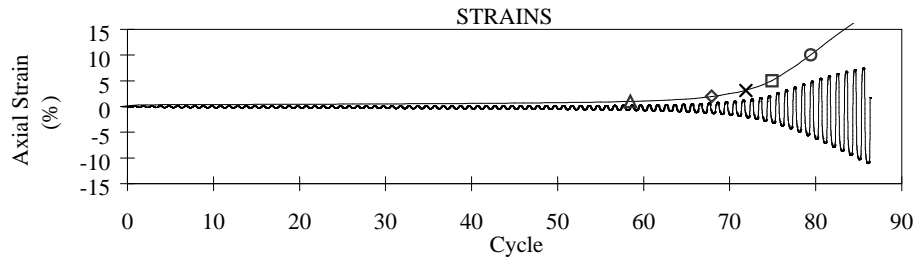
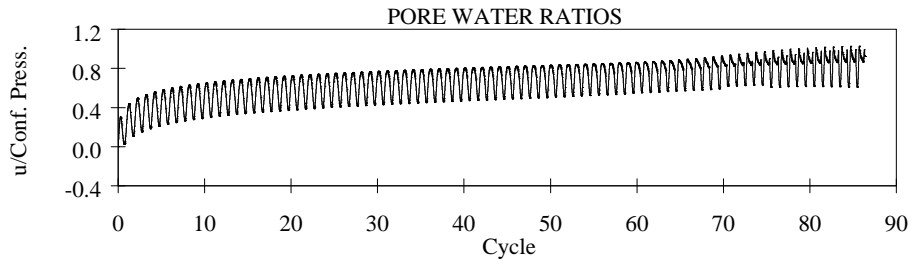
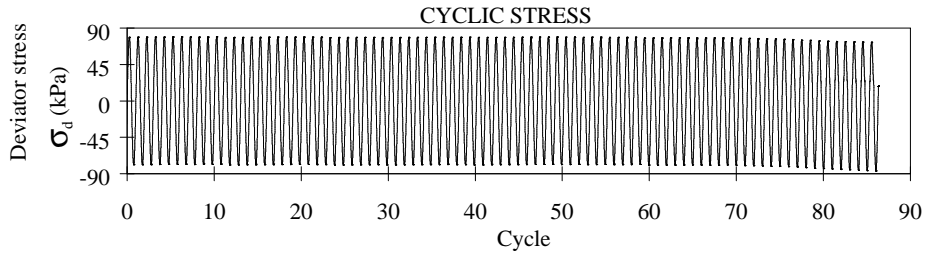
Relative Density (%): 31.5



Cyclic Stress Ratio: 0.2151

Effective Conf. Press (kPa): 100





SAMPLE PROPERTIES MC:5-A1

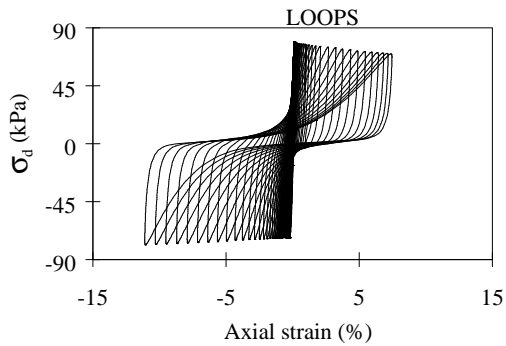
Mica Content (%) : 5.0

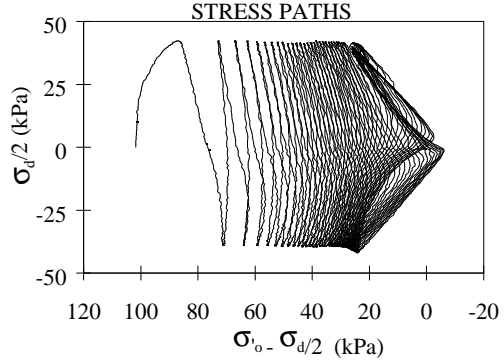
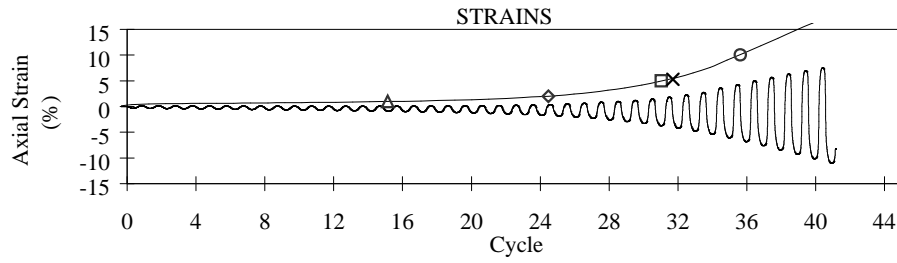
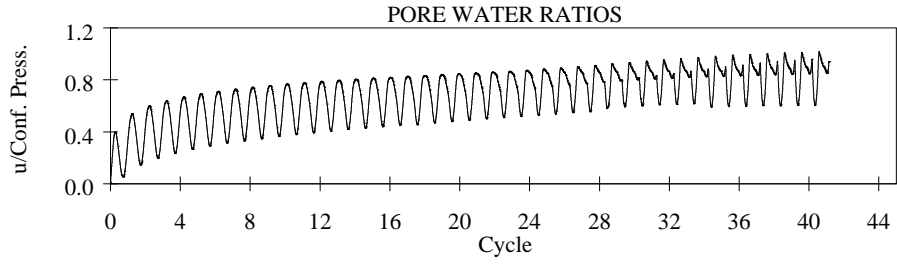
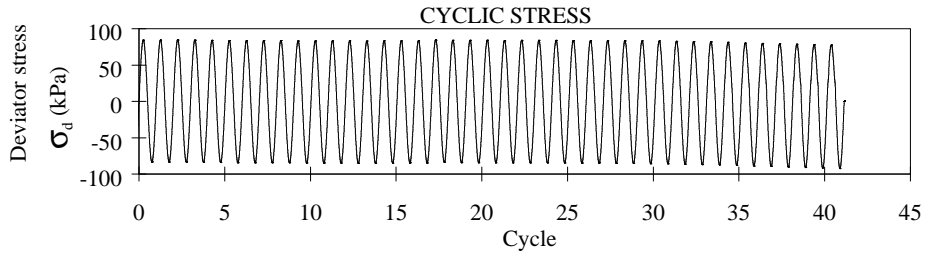
Non-Plastic Fines Content (%) : 0.0

Relative Density (%) : 79.00

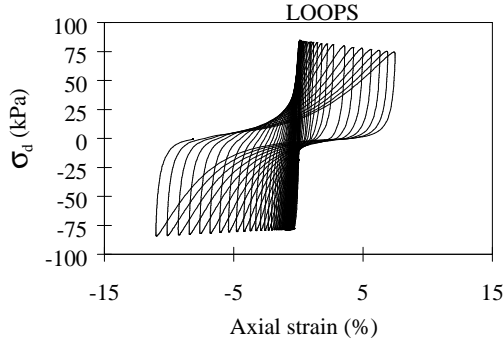
Cyclic Stress Ratio: 0.3980

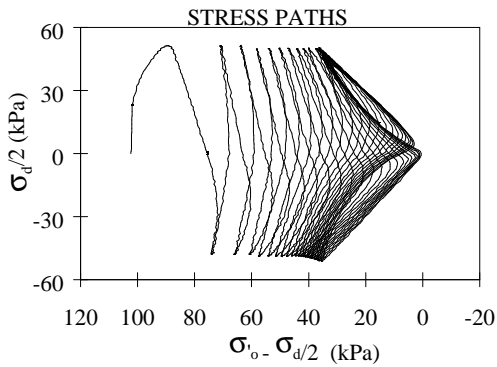
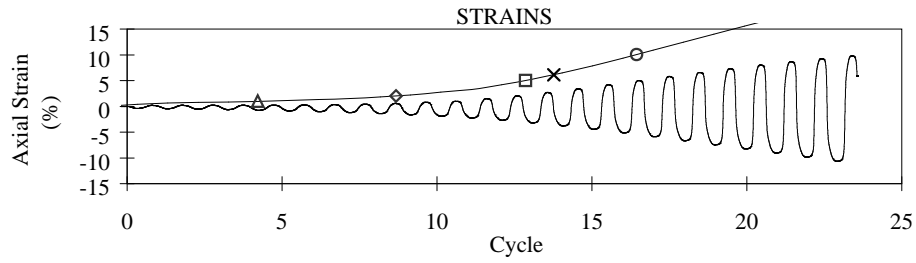
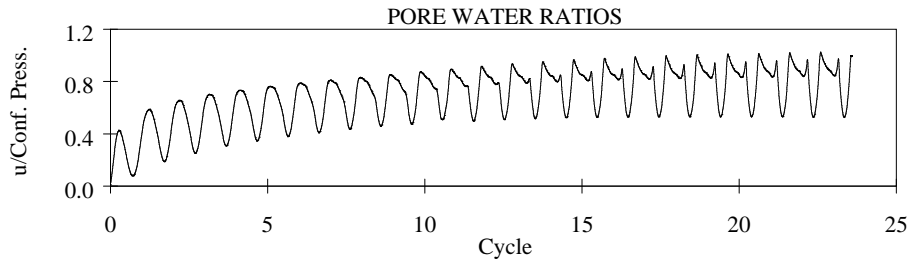
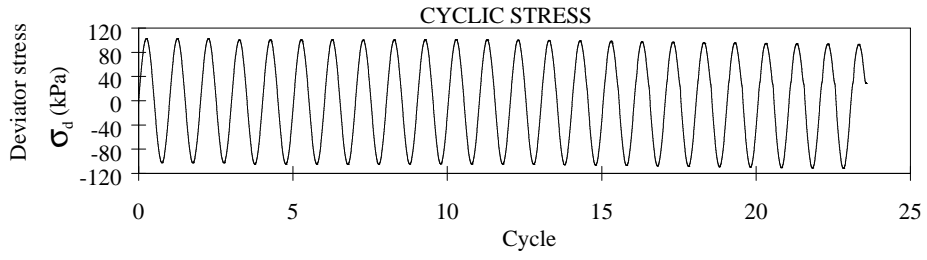
Efective Conf. Press (kPa): 102.3





SAMPLE PROPERTIES		MC:5-A2
Mica Content (%) :		5.0
Non-Plastic Fines Content (%) :		0.0
Relative Density (%) :		78.00
Cyclic Stress Ratio:		0.4232
Efective Conf. Press (kPa):		99.9





SAMPLE PROPERTIES MC:5-A3

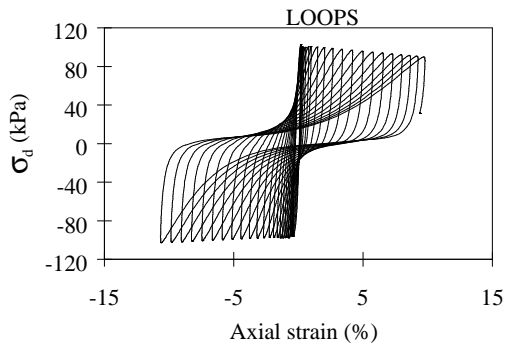
Mica Content (%) : 5.0

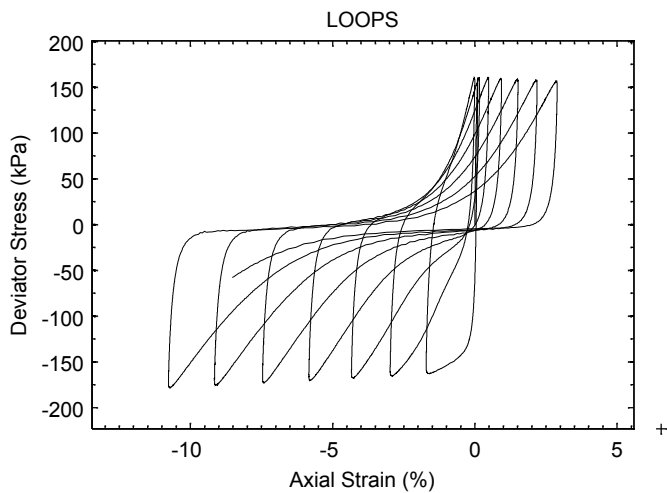
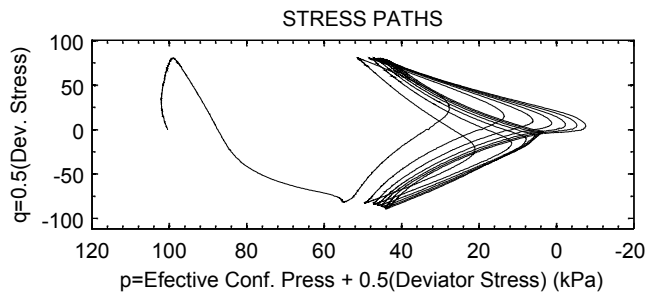
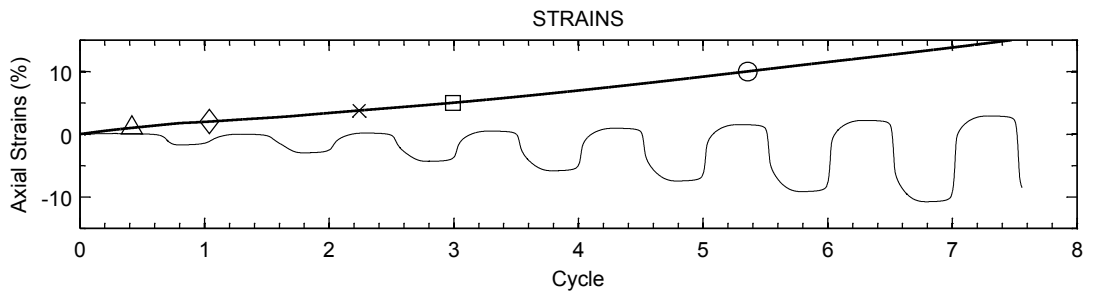
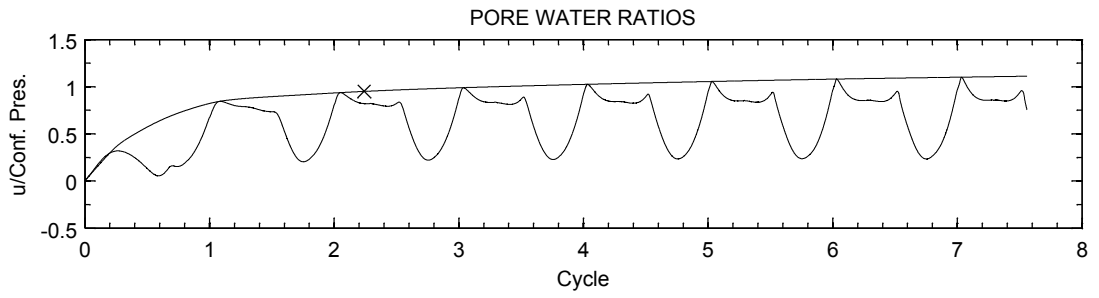
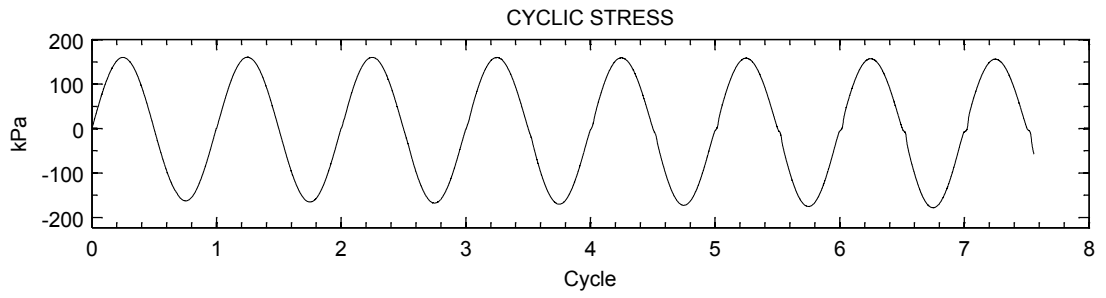
Non-Plastic Fines Content (%) : 0.0

Relative Density (%) : 78.30

Cyclic Stress Ratio: 0.5139

Efective Conf. Press (kPa): 101.9





SAMPLE PROPERTIES: MC:5-A4

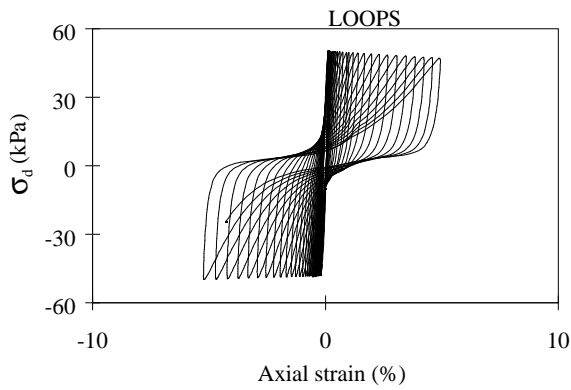
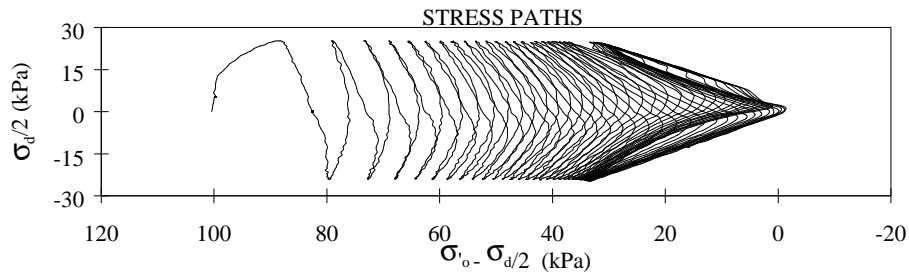
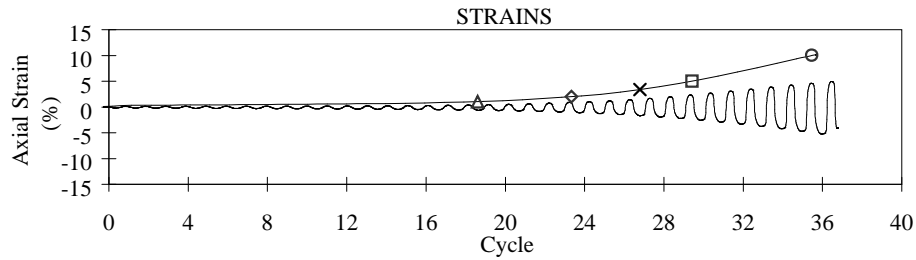
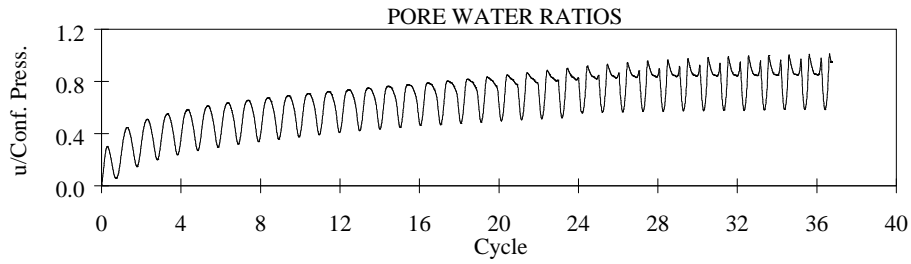
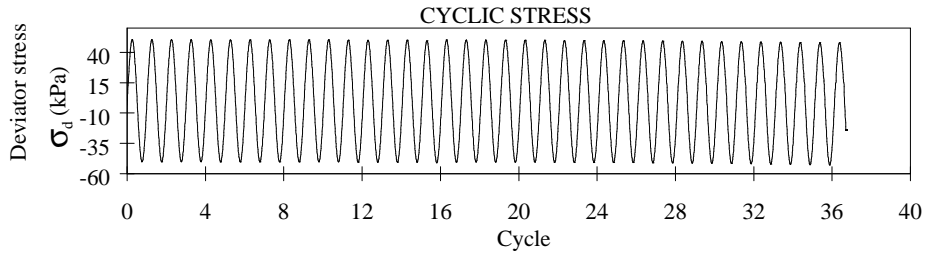
Mica Content (%): 5

Non-Plastic Fines Content (%): 0

Relative Density (%): 78

Cyclic Stress Ratio: 0.791

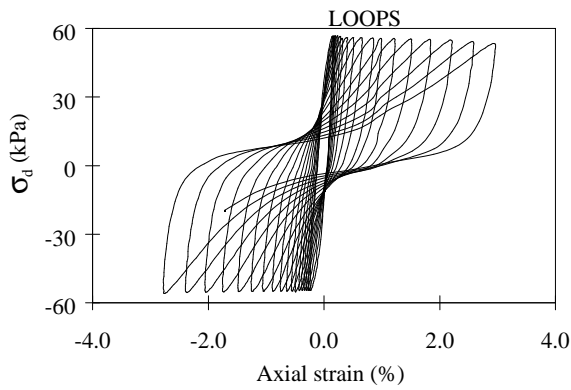
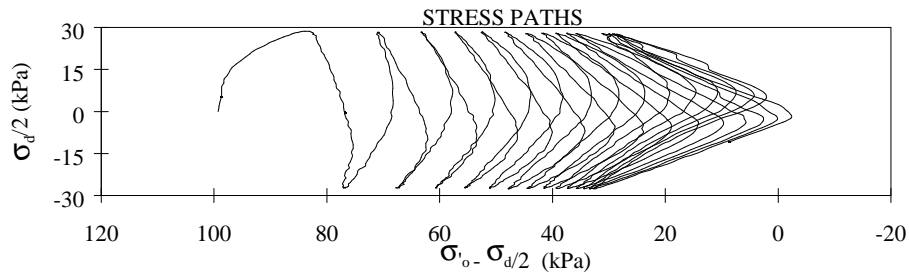
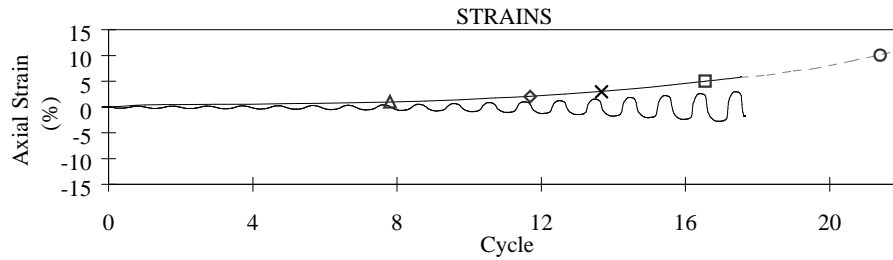
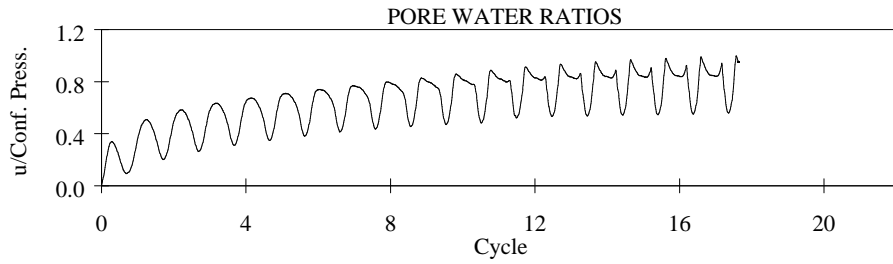
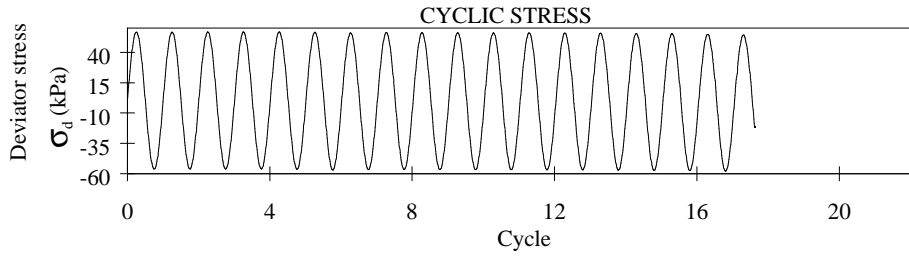
Efective Conf. Press (kPa): 101.1



SAMPLE PROPERTIES

MC:5-B1

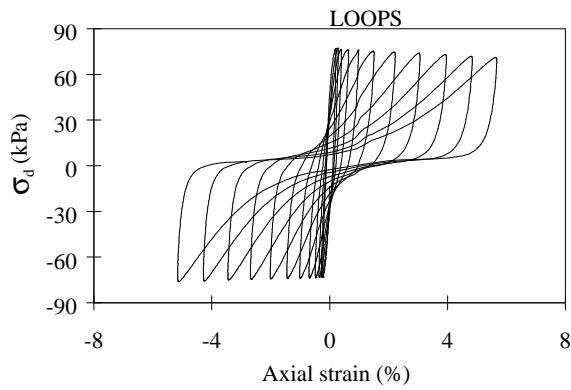
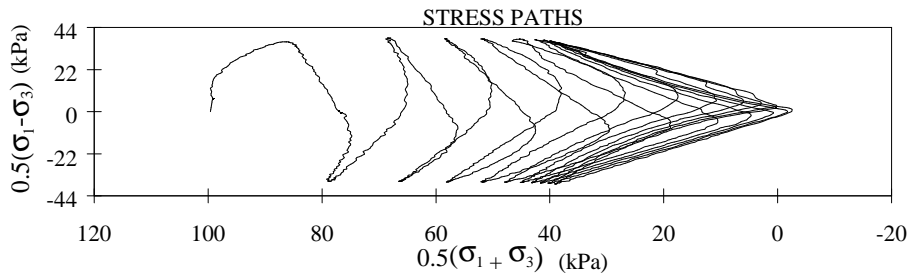
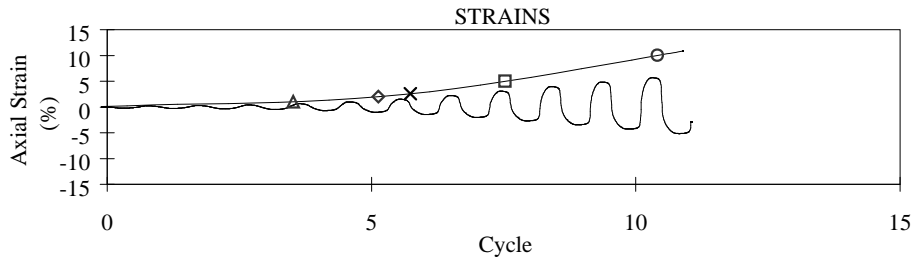
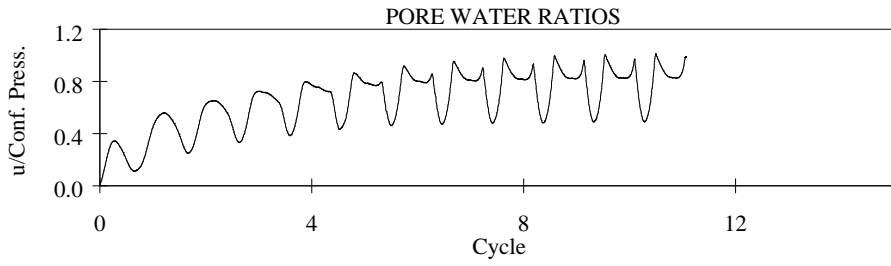
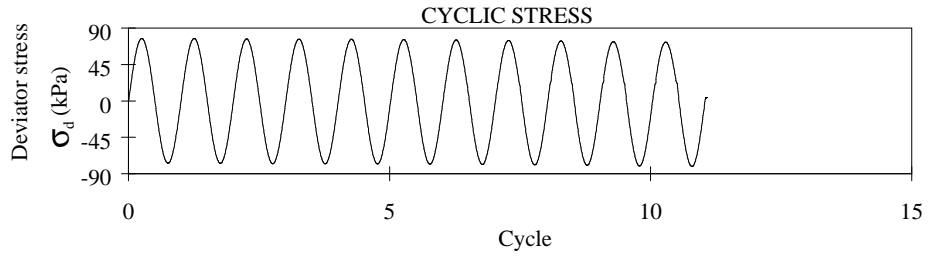
Mica Content (%) :	5.0
Non-Plastic Fines Content (%) :	0.0
Relative Density (%) :	63.00
Cyclic Stress Ratio :	0.2520
Effective Conf. Press (kPa) :	100.1



SAMPLE PROPERTIES

MC:5-B2

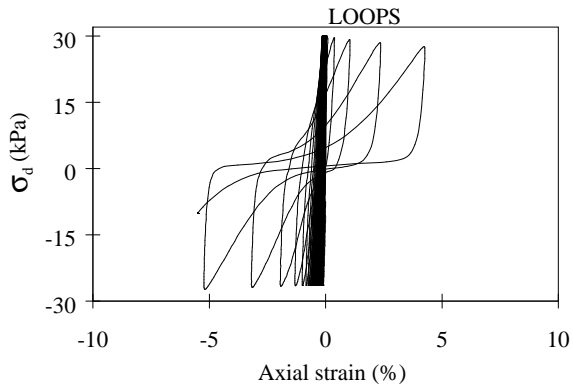
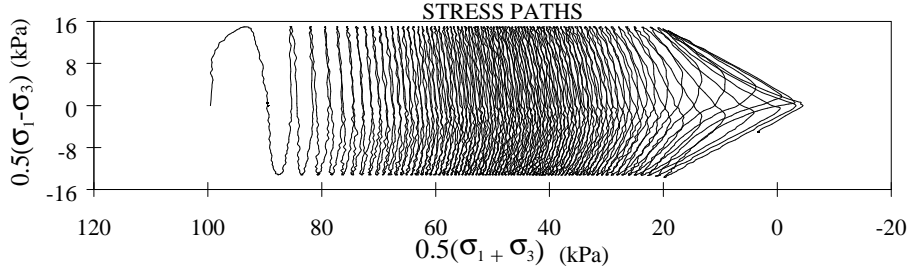
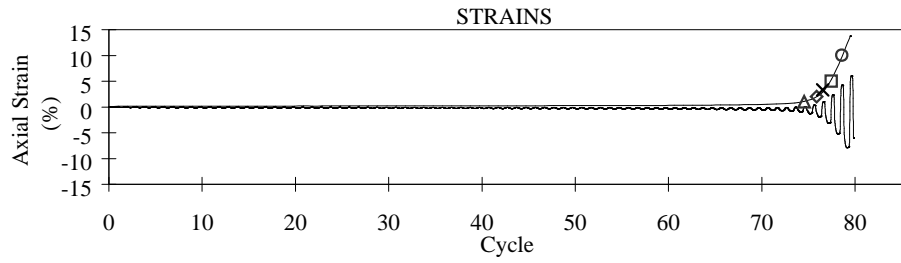
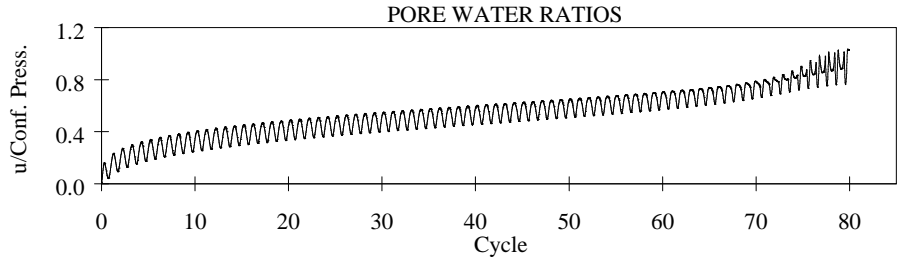
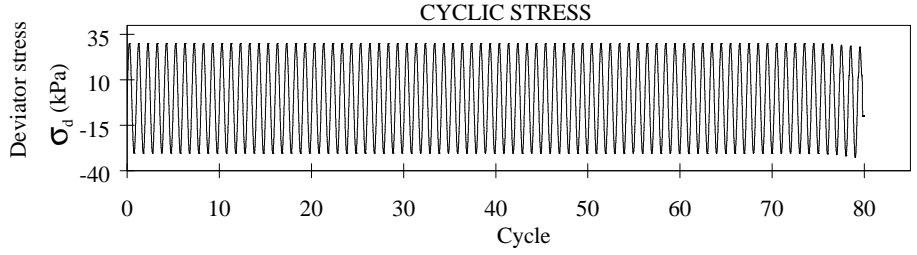
Mica Content (%) :	5.0
Non-Plastic Fines Content (%) :	0.0
Relative Density (%) :	64.00
Cyclic Stress Ratio :	0.2860
Effective Conf. Press (kPa) :	99.3



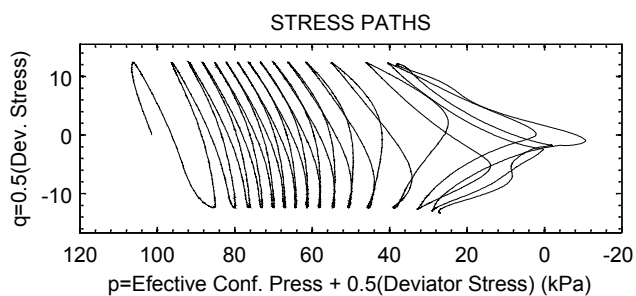
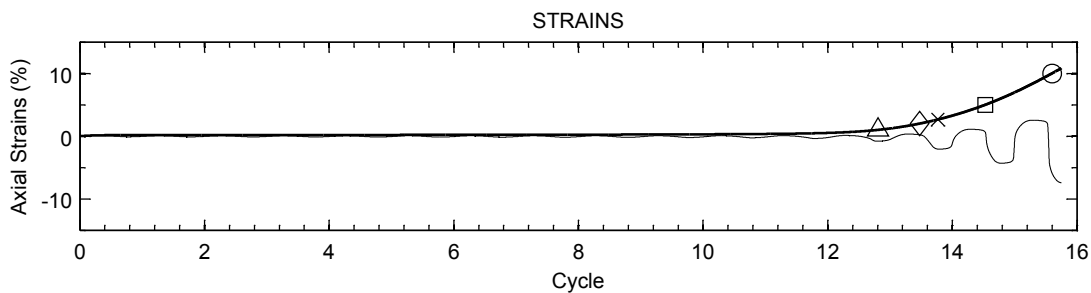
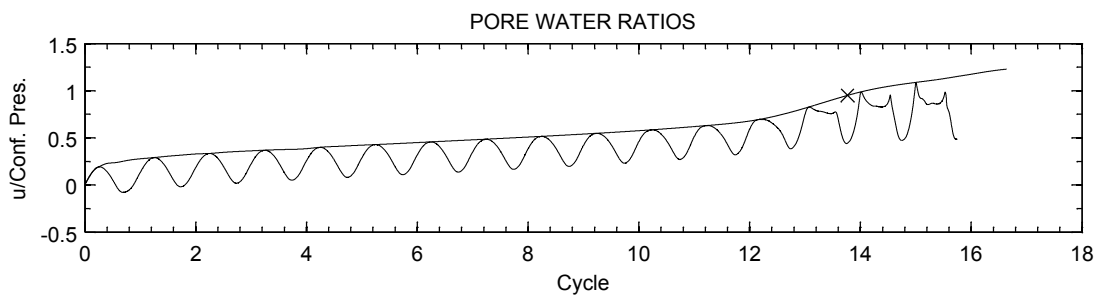
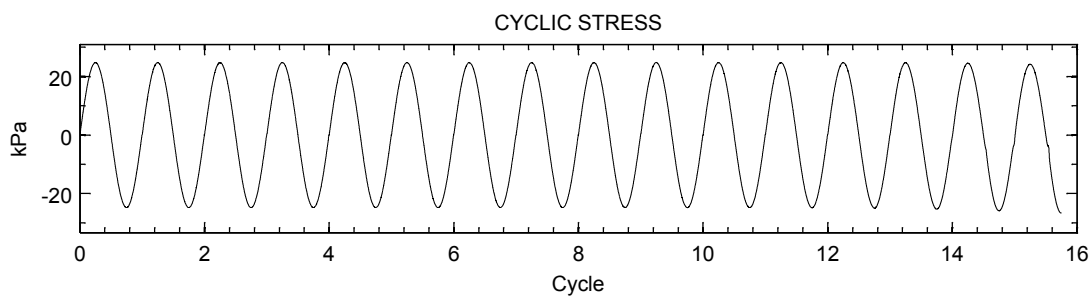
SAMPLE PROPERTIES

MC:5-B3

Mica Content (%) :	5.0
Non-Plastic Fines Content (%) :	0.0
Relative Density (%) :	63.90
Cyclic Stress Ratio :	0.3854
Efective Conf. Press (kPa) :	100.0



SAMPLE PROPERTIES		MC:5-C1
Mica Content (%) :	5.0	
Non-Plastic Fines Content (%) :	0.0	
Relative Density (%) :	46.20	
Cyclic Stress Ratio :	0.1507	
Effective Conf. Press (kPa) :	99.7	

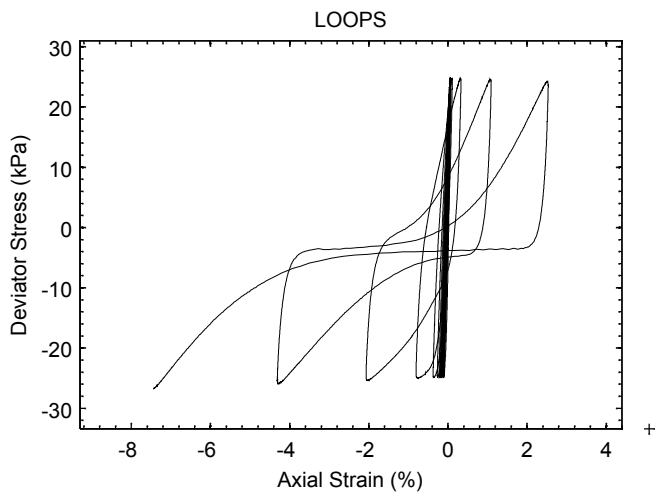


SAMPLE PROPERTIES: MC:5-C2

Mica Content (%): 5

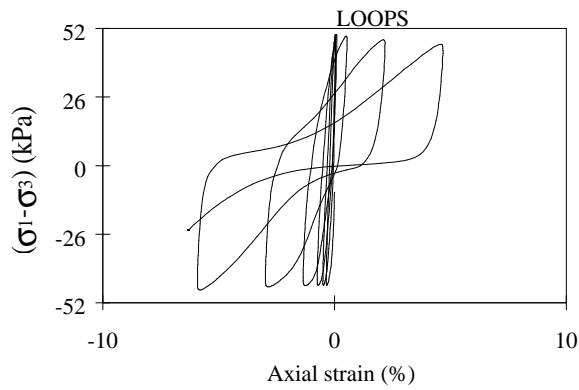
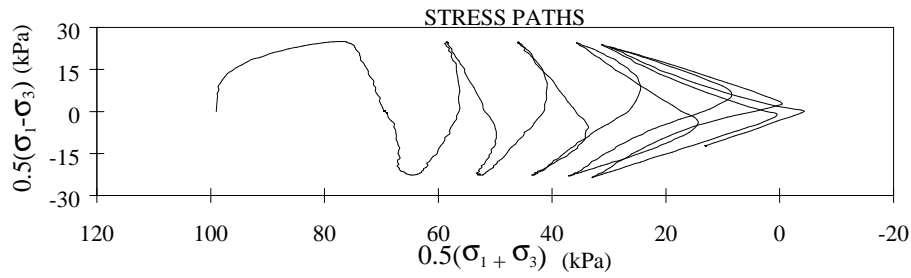
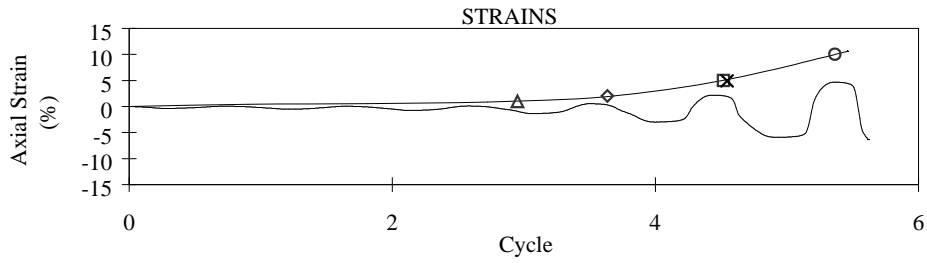
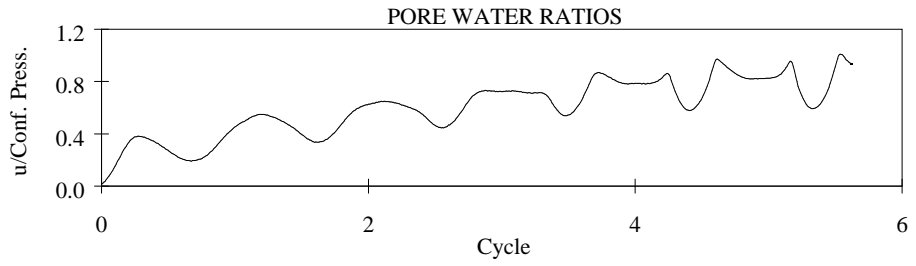
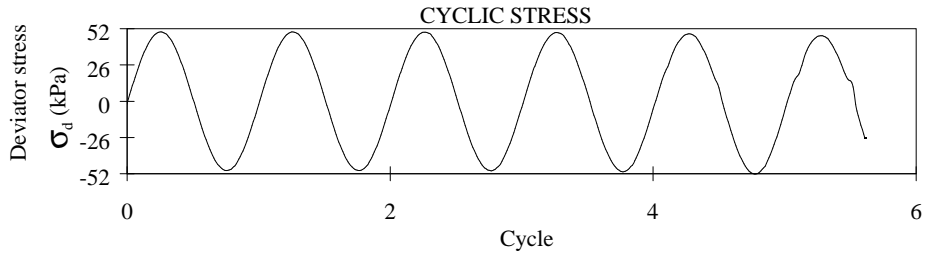
Non-Plastic Fines Content (%): 0

Relative Density (%): 45.1

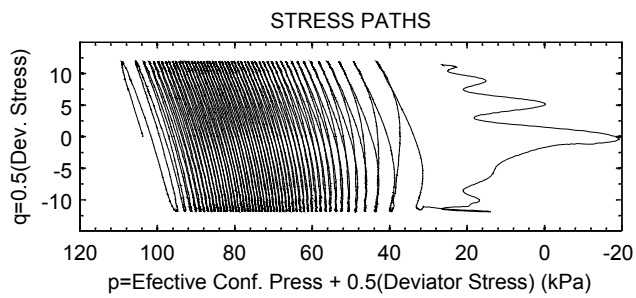
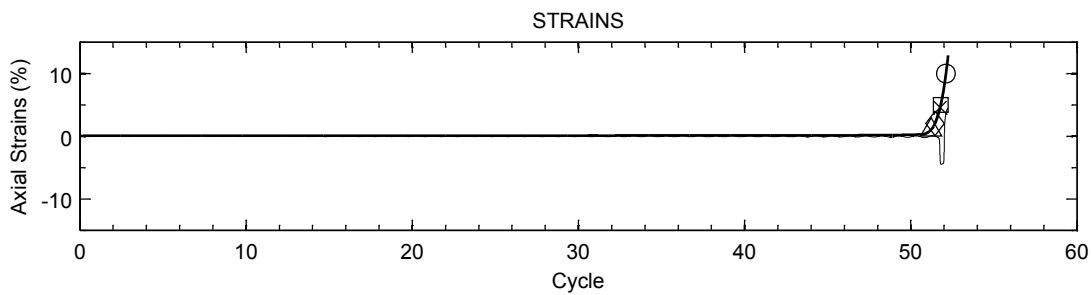
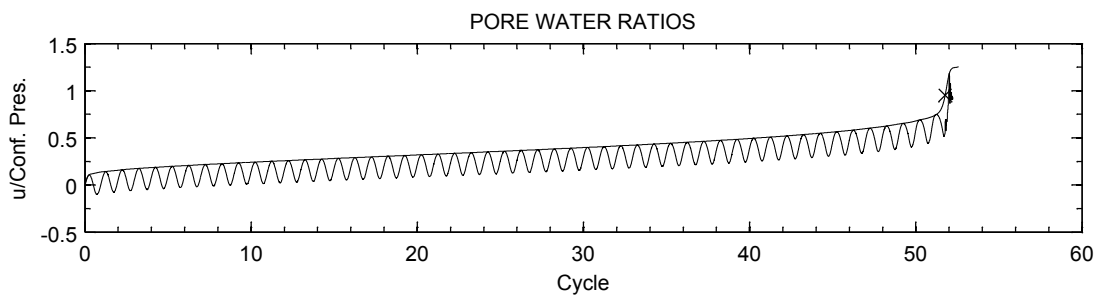
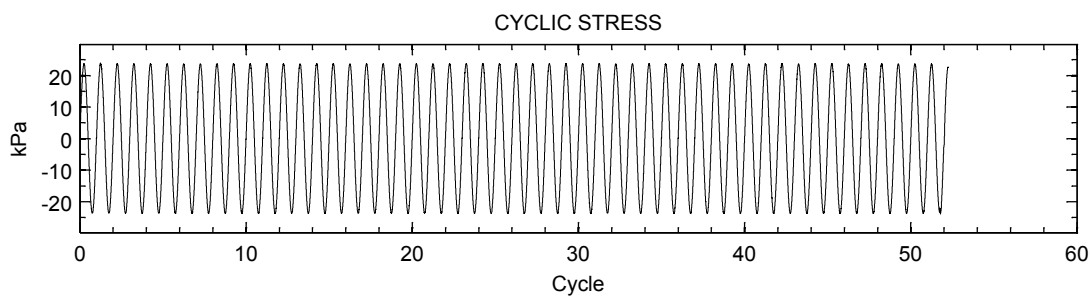


Cyclic Stress Ratio: 0.191

Effective Conf. Press (kPa): 102.1



SAMPLE PROPERTIES		MC:5-C3
Mica Content (%) :	5.0	
Non-Plastic Fines Content (%) :	0.0	
Relative Density (%) :	47.0	
Cyclic Stress Ratio :	0.249	
Effective Conf. Press (kPa) :	100.1	

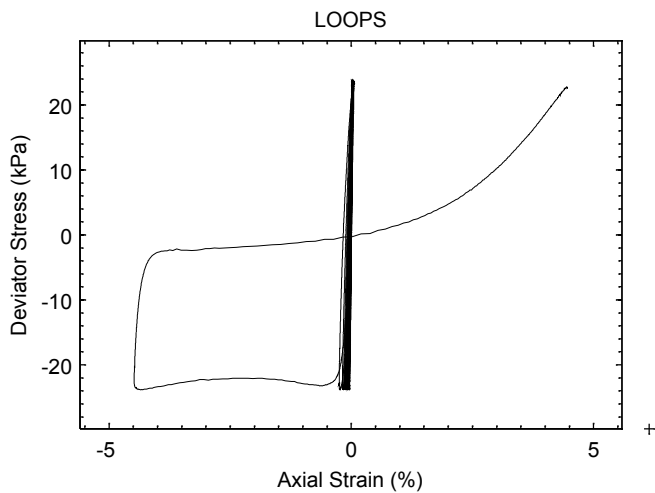


SAMPLE PROPERTIES: MC:5-D1

Mica Content (%): 5

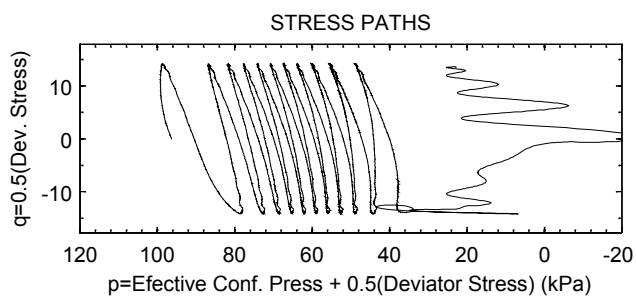
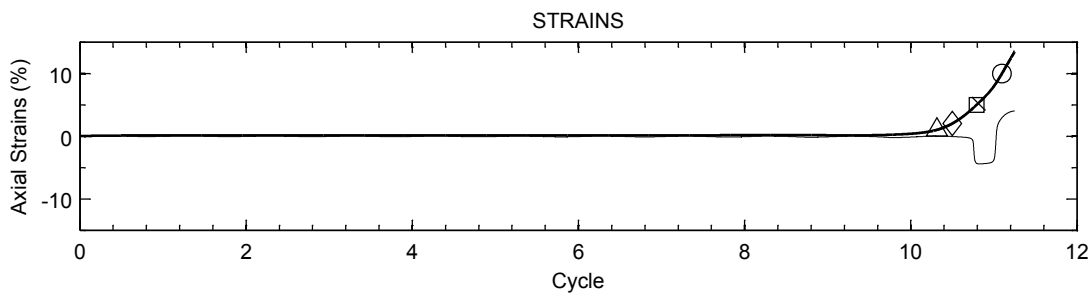
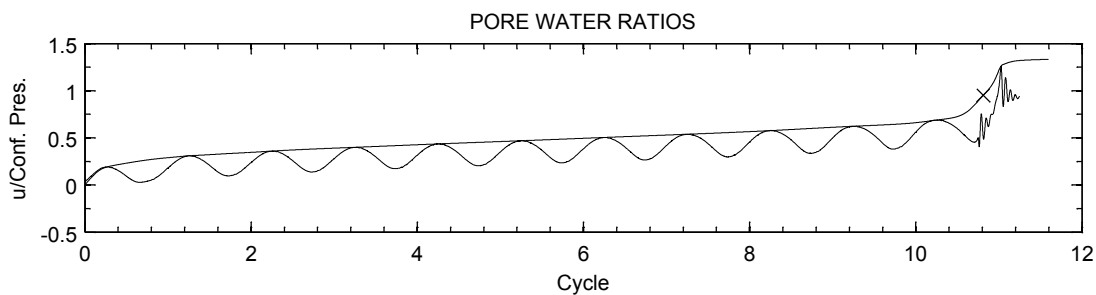
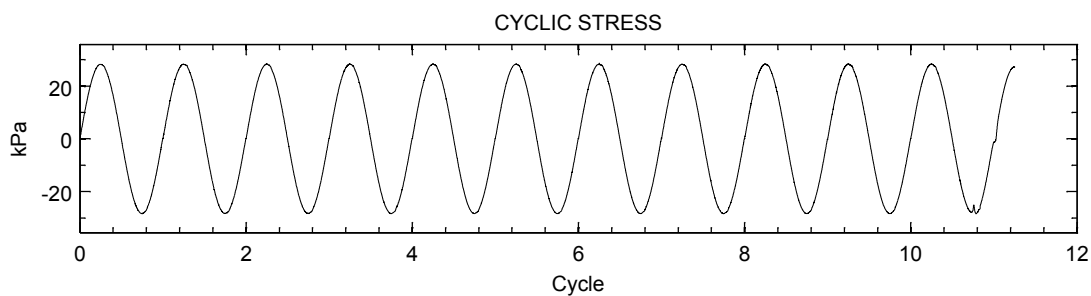
Non-Plastic Fines Content (%): 0

Relative Density (%): 32



Cyclic Stress Ratio: 0.1158

Effective Conf. Press (kPa): 102.5

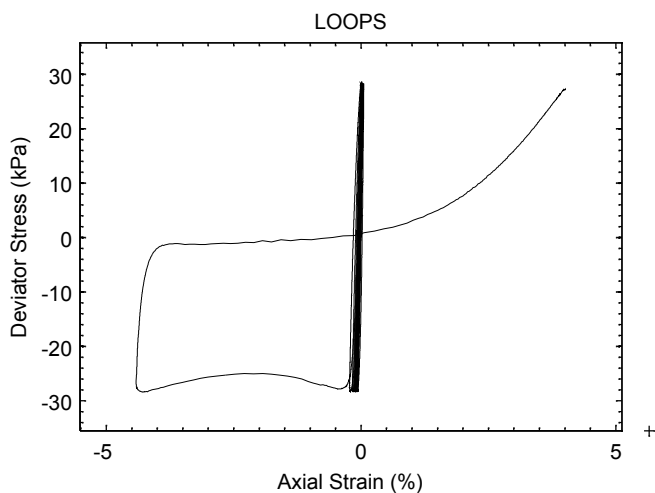


SAMPLE PROPERTIES: MC-5-D2

Mica Content (%): 5

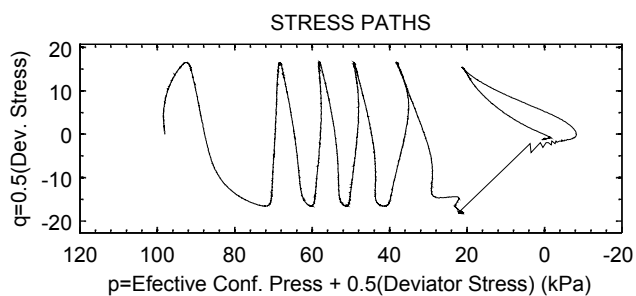
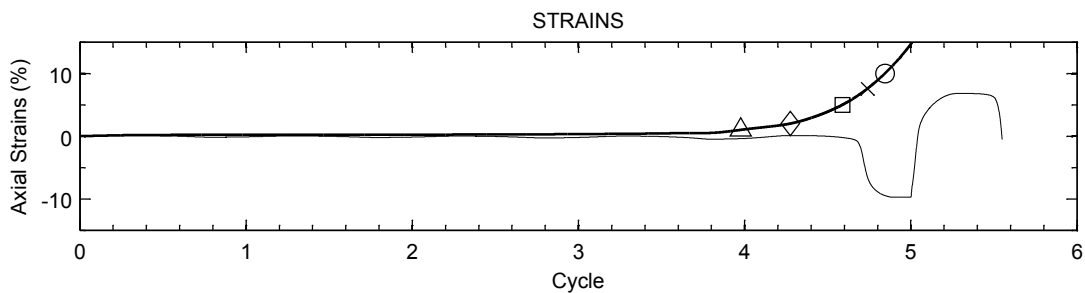
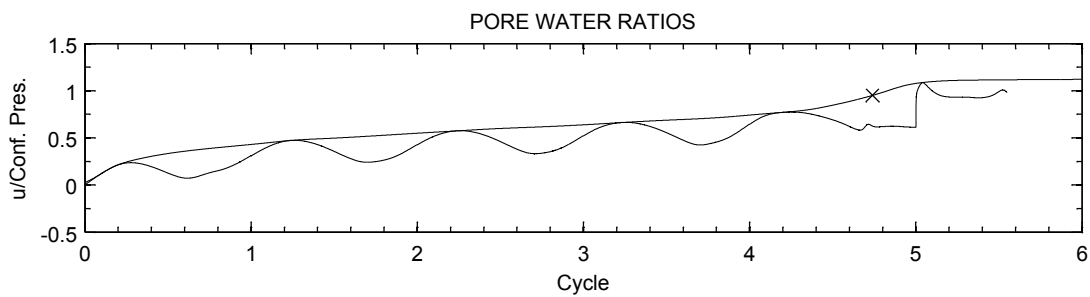
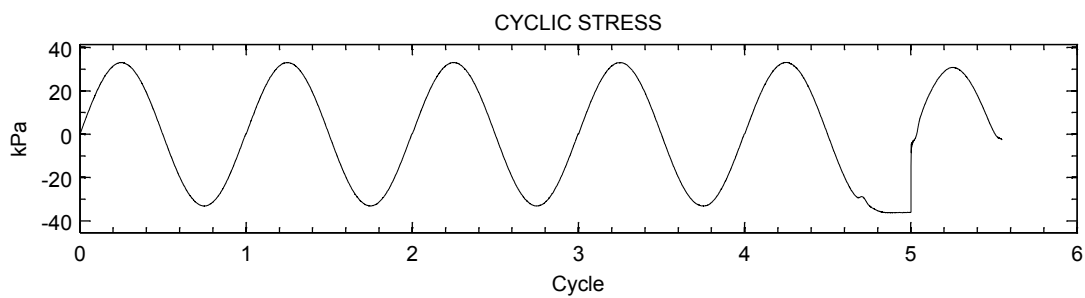
Non-Plastic Fines Content (%): 0

Relative Density (%): 32.5



Cyclic Stress Ratio: 0.1408

Effective Conf. Press (kPa): 100

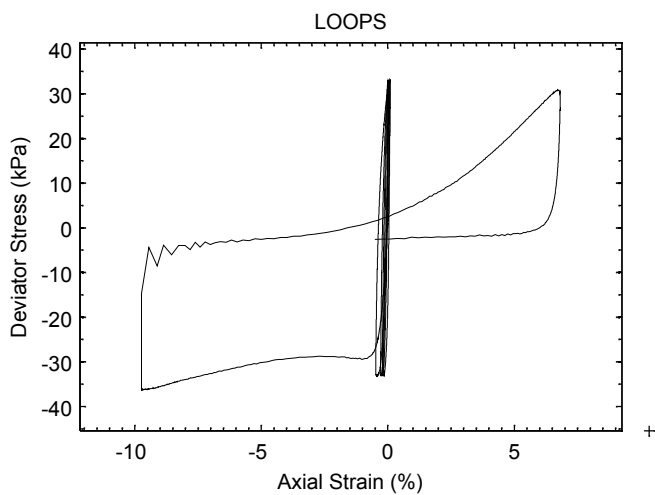


SAMPLE PROPERTIES: MC:5-D3

Mica Content (%): 5

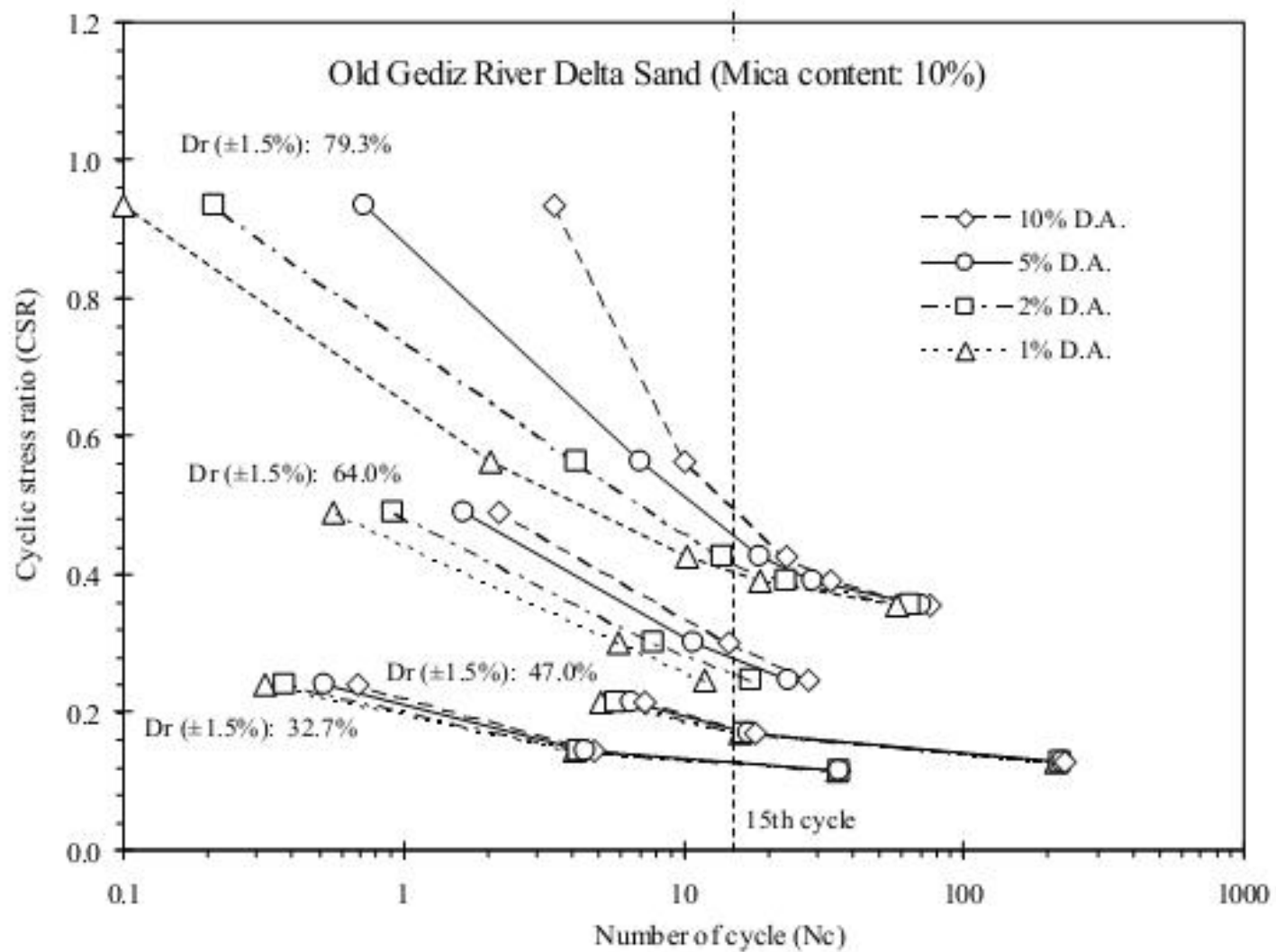
Non-Plastic Fines Content (%): 0

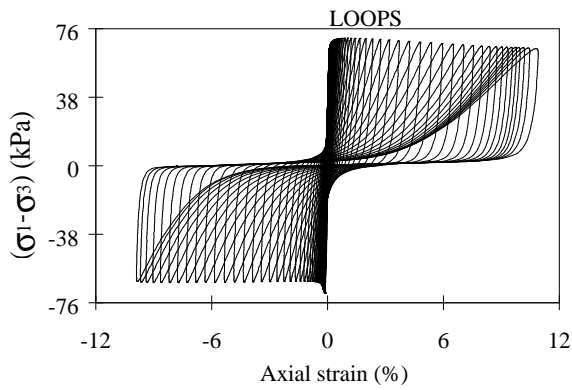
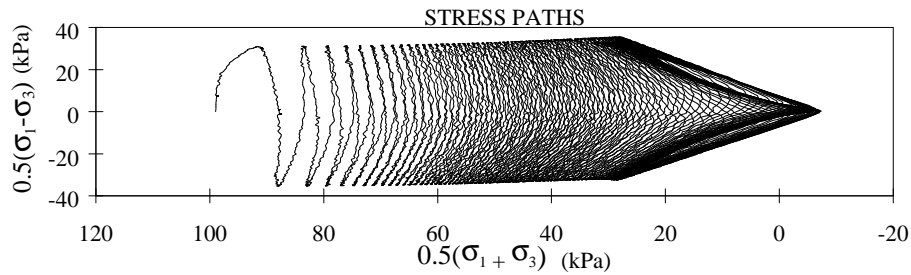
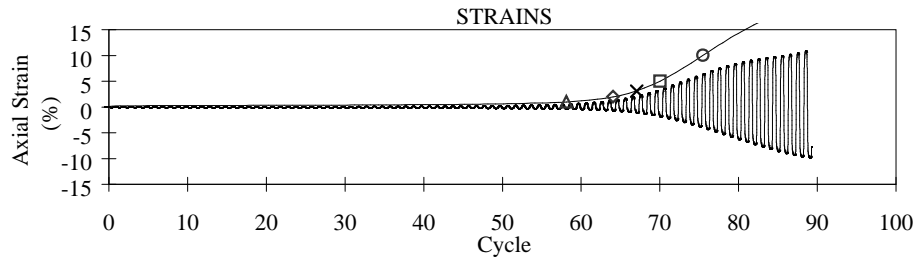
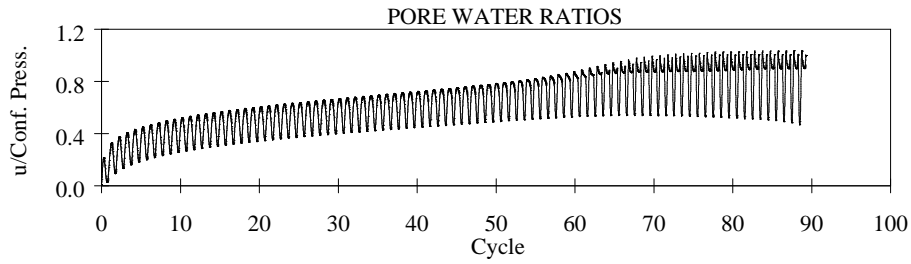
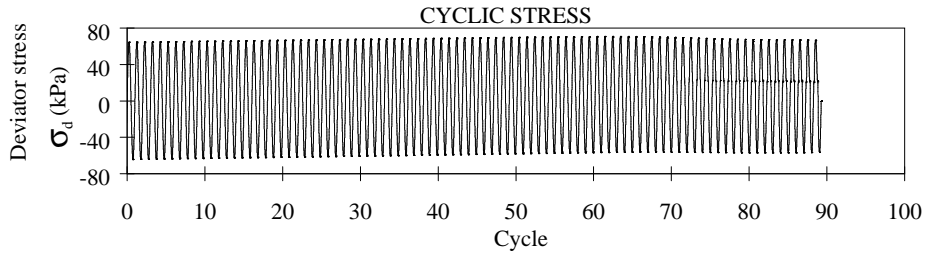
Relative Density (%): 31.5



Cyclic Stress Ratio: 0.163

Effective Conf. Press (kPa): 100.6

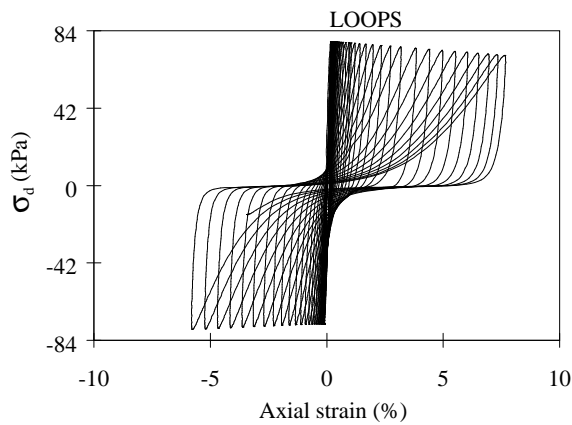
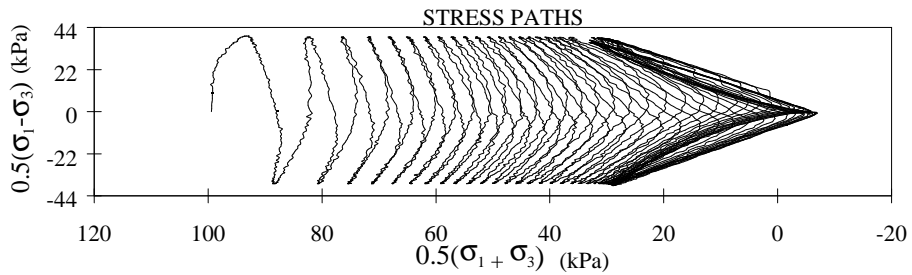
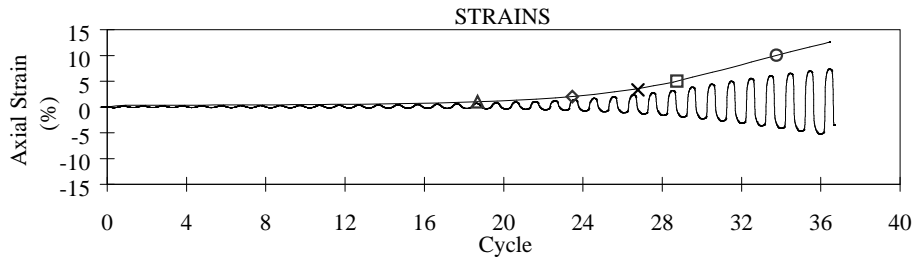
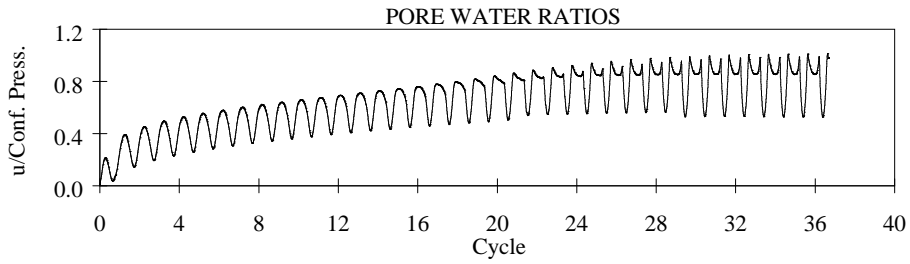
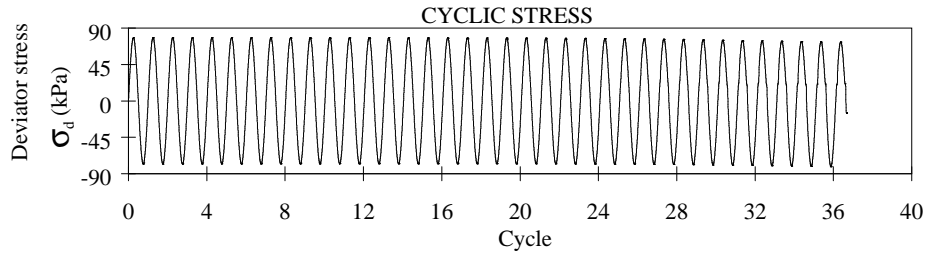




SAMPLE PROPERTIES

MC:10-A1

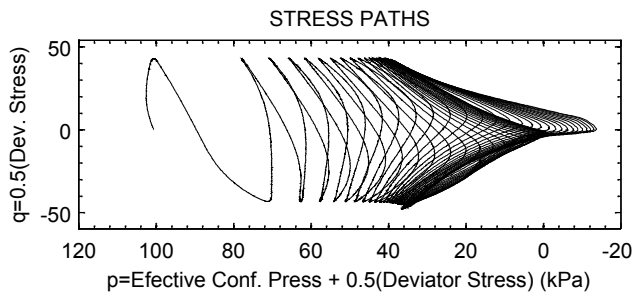
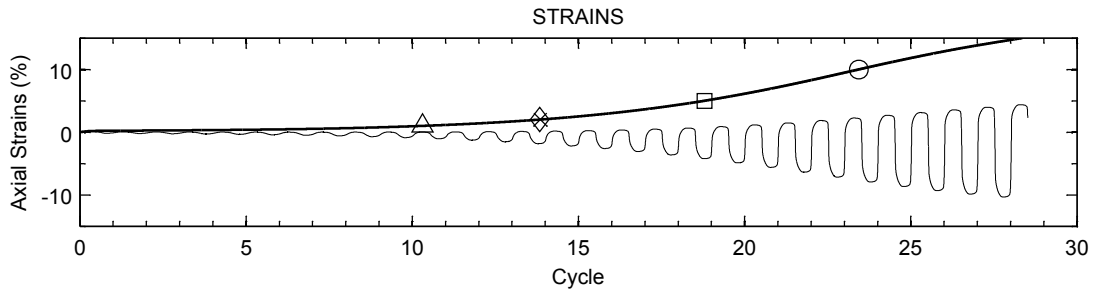
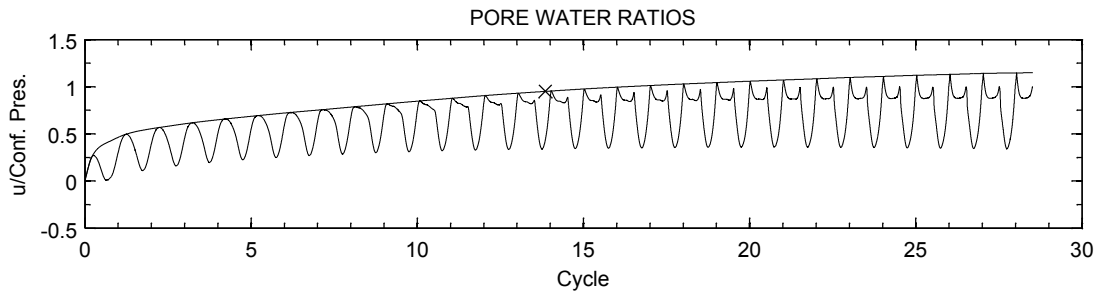
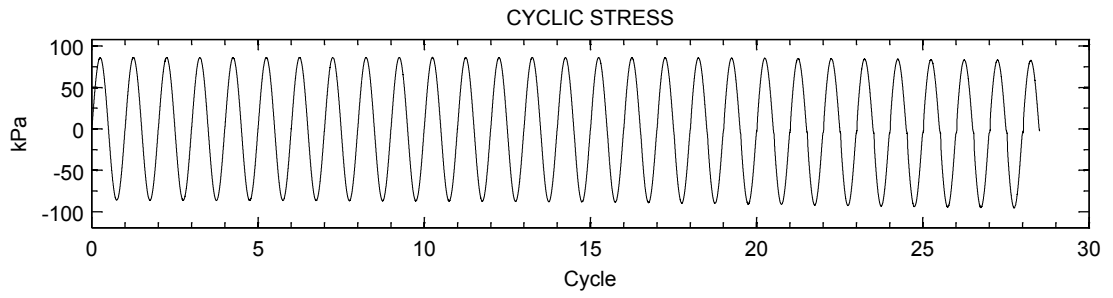
Mica Content (%) :	10.0
Non-Plastic Fines Content (%) :	0.0
Relative Density (%) :	80.5
Cyclic Stress Ratio :	0.355
Effective Conf. Press (kPa) :	100.0



SAMPLE PROPERTIES

MC:10-A2

Mica Content (%) :	10.0
Non-Plastic Fines Content (%) :	0.0
Relative Density (%) :	79.00
Cyclic Stress Ratio :	0.3924
Effective Conf. Press (kPa) :	99.4

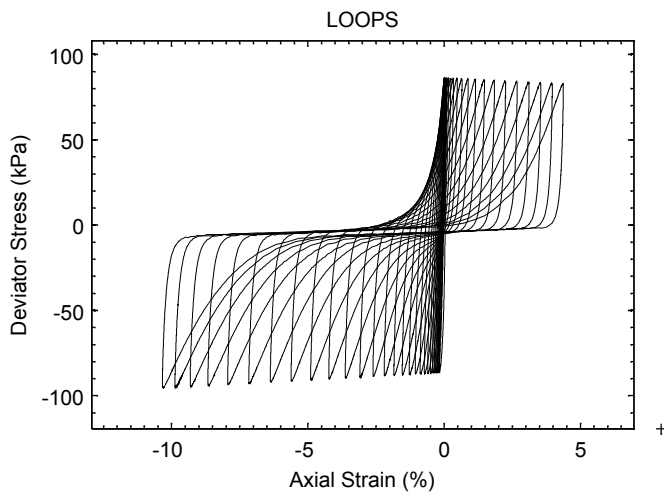


SAMPLE PROPERTIES: MC:10-A3

Mica Content (%): 10

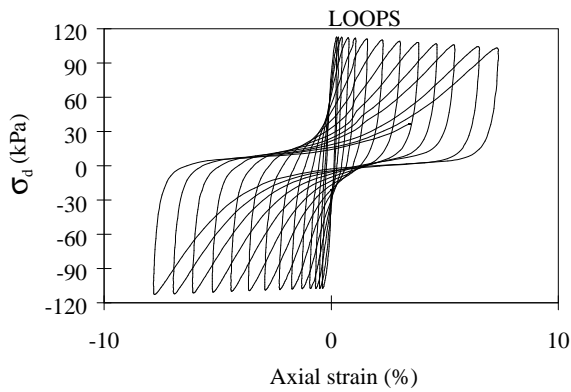
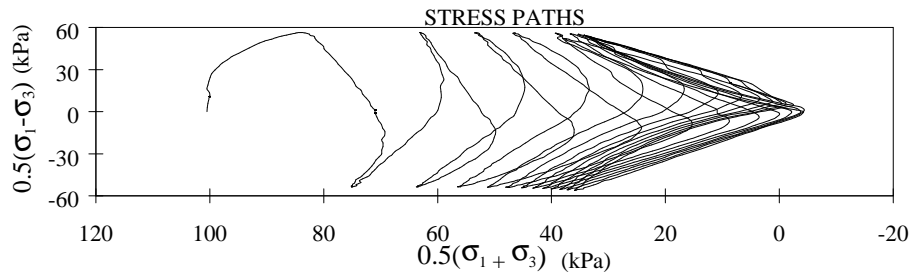
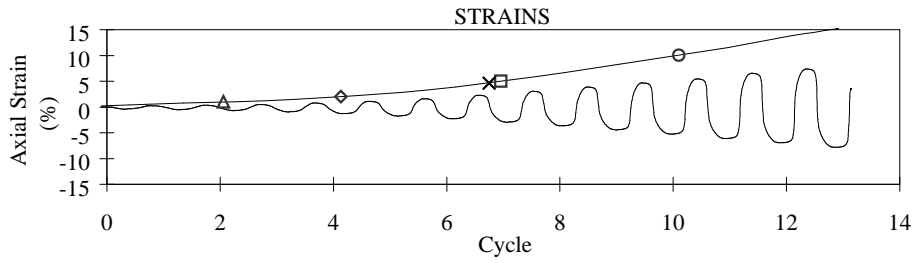
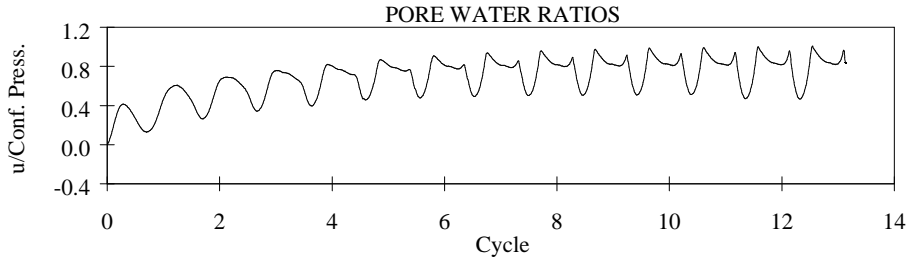
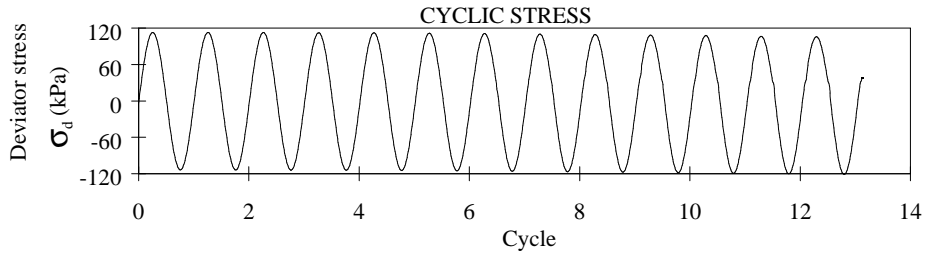
Non-Plastic Fines Content (%): 0

Relative Density (%): 78.8

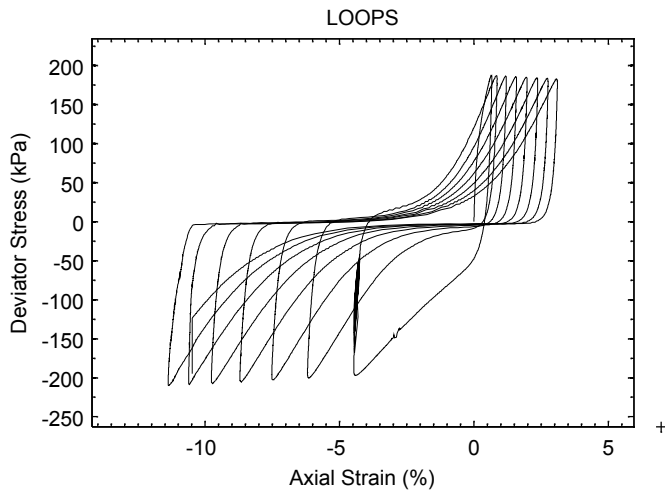
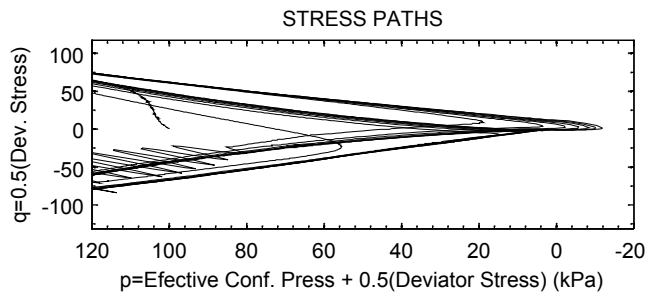
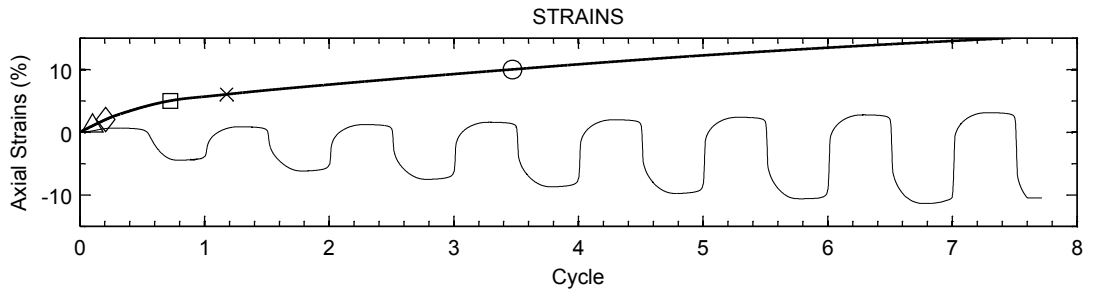
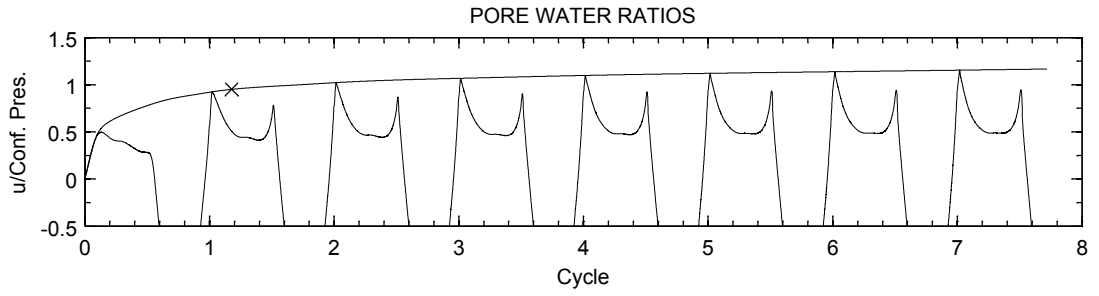
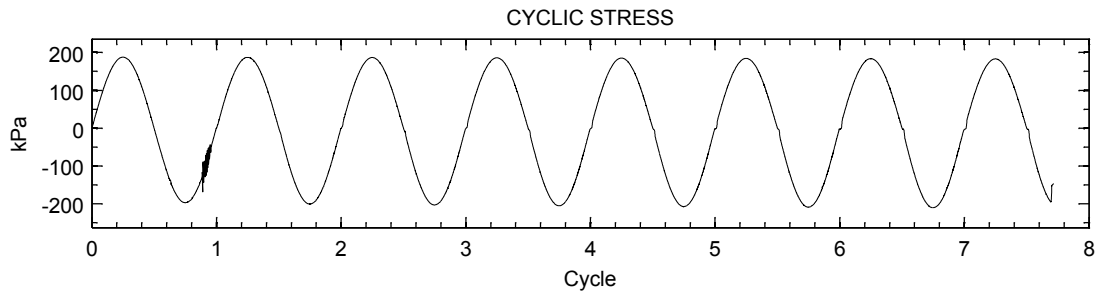


Cyclic Stress Ratio: 0.427

Effective Conf. Press (kPa): 100.9



SAMPLE PROPERTIES		MC10
Mica Content (%) :		10.0
Non-Plastic Fines Content (%) :		0.0
Relative Density (%) :		79.00
Cyclic Stress Ratio :		0.5635
Effective Conf. Press (kPa) :		100.1



SAMPLE PROPERTIES: MC:10-A5

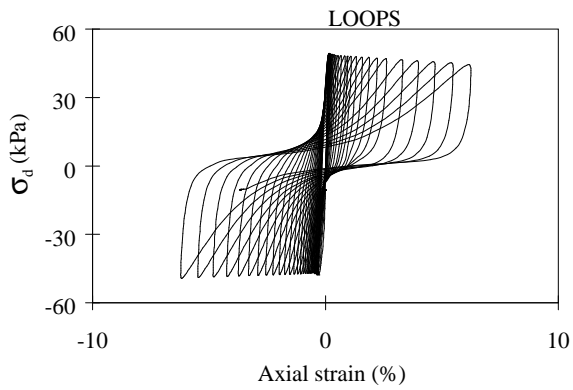
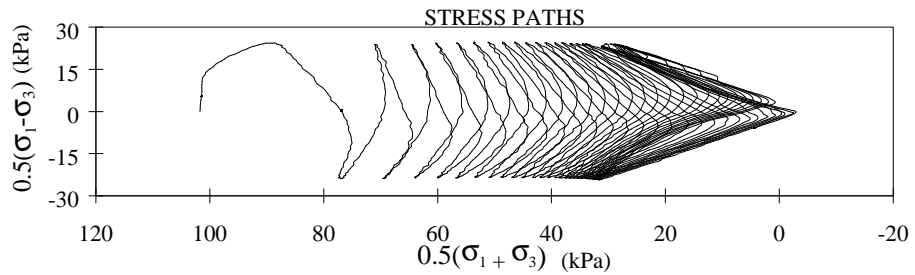
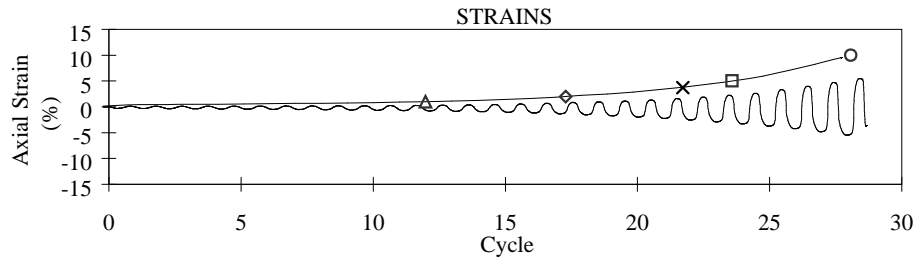
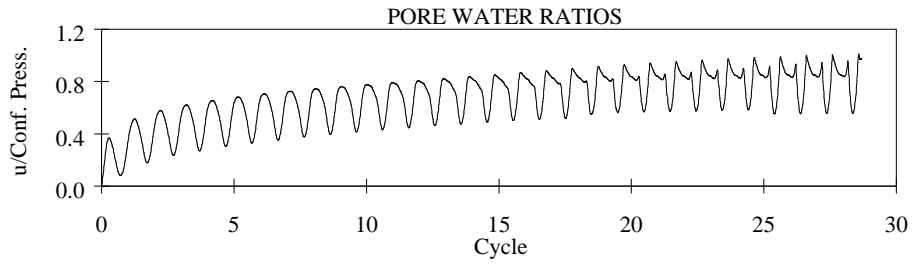
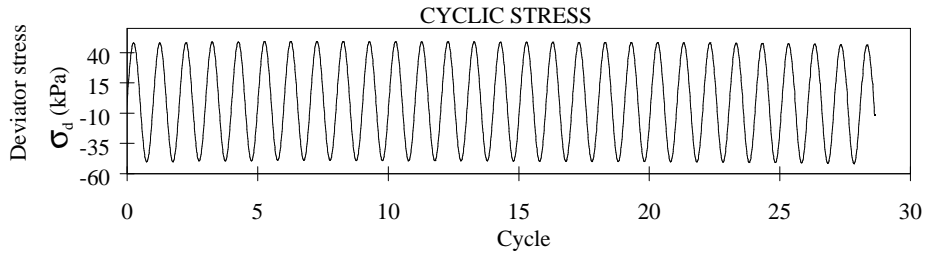
Mica Content (%): 10

Non-Plastic Fines Content (%): 0

Relative Density (%): 79.3

Cyclic Stress Ratio: 0.936

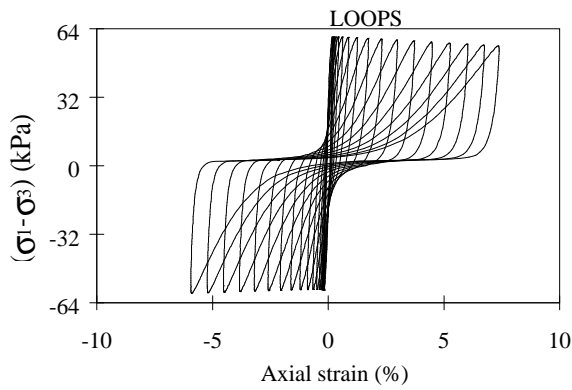
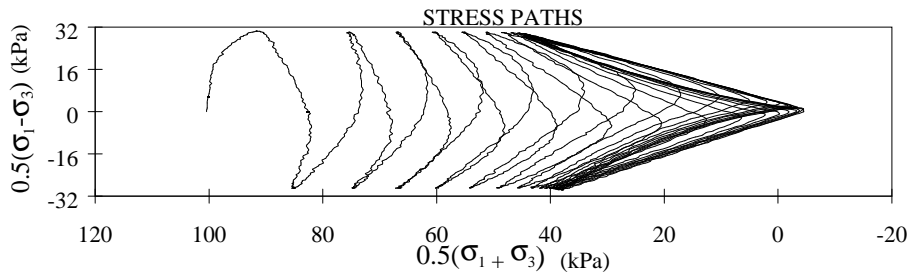
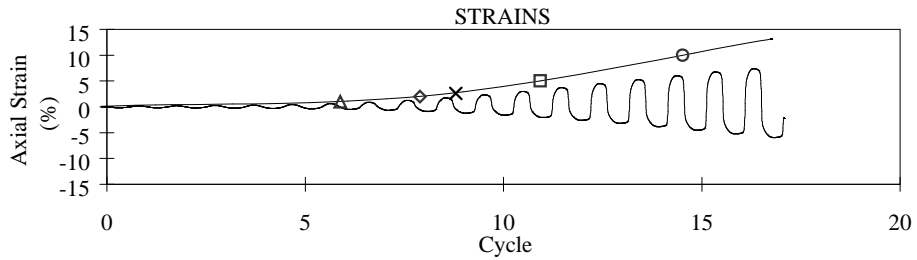
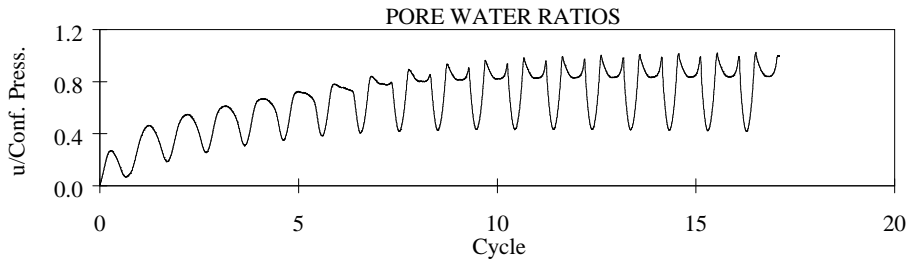
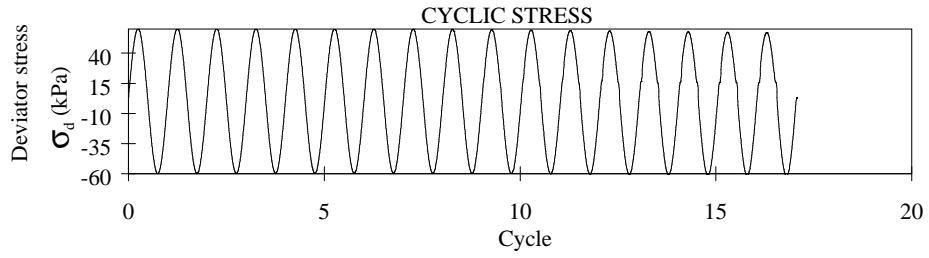
Efective Conf. Press (kPa): 100.7



SAMPLE PROPERTIES

MC:10-B1

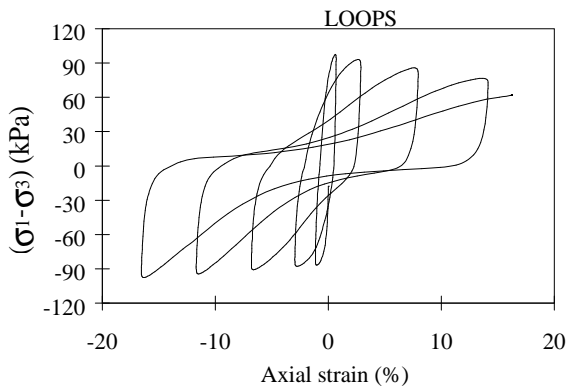
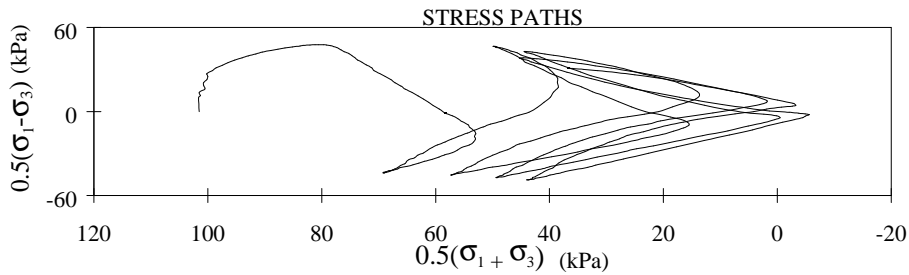
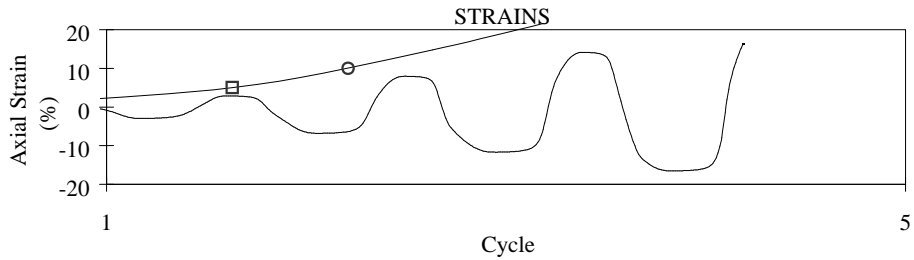
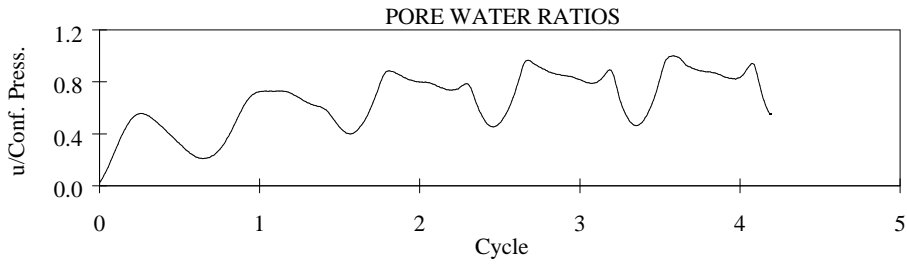
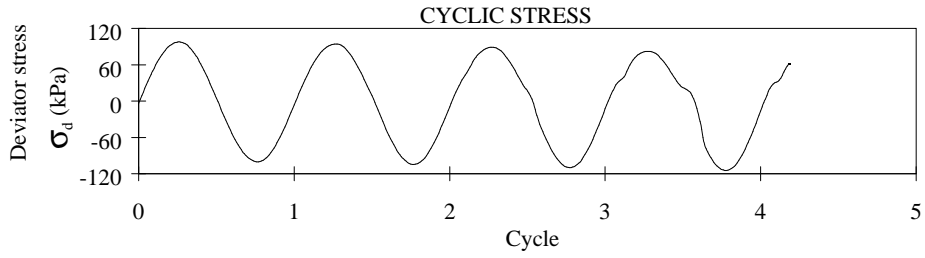
Mica Content (%) :	10.0
Non-Plastic Fines Content (%) :	0.0
Relative Density (%) :	65.00
Cyclic Stress Ratio :	0.2458
Effective Conf. Press (kPa) :	100.2



SAMPLE PROPERTIES

MC:10-B2

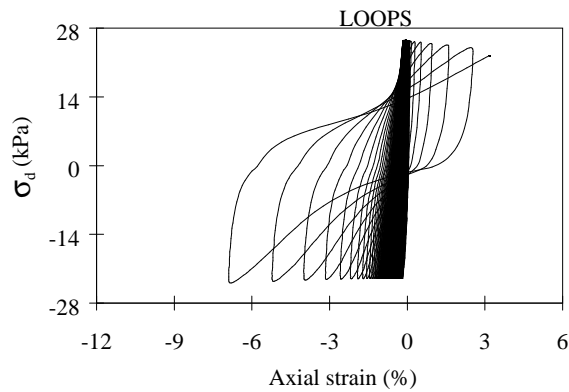
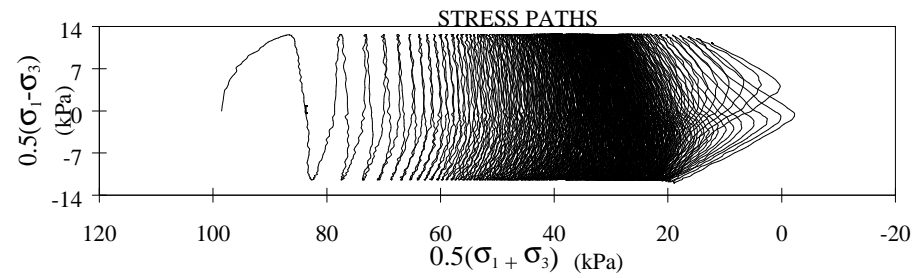
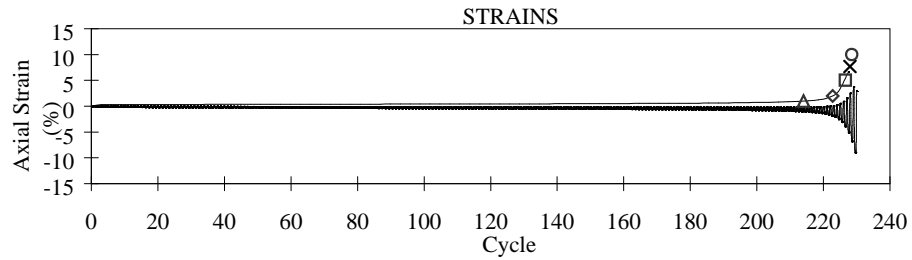
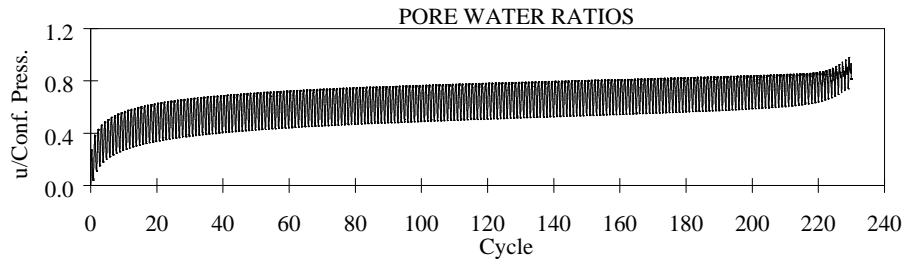
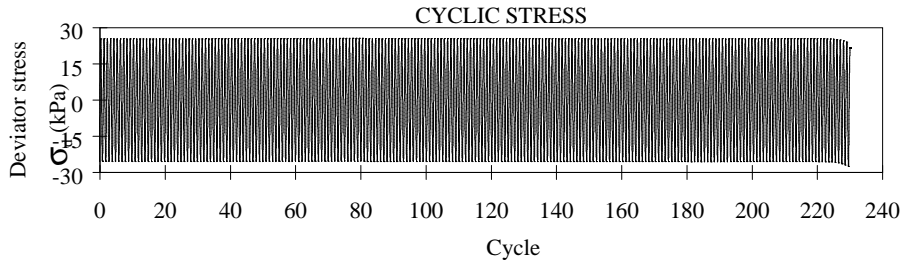
Mica Content (%) :	10.0
Non-Plastic Fines Content (%) :	0.0
Relative Density (%) :	64.0
Cyclic Stress Ratio :	0.301
Efective Conf. Press (kPa) :	100.0



SAMPLE PROPERTIES

MC:10-B3

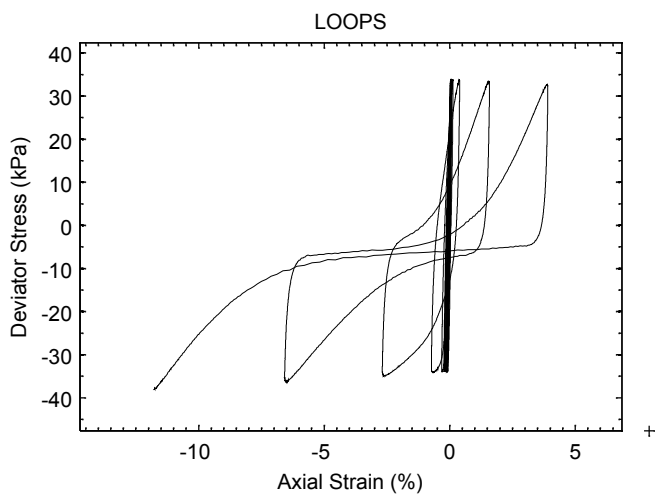
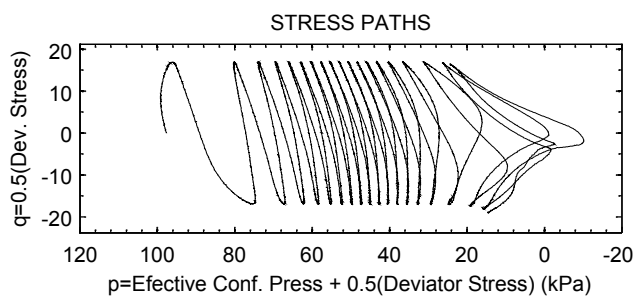
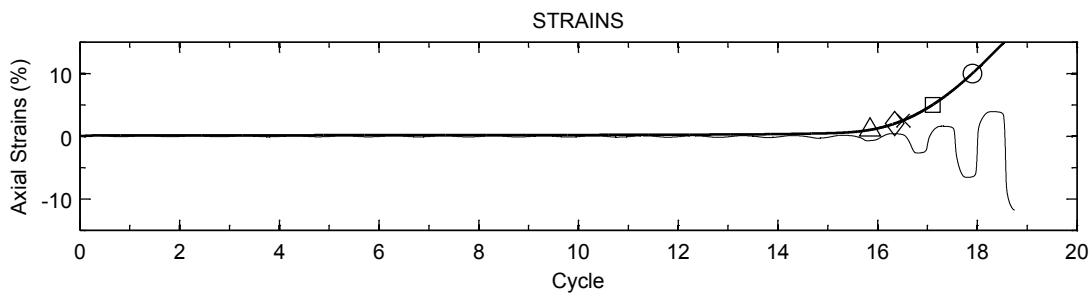
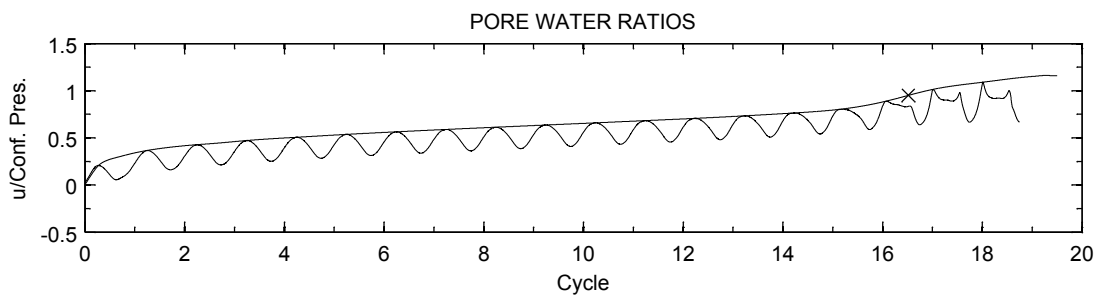
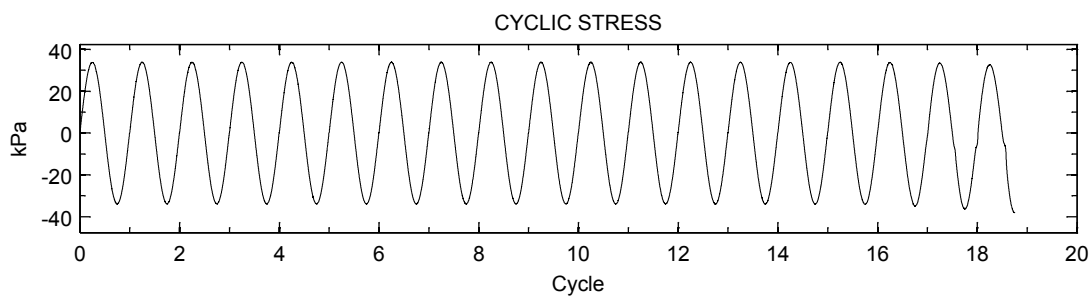
Mica Content (%) :	10.0
Non-Plastic Fines Content (%) :	0.0
Relative Density (%) :	63.0
Cyclic Stress Ratio :	0.490
Effective Conf. Press (kPa) :	99.6



SAMPLE PROPERTIES

MC:10-C1

Mica Content (%) :	10.0
Non-Plastic Fines Content (%) :	0.0
Relative Density (%) :	46.10
Cyclic Stress Ratio :	0.1281
Effective Conf. Press (kPa) :	99.9



+

SAMPLE PROPERTIES: MC:10-C2

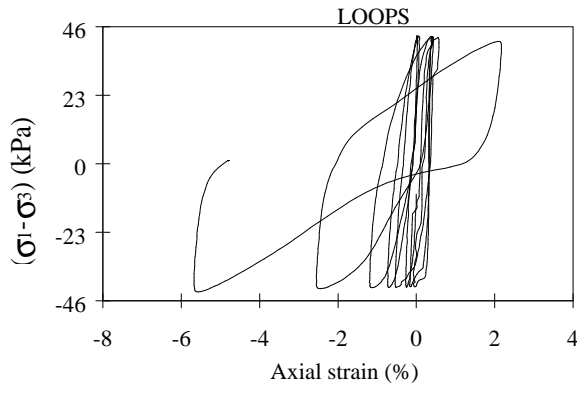
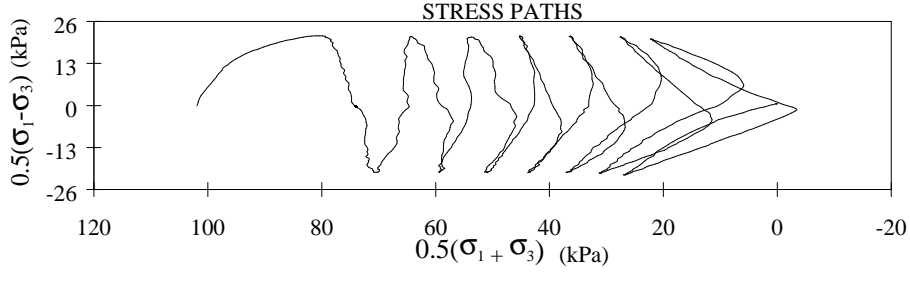
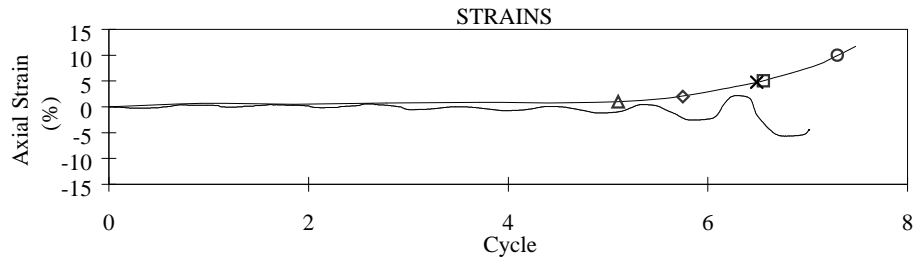
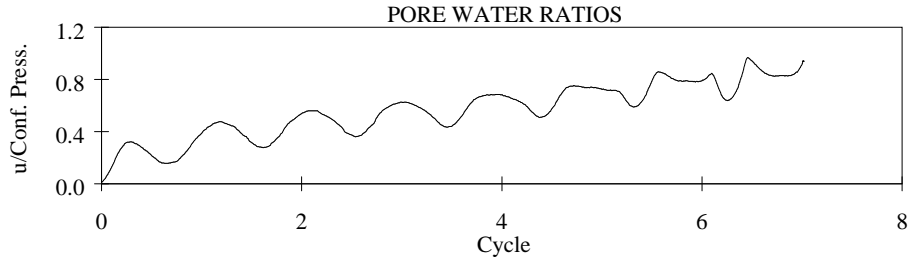
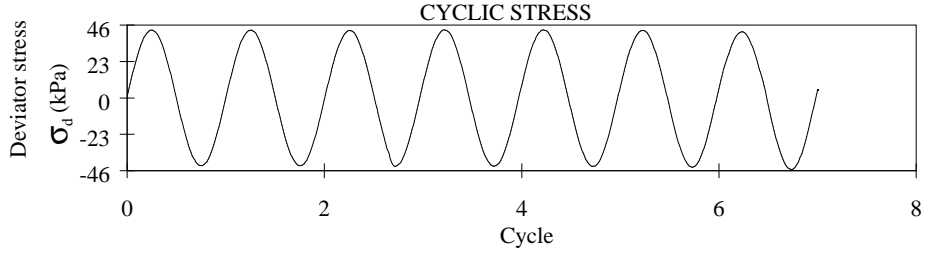
Mica Content (%): 10

Non-Plastic Fines Content (%): 0

Relative Density (%): 47

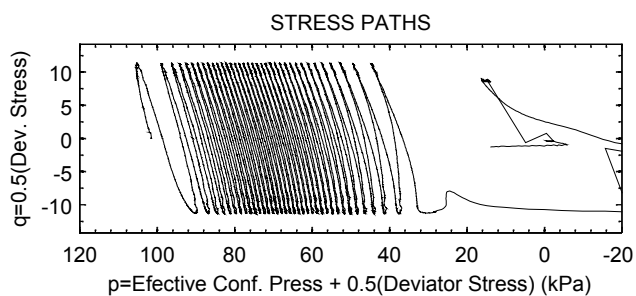
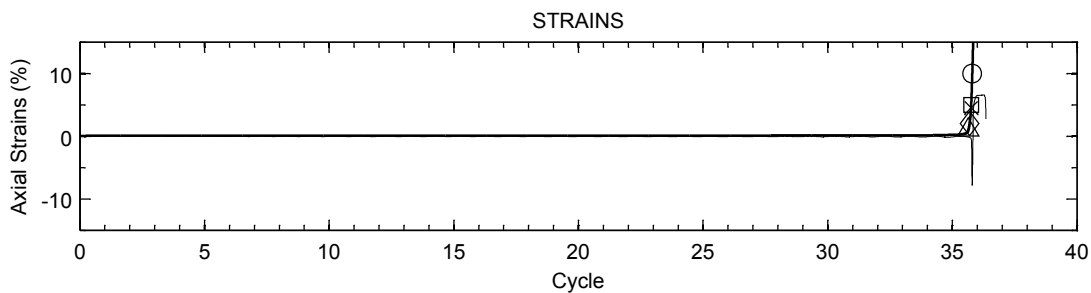
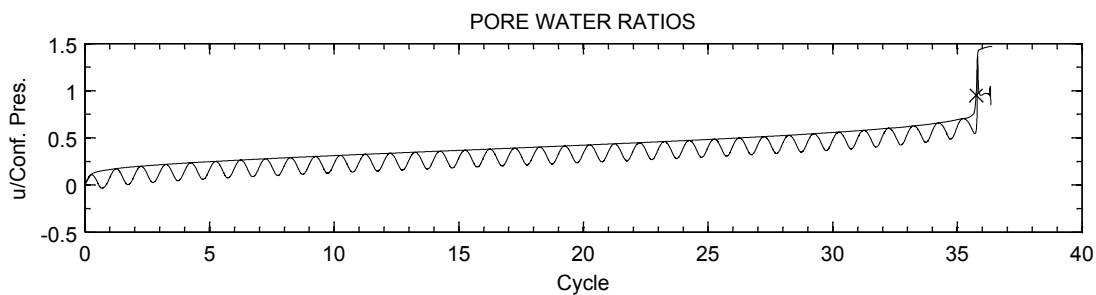
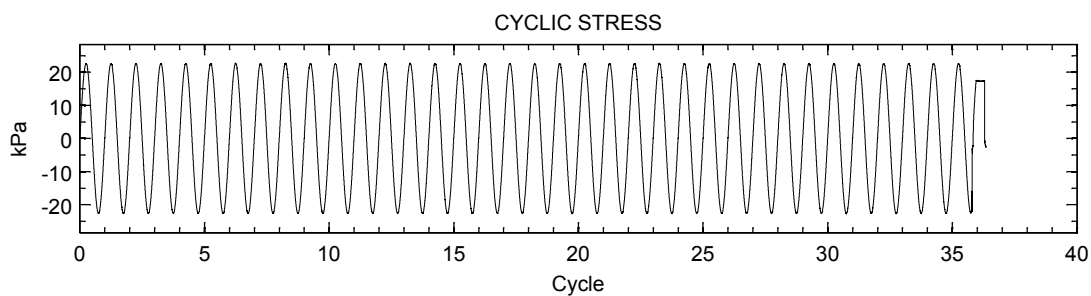
Cyclic Stress Ratio: 0.1691

Effective Conf. Press (kPa): 100.1



SAMPLE PROPERTIES MC:10-C3

Mica Content (%) :	10.0
Non-Plastic Fines Content (%) :	0.0
Relative Density (%) :	48.0
Cyclic Stress Ratio :	0.216
Effective Conf. Press (kPa) :	99.7

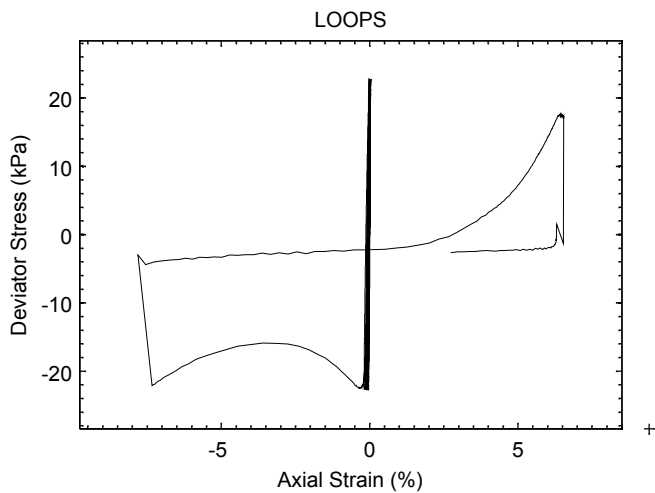


SAMPLE PROPERTIES: MC:10-D1

Mica Content (%): 10

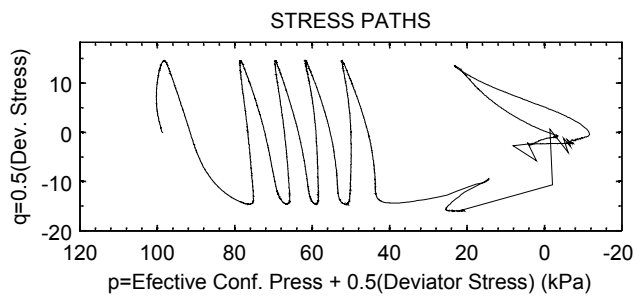
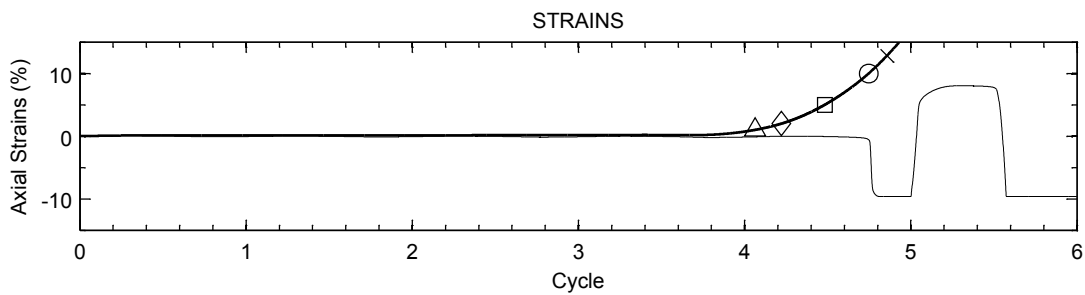
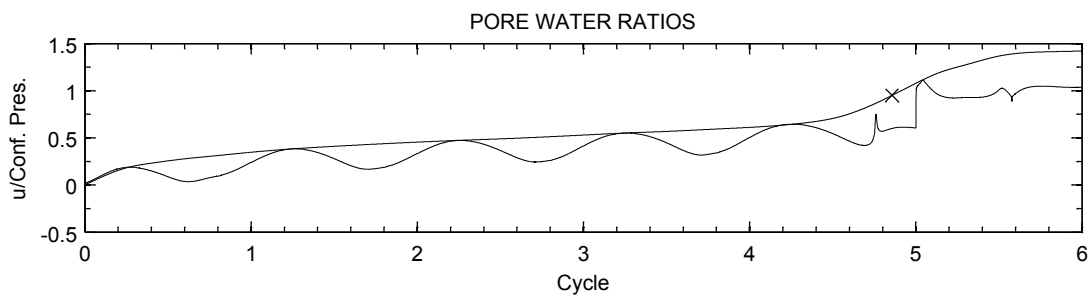
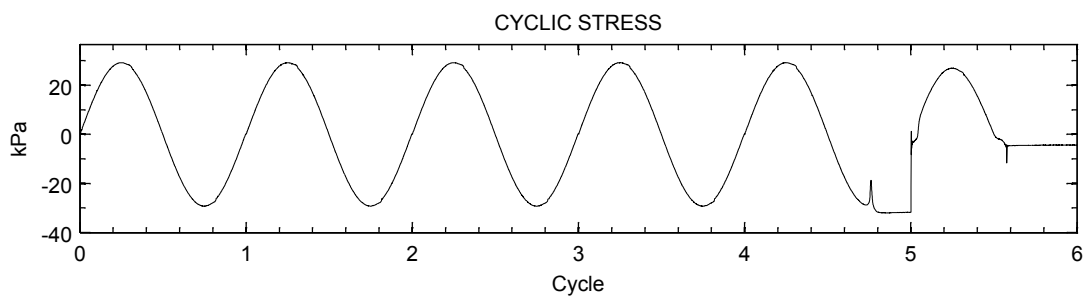
Non-Plastic Fines Content (%): 0

Relative Density (%): 33



Cyclic Stress Ratio: 0.1138

Efective Conf. Press (kPa): 101.9

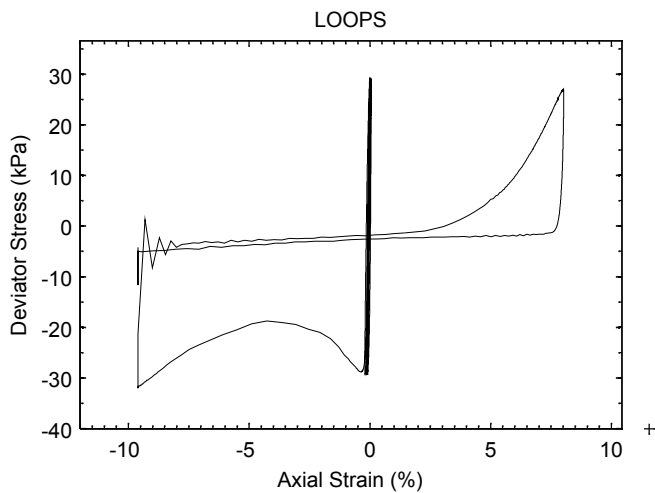


SAMPLE PROPERTIES: MC:10-D2

Mica Content (%): 10

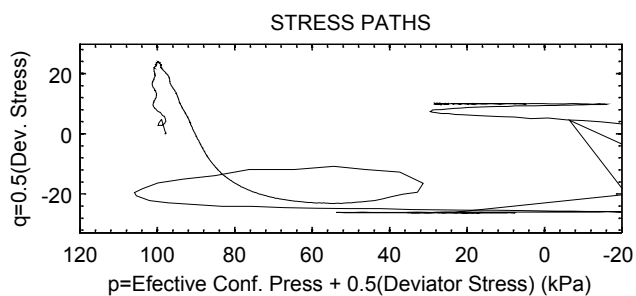
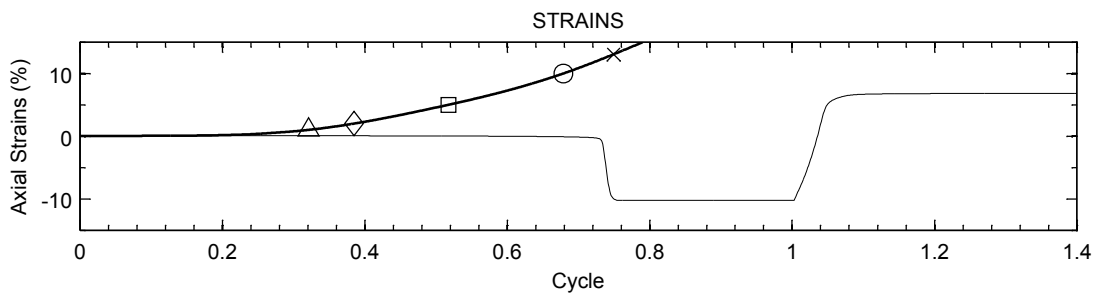
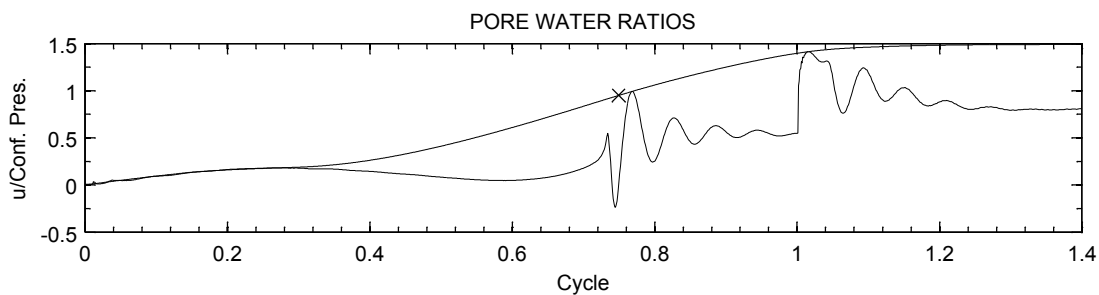
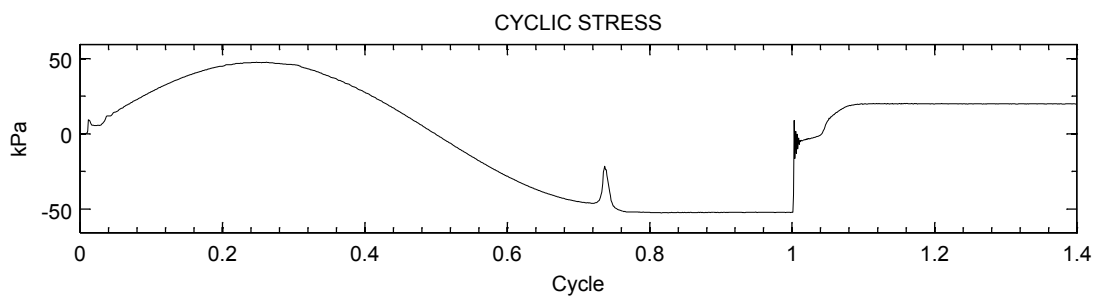
Non-Plastic Fines Content (%): 0

Relative Density (%): 33



Cyclic Stress Ratio: 0.1447

Effective Conf. Press (kPa): 100.4

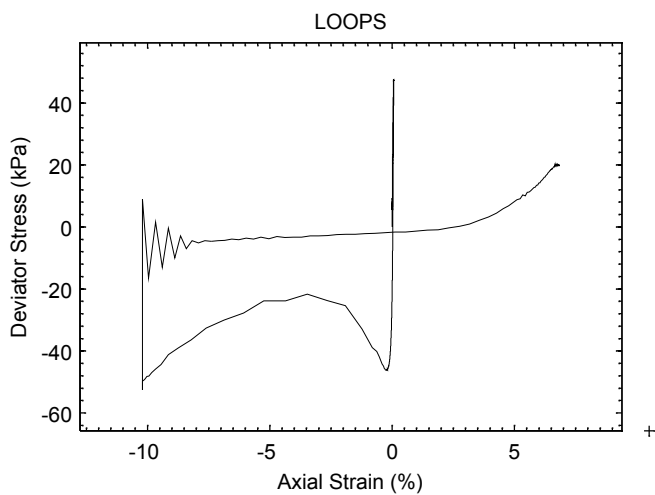


SAMPLE PROPERTIES: MC:10-D3

Mica Content (%): 10

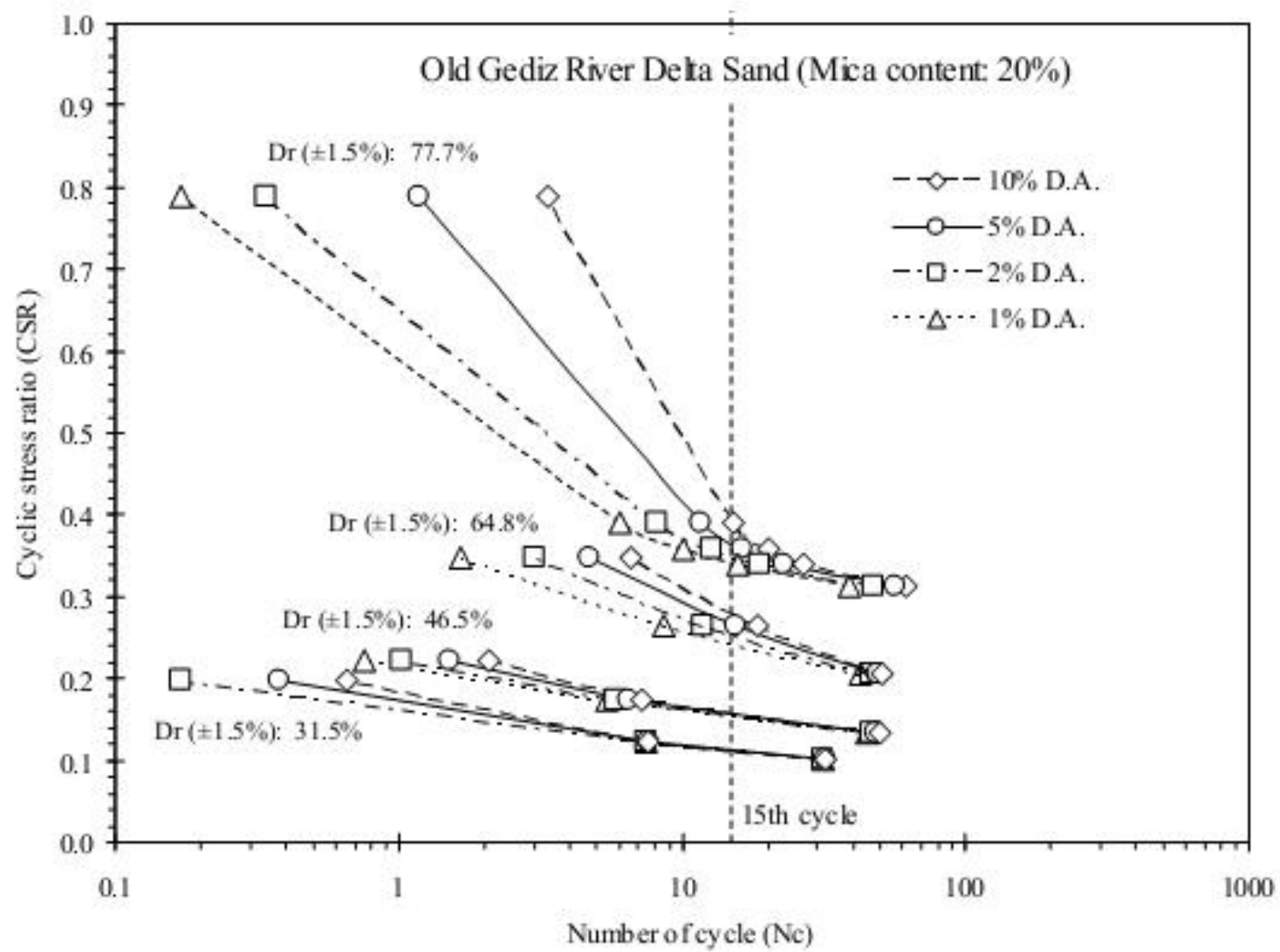
Non-Plastic Fines Content (%): 0

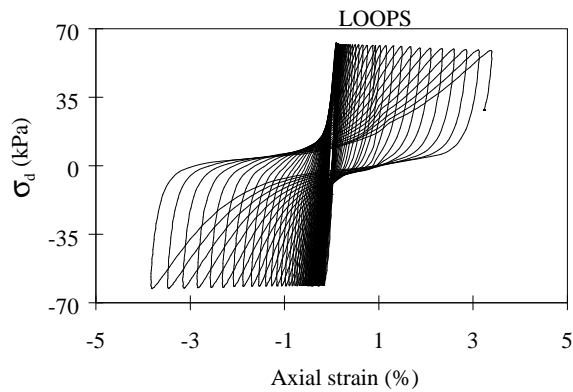
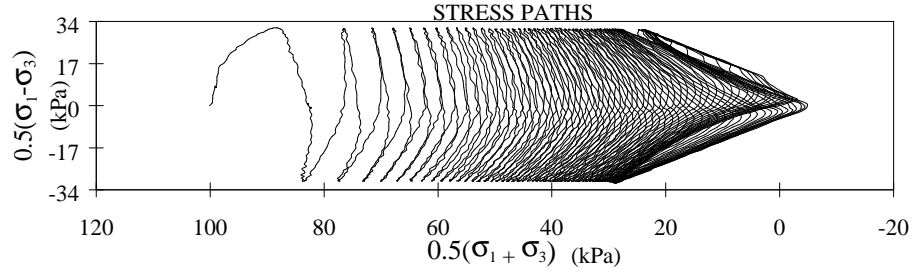
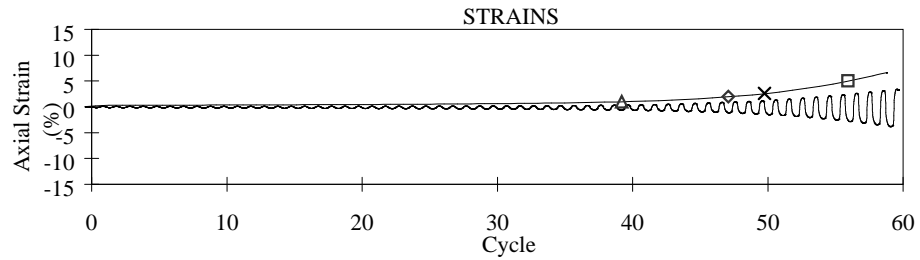
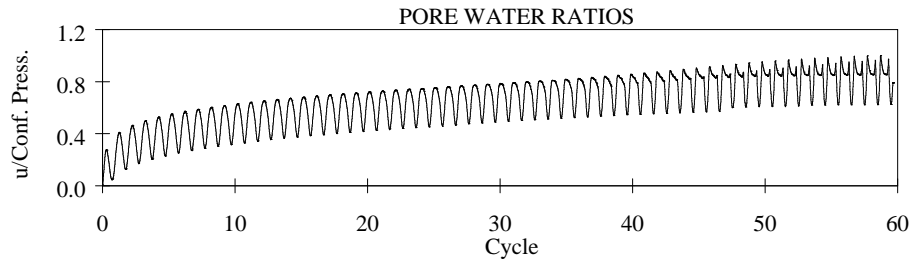
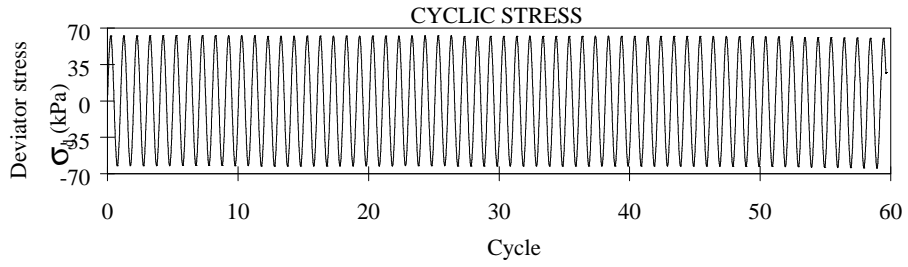
Relative Density (%): 32



Cyclic Stress Ratio: 0.24

Effective Conf. Press (kPa): 98.5

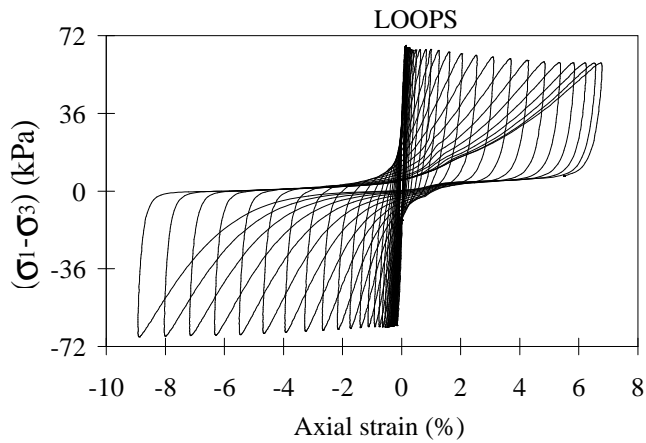
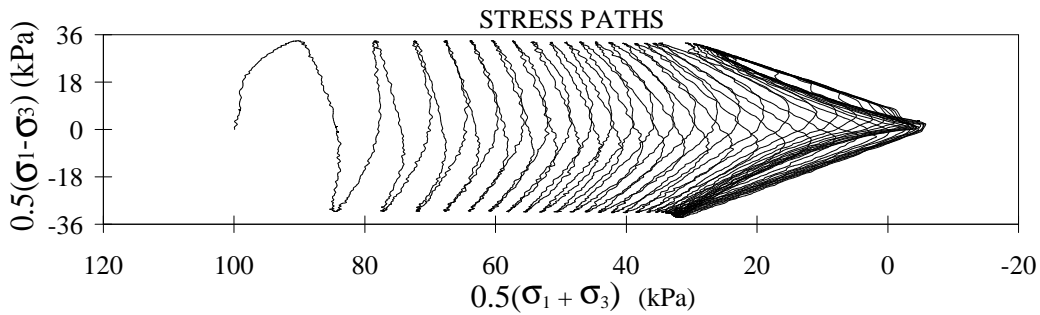
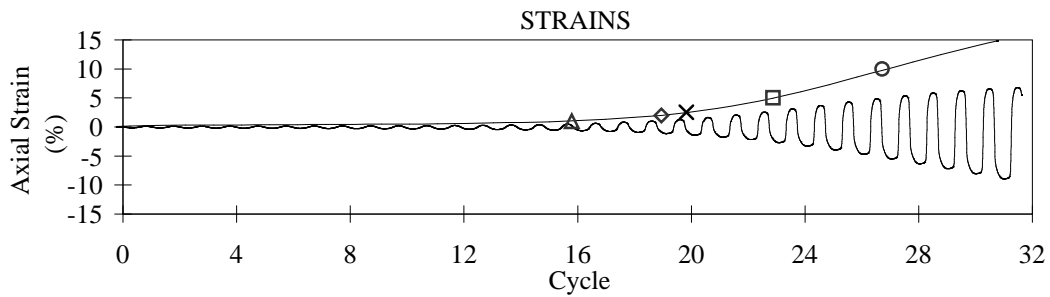
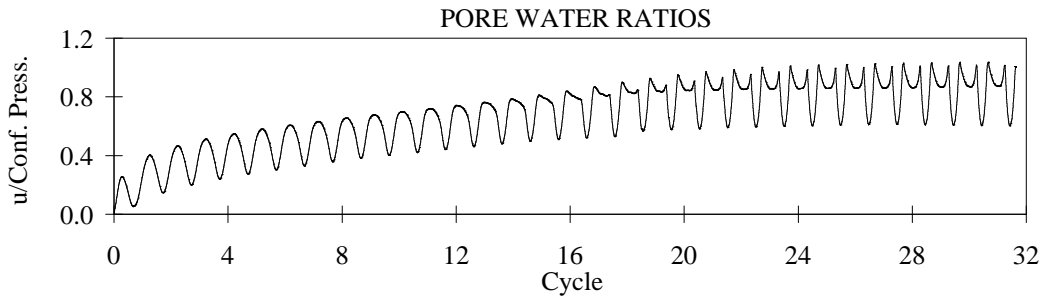
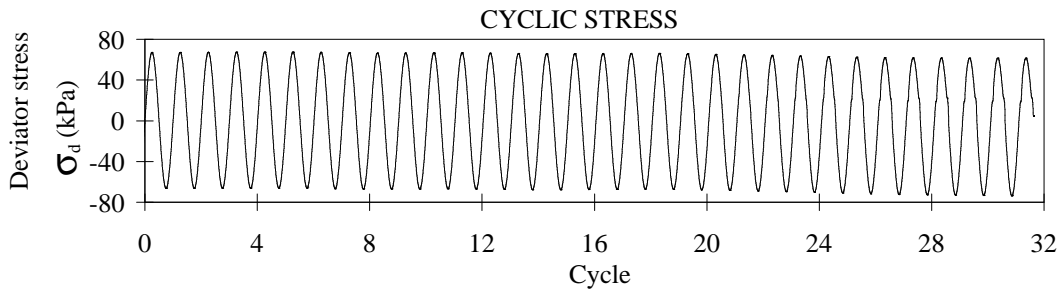




SAMPLE PROPERTIES

MC:20-A1

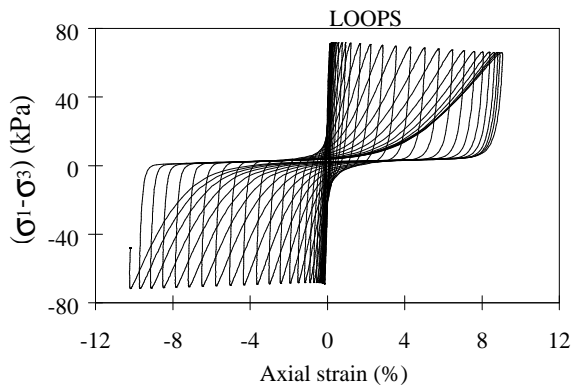
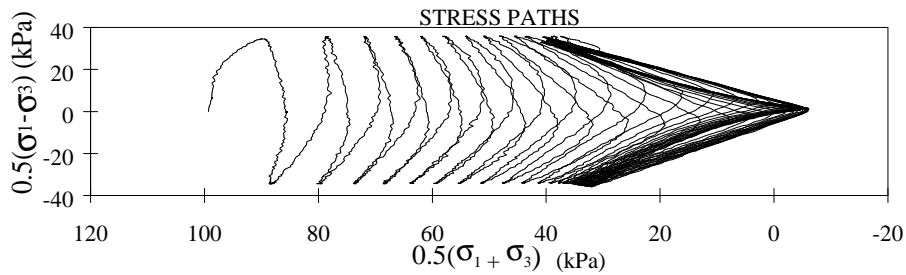
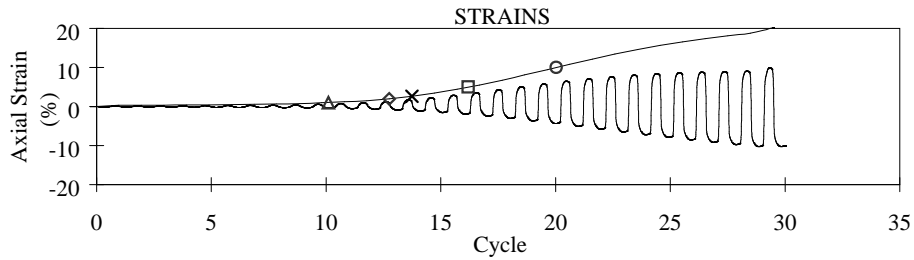
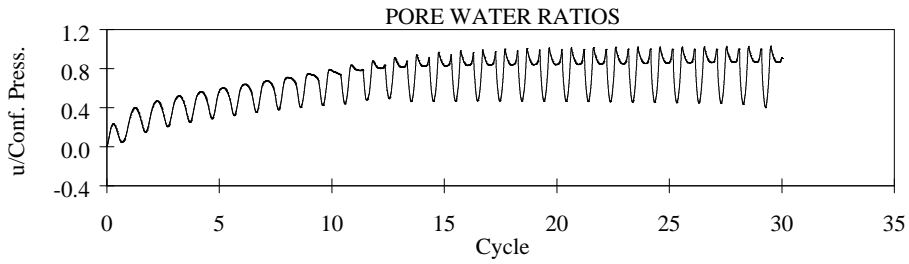
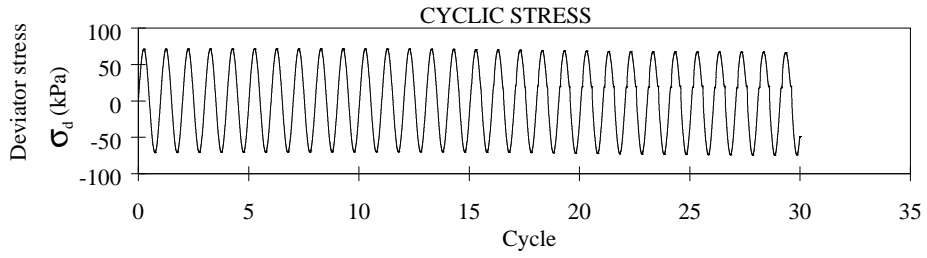
Mica Content (%) :	20.0
Non-Plastic Fines Content (%) :	0.0
Relative Density (%) :	77.80
Cyclic Stress Ratio :	0.3137
Efective Conf. Press (kPa) :	100.1



SAMPLE PROPERTIES

MC:20-A2

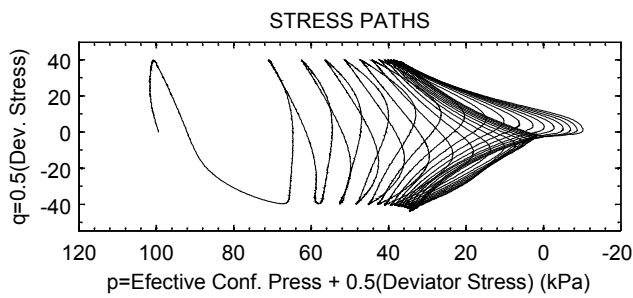
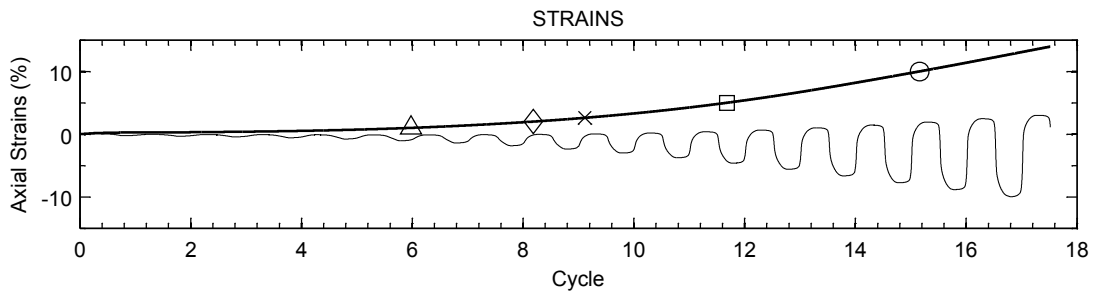
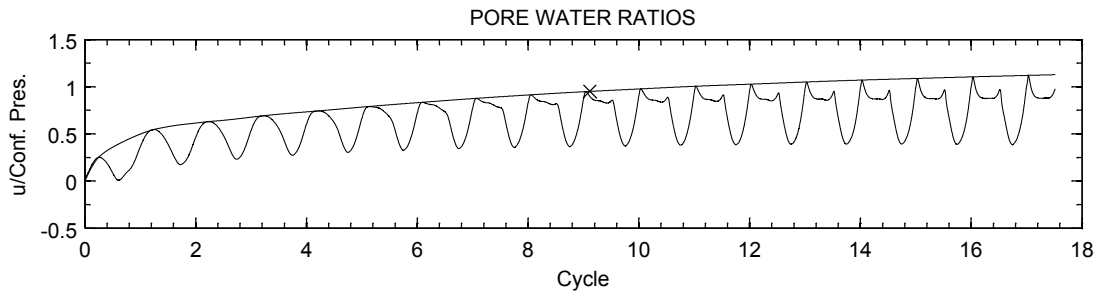
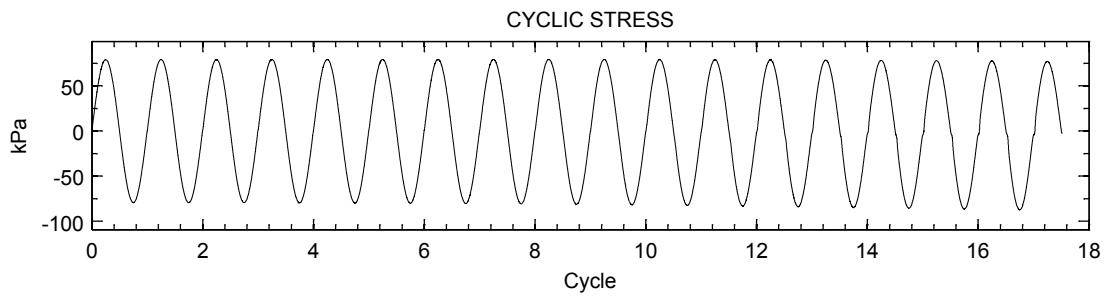
Mica Content (%) :	20.0
Non-Plastic Fines Content (%) :	0.0
Relative Density (%) :	76.9
Cyclic Stress Ratio :	0.338
Effective Conf. Press (kPa) :	99.6



SAMPLE PROPERTIES

MC:20-A3

Mica Content (%) :	20.0
Non-Plastic Fines Content (%) :	0.0
Relative Density (%) :	78.0
Cyclic Stress Ratio :	0.359
Effective Conf. Press (kPa) :	100.0

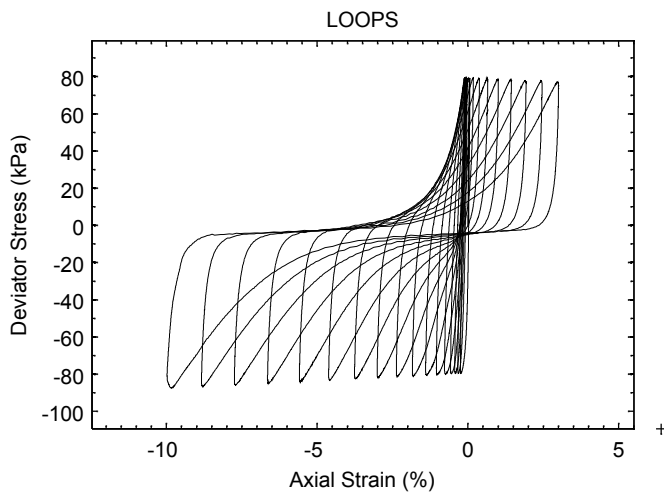


SAMPLE PROPERTIES: MC:20-A3

Mica Content (%): 20

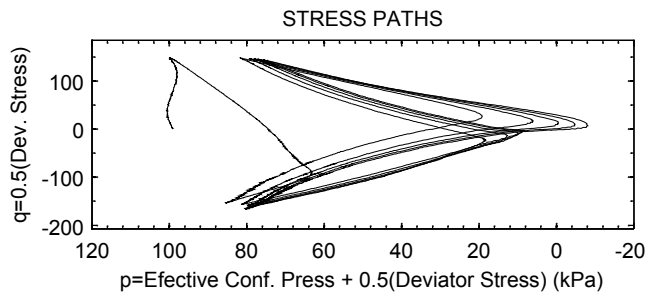
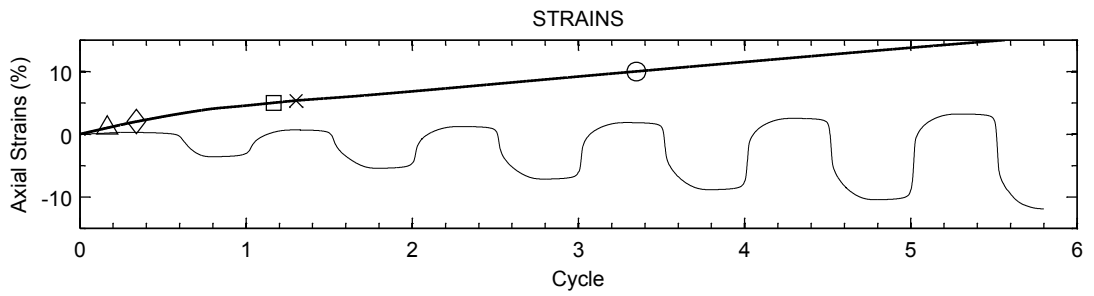
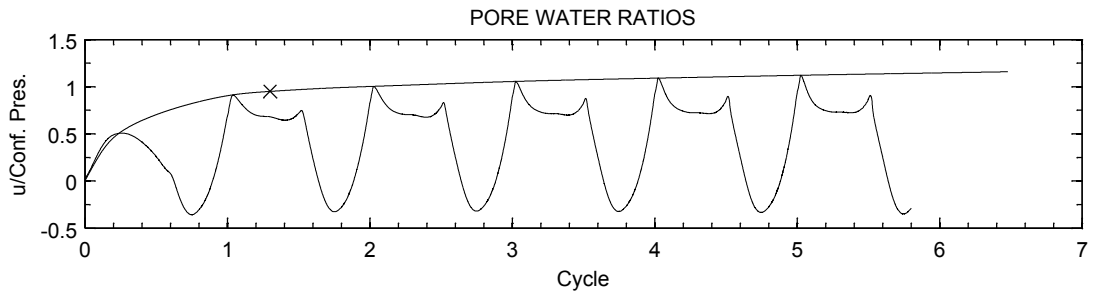
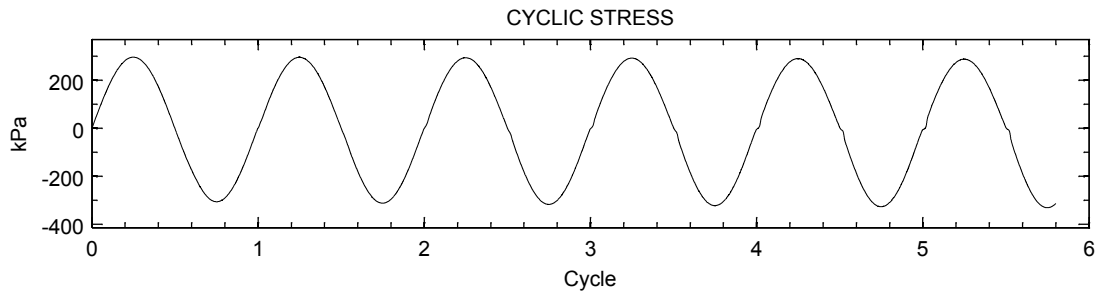
Non-Plastic Fines Content (%): 0

Relative Density (%): 77.8



Cyclic Stress Ratio: 0.391

Effective Conf. Press (kPa): 101

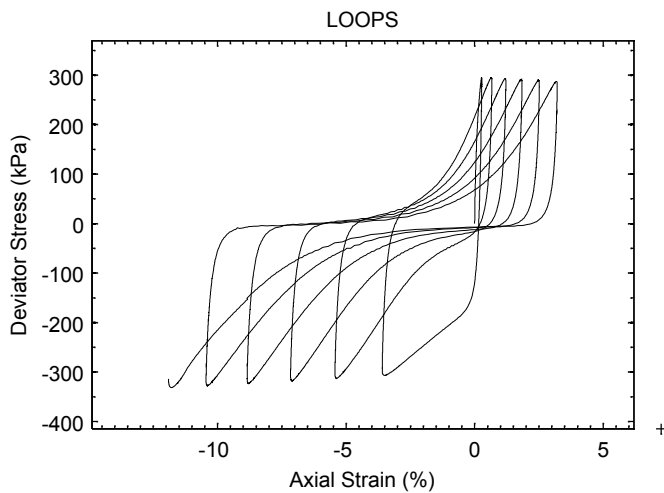


SAMPLE PROPERTIES: MC:49-A4

Mica Content (%): 20

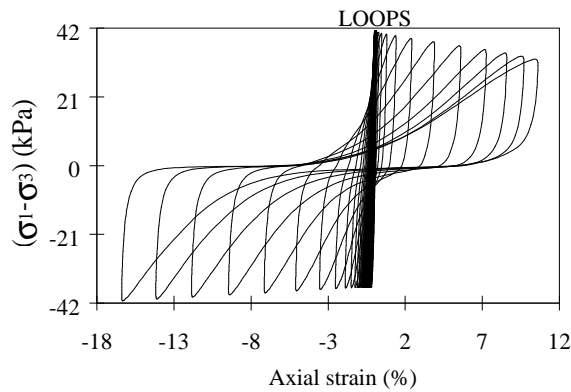
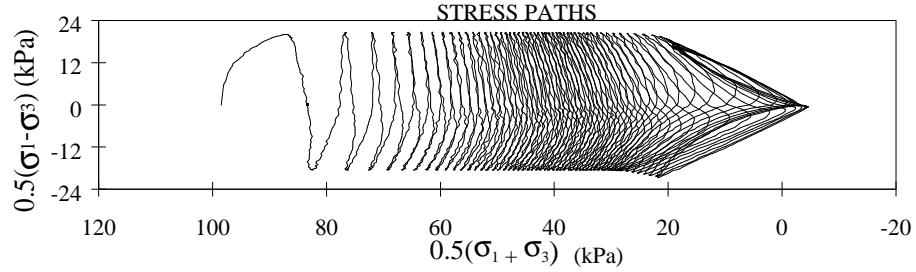
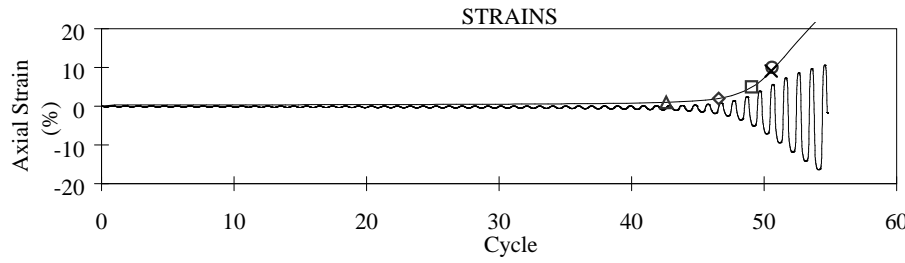
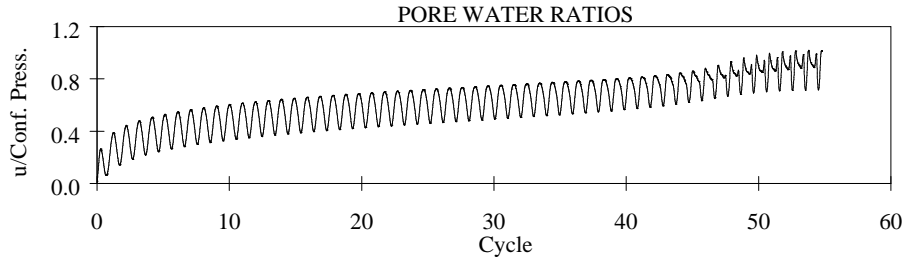
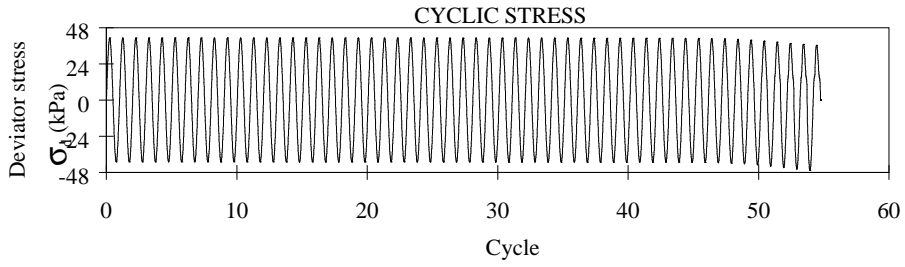
Non-Plastic Fines Content (%): 0

Relative Density (%): 78.2



Cyclic Stress Ratio: 0.79

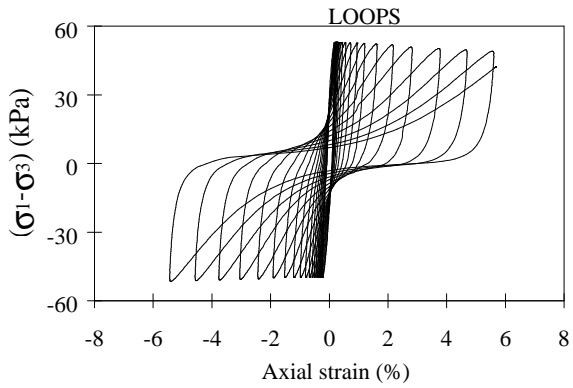
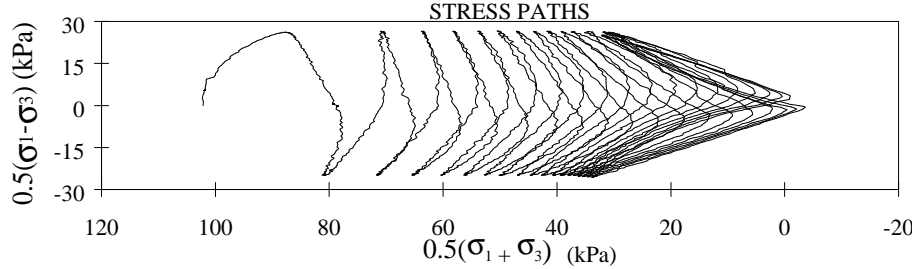
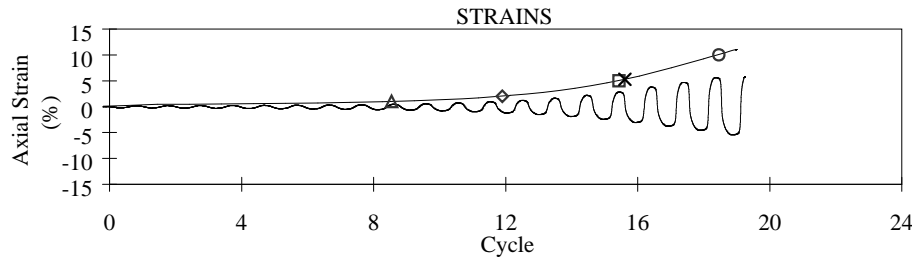
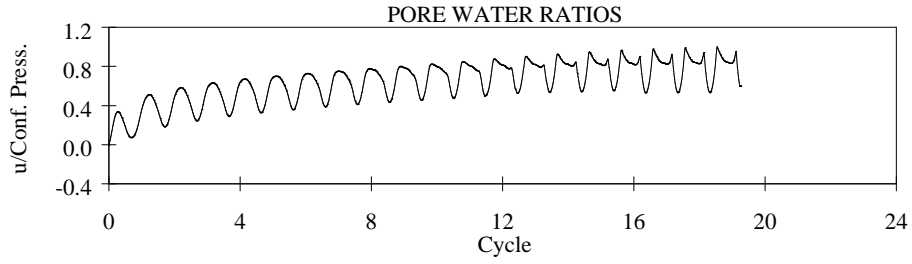
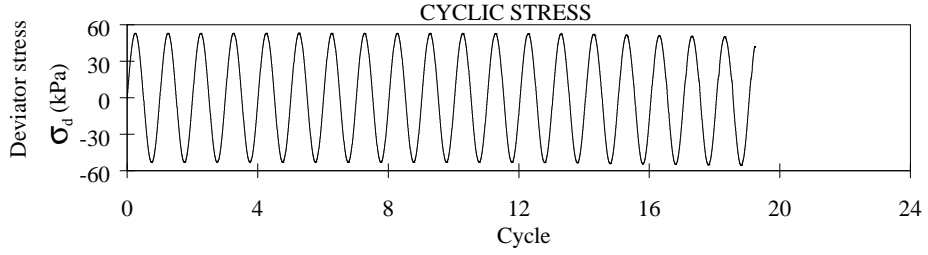
Effective Conf. Press (kPa): 101



SAMPLE PROPERTIES

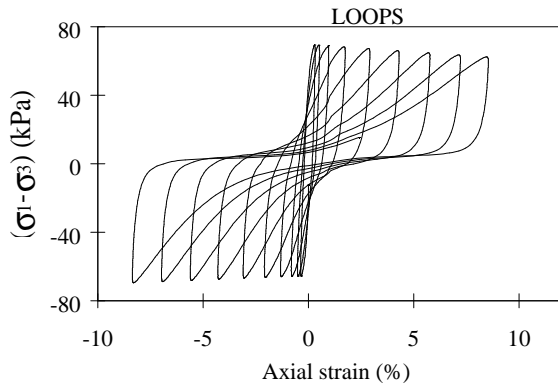
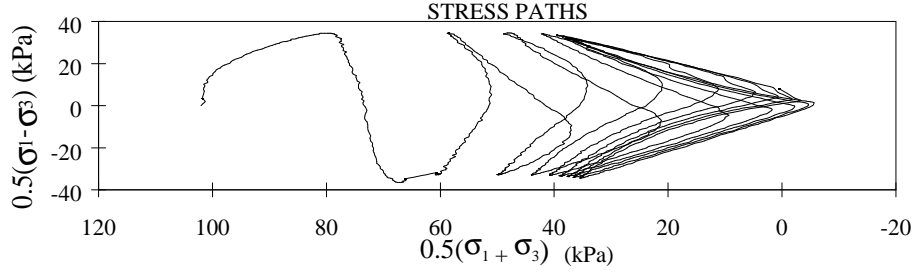
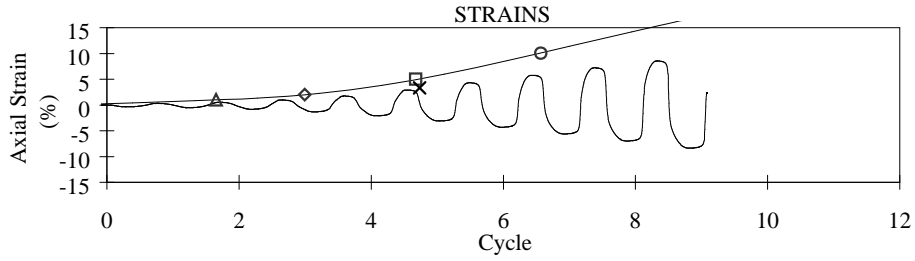
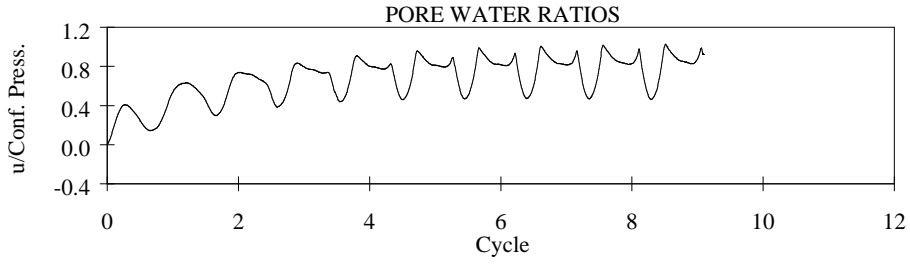
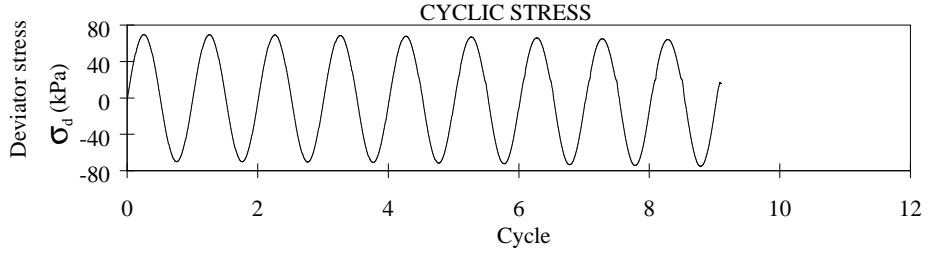
MC:20-B1

Mica Content (%) :	20.0
Non-Plastic Fines Content (%) :	0.0
Relative Density (%) :	65.3
Cyclic Stress Ratio :	0.207
Effective Conf. Press (kPa) :	99.8



SAMPLE PROPERTIES MC:20-B2

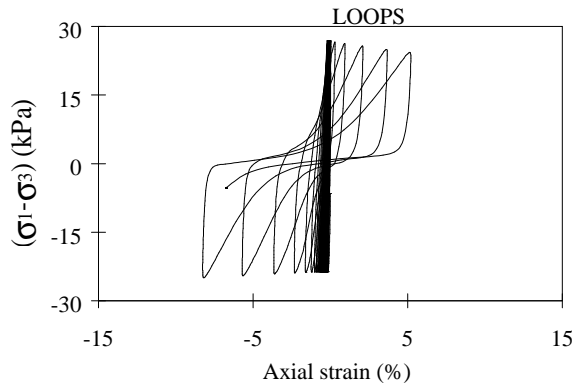
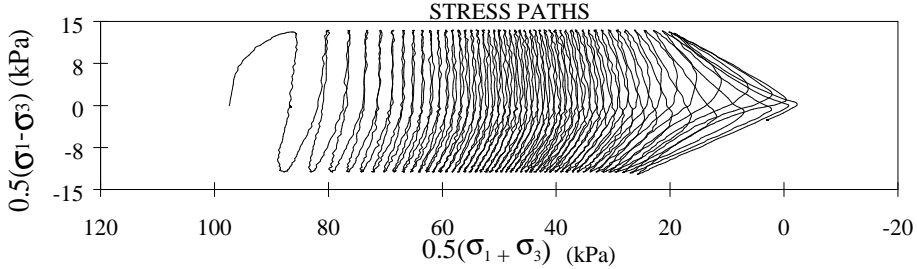
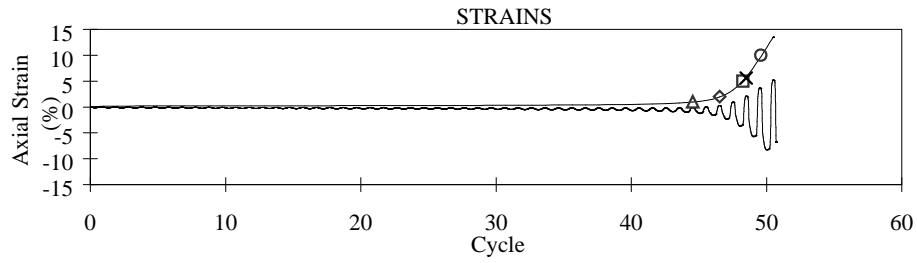
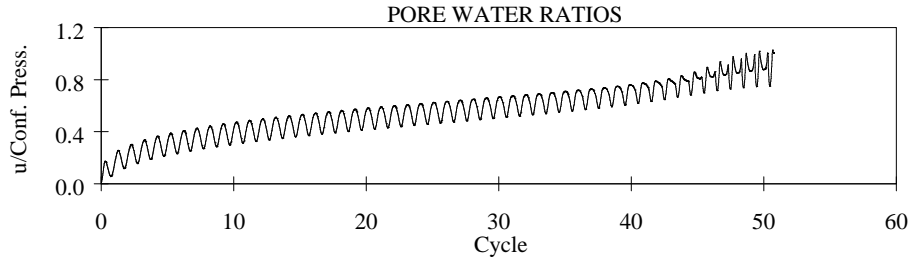
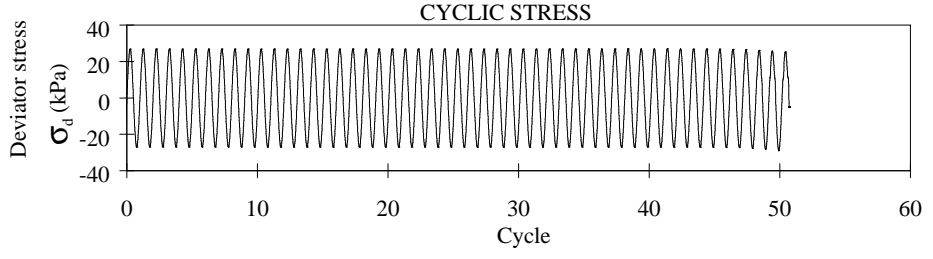
Mica Content (%) :	20.0
Non-Plastic Fines Content (%) :	0.0
Relative Density (%) :	64.3
Cyclic Stress Ratio :	0.265
Effective Conf. Press (kPa) :	100.1



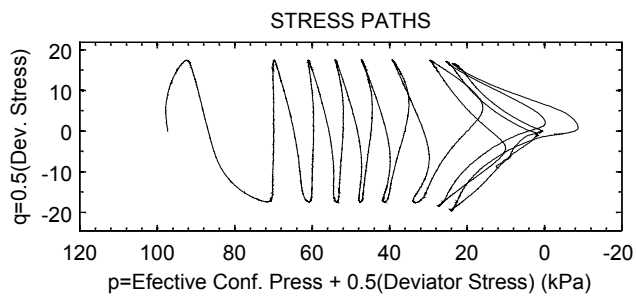
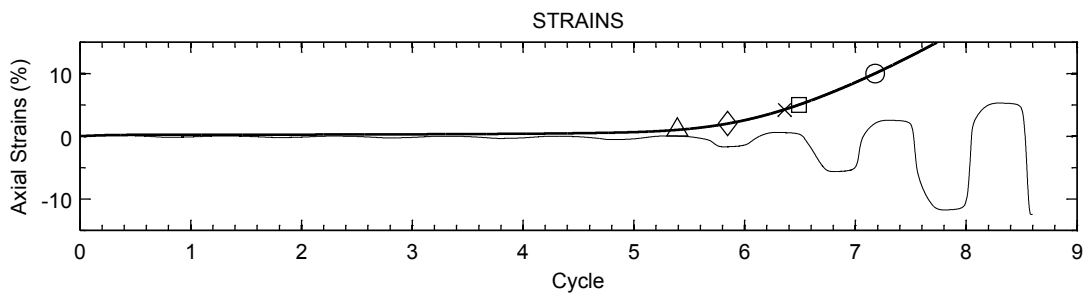
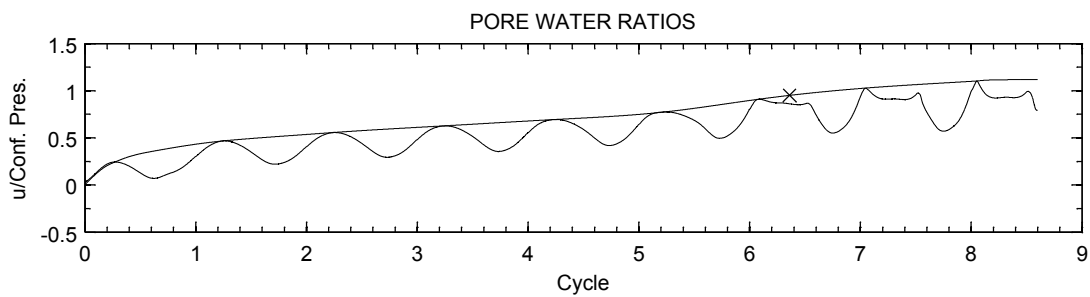
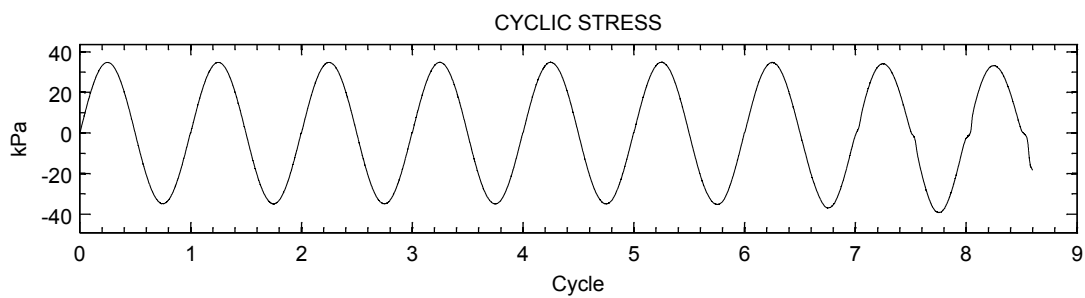
SAMPLE PROPERTIES

MC:20-B3

Mica Content (%) :	20.0
Non-Plastic Fines Content (%) :	0.0
Relative Density (%) :	64.8
Cyclic Stress Ratio :	0.348
Effective Conf. Press (kPa) :	99.7



SAMPLE PROPERTIES		MC:20-C1
Mica Content (%) :	20.0	
Non-Plastic Fines Content (%) :	0.0	
Relative Density (%) :	46.5	
Cyclic Stress Ratio :	0.135	
Effective Conf. Press (kPa) :	99.5	

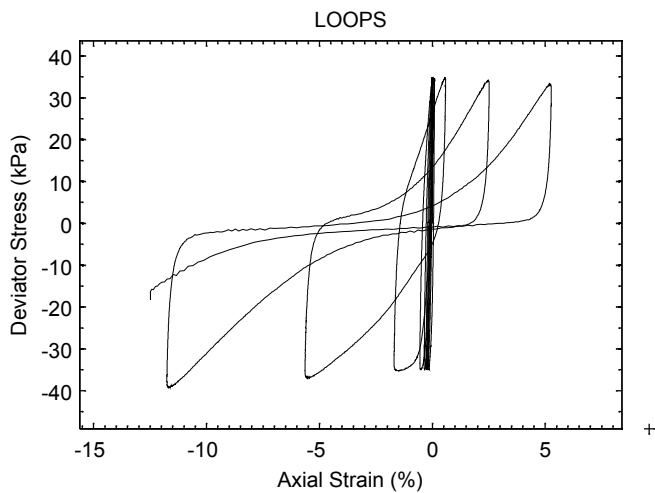


SAMPLE PROPERTIES: MC:20-C2

Mica Content (%): 20

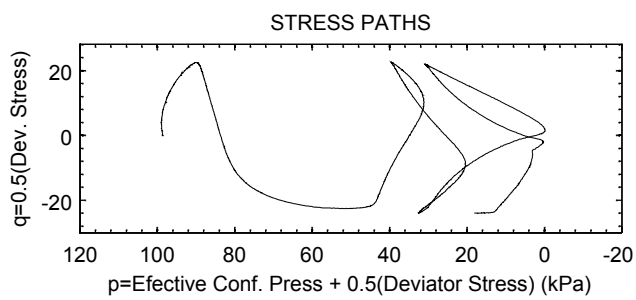
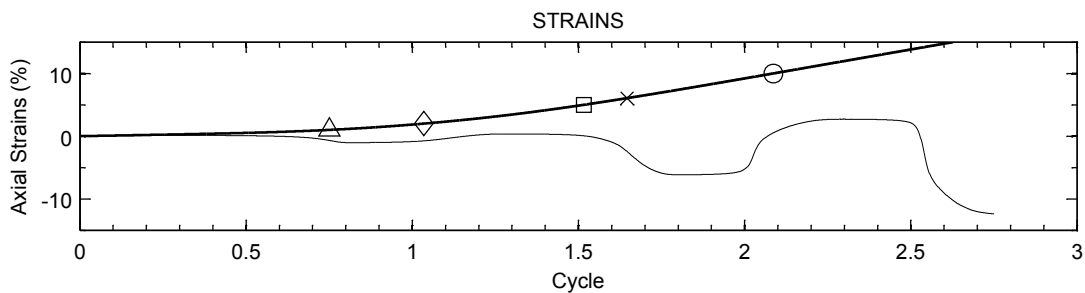
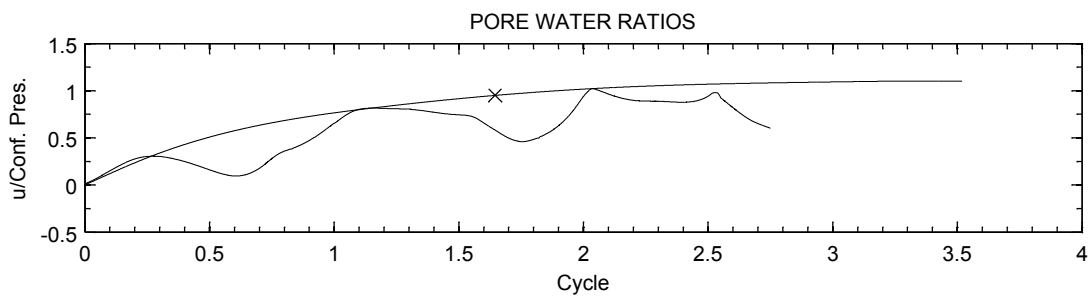
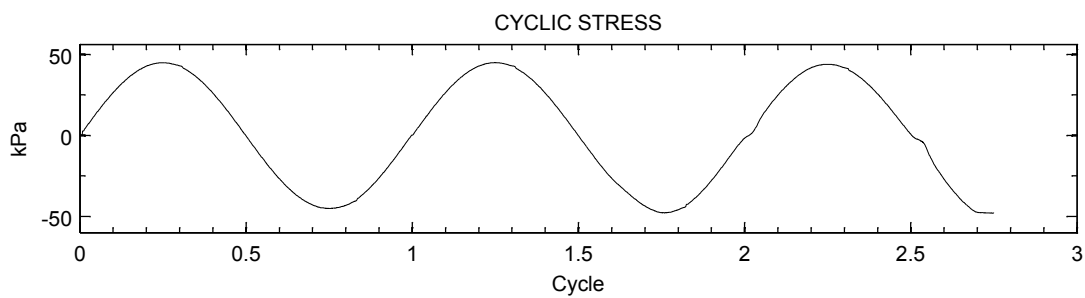
Non-Plastic Fines Content (%): 0

Relative Density (%): 46



Cyclic Stress Ratio: 0.1725

Effective Conf. Press (kPa): 99.8

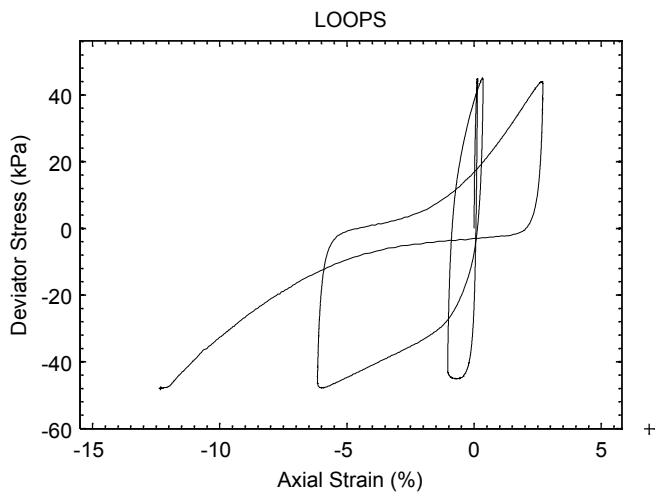


SAMPLE PROPERTIES: MC:20-C3

Mica Content (%): 20

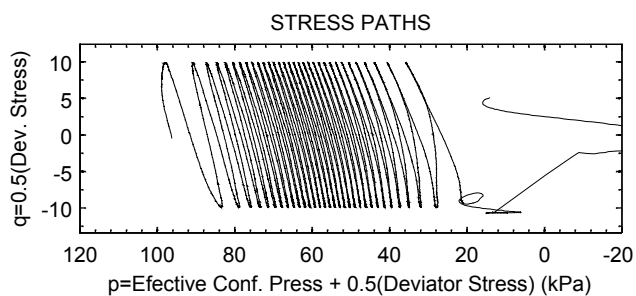
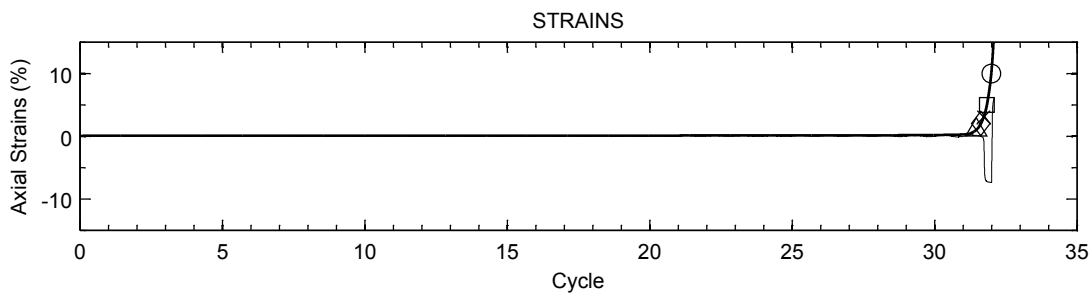
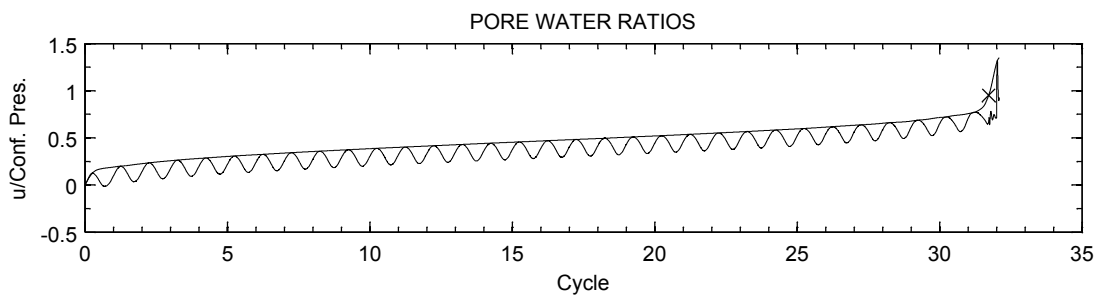
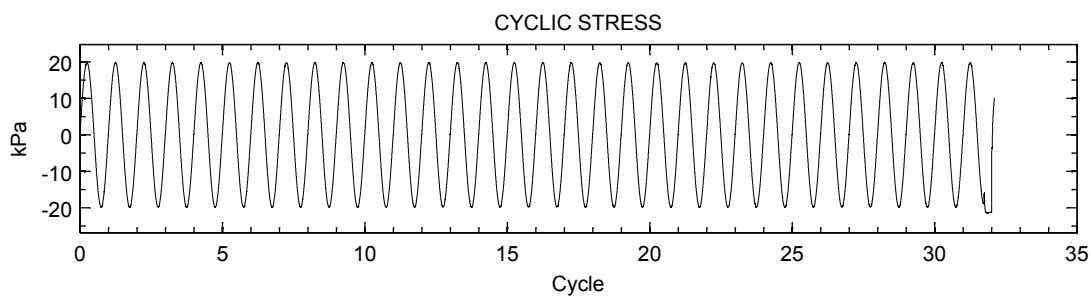
Non-Plastic Fines Content (%): 0

Relative Density (%): 47



Cyclic Stress Ratio: 0.2219

Effective Conf. Press (kPa): 99.9

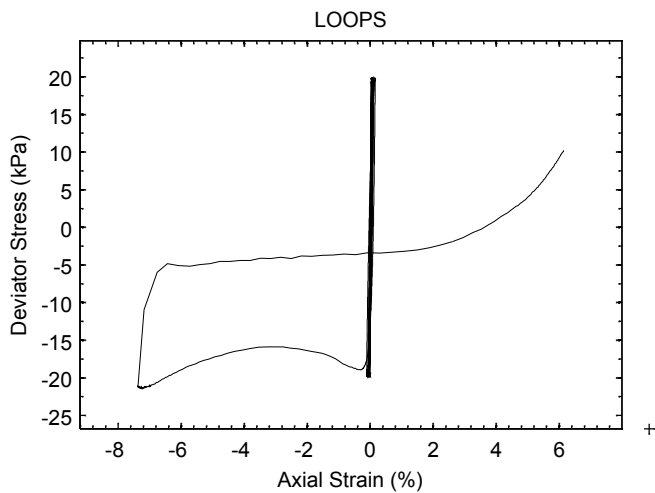


SAMPLE PROPERTIES: MC:20-D1

Mica Content (%): 20

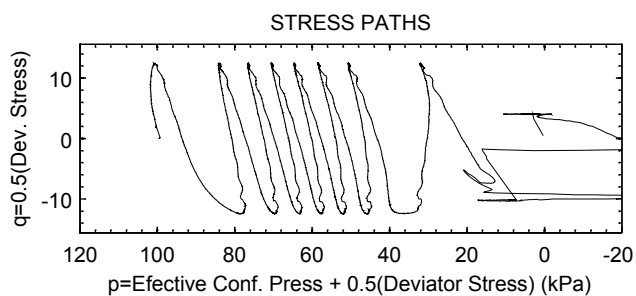
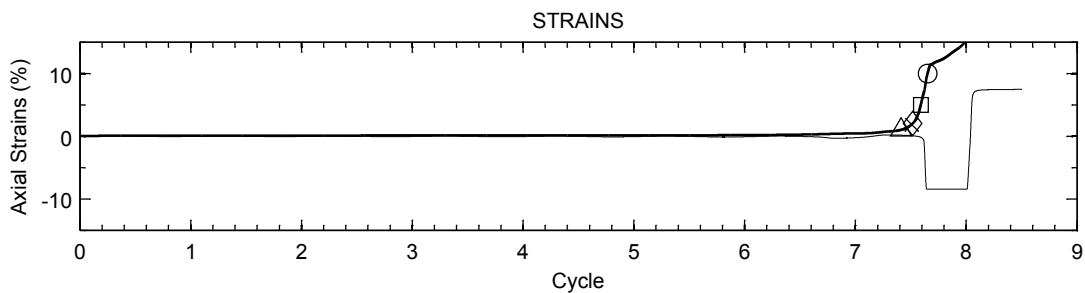
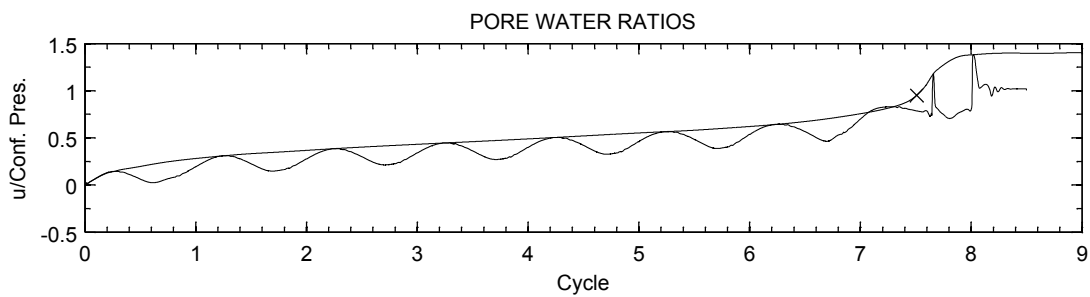
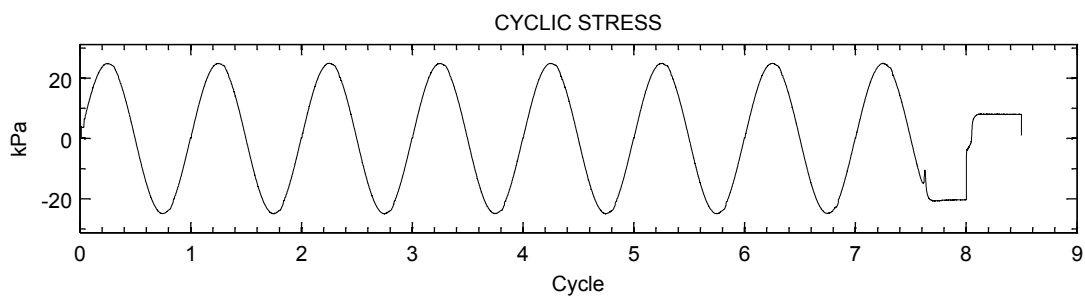
Non-Plastic Fines Content (%): 0

Relative Density (%): 31



Cyclic Stress Ratio: 0.1026

Efective Conf. Press (kPa): 96.1

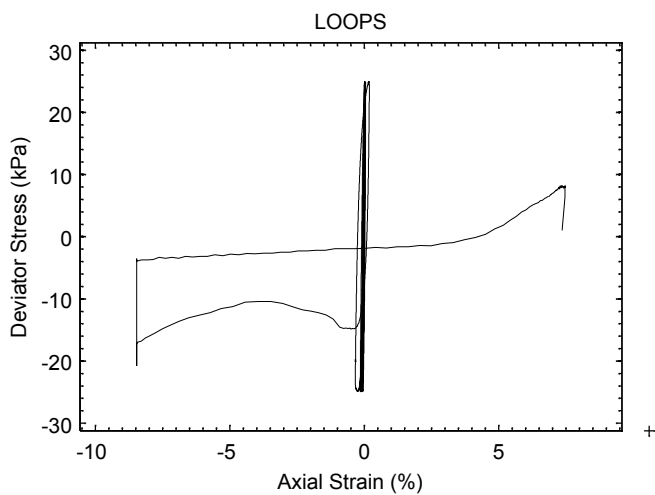


SAMPLE PROPERTIES: MC:20-D2

Mica Content (%): 20

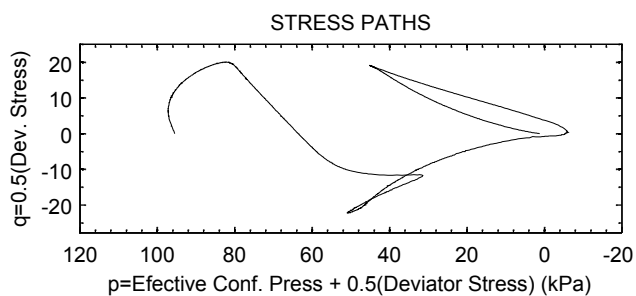
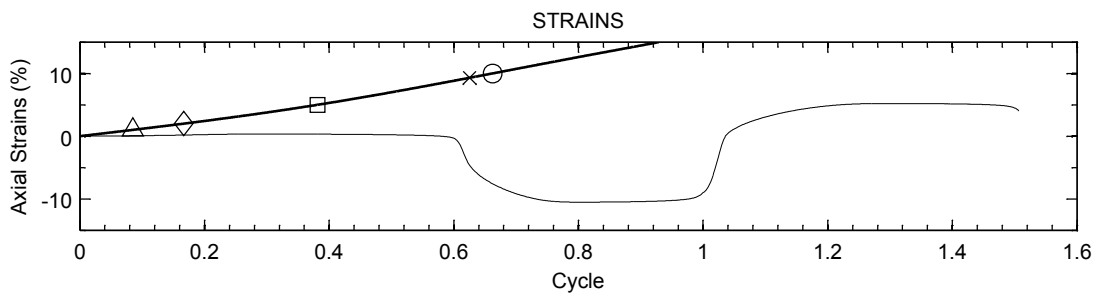
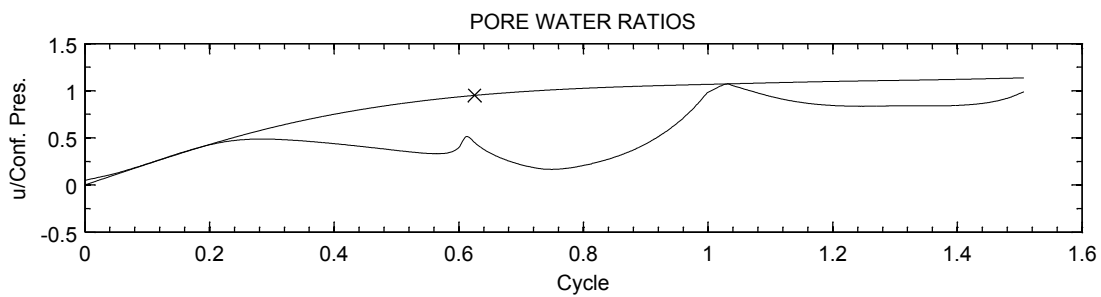
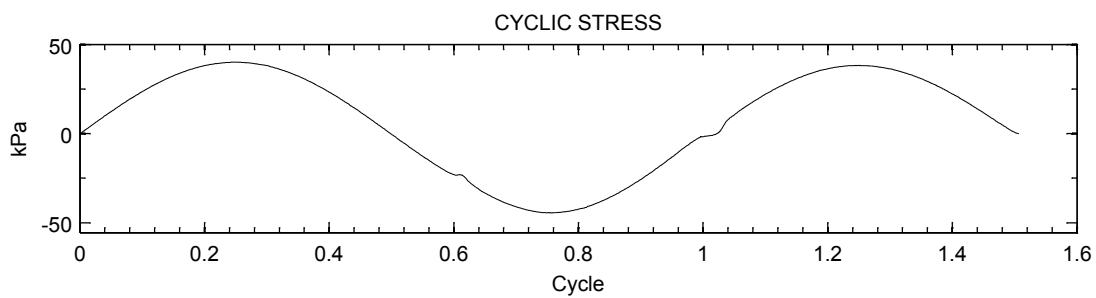
Non-Plastic Fines Content (%): 0

Relative Density (%): 31.8



Cyclic Stress Ratio: 0.1243

Effective Conf. Press (kPa): 99.9

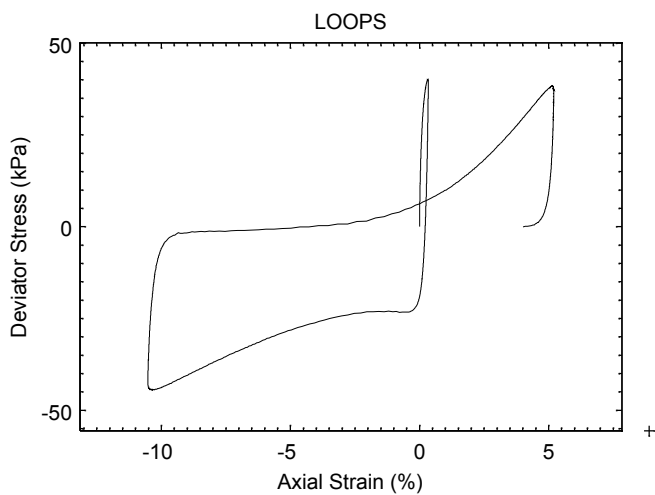


SAMPLE PROPERTIES: MC:20-E3

Mica Content (%): 20

Non-Plastic Fines Content (%): 0

Relative Density (%): 31.8

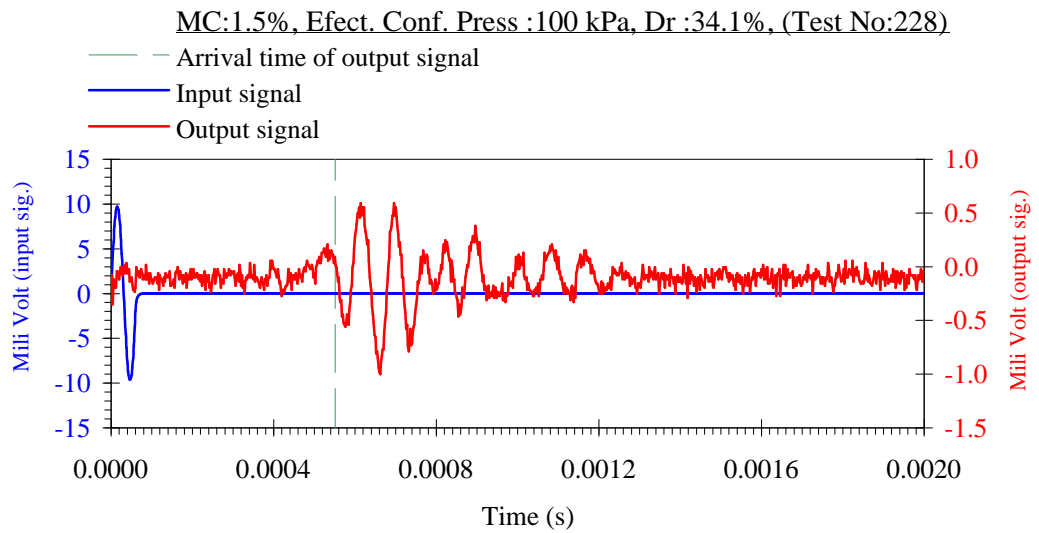
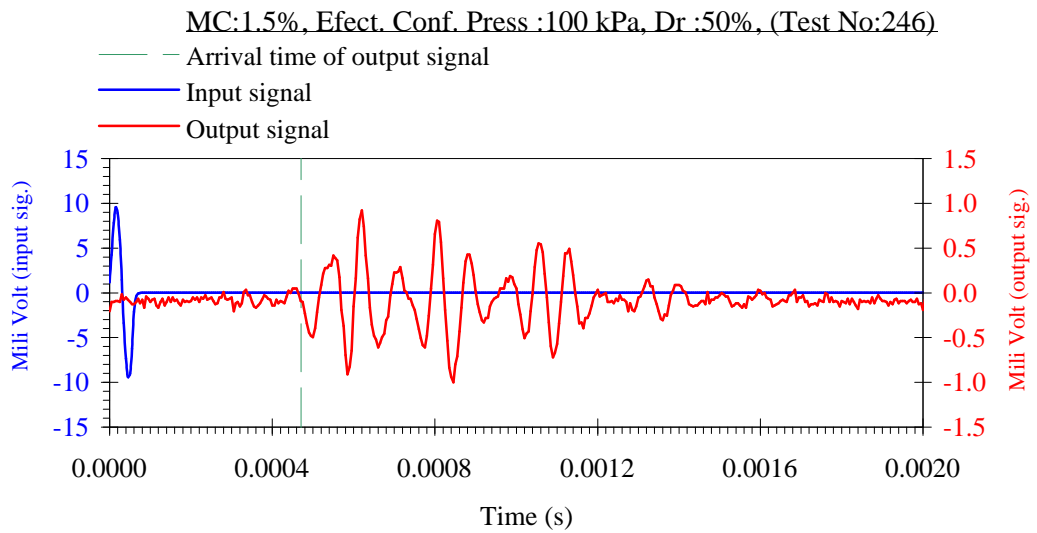
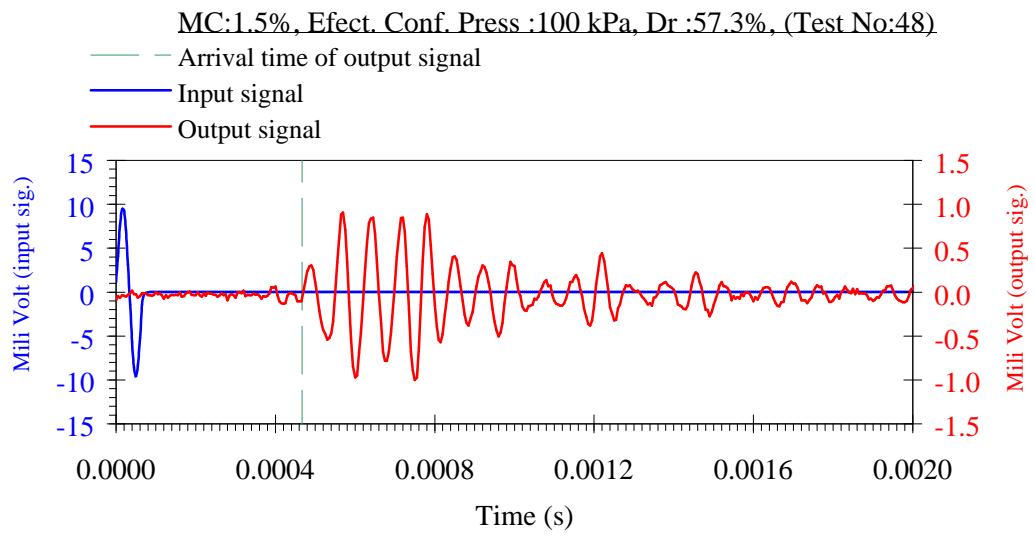


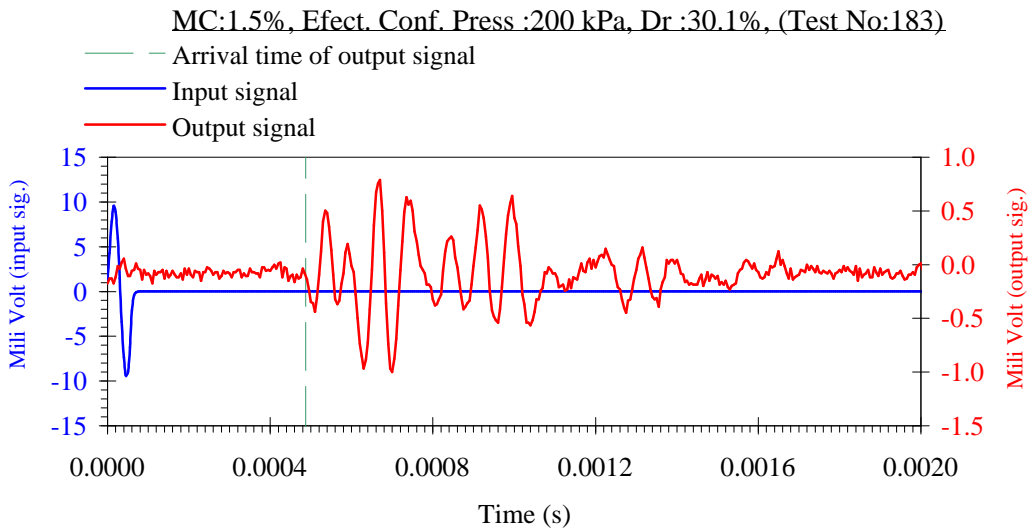
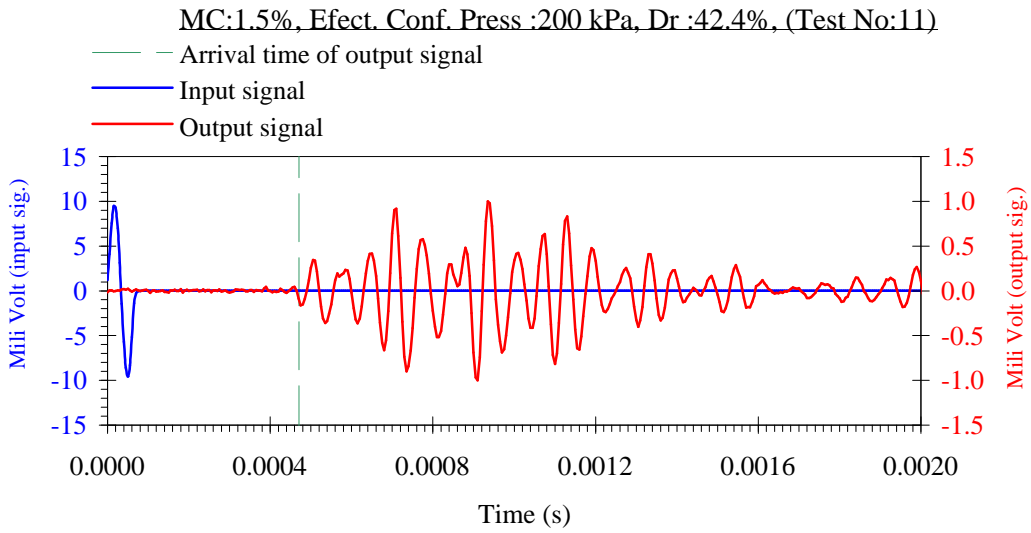
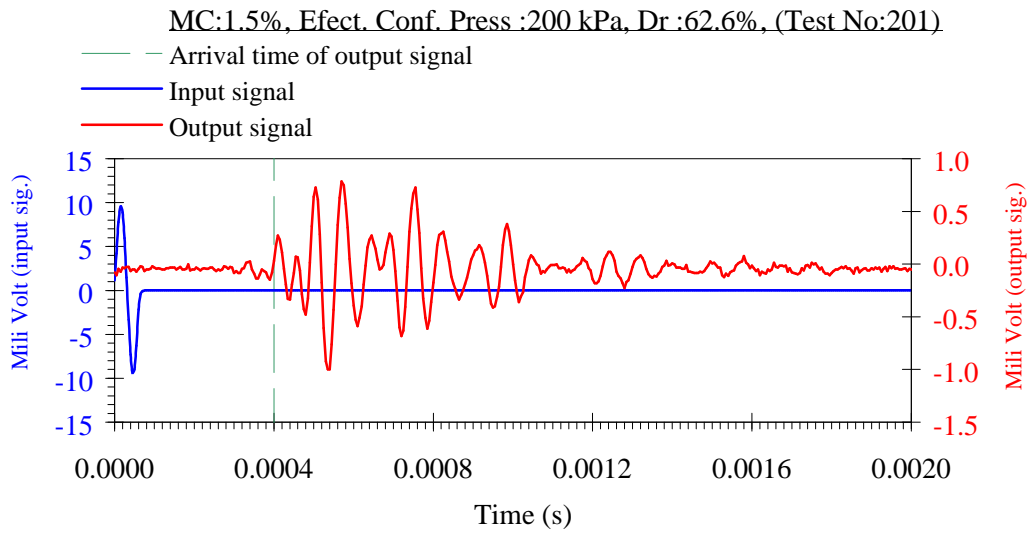
Cyclic Stress Ratio: 0.1987

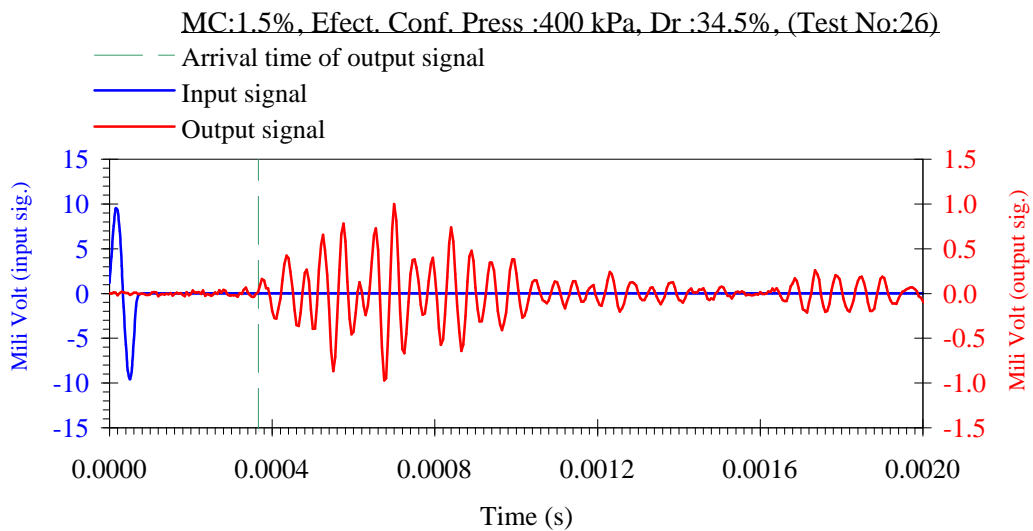
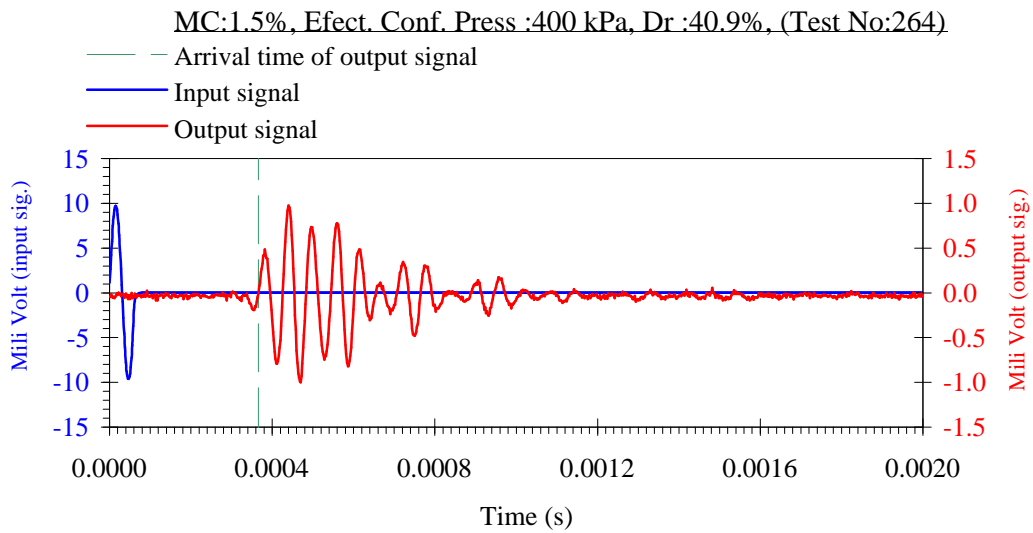
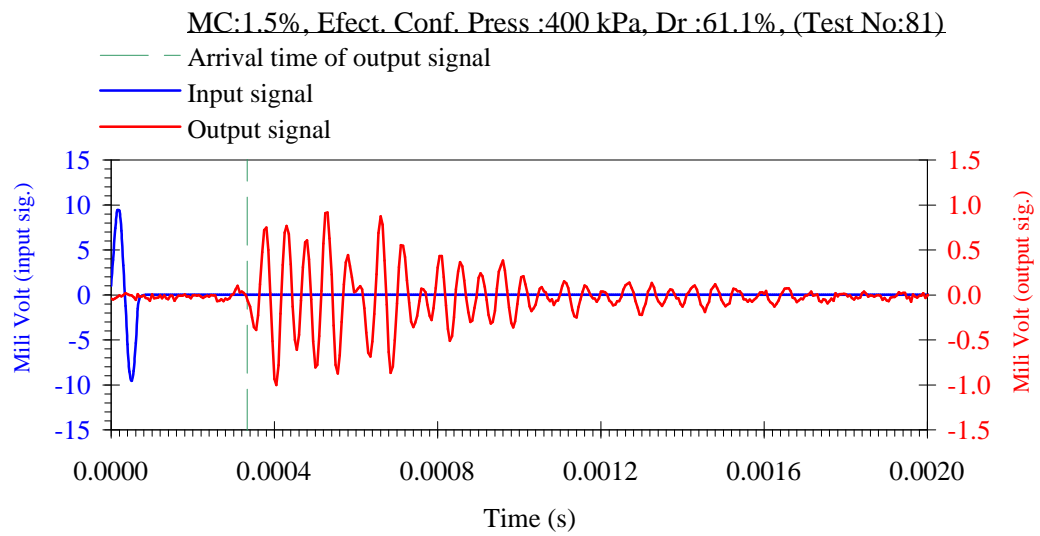
Effective Conf. Press (kPa): 100.5

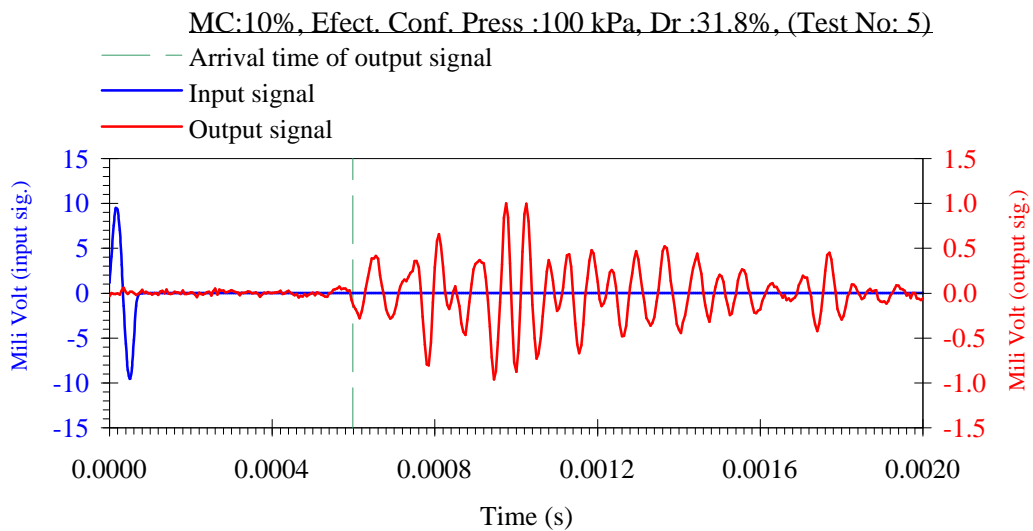
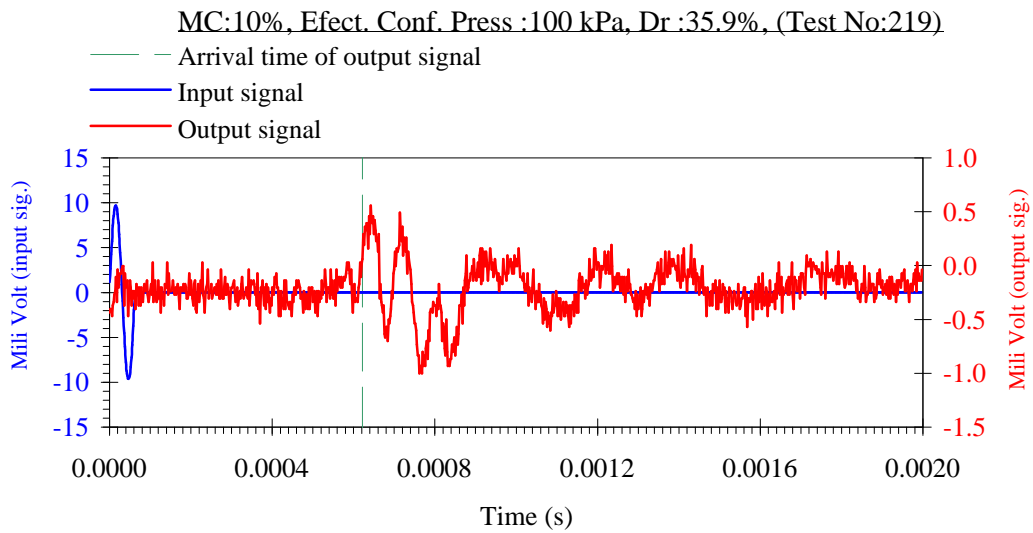
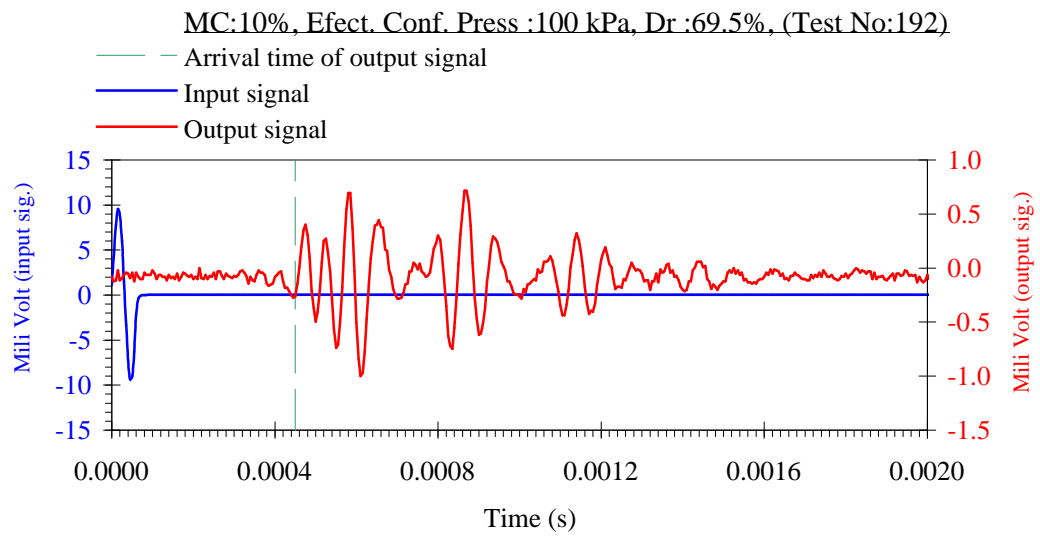
APPENDIX - B

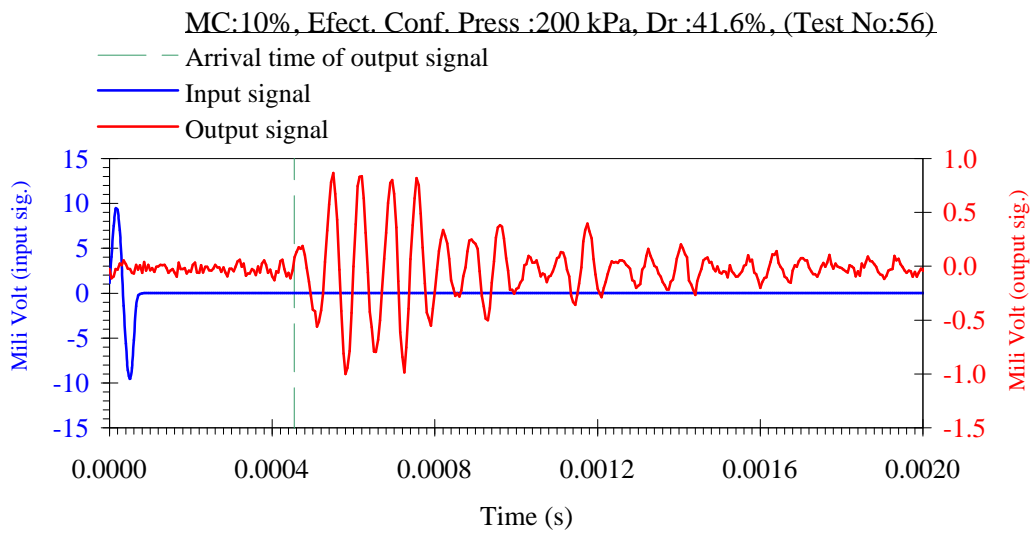
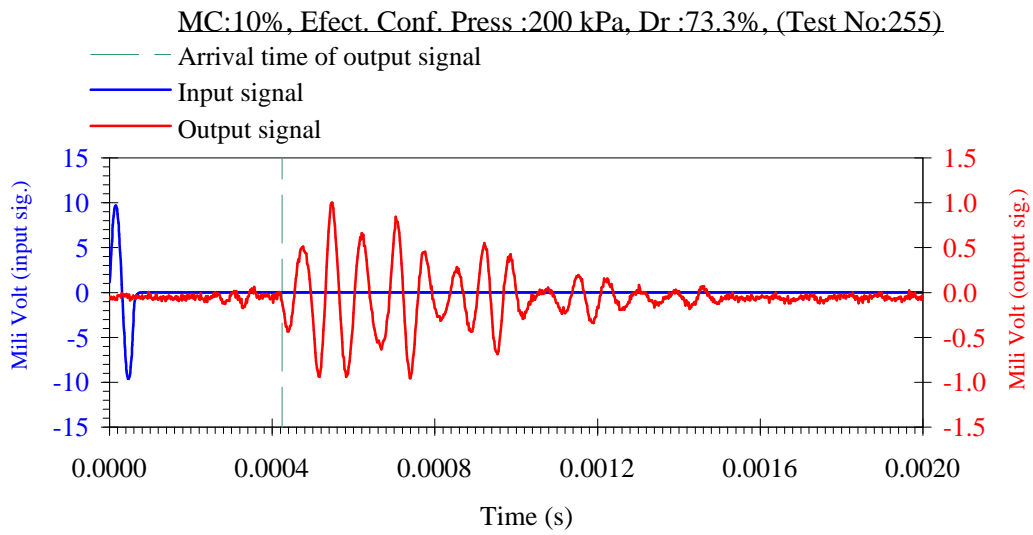
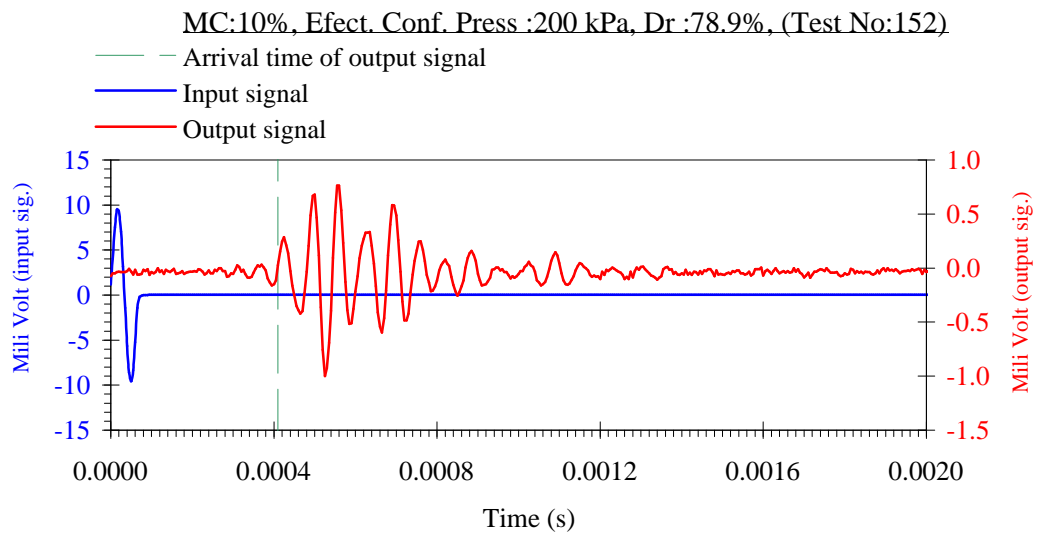
BENDER ELEMENT TESTS

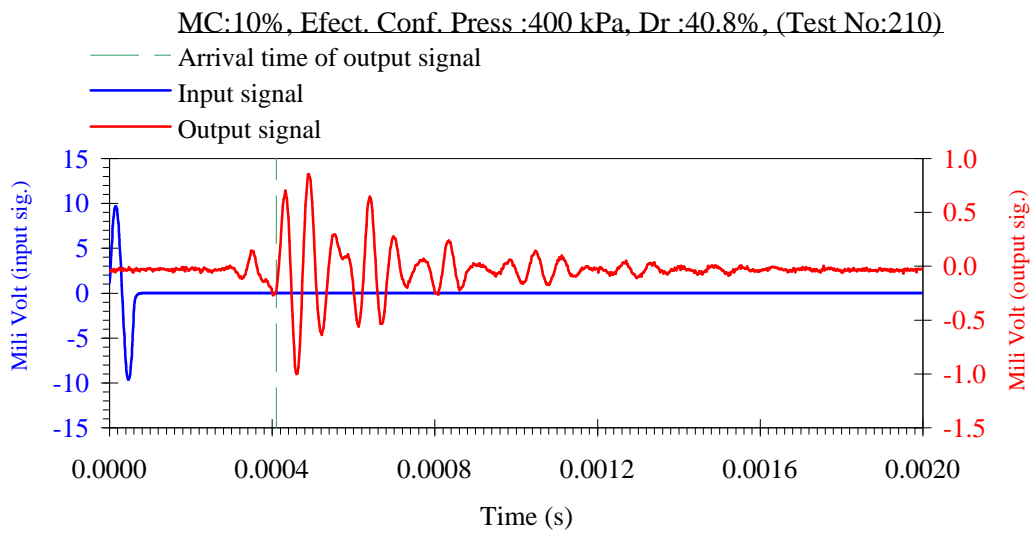
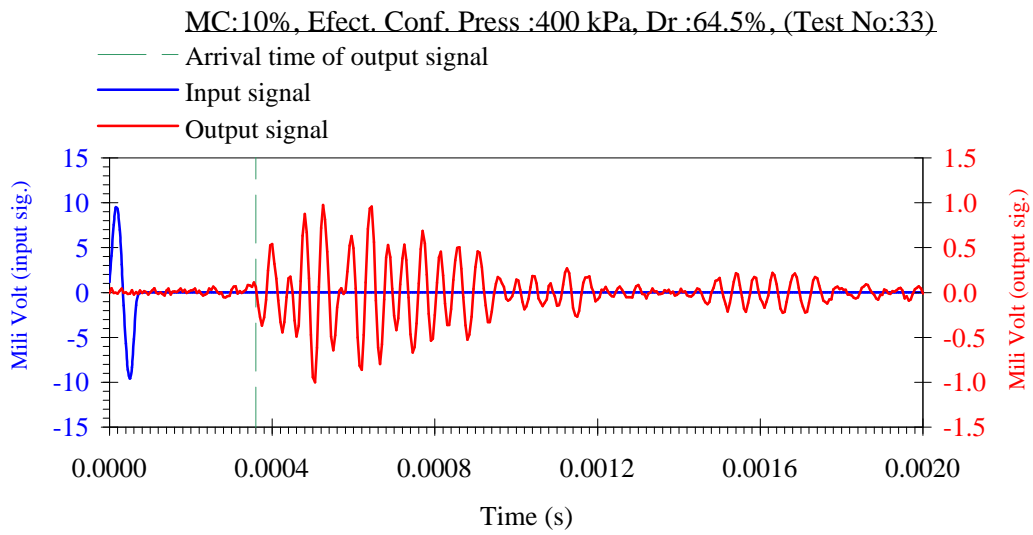
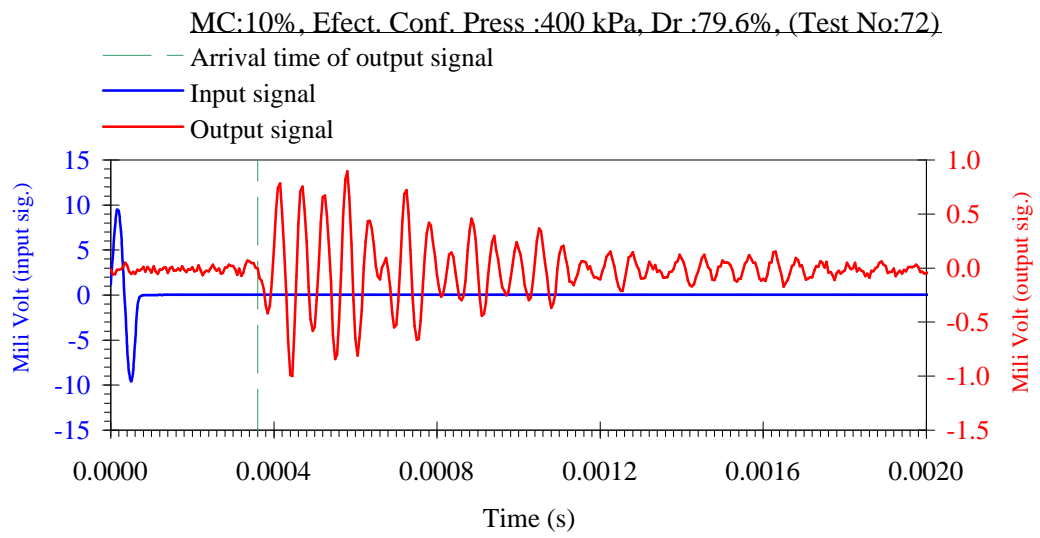


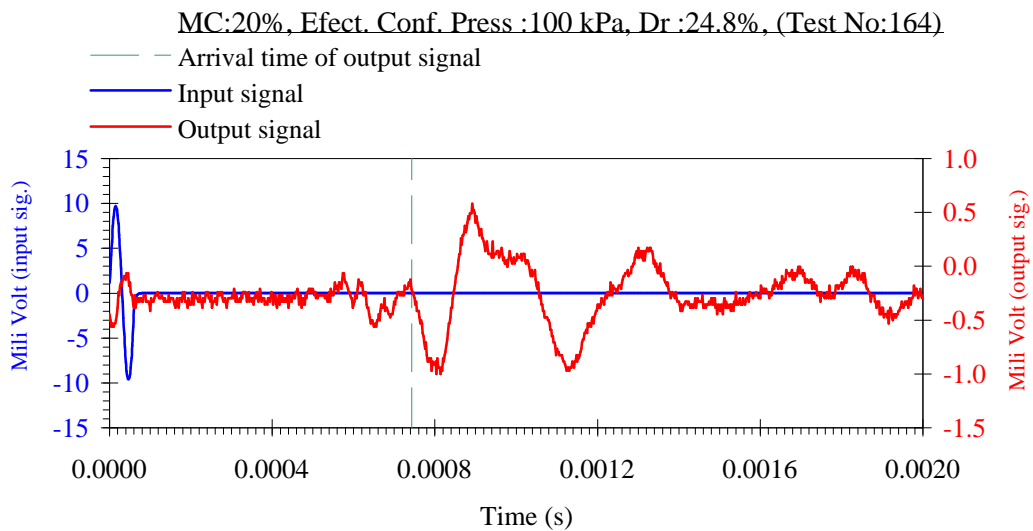
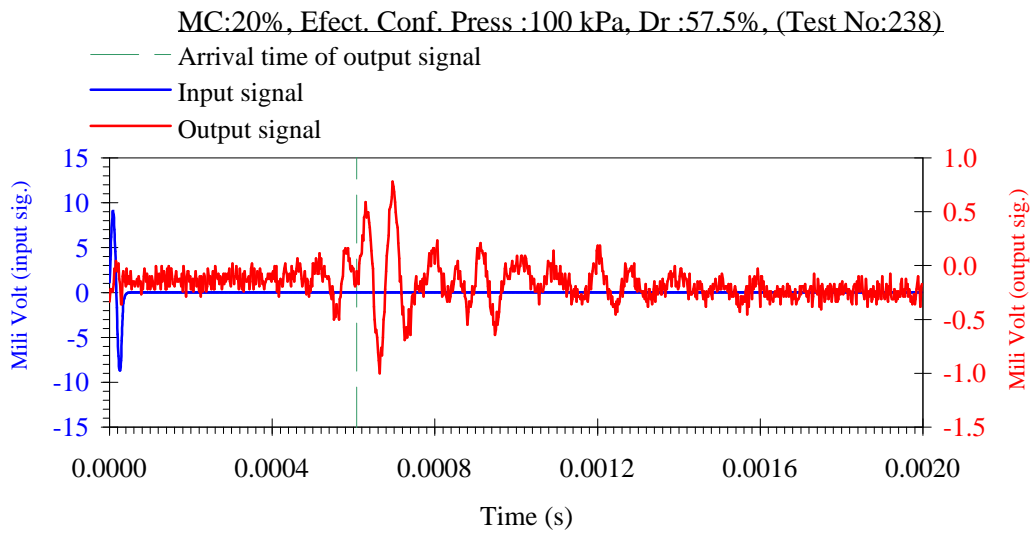
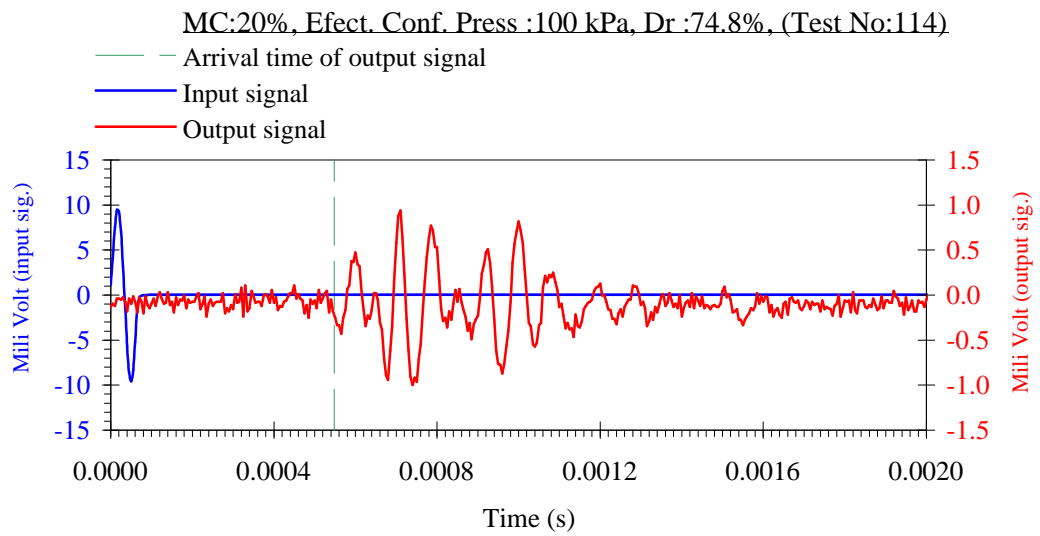


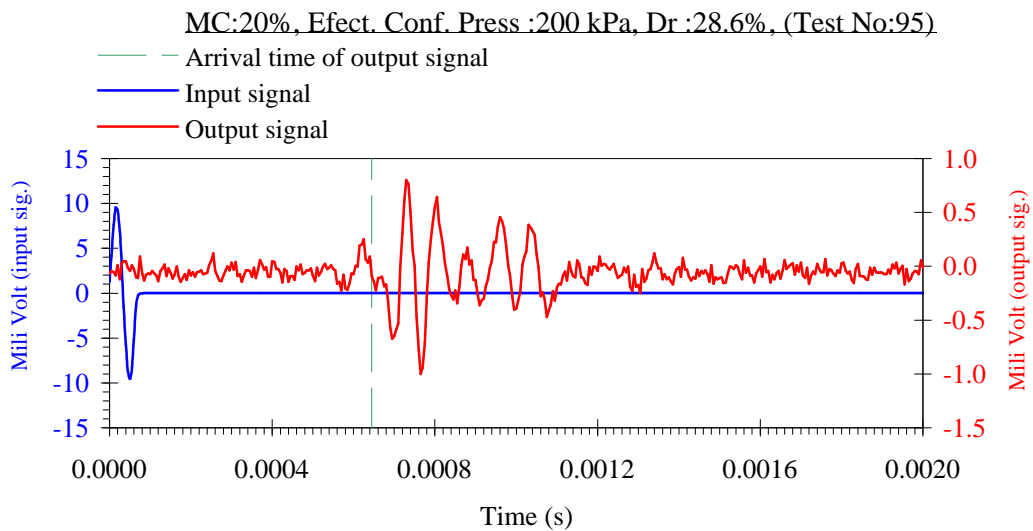
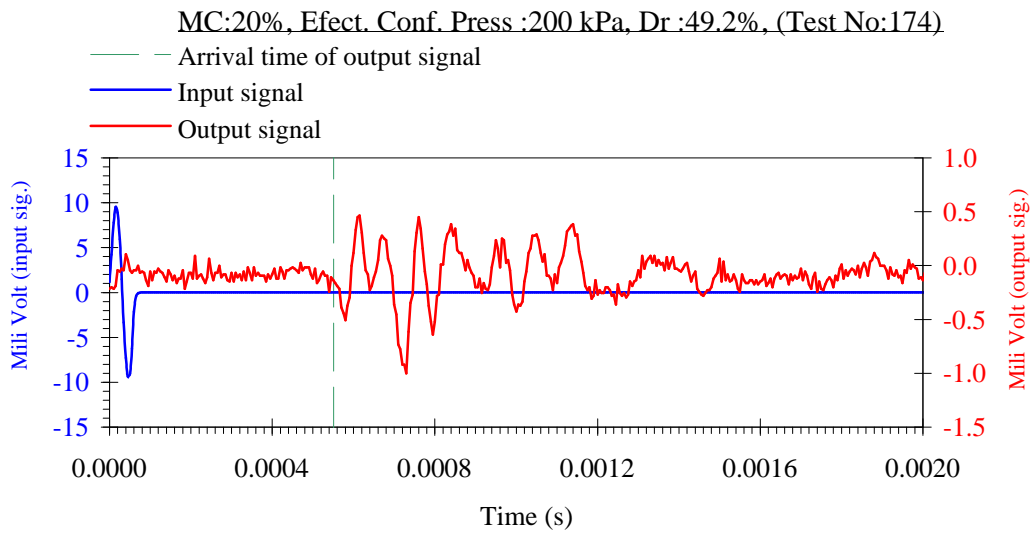
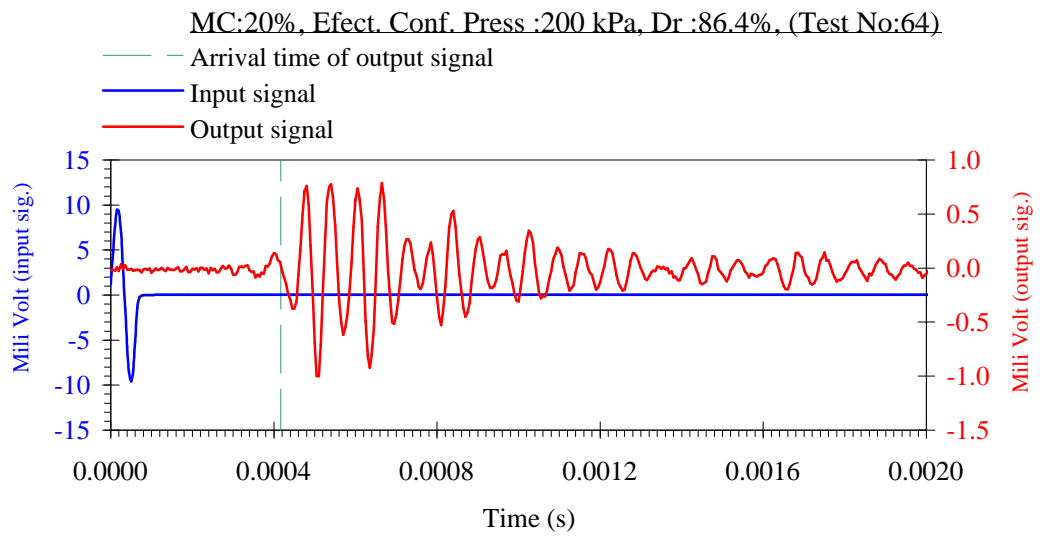


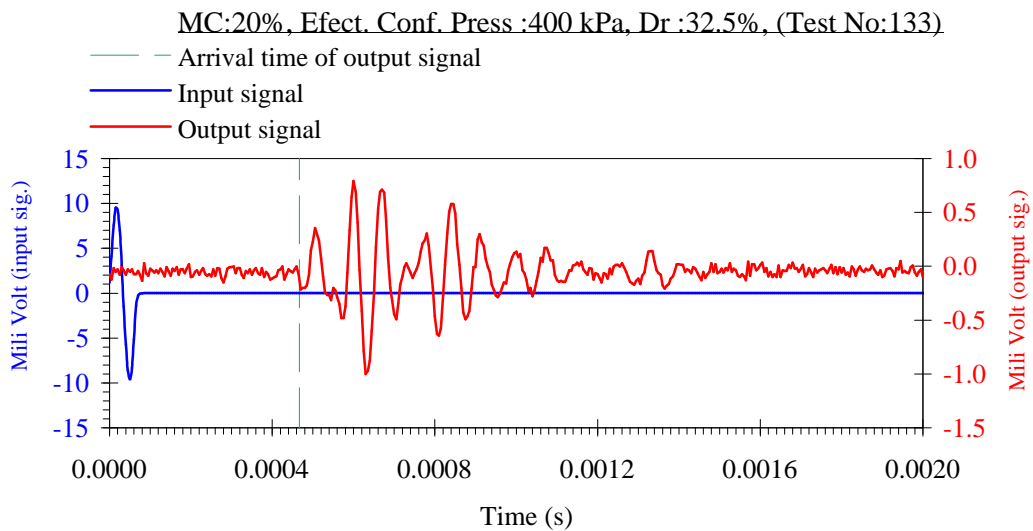
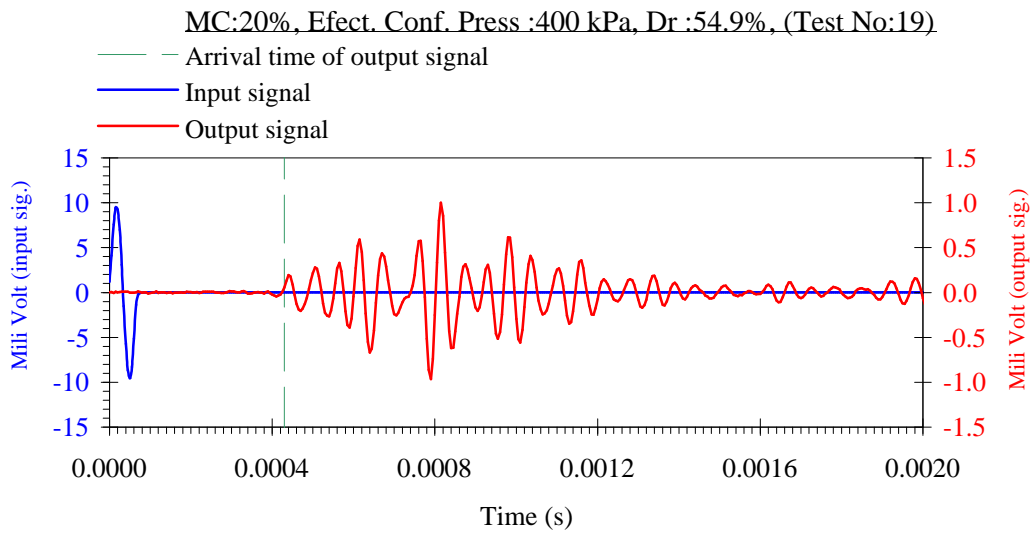
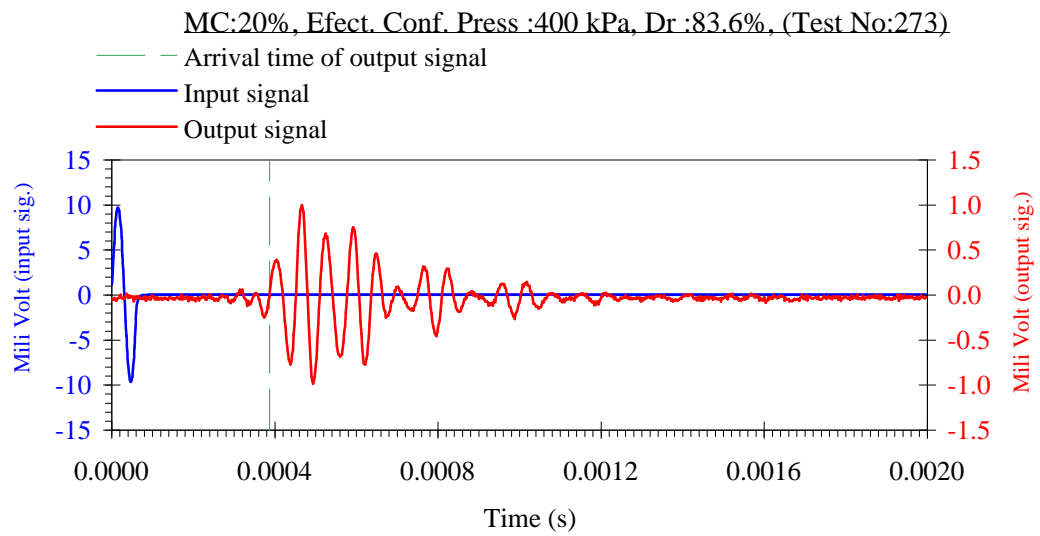








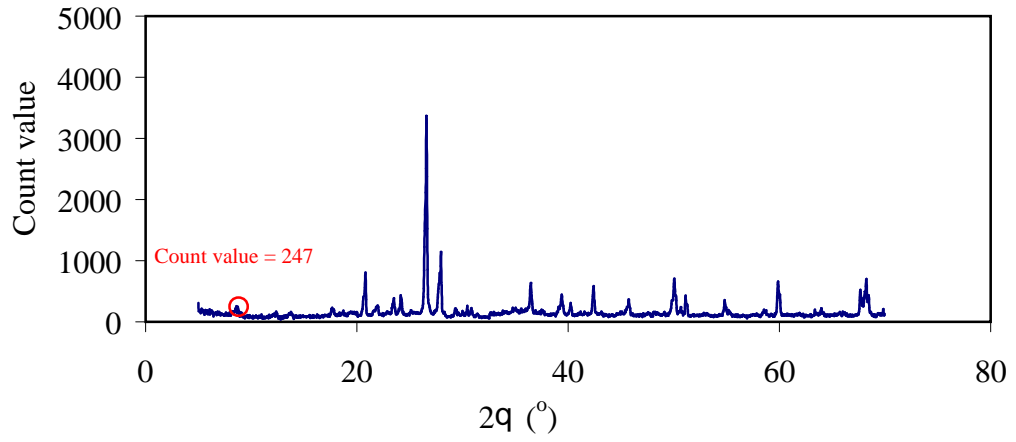




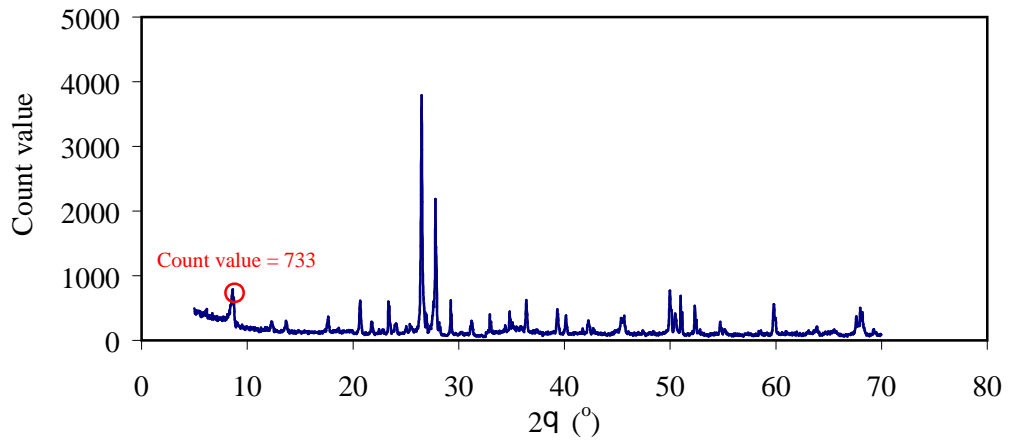
APPENDIX - C

X-RD TESTS

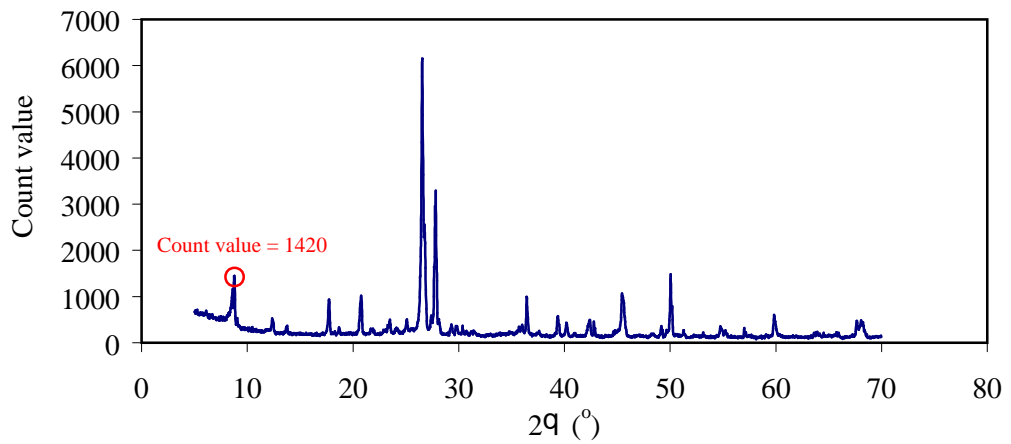
Sand-Mica Mixture (Sand=100%; Mica=0%)



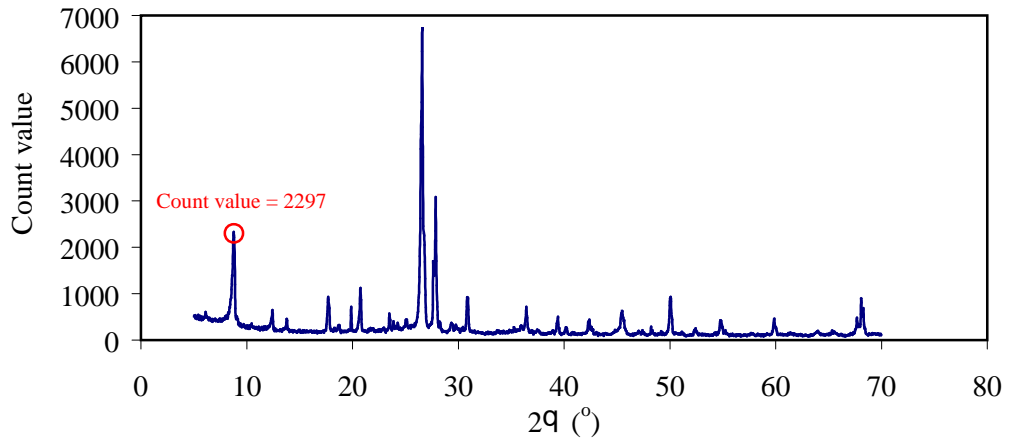
Sand-Mica Mixture (Sand=95%; Mica=5%)



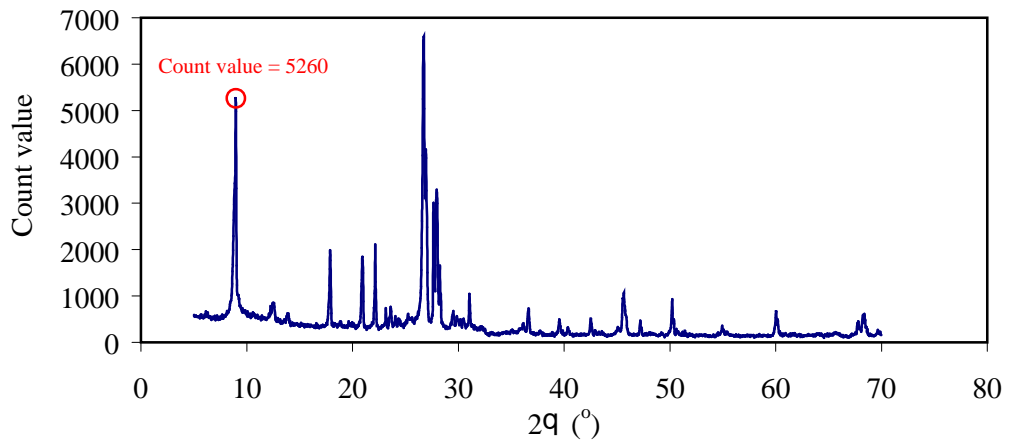
Sand-Mica Mixture (Sand=90%; Mica=10%)



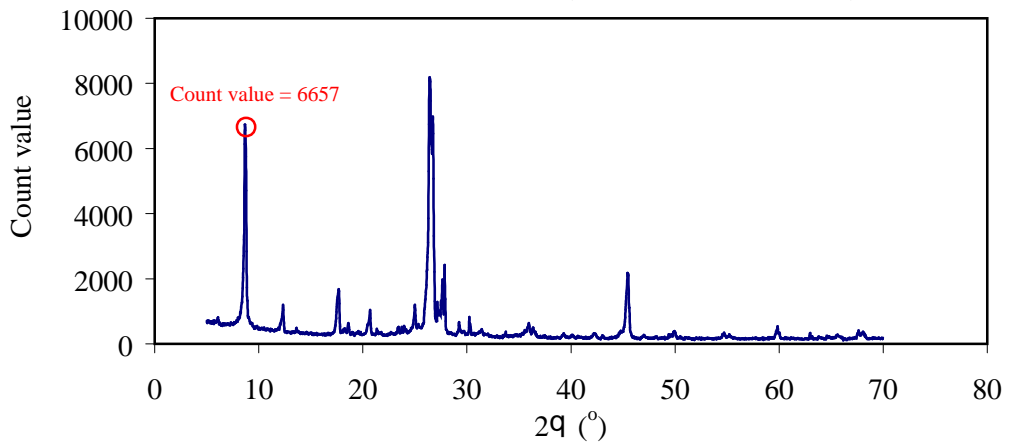
Sand-Mica Mixture (Sand=80%; Mica=20%)



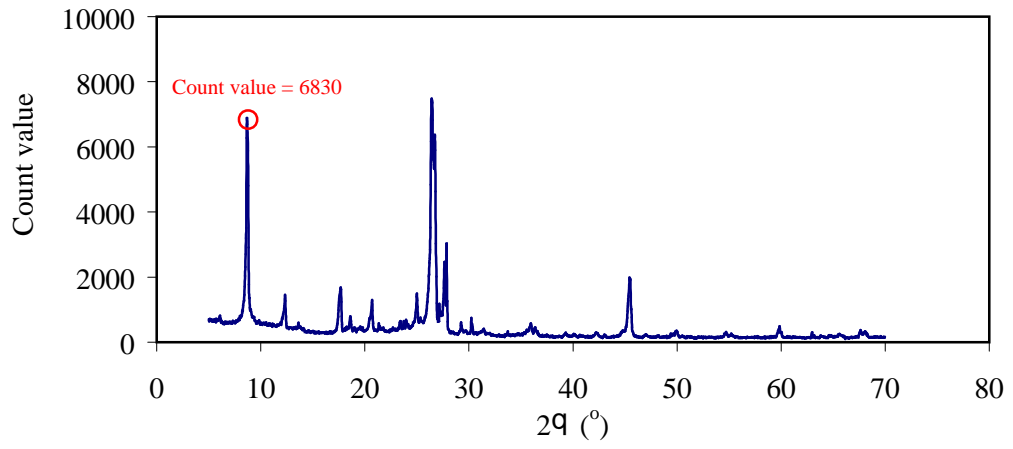
Sand-Mica Mixture (Sand=62%; Mica=38%)



Sand-Mica Mixture (Sand=44%; Mica=56%)



Sand-Mica Mixture (Sand=33%; Mica=77%)



Sand-Mica Mixture (Sand=0%; Mica=100%)

